ANNUAL REPORT

RESEARCH STUDY ON INSTRUMENT UNIT THERMAL CONDITIONING HEAT SINK CONCEPTS

67-2577
January 2, 1968

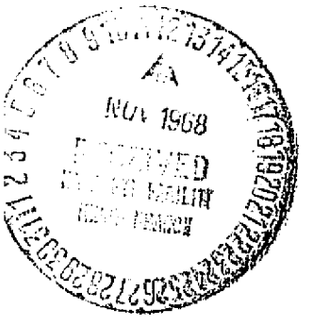

Prepared for

George C. Marshall Space Flight Center
Huntsville, Alabama
Contract No. NAS8-11291

GARRETT
AIRESEARCH MANUFACTURING DIVISION
Los Angeles, California

ANNUAL REPORT

RESEARCH STUDY ON INSTRUMENT UNIT THERMAL CONDITIONING HEAT SINK CONCEPTS

67-2577
January 2, 1968

Prepared by:

D. W. Graumann
G. R. Woods

Prepared for

George C. Marshall Space Flight Center
Huntsville, Alabama
Contract No. NAS8-11291

AIRESEARCH MANUFACTURING DIVISION
Los Angeles, California

FOREWORD

The work described in this report was accomplished under contract number NAS 8-11291 initiated by NASA Marshall Space Flight Center for a Research Study on Instrument Unit Thermal Conditioning Heat Sink Concepts. The contract was under the direction of Mr. F. Huneidi at the NASA and Mr. I. G. Austin at the AiResearch Mfg. Co.

The following members of the AiResearch program staff contributed to the report: D. W. Graumann, Thermal Analysis; G. R. Woods, Mechanical Design and Development.

CONTENTS

CONTENTS (Continued)

APPENDIXES

CONTENTS (Continued)

ILLUSTRATIONS

ILLUSTRATIONS (Continued)

ILLUSTRATIONS (Continued)

TABLES

NOMENCLATURE

a	tube radius
A	projected active wick area
A_c	wick free flow area
b	wick thickness
C	pore tortuosity
D	pore diameter
D_h	hydraulic diameter of steam passage
f	friction factor
g	acceleration of gravity
g_o	gravitational constant, 32.2 lb_f ft/lb_m sec^2
G	mass flux
h	vapor passage height
H_b	heat of vaporization
J	mechanical equivalent of heat, 778 ft-lb_f/Btu
k_w	effective thermal conductivity of wick-water matrix
L	active wick length
P	absolute pressure
P_B	breakthrough pressure
P_L	pressure on liquid side of vapor-liquid interface
P_s	steam passage pressure
P_v	local saturation pressure
P_V	pressure on vapor side of vapor-liquid interface
q/A	heat flux
Q/A	heat flux
Q	heat rate

NOMENCLATURE (Continued)

r	local pore radius
r'	minimum pore radius
r_n	radius of bubble nucleus
R	gas constant or pore exit radius
t	time
T	temperature
T_o	local liquid temperature
T_{sat}	saturation temperature
ΔT_{sup}	liquid superheat
ΔT	temperature difference
w	width of wick or steam passage
W	vapor mass flux
x	wick thickness
X	wicking length
θ	contact angle
λ	latent heat of vaporization
μ_ℓ	absolute viscosity of liquid
ν	kinematic viscosity of liquid
ρ_ℓ	liquid density
ρ_v	vapor density
σ	surface tension

SECTION I

INTRODUCTION

In the design of thermal control systems for spacecraft applications, there are essentially two approaches used in rejecting heat from the vehicle. The first is by radiation to the space environment, an approach which is ideal for extended duration missions and for applications where either large radiating surface areas or high surface temperatures are available. The second approach is to utilize the latent heat of an expendable evaporant, a concept which is more suitable to missions of short duration. Due to its relatively high latent heat of vaporization, water has proven to be an attractive expendable evaporant for this application.

Two concepts which utilize the expendable evaporant approach to heat sink design have been developed. These are the wick-type water boiler and the porous plate sublimater. In the former, water is transported by capillary action through the wicks to the heat input surface where evaporation takes place, and the water vapor is vented to space. The latter incorporates a porous plate barrier between the water and low pressure space environment. Upon exposure to the space vacuum the water which enters the pores of the porous plate freezes and then sublimes. The heat input is expended as the latent heat of vaporization in phase change from solid to vapor.

While units utilizing these concepts have performed adequately in their various spacecraft applications, they have been suspected of being non-optimum designs. For this reason, an analytical and experimental study was performed in order to develop optimized heat sink modules utilizing these concepts. In the water boiler study, wicking materials were investigated with regards to their water transport and heat dissipation characteristics, and water flow distribution and control, heat transport fluid temperature control, and module geometry were analyzed. A multi-wick boiler module and new type of control system were designed, fabricated and tested. Stacking studies were performed so that larger heat loads could be handled by using more than one module. On the basis of the analytical and experimental investigation, an optimized one kilowatt wick-type water boiler was designed.

The sublimator study involved an investigation of the performance characteristics of various porous plates during steady state, start-up, restart, and zero heat load operation. The effects of feed water pressure, steam plenum configuration, and water passage configuration were investigated, and the potential use of hydrophobic coatings on porous plates was studied. A multi-module sublimator core was designed, fabricated and tested. Stacking studies were performed and an optimized one kilowatt sublimator designed.

The second part of this Thermal Conditioning Heat Sink Study was an investigation of a thermal conditioning panel with a self-contained heat sink. Such a panel is used to cool electronic packages mounted upon it, and, being entirely self contained, may be located remotely to an active thermal conditioning system. Several thermal panel concepts were studied and the two most promising designs selected for further development. Test modules were designed, fabricated, and tested to substantiate the design procedure and performance predictions.

SECTION 2

WATER BOILER MODULE

INTRODUCTION

Wick-type water evaporators have demonstrated successful performance in a variety of spacecraft applications. However, due to a lack of basic performance data the existing water boilers have been suspected of being overdesigned, non-optimum configurations. It was desired, therefore, to conduct an analytical and experimental study program whereby a capillary-fed boiler would be optimized. The initial part of the study involved a basic investigation of wicking materials. Based upon past AiResearch development programs and information available in the literature, the best type of wicking material for this investigation was selected, and the various wick parameters were varied to determine their effect on water transport rate, evaporation performance, etc. Various methods of water flow distribution, water flow control, and heat transport fluid temperature control were analyzed. The evaporator module geometry was investigated with respect to wick-fin arrangement and flow configuration. A one-kilowatt boiler module and control system were designed, fabricated, and tested over a range of inlet temperatures and heat loads. Stacking studies were conducted to allow for heat loads larger than one kw. Based upon the wicking investigation, boiler operation analysis, and multi-wick module testing, an optimized wick-type water boiler was designed.

CONCLUSIONS AND RECOMMENDATIONS

The experimental and analytical investigation yielded the following conclusions and recommendations in the area of wick-type water evaporators.

1. Wicking rates may be successfully predicted analytically for a given wick as a function of pore size, contact angle, and tortuosity. The equations developed for pumping capacity and wicking rate in a zero g environment have been verified by horizontal wicking tests under one g conditions.

2. Stringent cleanliness requirements are essential to assure optimum performance of a wick-type evaporator. Surface activating agents should be further investigated as a means of overcoming system contamination and prolonging maximum boiler performance.

3. Good thermal control of a wick type evaporator may be achieved by the use of a single valve which provides back pressure and water on-off regulation utilizing a vernatherm element which senses the heat transport fluid outlet temperature. The chief advantage of this valve is that the vernatherm generates its own driving force making the control system independent of external power requirements.

4. Proper evaporator design should include a pressure drop distribution system in order to assure equal quantities of supply water to all boiler wicks. The primary importance of this system is realized in a 1-g environment when the effects of gravity are normal to the evaporator wicks.

5. The optimum boiler module configuration incorporates water feed from both ends of the wick with a centrally located steam duct. This technique offers the advantages of low steam side pressure drop, and, due to the shorter wicking length, the use of a minimum thickness wick, and more rapid distribution of water during a refill cycle.

6. A series of optimum one kw module water boilers may be combined to provide cooling for a wide variety of heat load applications.

WICKING INVESTIGATION

General

As the very principle of a wick-fed water boiler involves water distribution through and phase change from wicks, a major portion of any boiler optimization study is an investigation of wick materials. Among the evaluation criteria which are relevant to wick selection are wicking rate, evaporation performance, and structural integrity. Several investigations have been conducted on the wicking characteristics of various capillary materials. Among these Ginwala[1] obtained vertical capillary rise rates and water permeability data for various materials, primarily silica fiber materials, sponges, and felts. Langston, Sherman, and Hilton[2] obtained wicking rate data for sintered powder, sintered screen, and sintered fiber metal wicks, materials more suitable for plate-fin wick evaporators due to their structural integrity and compatibility with conventional joining techniques. Their results indicate that in a vertical attitude fiber metal wicks provide the most rapid liquid rise. AiResearch has conducted study and development programs in which wicks and their properties were investigated. The first generation of wicking evaporators utilized a glass fiber type of wicking material. Due to contamination problems and the desireability of a material with more structural integrity, subsequent units have incorporated sintered fiber metal wicks.

The major portion of tests conducted during the wicking investigation phase of this boiler optimization program were performed on sintered fiber metal wicking material. This was due to its superior wicking ability, compatibility with other evaporator components, applicability to conventional joining techniques, and in general, recognition of its superior applicability to state of the art wicking evaporators. The fiber metal material used is a randomly interlocked structure of metallic fibers, subjected to a sintering process in which metallic bonds are established at the fiber contact points. The material can be made in various densities and thickness by varying the size and type of fiber and manufacturing process. Ranges in density and thickness of 10 percent to 30 percent and 0.030 in. to 0.250 in., respectively were investigated as these appear to encompass the range of desirable properties.

Capillarity and Wick Flow

Equations defining the capillary rise in tubes and in wicks in any gravity field have been developed starting with the general differential momentum equation including surface tension, gravitational, frictional drag, and inertia (momentum) forces. Siegel[3] solved the equation for liquid penetration length in a tube in zero g and obtained the following result:

$$X^2 = \frac{1}{16}\,\frac{\sigma(2a)^3 g_0}{8\,\rho_\ell \nu^2}\cos\theta\,\left(e^{-8\nu t/a^2} - 1\right) + \left(\frac{1}{2}\,\frac{\sigma a\, g_0}{\rho_\ell \nu}\cos\theta\right) t \qquad (2\text{-}1)$$

For large values of time the first term in this equation becomes negligible, and the length, X, varies as the square root of time. The equation then becomes identical to that obtained if the inertia term is neglected in the original differential equation.

$$X^2 = \left(\frac{1}{2} \frac{\sigma\, a g_0}{\rho_\ell \nu} \cos\theta\right) t \qquad (2\text{-}2)$$

Since identical equations are obtained at large times with the inertia term included or omitted, it may be concluded that inertia forces are relatively unimportant in wick dynamics at large times. It should be noted that the term "large times" is somewhat ambiguous and what may be a large time for one wick or tube may not be for another. Solving equation (2-1) for the relative magnitude of the two terms on the right side, using the average pore diameter of typical fiber metal wicks used in wick evaporators reveals that the first term becomes negligible at times shorter than one second. "Large times" for these wicking materials therefore means times greater than one second. Since the significant time increment for the wicking heights of these wick materials are minutes rather than seconds, the validity of using simplified equations of the form of equation (2-2), which omits inertia effects, is established.

The equation developed in Appendix A for the wicking rate in zero g or in a horizontal attitude in one g is:

$$t_{g=0} = \frac{4\, \mu_\ell C X^2}{g_0\, D\sigma \cos\theta} \qquad (2\text{-}3)$$

which may be rearranged to obtain:

$$X^2 = \frac{1}{C}\left(\frac{1}{2} \frac{\sigma(D/2)\cos\theta}{(\rho_\ell \nu / g_0)}\right) t \qquad (2\text{-}4)$$

Equation (2-4) is identical to equation (2-2) except for the tortuosity term C which is defined as the ratio of the actual path length to the apparent length, X.

It is not possible to obtain a closed form solution to the differential equation defining vertical wicking in a gravity field if all the terms are included. Pickett[4] presents a finite-difference equation to obtain analytical solutions and Siegel utilized a digital computer to solve the equation numerically using the Runga-Kutta method of forward integration. Both of these investigators obtained good agreement with experimental data for tubes at small values of time. A closed form solution to the differential equation is possible if the inertia term is neglected. The equation defining vertical wicking in a gravity field developed in Appendix A is:

$$t_{g\neq o} = \left[\frac{32\, \mu_\ell C}{\rho_\ell g\, D^2} \frac{4\sigma \cos\theta\, g_0}{\rho_\ell g\, D} \log\left(\frac{1}{1 - \frac{\rho_\ell g\, D}{4\sigma \cos\theta\, g_0} X}\right) - X\right] \qquad (2\text{-}5)$$

To aid in selection of optimum wicks for a water boiler and to provide pumping rate data necessary for thermal panel design, horizontal and vertical wicking rate tests were performed. These data also served to verify the validity of equations (2-3) and (2-5).

The vertical wicking test involved mounting the wick specimens in a vertical position and immersing the bottom end of the wicks in water. A clock was started at the moment the wick was immersed and water level in the wick recorded at regular time intervals. Visual observations were supplemented by attaching litmus paper strips to the wicks. In the horizontal advance tests, the specimens were mounted in a horizontal position and water feed accomplished by using pieces of cellulose sponge to wet the bottom portion of the wick. Data were recorded in the same manner as in the vertical rise tests. Some difficulty was experienced with wick contamination which caused initial inconsistencies in the data; however, when it was learned how critical wick cleanliness was, additional care was taken to prevent contamination and good data were obtained.

In order to assure cleanliness of the test specimens, the following precautions were observed:

a. All testing was conducted in the AiResearch Altitude Laboratory Clean Room.

b. All specimens were thoroughly cleaned prior to testing.

c. Wick specimens were kept in nylon bags when not in use.

d. Wicks were handled only with tongs or clean rubber gloves.

e. Only distilled 1/2 micron filtered water was used in testing.

Data were obtained for nickel fiber felt wicks of various densities and thicknesses as given below.

Wick No.	Thickness, in.	Width, in.	Density, percent
1	0.132	1.25	20
2	0.061	1.01	20
3	0.031	1.02	30
4	0.034	1.02	20
5	0.031	1.01	15
6	0.093	1.00	10
7	0.060	1.00	15
8	0.125	1.24	30
9	0.062	1.01	30
10	0.122	1.25	15
11	0.250	2.49	15
12	0.090	1.00	15

The results of these tests are shown in Figures 2-1 through 2-4 as wetted length vs elapsed time. The solid lines in these plots are the values predicted by equations (2-3) and (2-5).

The numerical values of the parameters in these equations are fairly well defined in the literature except for the effective pore diameter, the tortuosity, and the contact angle of the wick. Wicks of this construction have a wide range of pore sizes, but the pore size variation is distributed evenly throughout the wick. The manufacturer quotes minimum, mean, and maximum pore diameters which vary with density but not with thickness. Wide variation in the values of contact angle on the same clean metal surface are quoted by the literature. It is also known that the contact angle varies greatly with the conditions of the surface and that surfaces may become contaminated during short exposure to a supposedly clean atmosphere.

Correlations of the horizontal data was attemped early in the program using assumed valves of tortuosity and contact angle of 1.5 and 45 degrees respectively, and it appeared that the best correlation was obtained using the minimum pore diameter. However, it was not possible to obtain agreement between the predicted and experimental vertical wicking data using these valves for C, θ, and D. More realistic valves of tortuosity were then obtained from water permeability data for this type of wicking material given in Reference 2. Values on the order of 1.1 were obtained which indeed seem more reasonable for materials which are from 70 to 90 percent void space. Contact angles on the order of 70 deg were obtained from vertical equilibrium wick height data.

Several important effects of gravity or the absence of it on the wicking characteristics are indicated by the equations and substantiated by the data. First, the predicted and measured wicking curves for different density wicks (different mean pore diameters) cross in a one-g environment. Initially, the wicks with the largest pores (lowest density) wick fastest but at large times as they approach their lower equilibrium height, the smaller pored wicks pass them. The denser wicks reach a higher equilibrium height because the height is inversely proportional to the pore size as shown by Equation (3) in Appendix A. In a zero gravity environment, or in a horizontal position in one-g, the wicks with the largest pores wick at a greater rate at all values of time; no equilibrium height is reached because there is no gravity head to oppose wicking, and the wick will continue to pump liquid until the wick is filled with liquid.

Wick Boiling

In order to determine the heat transfer performance of various wick materials and to obtain data upon which water boiler and thermal panel design could be based, water vaporization tests were performed on wick test modules. The wicks tested were oriented in a vertical position so that water resupply by capillary forces in the wick was against gravity.

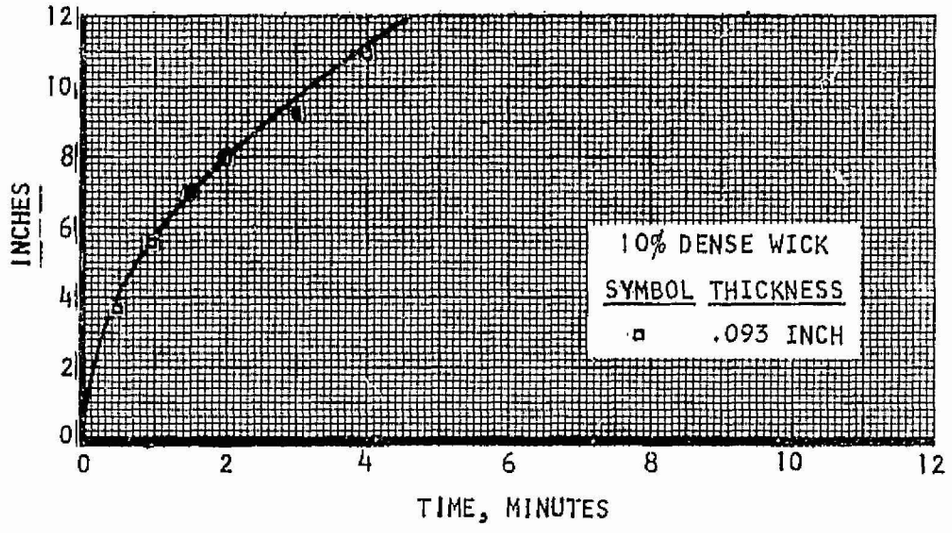

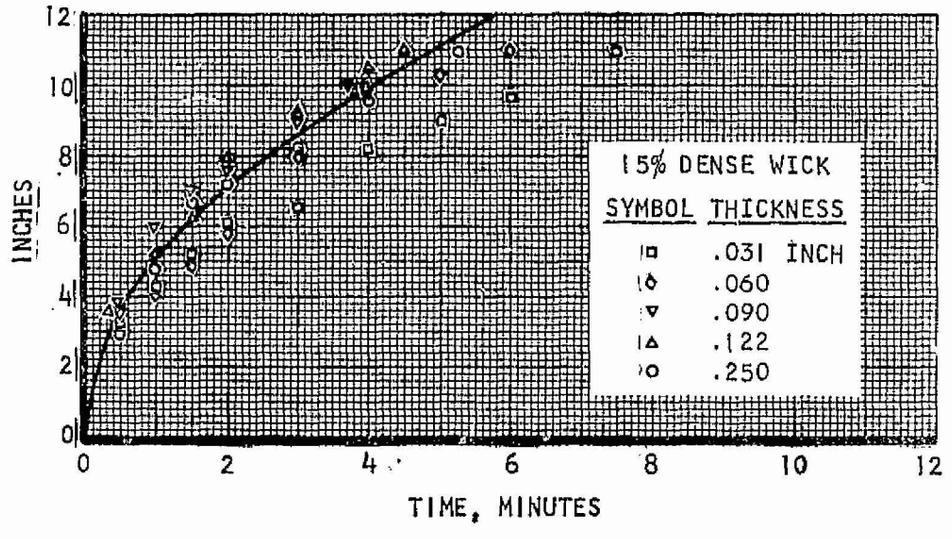

A-28754

Figure 2-1. Horizontal Wicking In One-G

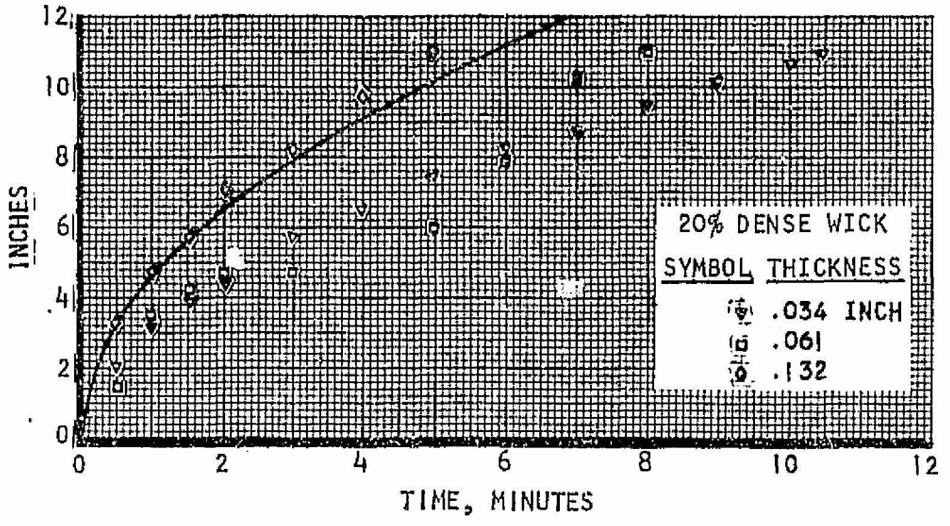

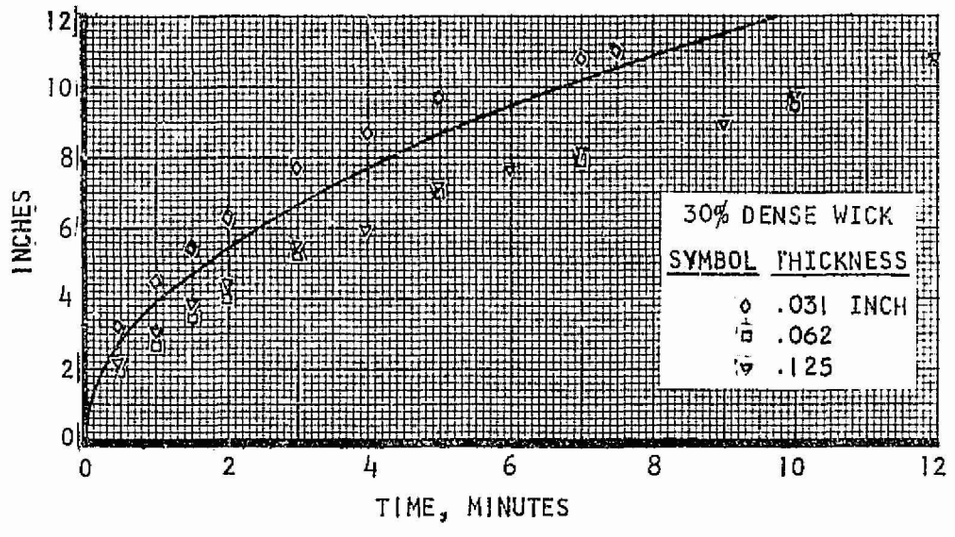

Figure 2-2. Horizontal Wicking In One-G

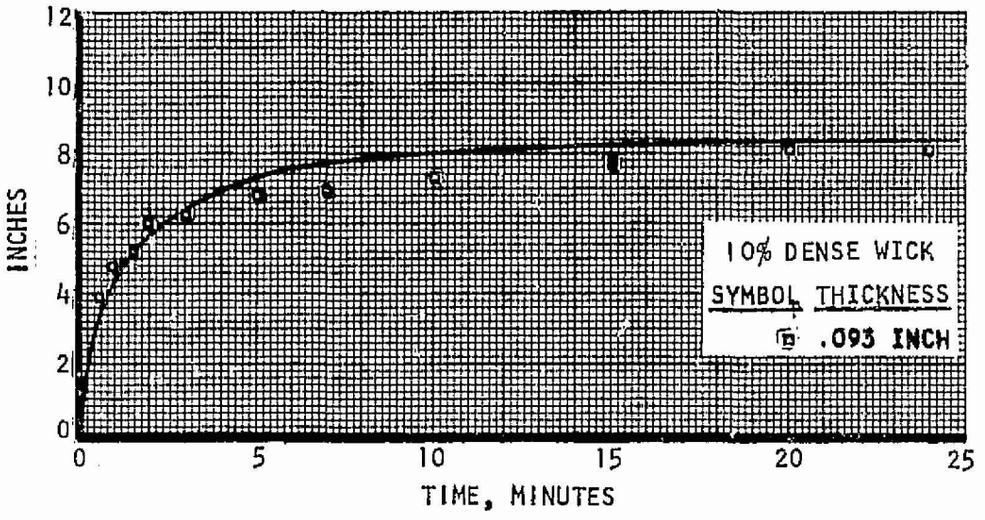

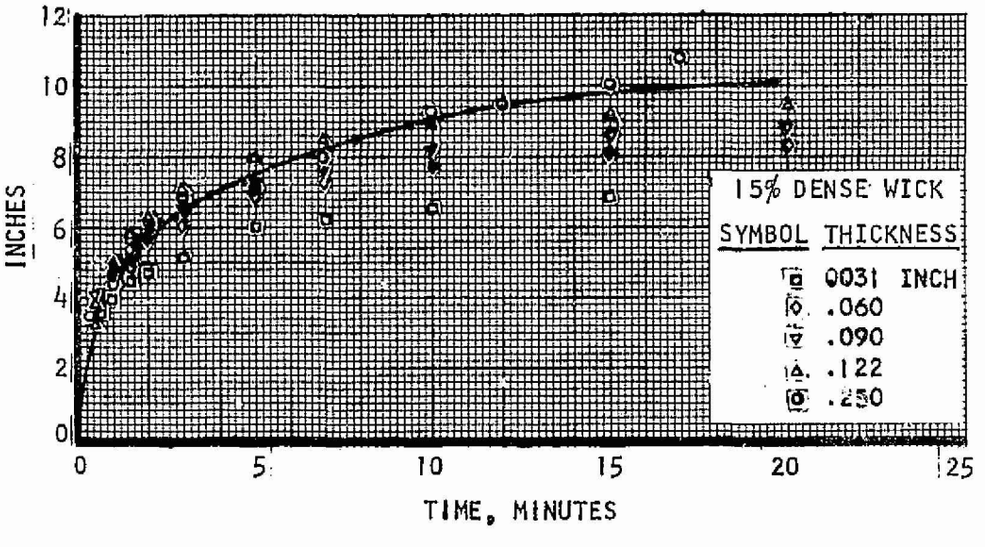

Figure 2-3. Vertical Wicking in One-G

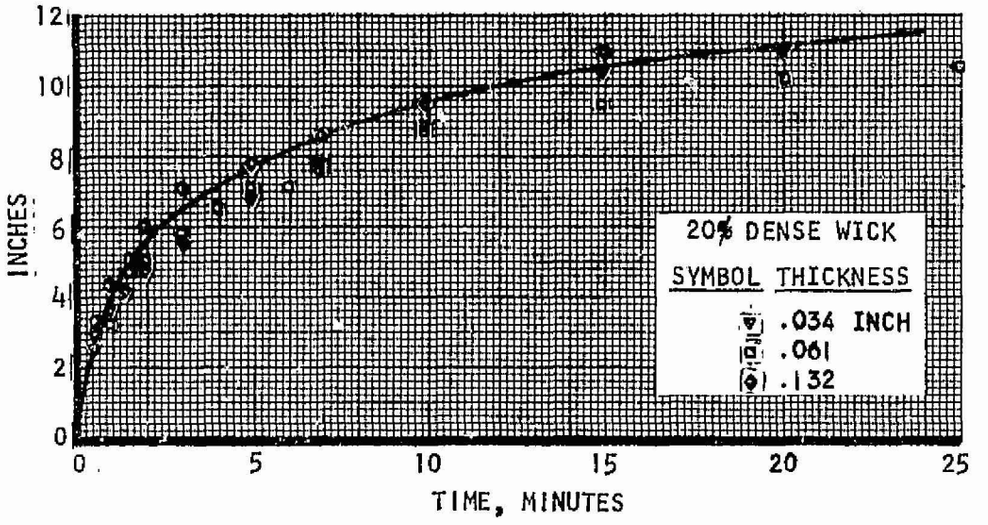

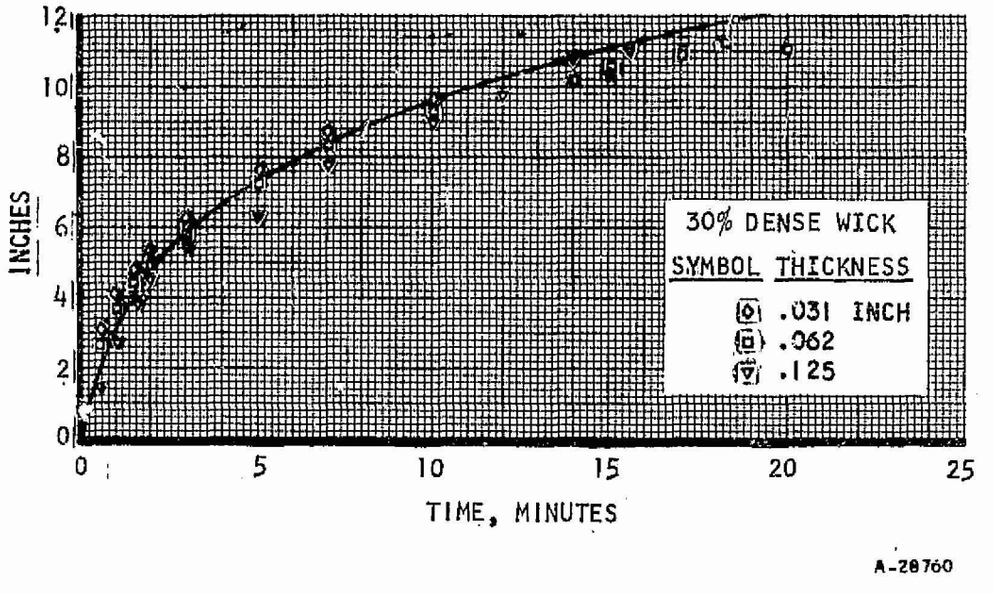

Figure 2-4. Vertical Wicking In One-G

The original test modules were large flat units, the components of which are shown in Figures 2-5 and 2-6. Figure 2-5 shows the electrical heater and the heavy copper plate to which it was attached. Electrical heaters were chosen for simplicity of operation and to provide better heat balances, while the copper plates assured uniform heating and more precise definition of the temperature boundary conditions. Copper-constantan thermocouples were imbedded in the copper plate at six locations at two elevations so that the heater temperature could be recorded as a function of position. The heater was attached to the copper plate with RTV silicon rubber. Figure 2-6 shows the fins and wick, in addition to the heater and copper plate. The fins shown are rectangular offset; however, triangular fins also were tested with this unit.

A photograph of the test setup is shown in Figure 2-7. The wick module was enclosed in a bell jar so that the boiling temperature could be controlled by reducing the pressure. Separate power input was supplied to each heater plate and individual voltmeters, ammeters and variacs were provided. The water from the supply tank was filtered through a 1/2 micron absolute Millipore filter, and metering was provided for extended duration testing. The test section was wrapped with multiple layers of aluminized Mylar to reduce the heat losses.

Two series of boiling tests were performed on this type of unit: one with rectangular fins between the wick and heater plates and the other with triangular fins. Both units were 4.5 in. high by 6 in. wide, contained 15 percent dense nickel fiber wicks, and had the fins brazed to the wicks. The wick in the rectangular finned unit was 0.090 in. thick, and the one in the triangular finned unit was 0.080 in. thick. Tests were performed at saturation temperatures of 40, 50, and 60°F, and heat fluxes as high as 8500 Btu per hr sq ft were reached. Effective boiling coefficients of from 100 to 300 Btu per hr sq ft °F were obtained. It was determined from these tests that variations in the performance between rectangular and triangular fins were slight.

Two problems were encountered with these test units which prompted a redesign of the wick boiler test module. The first of these was a vertical variation in plate temperature (or h). The fairly large temperature differences which existed, caused substantial heat conduction in the vertical direction and were suspected of having a pronounced effect on the performance and the data obtained. The other problem was due to the relatively wide (6 in.) heater plates. For unbrazed modules, it was difficult to obtain good contact between the wick and fins at the middle of the wick due to a tendency of the wide copper plates to bow.

In order to eliminate the problems encountered, a new test module was designed and fabricated. The new module shown in Figures 2-8 and 2-9 incorporated a series of heater plates, each thermally isolated from the next. Triangular fins were machined into the copper heater plates so the need for providing additional heat transport surface was eliminated. The wick specimen was placed between the two rows of heaters which were then clamped tightly to the wick until they slightly deformed the wick surface. Each copper plate had a copper constantan thermocouple inbedded in it and good thermocouple

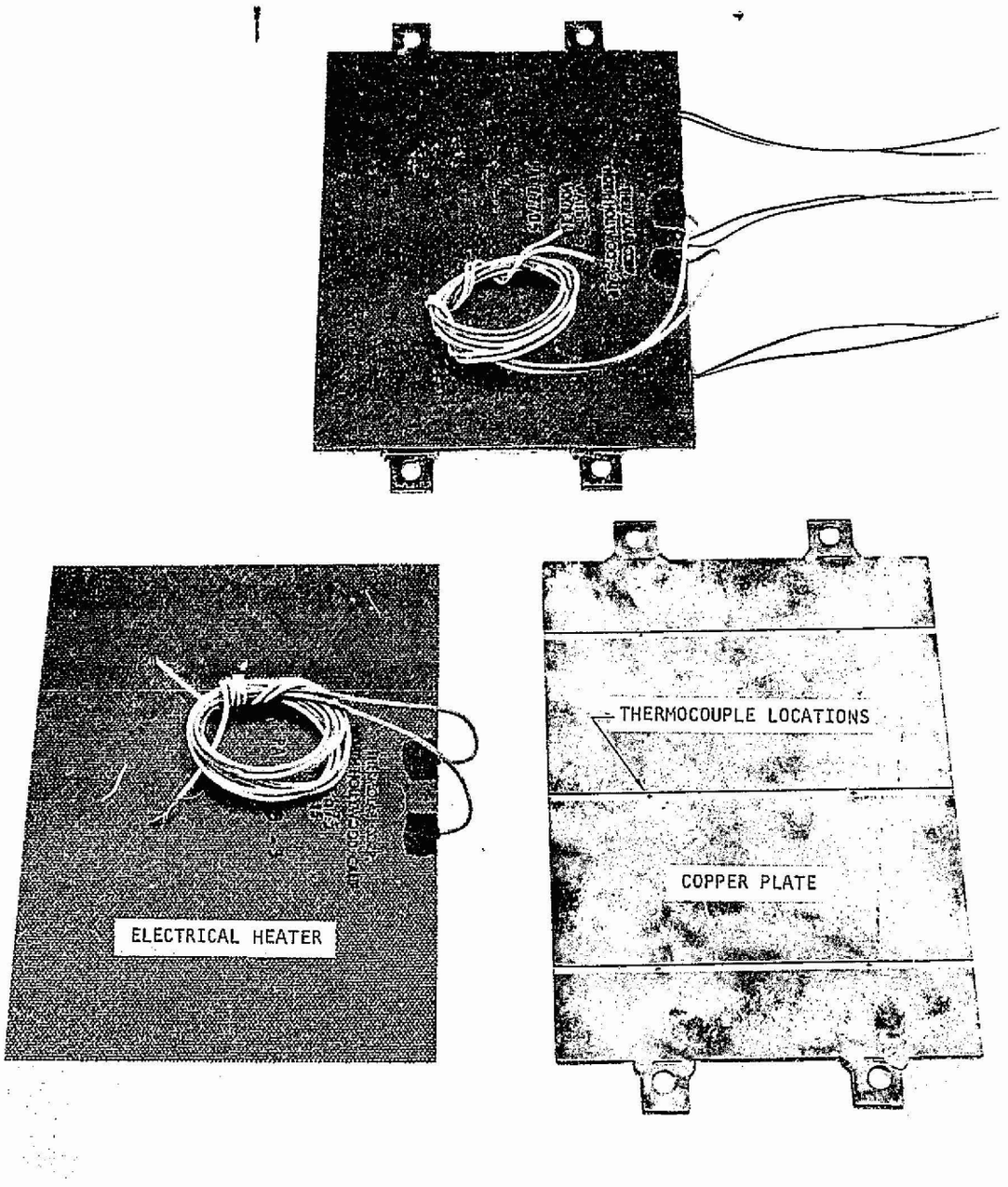

F-5745

Figure 2-5. Wick Performance Test Module Heater Plate

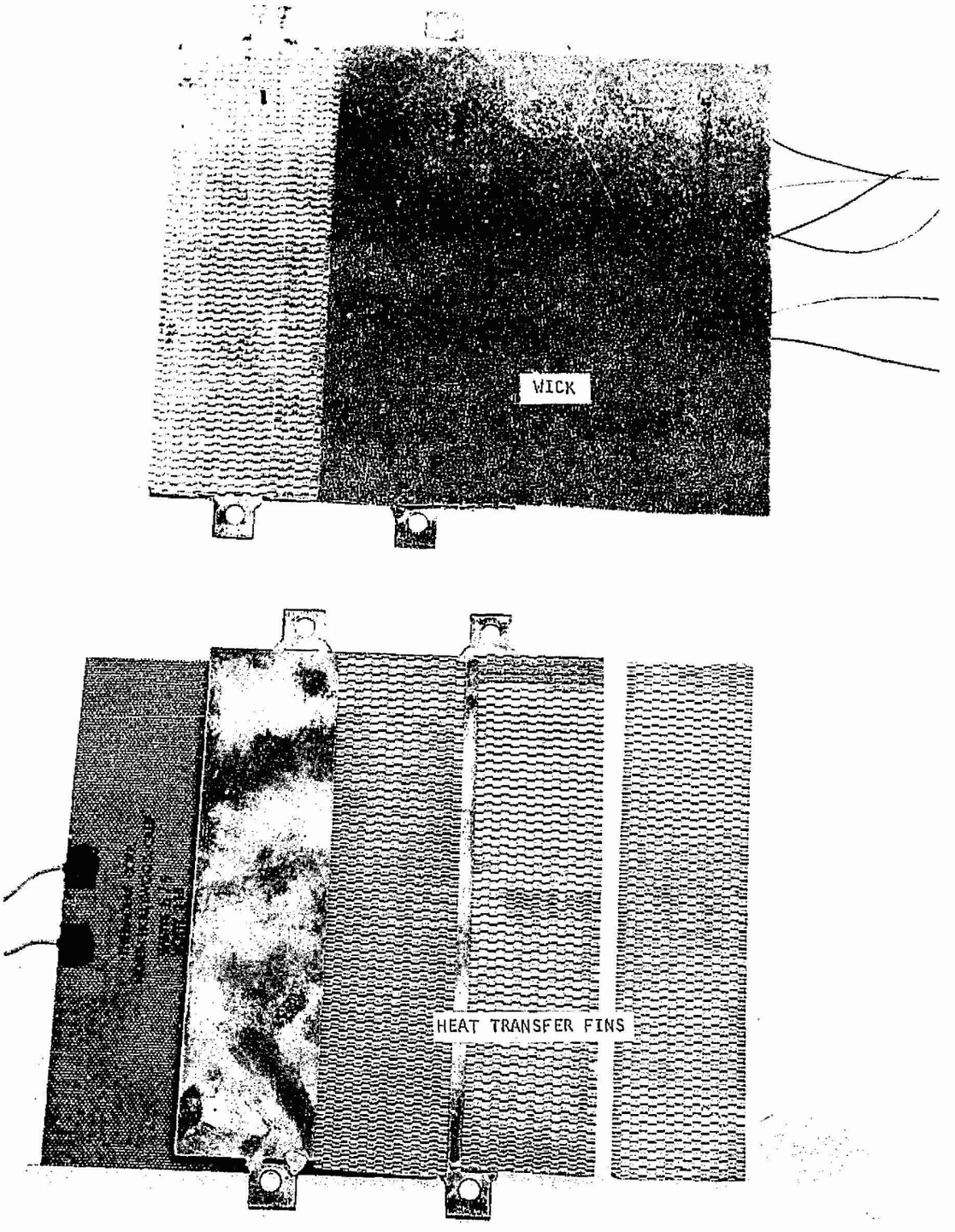

F-5746

Figure 2-6. Wick Performance Test Module Assembly

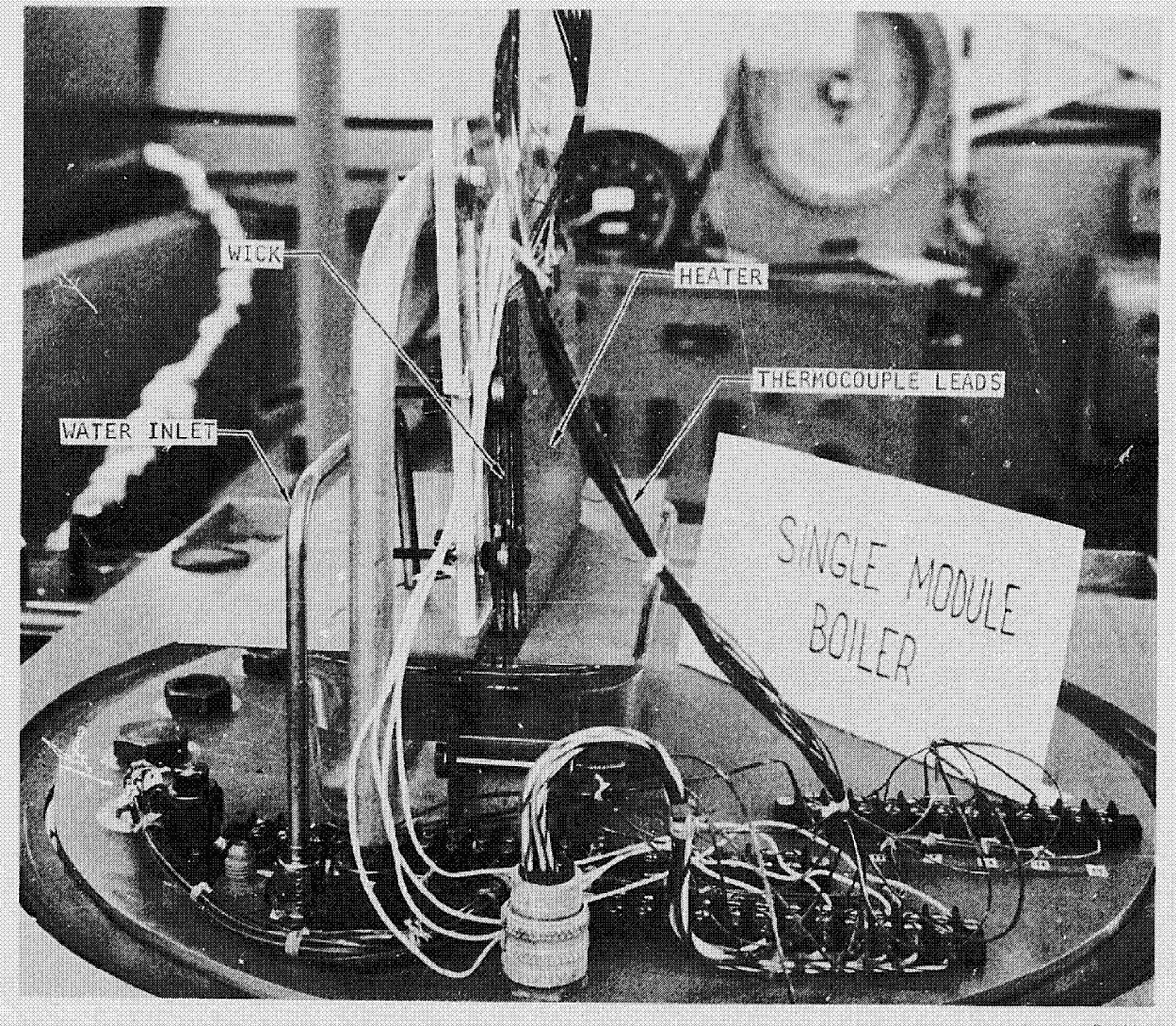

F-6004

Figure 2-7. Single Wick Boiler Module

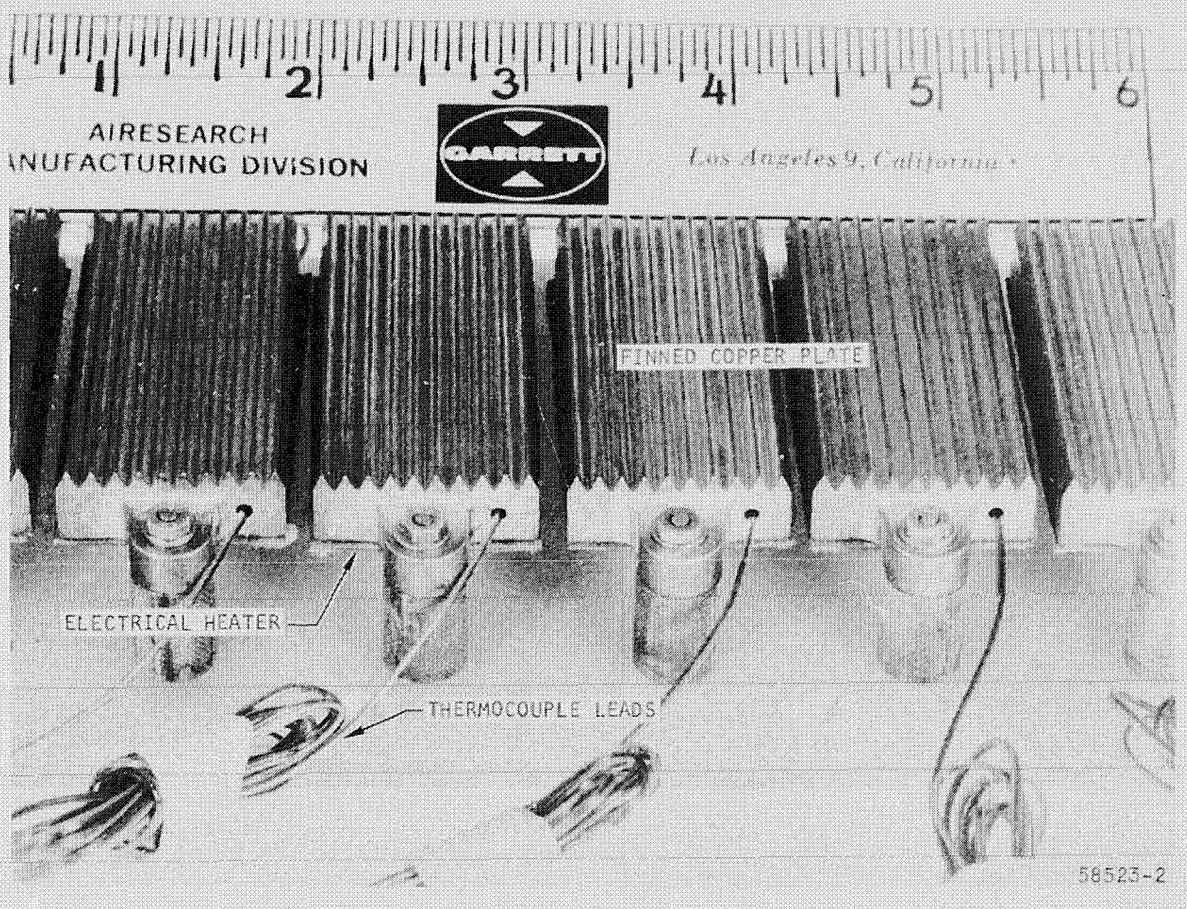

Figure 2-8. Wick Module Heater Plate Assembly

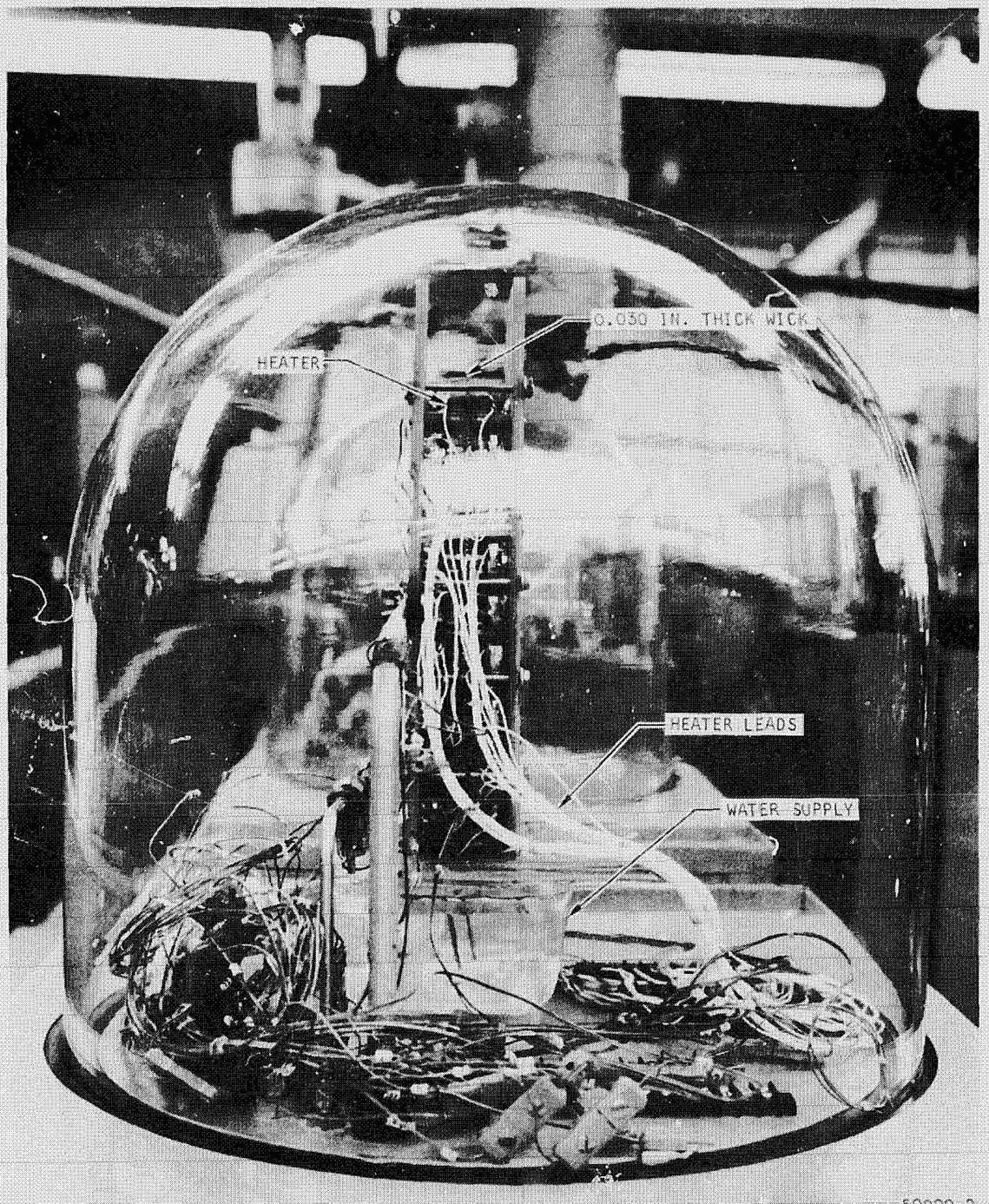

Figure 2-9. Wick Performance Test Apparatus

contact was assured by holding the thermocouple to the plate with a set screw. The three plates at the bottom of the module on each side contained two thermocouples located near the top and bottom of the plate; these were used to verify the prediction of an essentially constant temperature in each plate. Eleven heaters on each side allowed for the testing of wick samples 2 in. wide and up to 12 in. long. The separate heaters eliminated vertical conduction problems and enabled the heat flux to be varied in the vertical direction.

A schematic of the test setup is shown in Figure 2-10. Heat transfer tests were performed on the wicks shown in Table 2-1. Heat flux, heater temperature, saturation pressure, and water reservoir temperature data were obtained at saturation temperatures of 40, 50, and 60°F and heat fluxes to 12,000 Btu per hr sq ft. Effective boiling coefficients were obtained by dividing the heat flux (based upon projected wick area) by the heater to saturation ΔT and the results are shown in Appendix B as film coefficient vs $\Delta T_{\text{heater to saturation}}$. Coefficients are shown also as a function of vertical position.

A summary of the data obtained for wicks approximately 15 percent dense of various thicknesses is shown in Table 2-2. The mean film coefficients at various ΔTs are shown for the three saturation pressures. Some wicks experienced a slight decrease in coefficient with increasing $\Delta T_{\text{heater to saturation}}$ while others had an increase. The data indicate a slight increase in the evaporation coefficient with increasing saturation pressure, at least over the 0.122 psi to 0.256 psi range tested. These same trends were evident for the higher density wicks.

Several significant points other than the magnitude of the coefficient were learned from these tests and are indicated by the data shown. First, there is no consistent or uniform decrease in coefficient with height. A fairly uniform coefficient exists up the wick to a certain level above which it drops rapidly to essentially zero. This level decreases with increasing heat flux as is indicated by the fewer number of data points at large ΔT's and is due to the inability of the wick to deliver water to the higher elevations. There were two wicks which proved to be exceptions to this behavior, the 0.030 in. thick 20.2 and 26.8 dense wicks. These two, as indicated, did exhibit a consistent decrease in h with elevation. The reason for this is not known although it is thought to be due in part to the small thickness of the wicks limiting the water supply. It is noted that this did not occur for the other 0.030 thick wick tested, the 15 percent dense one, however, the lower density wicks are better pumpers which may offset the effect of thinness.

As indicated in Table 2-1, all the wicks tested were nickel except for one copper wick and one refrasil wick. In general, higher effective evaporation coefficients were obtained for the nickel fiber metal wicks than for the copper and refrasil wicks. This is consistent with data obtained during previous programs and for this reason as well as for the fact that through experience it has been learned that nickel wicks are less susceptible to contamination the majority of data were obtained for the nickel fiber wicks.

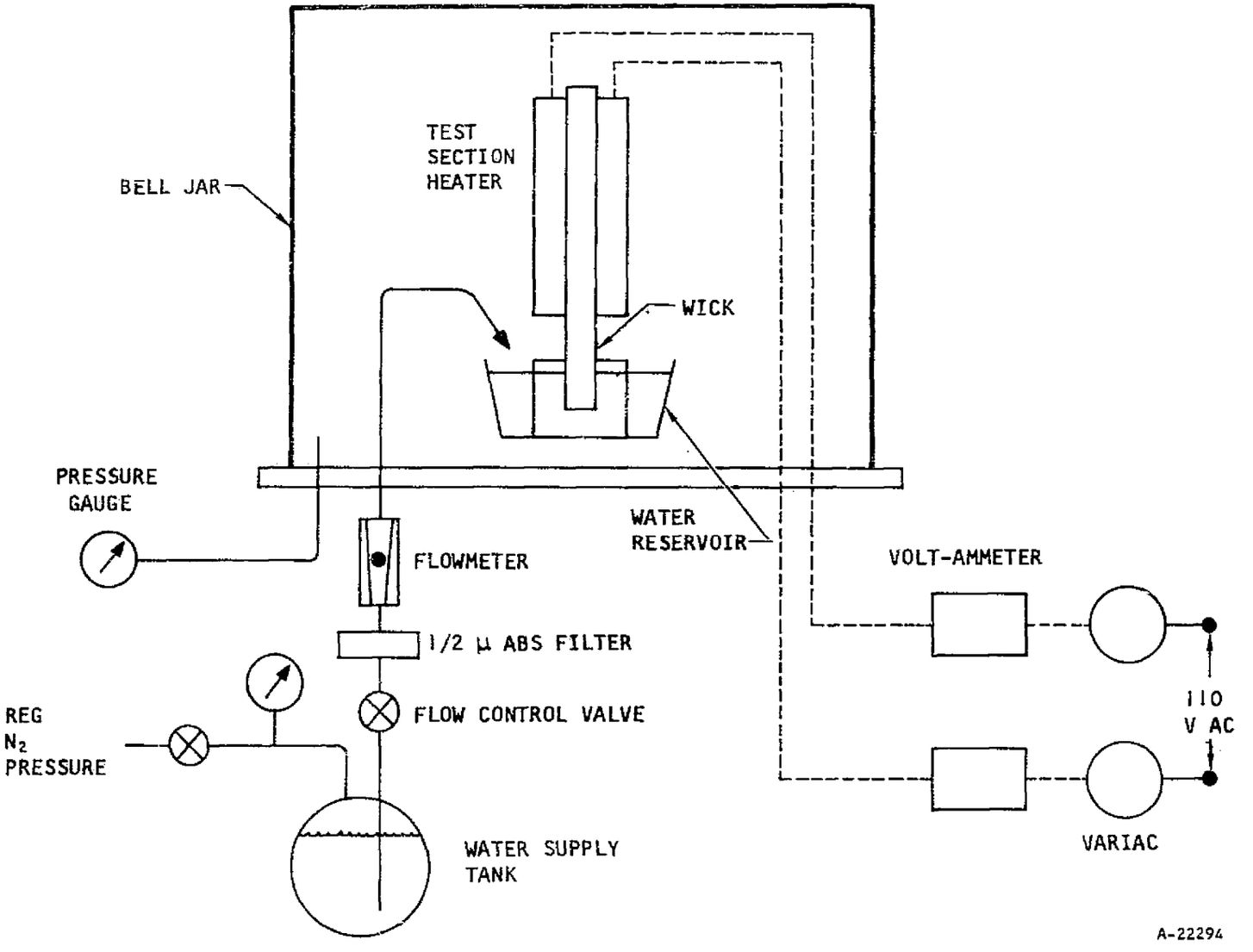

Figure 2-10. Wick Heat Transfer Performance Test Setup

TABLE 2-I

WICKS TESTED IN SINGLE WICK BOILER MODULE

Wick No.	Density, percent	Thickness, in.	Material
1700	13.8	0.028	Nickel
1800	14.6	0.057	Nickel
1100	14.5	0.092	Nickel
900	15.6	0.121	Nickel
1900	15	0.250	Nickel
1400	20.2	0.030	Nickel
1200	17.2	0.062	Nickel
1600	18.7	0.124	Nickel
1500	26.8	0.033	Nickel
1300	25.4	0.061	Nickel
700	28.7	0.250	Nickel
--	20.7	0.100	Refrasil
--	4.0	0.132	Copper

TABLE 2-2

MEAN FILM COEFFICIENTS FOR VARIOUS THICKNESS WICKS OF APPROXIMATELY 15 PERCENT DENSITY AT VARIOUS HEATER TO SATURATION ΔTs

Wick No.	5°F	10°F	15°F	20°F	25°F	30°F	35°F	T_{sat}
1700	350	360	360	340	325	305	285	40
	--	390	410	410	400	400	--	50
	450	480	480	460	430	400	--	60
1800	420	400	390	370	350	330	315	40
	480	480	460	450	430	--	--	50
	370	450	480	470	460	430	--	60
1100	--	195	230	245	250	255	260	40
	--	150	210	240	260	270	280	50
	--	165	220	250	270	280	280	60
900	--	150	180	200	200	210	210	40
	--	130	190	220	240	250	260	50
	--	150	200	225	240	250	260	60
1900	460	440	415	400	380	370	360	40
	410	400	400	400	390	390	390	50
	520	460	430	410	390	380	370	60

No consistent dependence upon either wick thickness or wick density was evident with regards to the magnitude of the coefficient; however, the wick thickness did have a pronounced effect on the elevation to which evaporation occurred as explained below. Some scattering of data is evident, that is, at any heat flux data point, the temperature of the various heaters were not identical which results in different film coefficients. Some of this scatter is due to inaccuracies in data collection, as evidenced by greater scatter at the low ΔT range. The rest is thought to be due to local nonwetting of the wick or possible poor contact between the wicks and the clamped on heaters. For the most part the scatter is within ±20 percent of a line drawn through the middle of the data points.

The wicking and heat dissipation abilities of any wick material interact with each other. For example, in order for a saturated wick to pump more water from a reservoir, some of the liquid in the wick must be removed. The following equation defining the relationship between the maximum heat flux which a wick can maintain and the active wick length for a uniform heat flux boundary condition is developed in Appendix A.

$$L^2 + \frac{D^2 g\rho^2 \lambda\left(A_c/w\right)}{32\, C\mu_\ell (Q/A)} L - \frac{g_o D\sigma \cos\theta\, \rho\, \lambda\left(A_c/w\right)}{8\mu_\ell\, C(Q/A)} = 0 \qquad (2\text{-}6)$$

For a zero gravity environment, the second term becomes zero and L increases. The effect of heat flux on the active wick length for a vertical wick in one g is shown in Figure 2-11 for various thickness 15 percent dense wicks as predicted from equation (2-6). The values of D, θ, and C used for the prediction are the same as those used in the wicking rate predictions. Also shown on the plot are experimental data obtained in the single module tests. The analytical derivation predicts an increased active wick length for lower heat fluxes and thicker wicks. These two trends are expected, for at low heat fluxes, less liquid is evaporated near the bottom and more is available to be pumped higher, and thicker wicks merely represent more free flow area through which liquid may be supplied. Reasonable agreement between the data and predictions was obtained, at least as far as the two trends are concerned. The deviation evident is probably due to a difference in the actual contact angle and that used in equation (2-6) as it is known that this parameter may vary significantly.

Wick Endurance Testing, Wick Contamination, and Surfactants

AiResearch conducted a series of 1000-hr wick performance tests as part of the Apollo glycol evaporator program. The series of tests of specific interest involved 3 in. high by 6.4 in. wide nickel felt metal wicks of 15 percent density, with an average pore size of 0.00165 in. These wicks were heated on both sides with electrical heaters separated from the wicks by offset rectangular fins. Four thermocouples were used to measure the plate temperatures, two adjacent to the top half of the wick, and two adjacent to the bottom half of the wick.

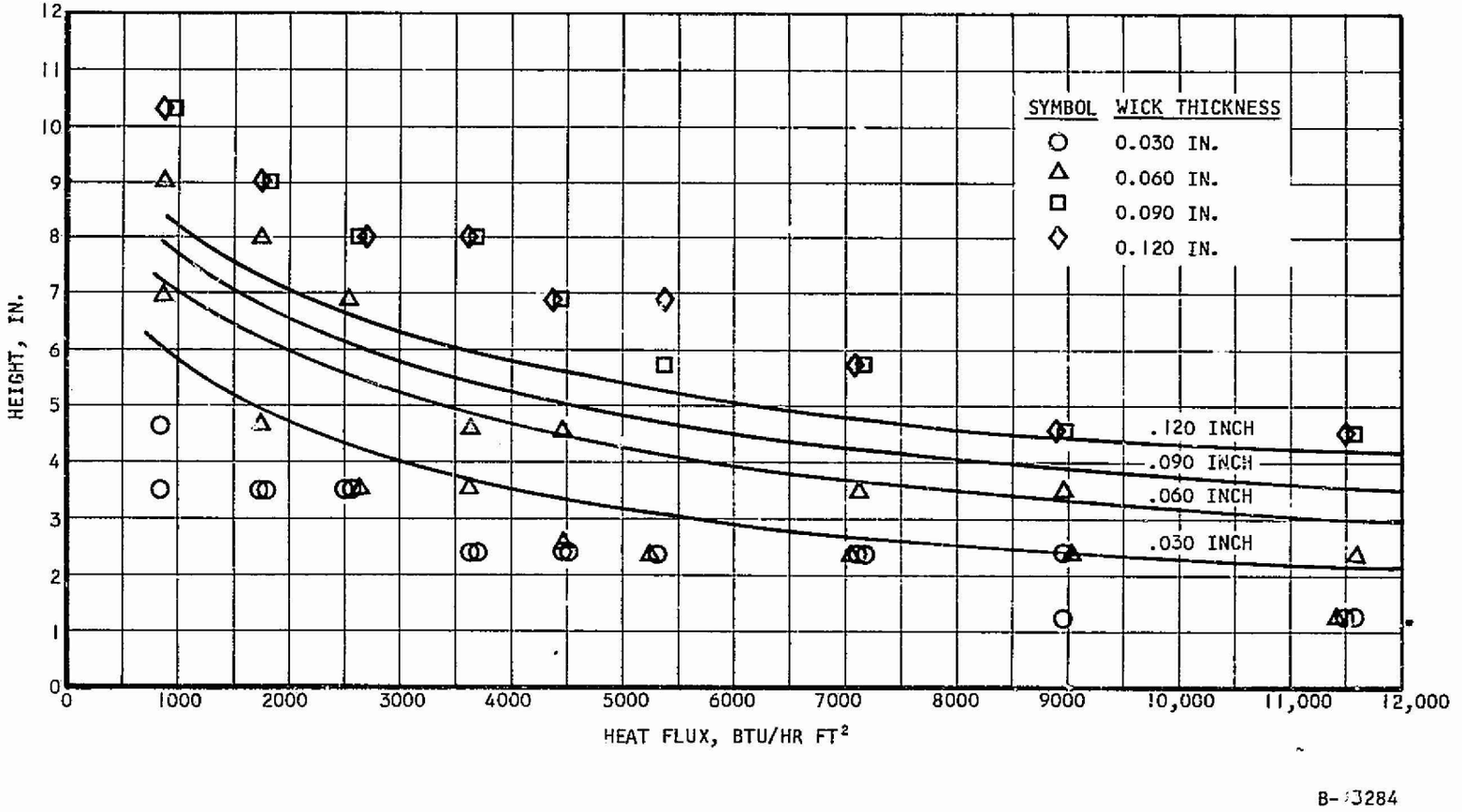

Figure 2-11. Effect of Heat Flux on Active Wick Length in One G

Five different types of tests were run. Two of the wicks were brazed as received, two were oxidized at 800°F in air and one was saturated with a 0.1 percent solution of Sterox NJ, a surface-active agent. To investigate the effect of water filtration some of the samples were fed water that had gone through a 10 micron filter, while the others were fed water that had gone through 1/2 micron filtration. Table 2-3 shows the results. On the basis of performance change, the best performance was obtained with the surfactant-treated wick, which actually increased 19 percent in performance over the 1000-hr test. The best overall performance of the five specimens tested was the brazed-as-received wick with 1/2 micron water filtration, which declined in performance only 5 percent. The [illegible] which were fed 10 micron water had performance degradations of 5[illegible] 36 percent, respectively, while the oxidized wick which had 1/2 micron [illegible] water, had a performance degradation of 23 percent. While the surfactant apparently prevented any degradation and actually led to a significant increase in performance with time, the effect of the surfactant was also to decrease initial performance by a significant amount.

The following conclusions can be drawn from these 1000-hr tests.

a. Water filtration and water purity is of great importance. Water that was filtered through a 1/2 micron filter led to much less degradation of wick performance than water which was filtered through a 10 micron filter.

b. The oxidation of the nickel wicks in air leads to reduction in performance, and does not reduce susceptibility to degradation with time.

c. Treatment of wicks with surfactant may lead to considerable reduction in susceptibility of the wick to performance degradation with time. However, the surfactant may reduce the wicking rate of the wicks significantly. An interesting possibility would be to use wicks which had an initial wicking rate considerably in excess of that required, and treat these with surfactant. Based on the results of the above tests, it might be possible to obtain immunity from performance degradation, without the sacrifice of performance that would be obtained by treating the same wick with a surface active agent.

The importance of maintaining clean and uncontaminated wicks was demonstrated in both the wicking rate and evaporation tests. Initial wicking rate tests yielded inconsistent results until the importance of absolute cleanliness on the wick rate was realized. The same tests, when conducted on properly cleaned wick materials, produced test results consistent within themselves and with predicted values. The problem of wick contamination is further complicated by the results of wicking rate tests performed on evaporation test samples after completion of the boiling tests. The tests showed that in most cases the wicks that had been tested would not wet after they were dried. This indicates that trouble might be encountered in trying to restart an evaporator which has been dried out completely. It should be noted that the wicks were still functioning quite well at the end of the evaporation

tests so that the contaminants did not cause the wicks to fail as long as they remained wet. The contaminants may exist in suspension as long as water remains in the wick, but once the wick is dried, the solids settle on the metal fibers causing a hydrophobic effect. This is consistent with other test results that show wicks that would not wet by capillary forces, would perform satisfactory in an evaporator when forcibly wet.

One of the nonwetting wicks obtained in the boiling tests was submitted for a chemical analysis in an attempt to identify the cause of contamination. The results of this analysis listed an unidentifiable amide compound and a small quantity of a low molecular weight methyl silicone polymer. The silicone base was traced to the adhesive compound used to bond the electrical heaters to the copper bars used in the test setup. To eliminate the silicone as a source of contamination the heaters were baked at temperatures 100°F above the test temperatures to drive off any of the silicone compound which remained. Subsequent testing showed that the test samples would not wet in those areas where evaporation had taken place. A sample of the test water was then submitted for chemical analysis and the amide found on the wick sample was once again discovered in the water. The quantity of amide present in the water was not, however, sufficient to permit its identification.

As a portion of the Apollo glycol evaporator program, a series of tests were conducted to establish a standard cleaning procedure for wicks known to contain contamination. Wick samples were prepared by measuring the initial wick rate and then applying known sources of contamination. After contaminant application none of the wicks would wet. Of the many cleaning techniques tried, the most successful was a high temperature soak under vacuum conditions. Samples were run at 5×10^{-5} torr and 500°F, 600°F, 700°F, 800°F, and 900°F. The samples run at 900°F and 5×10^{-5} torr produced wick rates after cleaning equal to the initial values recorded and this 900°F vacuum cycle has been adopted as the standard cleaning procedure for fiber metal wicks.

Although no specific tests were performed during this program on surface activating or wick wetting agents, investigations conducted on other programs have indicated that such compounds can prevent a surface from becoming nonwetting. Some of the solution treatments tested at AiResearch include: Ethylene diaminete acetic acid in combination with Aerosol MA and Aerosol OT applied by dipping dry wicks in the respective solutions and then drying them at 212°F overnight; Aerosol OT and Aerosol 18 applied by themselves with the same technique as above; and Sterox NJ solution also applied by dipping. In general, most of the surfactants tried tended to reduce the surface tension force of the water to such an extent as to reduce the wicking rate to as little as 1/10 of the original rate. In some cases, although noticeably reduced, the wick rates did remain high enough to allow the use of surface treated wicks in an evaporator. The use of wetting agents to overcome contamination problems is a subject which will be pursued in the follow-on effort of this program.

TABLE 2-3

1000 HR ENDURANCE TEST RESULTS
15 PERCENT DENSE NICKEL FELTMETAL WICKS

Wick Description	Location Number	$h_{initial}$ Btu per hr sq ft ^{0}F	h_{final} Btu per hr sq ft ^{0}F	$\frac{h_{final}}{h_{initial}}$	Average Performance Change percent
Brazed as received 10 micron water filtration	Top 1	176	106	0.60	-51
	Top 2	240	66	0.28	
	Bottom 1	156	91	0.58	
	Bottom 2	139	71	0.51	
Brazed as received 1/2 micron water filtration	Top 1	203	240	1.18	-5
	Top 2	240	220	0.92	
	Bottom 1	120	106	0.88	
	Bottom 2	132	106	0.80	
Brazed after heating in air, 800^{0}F, 30 min 10 micron water filtration	Top 1	83	61	0.75	-36
	Top 2	91	45	0.49	
	Bottom 1	102	66	0.65	
	Bottom 2	102	66	0.65	
Brazed after heating in air, 800^{0}F, 30 min 1/2 micron water filtration	Top 1	106	80	0.76	-23
	Top 2	132	132	1.00	
	Bottom 1	91	64	0.71	
	Bottom 2	115	71	0.62	
Brazed as received saturated in 0.1 percent solution of Sterox NJ. 1/2 micron water filtration	Top 1	61	126	2.04	+19
	Top 2	115	132	1.15	
	Bottom 1	115	78	0.68	
	Bottom 2	115	102	0.88	

WATER BOILER DESIGN CONSIDERATIONS

Boiler Water Flow Distribution

A large amount at work has been done at AiResearch on techniques for feed water distribution to a wick fed water boiler. The primary goal in these studies has been the development of a system which would provide equal quantities of water to all portions of a wick boiler independent of the orientation of gravity. The best of the systems is a distribution plate-cellulose sponge-wick system developed for use on the Apollo Glycol Evaporator and applied to the 1 kw module water boiler built during this program.

The most important features of the glycol evaporator are shown in Figure 2-12. Water is pressure-fed into the boiler after passing through a filter and a solenoid valve. There are nine groups of distribution plates composed of stacks of six plates each, with each plate containing five holes, 0.0045-in. in diameter. The high flow restriction in the distribution plate is required for two reasons: (1) to make the pressure drop across the distribution plate great enough to minimize the effect of gas evolution (upstream of the boiler) on flow distribution, and (2) to make the head of water (when the boiler is tested on its side and end) small compared with the pressure drop across the plate, so that gravity has a negligible effect on boiler performance during ground tests in various attitudes.

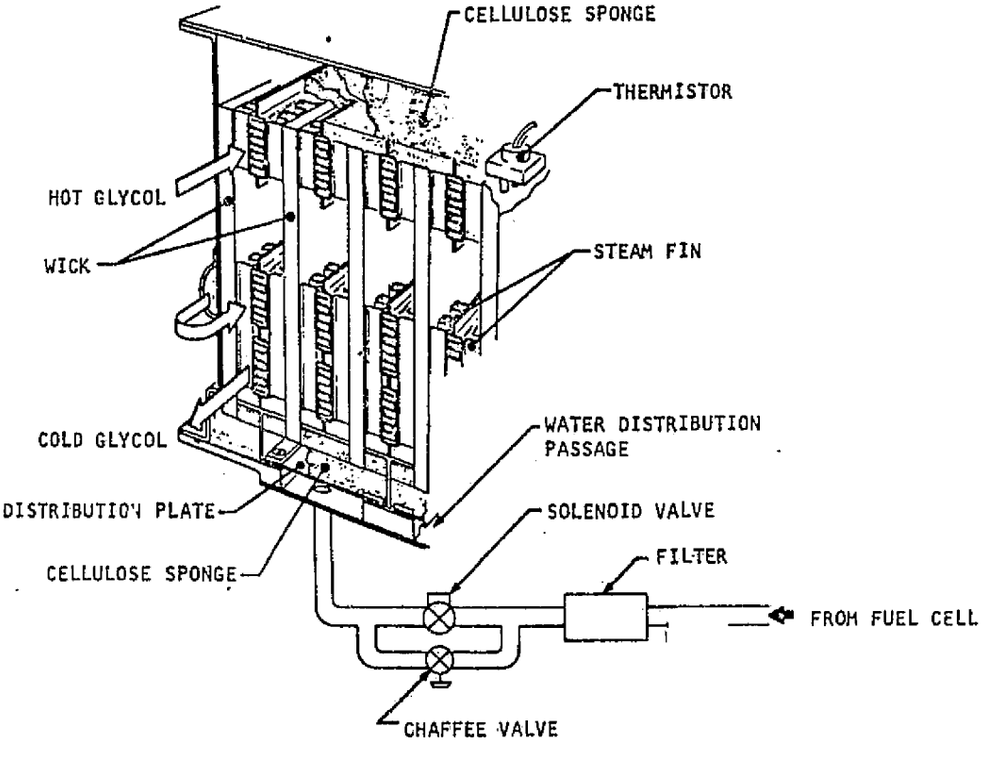

Figure 2-12. Glycol Evaporator

After the water passes through the distribution plate, it impinges upon a cellulose sponge that is in contact with 21 feltmental wicks, five of which are shown in the figure. The wicks pull water from the sponge as a result of capillary action; the water flow from the sponge to the wicks continues until the wicks are saturated. The glycol flow passages are attached to the wicks by nickel steam fins as shown. Heat is transferred, by conduction across the fins, from the hot glycol to the surface of the wicks where water is evaporated. When evaporation occurs, water is continually drawn from the sponge near the distribution plate and fed to the surface of the wicks by capillary forces. The steam that is generated flows in the steam-fin passages to the center section of the core, where it makes a 90-deg turn and flows out the end of the evaporator. The steam exhaust section is in the interior of the evaporator; this enables performance requiements to be met with the evaporator both in the launch attitude, as shown in the figure, and upside down. To improve performance when the unit is in the inverted position, a cellulose sponge is placed on the top edges of the wicks to redistribute water from the wetter wicks to the dryer ones.

The simplified schematic of the qualification test boiler subsystem presented in Figure 2-13 shows the way in which the distribution plates, located in the sump pan, and the sponges are segmented to make it possible for the boiler to meet performance requirements when turned on its end or

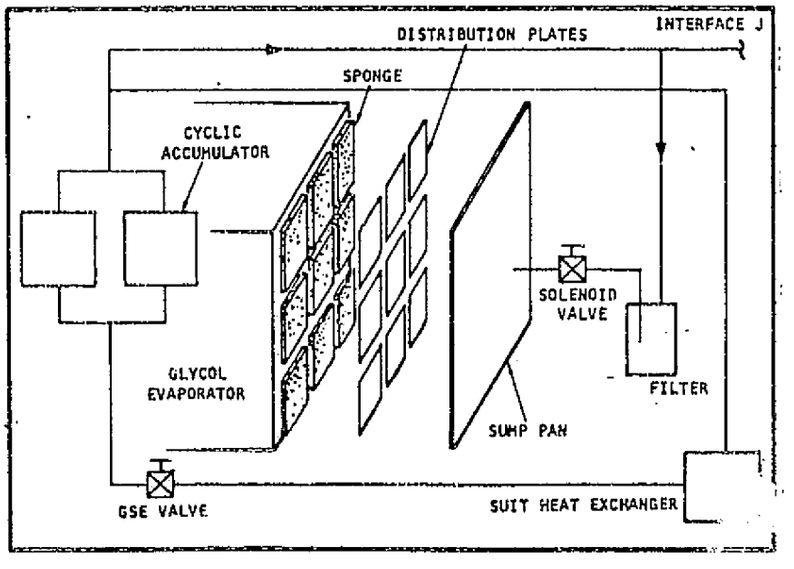

Figure 2-13. Qualification Test Boiler Subsystem

side in a 1-g environment. Nine separate distribution plates and sponges that independently feed the required quantity of water to each segment of the boiler are used. If this were not done, when the boiler was operating on its side, as shown, in a 1-g environment, the pressure difference across the distribution plate at the bottom of the boiler would be greater than that at the top, because of the head of water in the sump pan. A disproportionately high flow of water, therefore, would be forced into the bottom of the boiler, while the top would be deficient in water. This system has been successfully qualified for the Apollo boiler and proved quite satisfactory on the 1 kw boiler tests.

Water Flow Control Systems

Several concepts have been proposed for the supply of water to a wick type evaporator, and each system has its own advantages and disadvantages when examined in light of a particular problem statement. The actual performance of most of the proposed concepts has been evaluated at AiResearch in connection with evaporators built to satisfy a variety of design requirements. The following paragraphs discuss each concept, explaining its operation and particular characteristics.

1. Wick Temperature Sensor

This system controls the flow of water to wicks in an evaporator core in an on-off manner as a function of wick temperature. In a wick evaporator, when the wicks are wet, the temperature of the wicks remains close to the water saturation temperature. As the wicks become dry however, the heat conducted from the hot side fluid through the steam fins raises the wick temperature to a level near that of the hot fluid. The water flow control system is based on this characteristic. A thermistor is located in selected wicks, generally in that portion of the wick most remote from the source of supply water. As long as the thermistor senses a temperature close to the water saturation temperature, adequate water is available within the boiler and the accompanying water solenoid valve remains closed. Whenever the thermistor senses a temperature approaching the hot side fluid temperature, the water solenoid valve is opened and water flows from a pressurized source to the evaporator where the distribution system divides the water among the evaporator wicks. Thus, the water flow is controlled so that sufficient water to meet the heat load is always in the evaporator, but boiler flooding and water carry-over are prevented, because no more water is fed into the boiler than can be contained in the wicks and boiler sponges.

This type of system provides a very effective control of water flow, in that while the temperature sensed by the thermistor may vary a few degrees, the hot fluid outlet temperature will vary only slightly. This is possible because the thermistor located remote to the water source may sense a dry wick, but the remaining wicks can contain enough water to provide cooling until a fresh water supply can be introduced by the opening at the solenoid valve. The almost instantaneous reaction of the solenoid upon signal makes a variation of $\pm 2^{\circ}F$ possible with this system. The disadvantage of this technique lies in its complexity as compared to other candidate concepts. The output signal of the thermistor requires amplification to actuate the solenoid and the power

requirements involved, while limited and intermittent, do represent a dependence of the water control on the rest of the system. However, where electrical power is available, the wick temperature does provide a close reliable control as demonstrated by its use on the Apollo glycol evaporator.

2. Outlet Temperature Sensor

Control of supply water with this technique is a function of the heat transport fluid temperature level as the fluid leaves the evaporator. This temperature can be sensed by a wax type vernatherm element or an electrical signal, with the Vernatherm element being the simplest in operation and the electrical signal providing the most rapid response to a change in outlet temperature. In either case, the control principle is the same, that is, when the evaporator wicks begin to dry, less water is available for cooling and the heat transport loop temperature begins to rise. At this increase in fluid outlet temperature, the water control valve opens, permitting water to flow from a pressurized source to the evaporator. The valve remains in the open position until the heat transport outlet temperature drops to the normal operating level. This drop in temperature corresponds to a sufficient water supply in the wicks to meet the heat load.

The disadvantage of this technique, when compared to a wick wetness sensor, is that the valve actuating characteristic is a secondary one. The relative dryness of the evaporator wicks is sensed by the result of that dryness or a change in heat rejection and not directly at the wicks themselves. The advantage of the concept is derived from the use of a Vernatherm element to sense fluid outlet temperature. The Vernatherm element provides an actuating force by the melting of a wax mixture and can be coupled to a simple valve mechanism, thus eliminating the relative complexity and the power requirements of an electrical system.

3. Constant Water Flow

This concept is the simplest of all those considered. It involves merely turning on a constant pressure supply of water to the evaporator at the same instant that the evaporator itself is activated or at a command signal when the need for cooling arises. Its application is, however, limited to the circumstance where the evaporator heat rejection is constant. In this case, the water flow could be metered such that only enough water to meet the heat load would be allowed to enter the wicks. In a system where a fluctuation in heat load is expected, the use of this system would permit, at low heat loads, an excess of water to enter the evaporator under pressure, resulting in boiler flooding and water carryover.

A slight modification to this concept has been employed on the PECS (Portable Environmental Control System) evaporator. This unit consists of an evaporator mounted atop a wick lined water reservoir, with a wick circuit between evaporator and reservoir continually open. As the evaporator wicks begin to dry an imbalance in surface tension forces between the water in the evaporator wicks and the reservoir water draws water through the wick matrix to the boiler core. The difficulty encountered with this wick reservoir concept occurs when, on startup, a sudden decompression of the evaporator steam

plenum causes an initial water carryover which continues until the system pressure level has been equalized. This drawback can be overcome if it is possible to reduce the pressure level slowly and use chilled water in the reservoir.

4. Inlet Temperature Sensor

Control of water flow with this technique is based on a change in evaporator inlet temperature and the constant heat rejection capability of the evaporator. The actual flow control is accomplished with a modulating valve which converts a change in the amount of water allowed to enter the evaporator wicks. The modulating function creates the chief disadvantage of this system, in that it requires a perfect correspondence between the system heat load - temperature relationship and the temperature - water flow characteristic. If, for example, the system flow rate is not constant with time a change in the inlet temperature could represent any number of heat rejections and required feed water flow rates. The net result for the evaporator would be too much or too little supply water, depending on whether the heat transport flow were lower or higher than that for which the valve was calibrated. For a system where the heat transport fluid flow is constant, the modulating valve calibration would have to be exact, because a slight discrepancy between the actual water flow and the required amount of water could result in flooding of the boiler or a drying of the wicks.

Evaporator Temperature Control

In a typical system where a wick type evaporator is used to provide cooling, there exists both a maximum and minimum desired heat transport fluid temperature. As the temperature of the heat transport liquid entering the evaporator is determined by addition of heat from external sources, the system temperature can be regulated only by varying evaporator heat rejection. The most common technique for regulating the amount of cooling obtained is by backpressurizing the evaporator steam plenum. Varying the steam plenum pressure provides a strong and direct effect on the temperature difference between heat transport fluid and evaporator water temperature. This is accomplished by altering the water saturation temperature and results in a direct control of the heat rejection capacity of the evaporator. Proper design of this type of system will allow the boiler to operate between 0 and 100 percent of the maximum heat load.

Two methods of effective backpressure control are available. The first method, which maintains a constant sink temperature, utilizes a pressure transducer placed in the evaporator steam plenum. The output signal from the transducer is converted to an opening or closing of an electrical backpressure valve. An increase in the heat transport fluid inlet temperature causes an increase in the amount of water evaporated and a rise in the steam plenum pressure. The backpressure valve reacts by opening and reducing the plenum pressure to a level which will provide sufficient heat rejection to maintain a constant heat transport fluid outlet temperature. Backpressure by this technique requires a constant heat transport fluid flow rate, and electrical signal amplification, and depends on the availability of a power source.

The second alternative for backpressure control utilizes a temperature sensitive element to monitor fluid outlet temperature and regulates the sink pressure as a function of this temperature. A change of the total heat rejection of the evaporator is therefore achieved by varing the driving force temperature difference between the heat transport fluid and evaporator water. Typically this valve is driven by a Venatherm element sensing the fluid outlet temperature and supplying, with a change in temperature, a change in the position of the backpressure poppet. The valve is designed to operate between two limits in heat transport fluid outlet temperature, with the backpressure poppet sized to allow a steam free flow area which will produce the desired steam side pressure drop at the maximum heat load condition, and a Vernatherm piston travel that will insure a closed poppet at the zero heat load condition. This type of valve has been used successfully on the Gemini evaporator, PECS evaporator and 1 kw module water boiler built for this program. The concept offers the advantages of simplicity of design, no external power requirements and a direct sensing of the evaporator outlet temperature. The resulting control band ($\pm 3^{0}$F for heat transport fluid temperature) is, however, not as narrow as that which can be achieved with an electrical system.

Another suggested technique for control of the system temperature is the use of a bypass valve sensing evaporator outlet temperature and regulating the percentage of fluid traveling to the boiler core. This technique can be used only in conjunction with backpressure valve, which will close completely where the steam plenum pressure falls below the water triple point pressure. A bypass valve and on-off backpressure valve combination can be effectively used where a limited power supply is on hand to energize a solenoid type steam plenum shutoff valve.

Module Geometry

Design of a boiler module core involves selection of the specific wick and fin, wick-fin arrangement, core dimensions, steam duct location, and flow configuration. While some of these parameters may be selected independently, others, such as wick selection and core dimensions are directly related and must be considered together.

1. Wick-Fin Configuration

The geometry used exclusively in current wick evaporators is the heated surface-fin-wick configuration shown in the sketch, in which heat is conducted through fins in the steam passage to the wick. Another geometry which has been suggested and subjected to limited testing is the heated surface-wick-fin geometry in which the wick is in direct contact with the heat input surface as shown in the sketch on the following page.

The reason that the former geometry has been used exclusively is the desire to avoid vapor formation in the wick at a location where the vapor cannot escape, namely at the wall. If vapor is formed in a heated surface-wick-fin geometry, it will likely occur as bubble nucleation at the wick-wall interface, the hottest location. Analysis has shown that in this case the surface tension forces dominate and buoyancy forces are insignificant. Vapor formed at the wall will remain there and form an insulating blanket, decreasing

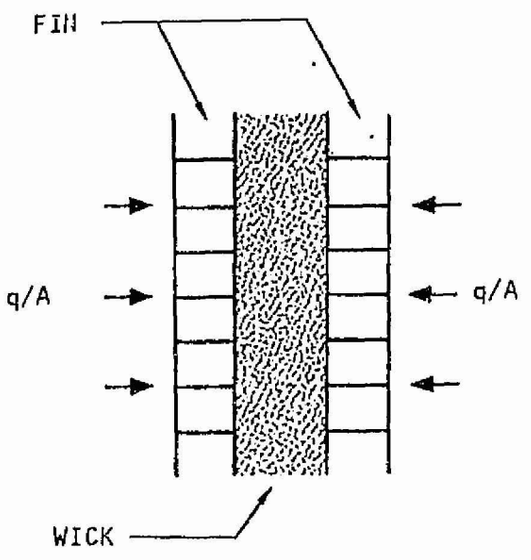

HEATED SURFACE-FIN-WICK

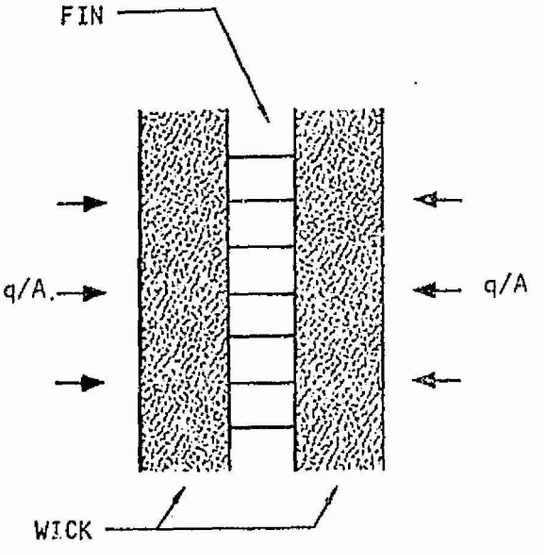

HEATED SURFACE-WICK-FIN

the heat transfer capability significantly. Only if the wick is thin enough, will nucleating bubbles grow to sufficient size to reach the surface and be forced out by surface tension drawing the liquid around them before a continuous vapor blanket is formed.

If nucleation does not occur within the wick in this configuration, the heat transfer mechanisms are conduction across the wick-water matrix and evaporation at the surface of the wick. In this case, unless the wick is extremely thin, conduction is the controlling mechanism and the major temperature drop occurs in conduction across the wick.

The desire to avoid the performance degrading phenomenon of nucleation within the wick and the uncertainty as to the method of predicting analytically the criteria for nucleation, along with the realization that if phase change occurred as evaporation at the wick surface, a sizeable temperature gradient would exist in the wick, has resulted in the use of a fin between the heat source and the wick.

Recent investigations of heat pipes and phenomena associated with their operation have indicated that analytical predictions of the conditions which must exist for nucleation to occur in the wick may be made by applying the

same criteria as those which apply to nucleate boiling. In that case, according to Tong[5] a bubble nucleus will grow when the liquid surrounding it is superheated by an amount:

$$\Delta T_{sup} \geq \frac{2 \sigma T_{sat}}{\lambda r_n \rho_v J} \tag{2-7}$$

The local temperature required for nucleation to occur is:

$$T_o = T_{sat} \left(1 + \frac{2 \sigma}{\lambda r_n \rho_v J} \right) \tag{2-8}$$

In the capillary structure r_n cannot exceed r/cos θ where r is the pore radius and θ the contact angle. Thus as long as:

$$T_o < T_{sat} \left(1 + \frac{2 \sigma \cos \theta}{r \lambda \rho_v J} \right) \tag{2-9}$$

the bubbles cannot grow beyond this critical size and nucleate boiling will not occur. It is therefore possible to predict the occurrence of nucleation in a wick and design accordingly. Thus the heated surface-wick-fin geometry is an acceptable configuration which should be considered in wick evaporator design.

Selection of the wick-fin configuration cannot be made independent of other system parameters such as core dimensions and wick selection and is discussed below with these items.

2. Fin and Wick Selection

In selecting the components for the evaporation side of a wick boiler, the following concepts are relevant. First it is desirable to minimize heat transfer resistances in the core in order that the size and weight of the unit may be minimized. Sufficient capillary material should be provided so that adequate water is supplied to all areas of the unit. Pressure drops should be minimized so that maximum ΔTs are available for heat transfer.

If the configuration is heated surface-fin-wick, wick thickness is related to the heat flux and the height of the unit as described by Equation (2-6). The larger the heat flux and/or the dimension perpendicular to the plane of water supply, the thicker the wick must be. Since all the heat is conducted across the steam passage, the fins must be sized so as to minimize the heat transfer resistance. This means short, thick, high conductivity fins are desirable. Sufficiently high heat transfer conductances are generally obtained using high fin-density surfaces typical of those utilized in state-of-the-art aerospace heat exchangers; the major temperature drop is still associated with phase change at the wick. Care must be exercised so that such restrictive configurations that would give large pressure drops are not used.

If the configuration is heated surface-wick-fin, wick thickness is related not only to the height and heat flux but also to the degree of superheat allowable before nucleation. Whereas for the previous configuration it is possible to select a wick thickness which will satisfy a given heat flux and wick height (provided the height is not greater than the veritical equilibrium height for operation on the ground), it is not necessarily possible to do this for the heated surface-wick-fin configuration. This is due to the inverse dependence of the heat flux on the wick thickness because of the controlling conduction mechanism as described by:

$$q/A = \frac{k_w}{X} \Delta T \qquad (2\text{-}10)$$

where k_w = the effective thermal conductivity of the wick-water matrix

X = wick thickness

ΔT = the temperature difference between the two surfaces of the wick

Again Equation (2-6)(modified for one sided heating) applies, and an increase in heat flux for a given wick length requires a corresponding increase in wick thickness (A_c) to sustain operation. From (2-10) which also applies, an increase in heat flux requires a decrease in thickness. Compatibility of Equations (2-6) and (2-10) is necessary in designing a unit of this configuration. The fin which appears between the wicks in this configuration is there only for structural purposes and therefore can be a "looser" surface (i.e., fewer fins per inch and higher) than is required for the conventional design. This may in some cases prove to be significantly advantageous from a pressure drop standpoint, as a less restrictive fin causes less friction ΔP.

In general, if the configuration is heated surface-fin-wick, the lowest density wick should be chosen because, since it has the largest pores it will be the best pumper and because it is least dense, it will be lighter. This is of course based upon the assumption that the height of the unit (for operation in one g) is sufficiently less than the equilibrium wicking height. The least dense wick is not necessarily the best wick for the heated surface-wick-fin geometry because as the density decreases, the thermal conductivity of the wick-water matrix decreases, increasing the thermal resistance. Since conduction across the wick-water matrix is a significant heat transfer mechanism for this configuration, an increased resistance will give worse performance. A trade-off must be made therefore between the heat transfer process (large density desirable) and the water transport process (small density desirable).

3. Flow Configuration

On the heat transport fluid side of the wick boiler, the heat transfer coefficient is generally much higher than the evaporant coefficient and is predicted based upon well established equations. Since the evaporant side is the controlling side of the heat exchanger, selection of fins for the transport fluid side is not so critical. Again high fin density state-of-the-art finned surfaces are quite adequate to assure sufficient conductance on the hot side to make the cold side controlling.

It is well understood that in an evaporator or a condenser, the flow configuration has no effect on the heat transfer performance. This is true of course only if one side of the unit operates isothermally, which in the case of a wick evaporator means that the friction pressure drop should be small enough as not to change the saturation temperature significantly. From this standpoint the flow configuration could be counterflow, or crossflow with any number of passes and the same performance would be obtained. There are however some noteworthy reasons for choosing a specific configuration, reasons which are directly related to the overall performance of the unit and manufacturing considerations. Possible flow configurations are shown in Figure 2-14. The first configuration (A) is the simplest one; the glycol makes one pass through the unit and the water enters at one face as liquid and leaves at the opposite face as steam. In configuration, (B) the glycol makes two passes through the unit. The water inlet face may be adjacent to either the glycol inlet pass or outlet pass with the steam outlet on the opposite face. Configuration (C) is another two-pass unit, however this unit has the steam outlet duct in the middle of the core. Again the water inlet may be adjacent to either the glycol outlet or the inlet. Configuration (D) goes one step further in that it incorporates water feed through two faces of the unit.

The differences between configurations (A) and (B) are slight. The glycol passage free flow areas and the flow lengths differ by factors of two, however little advantage is realized with the higher mass flow rate of (B) since the flow rates in conventional units are so low that flow is in the laminar regime and only small increases in the heat transfer coefficient are realized. Since the evaporant side is controlling, small increases in h on the glycol side are insignificant. Also, the longer flow length results in a higher glycol pressure drop. Some advantage in control may be possible with configuration (B) since the water inlet may be adjacent to the hot or cold glycol pass.

Configuration (C) places the steam plenum at the middle of the unit. Two advantages are realized with this configuration. First, with the steam exhaust duct at the center of the core the vapor flow length in the steam fin is reduced in half. This reduces the vapor ΔP and provides a uniformly lower saturation temperature. Also a sponge redistribution pad may be provided at the face opposite the water inlet for liquid redistribution whereas in (A) and (B) this is not possible and water may drip from the end of the wick into the exhaust duct under certain conditions.

The last configuration is similar to (C) but in addition to cutting the steam flow length of (A) and (B) in half, the wicking length is reduced by a factor of two. This is accomplished by feeding liquid from two faces. Reducing the wicking length allows for the use of thinner and lighter wicks, and provides for more rapid distribution of water to all areas of the unit when additional liquid feed is required. Configuration (D) represents the optimum design.

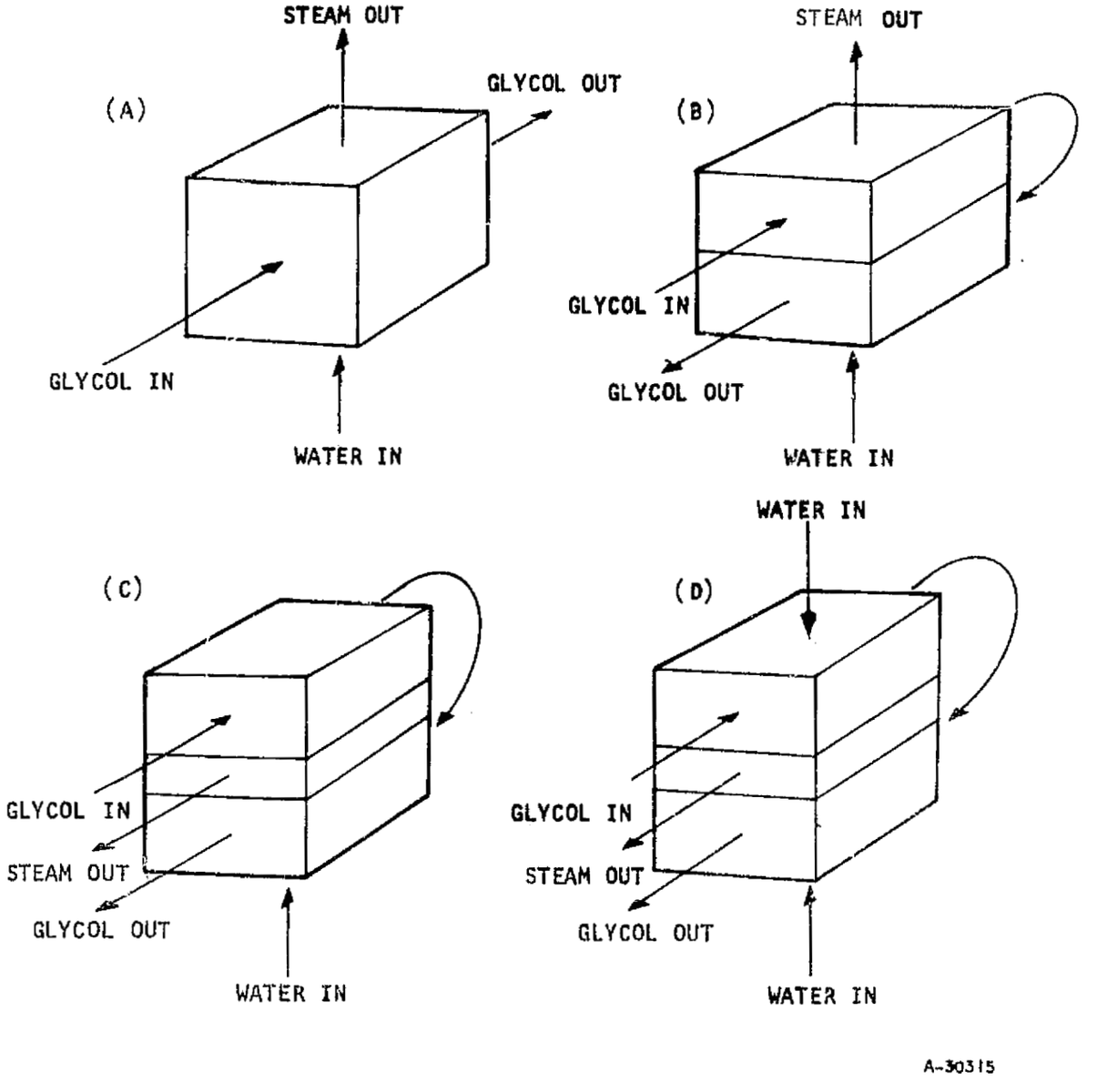

Figure 2-14. Water Boiler Flow Configuration

ONE KW BOILER MODULE

General

In order to obtain performance data from a complete wick evaporator unit and to evaluate experimentally the new control valve, a one kilowatt wick boiler and control system was designed, built, and tested. Since in order to allow sufficient time for fabrication and testing it was necessary to begin design of this unit while the wicking investigation and the design studies were in progress, this unit is not necessarily an optimum design. However, wick selection and unit configuration were based upon what appeared to be the best choices at the time of design. An optimum design was not essential since the unit constructed was for test purposes.

Boiler Design

1. Evaporator

Since the primary objectives of the one kilowatt test module were to verify analytical procedures and to evaluate the performance of a new control system, the design was based to some extent upon configurations and components whose operation was clearly understood. This was to assure that the core itself would not limit the performance and hinder the accumulation of control system data. The configuration utilized in the steam passage was the heated surface-fin-wick type which has proven quite adequate in past designs. Fiber metal wicks 15 percent dense and 0.080 in. thick were selected as the capillary structure. These wicks are good capillary pumpers, light weight, provide adequate film coefficients and have given good performance in the past. The fin employed in the steam passage was 0.002 inch thick, 0.050 inch high and contained 20 nickel fins per inch of flow width. Nickel was used because the high thermal conductivity gives a smaller conduction temperature drop across the steam passage. The large number of fins and short fin height also reduce the conduction ΔT while not being so restrictive as to increase significantly the pressure drop. An identical fin configuration was used in the heat transport fluid passage, however the material was stainless steel because it is more compatible with the water-ethylene glycol heat transfer fluid. This compact, high area density fin was used to increase the conductance on this side of the unit.

A two pass configuration with the steam passage in between was used with water feed on one face only. The advantages of this design were given above in the discussion on flow configuration. Water feed was directly into a cellulose sponge in which the metal wicks were imbedded. This sponge which was 1 inch thick served to distribute the water to all the wicks across the face of the unit. The control scheme utilized an on-off water control so the sponge also served as a water storage facility between periods of feed. Another thinner sponge is located on the face opposite the water feed face and serves to redistribute water from faster pumping wicks to slower pumping wicks as well as storing water.

2. Control Valve

The control system for the boiler is a new concept combining water supply on-off control and steam pressure modulation in one valve bolted to the boiler core. The valve, shown in a section view in Figure 2-15, is Vernatherm actuated with the thermostat element sensing coolant outlet temperature. A control band of 40^0 to 50^0F was chosen for the unit in order to make use of available Vernatherm elements. The control scheme operates as follows: as the coolant temperature increases above 40^0F, the thermostat begins its stroke, opening the steam poppet, thereby reducing pressure in the steam plenum and providing additional cooling to the boiler. As the boiler uses all the available water in the wicks and storage sponge, the coolant outlet temperature continues to rise and the thermostat increases its stroke. At a pre-set coolant temperature, the thermostat piston actuates a second valve mechanism opening the water control poppet, allowing water to flow to the boiler from a pressurized water storage tank. Coolant temperature continues to rise for a few minutes until feed water reaches the wicks and the coolant outlet temperature drops. Steady state cooling continues until the coolant temperature again increases, at which time the cycle is repeated. The duration of each cycle is determined by the valve dimensions, boiler characteristics and the size of the sponge reservoir. The amount of sponge used may be varied, and the water on-off valve is independently adjustable, making it possible to change both the cycle time and the control temperature to obtain optimum operating characteristics.

Water Boiler Fabrication

The 1 kw module evaporator is essentially a brazed stainless steel heat exchanger using nickel feltmetal wicks to transport the evaporant. Brazing of the boiler core is accomplished in modular form with an initial braze operation joining the primary fluid (water glycol) fin passages and a second braze operation adding the steam fins and nickel feltmetal wicks to these modules. Two nickel base braze alloys with different melting points are used for these operations. Figure 2-16 shows the completed braze assembly of the boiler module. Final assembly of the boiler module is made with the weld of the water glycol inlet-outlet pans and the steam backpressure valve mounting pad to the brazed assembly. The boiler core is completed by final machining of the flange surfaces, followed by cleaning of the entire assembly. The water on-off steam packpressure valve is essentially a machined aluminum structure with the water control valve mounted to the backpressure valve which is in turn bolted to the evaporator assembly. Prior to performance testing of the unit, the supply water sponges are cleaned and installed, and the control valve calibrated to the desired temperature settings.

A photograph of the boiler module and control valve is shown in Figure 2-17.

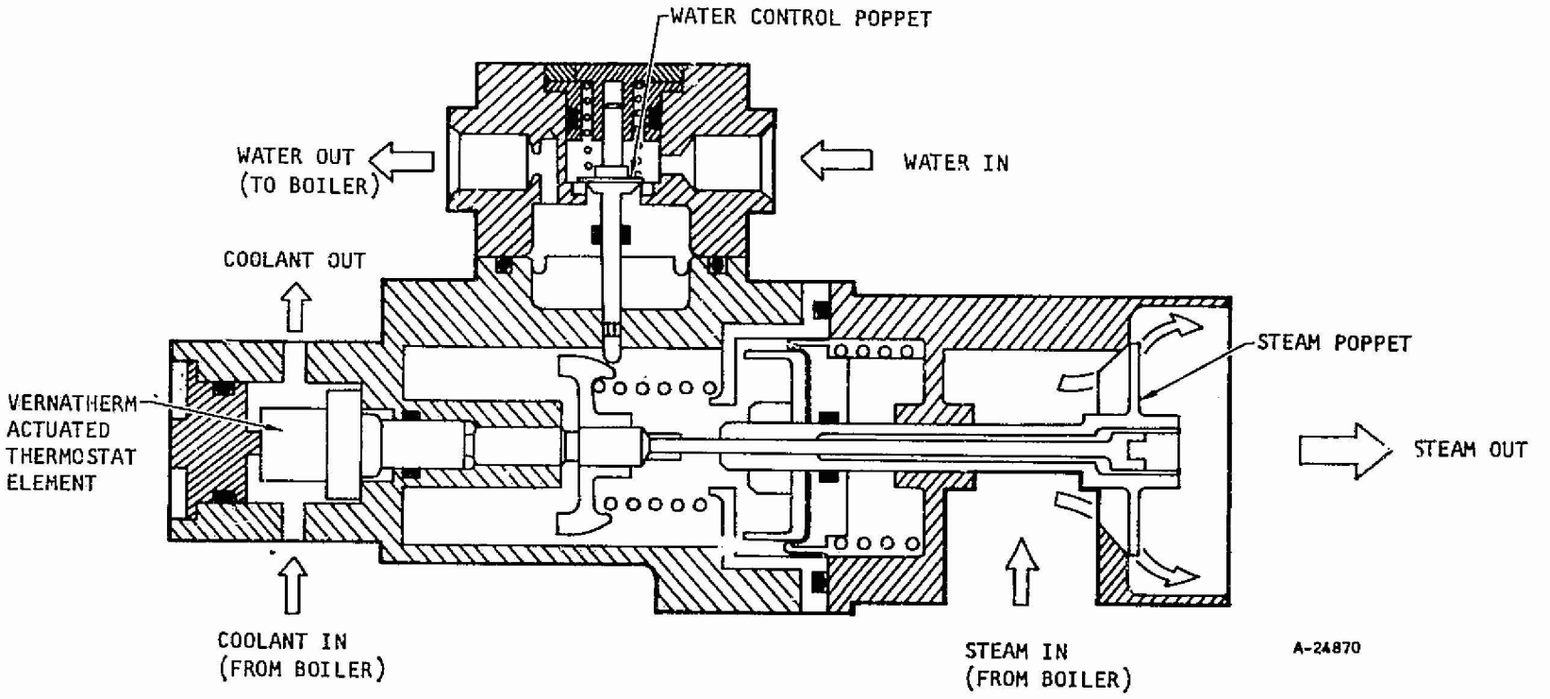

Figure 2-15. Water Boiler Control Valve

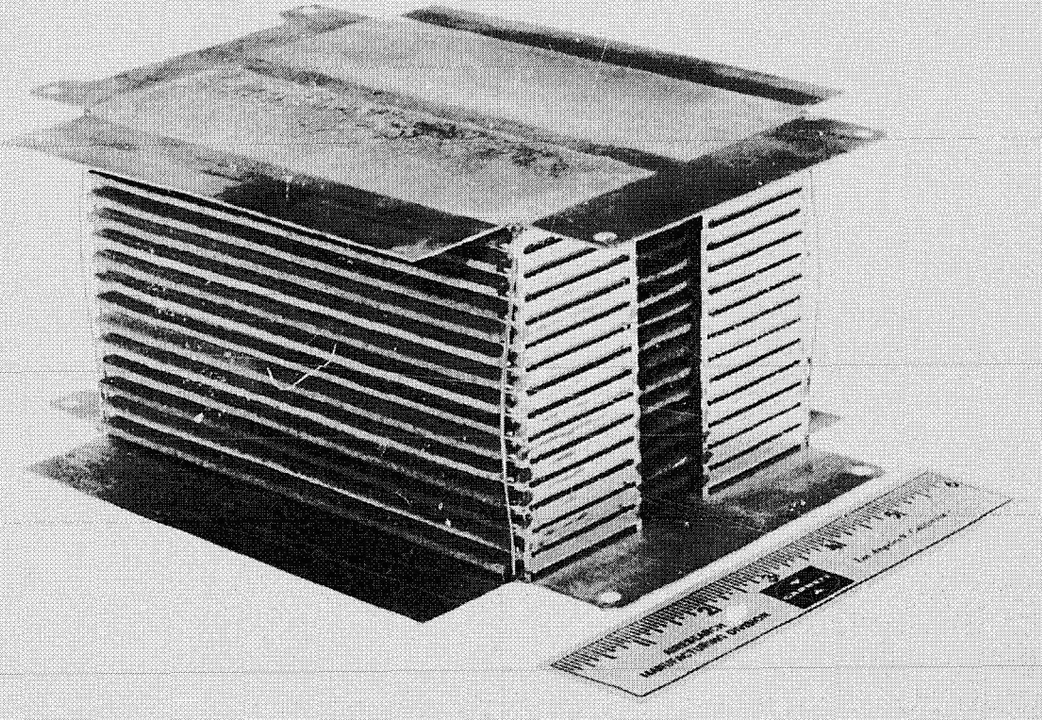

59844-2

Figure 2-16. Wick Boiler Incorporating Modular Brazed Assembly

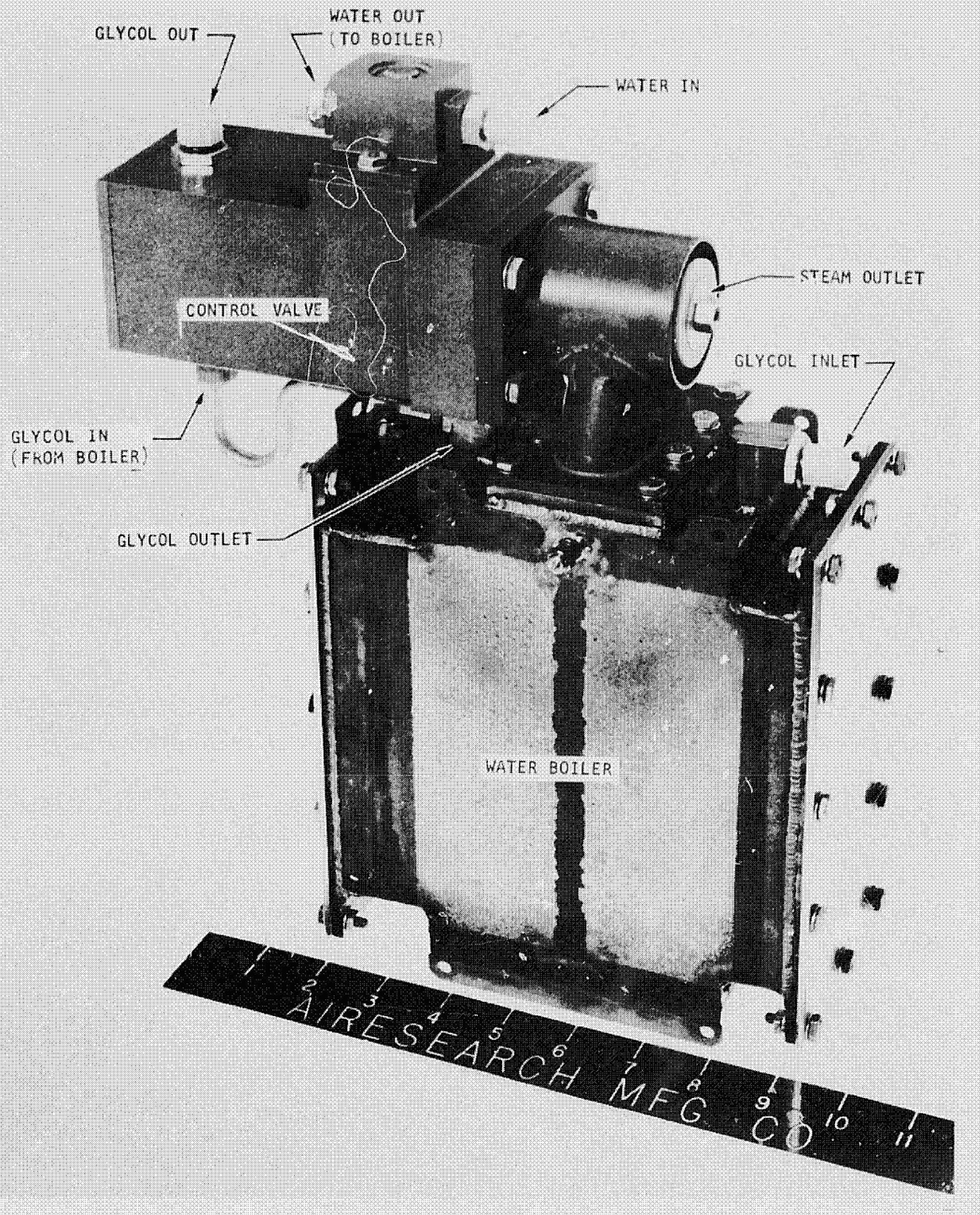

Figure 2-17. One KW Boiler Module and Control Valve F-8071

Boiler Testing

Tests were performed on the wick boiler and control valve combination to evaluate its performance and to verify the design procedure. Figure 2-18 shows the boiler module instrumented for testing. Water was used as the heat transport fluid, and various heat loads, inlet temperatures, and flow rates were examined. A summary of the test conditions is given below.

Run No.	$W_{coolant}$ lb per hr	$T_{coolant\ in}$ °F	$T_{coolant\ out}$ °F	Q Btu per hr	
103-106	70	90	44	3250	
204-208	70	76	42	2380	
201-203	70	60	38	1540	
209-211	70	90	44	3260	(unit inverted)
101-102	211	68	47	4430	
113-116	226	61	46	3500	
107-112	109	76	45	3490	

Portions of the coolant inlet and outlet temperature traces are given in Appendix B.

For a coolant flow rate of 70 lb per hr, runs were made at approximately full, 2/3, and 1/2 of the design heat load to determine the effect of a reduced heat load on performance. Examination of the coolant outlet temperature for these three cases indicates that as the heat load decreases, so does the average outlet temperature of the coolant. For 90, 76, and 60°F inlet temperatures the steady state outlet temperatures are 44, 42, and 38°F, respectively. This is an expected characteristic which is built into the system in the control valve. The outlet temperature controls the opening of the steam poppet. At lower inlet temperatures (lower heat loads for the same flow rate) less steam is generated so that a smaller pressure drop exists across the poppet. Since the sink pressure is constant this decreases the saturation pressure and temperature in the core, reducing the outlet temperature of the heat transport fluid. This reduced temperature is sensed by the control valve and causes the steam poppet to close, increasing the ΔP across it. Equilibrium is established at a smaller poppet opening and a lower outlet temperature for a decreased heat load.

The three plots beginning with runs 103, 204, and 201 (Appendix B) also indicate the cycle time associated with the different heat loads. For full, two-thirds, and half of the design heat load the average amount of time between water feeds was 15.2, 26.7 and 34 min, respectively. Prediction of

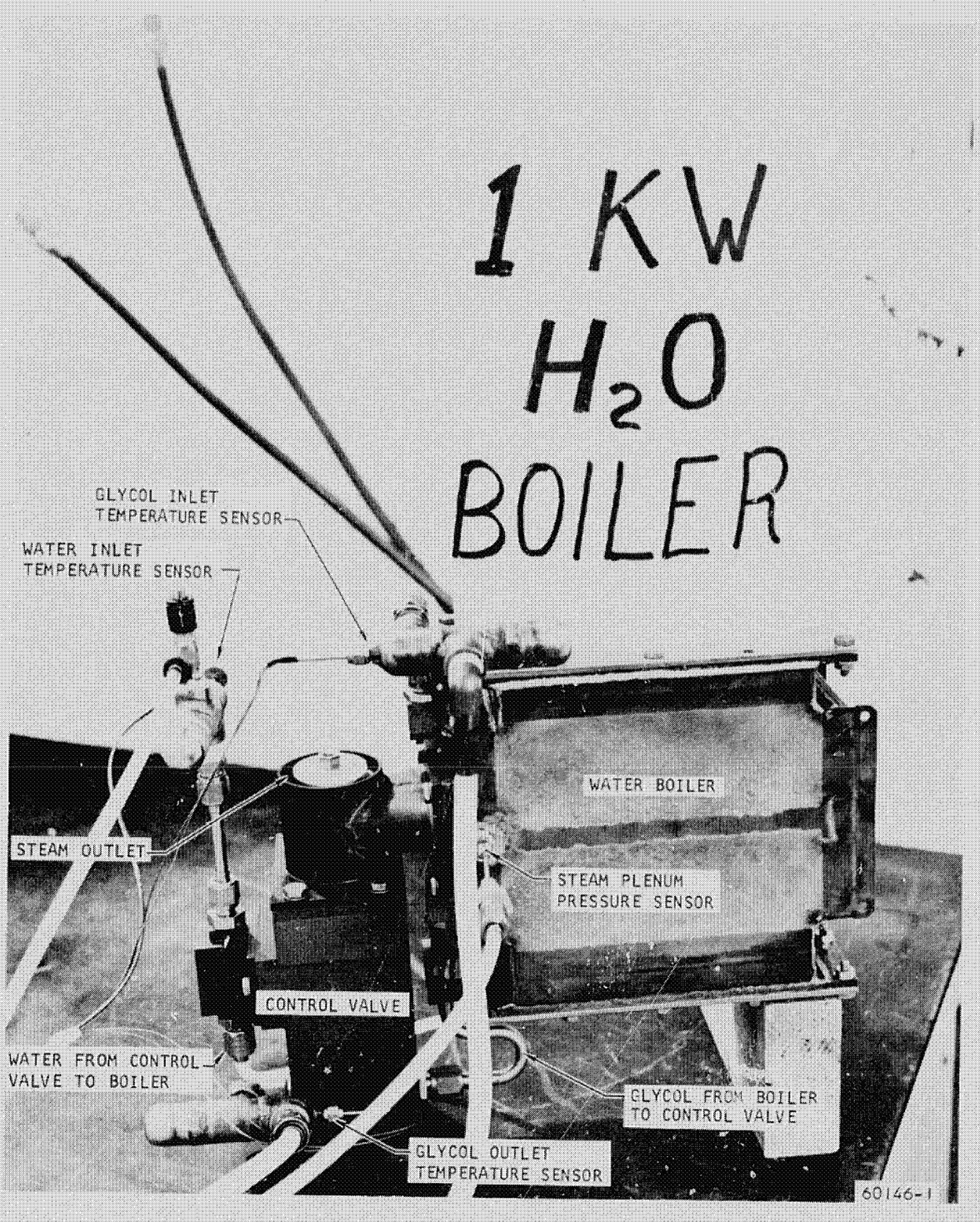

F-8101

Figure 2-18. Instrumented One KW Boiler Module

the cycle times were not made because it was not known what percentage of the water in the wicks and sponge could be pumped out. The data do indicate that the time between water refills increases roughly as the inverse of the heat load. This would be the expected tendency if the same amount of water were added during each refill period regardless of the heat load. The data also indicate that this is the case. The control valve was calibrated to open the water flow poppet when the coolant outlet temperature reached 50°F and close when it reached 48.5°F. Observations conducted during the testing indicated however that water flow began at 51°F and ceased at 47°F. Since for these three runs a constant water feed pressure was used, the amount of water flowing into the unit was directly proportional to the time the water valve was open. This time is indicated by the outlet temperature trace; the elapsed time between the 51°F reading and the 47°F reading is the time during which the valve was open. For full, two-thirds, and half heat loads the average fill times were 1.82, 1.72, and 1.90 min, respectively, indicating essentially no difference in the amount of water fed during each refill period. As stated above this is consistent with the recorded cycle time.

Runs 209 to 211 were also made with a full heat load and a coolant flow of 70 lb per hr, however, the unit was run in an inverted position, that is, with the water-feed face located on the top of the unit instead of on the bottom. As is indicated in the temperature trace, the outlet temperature of the coolant was 44°F, the same as that recorded with the feed on the bottom of the unit. The one significant difference between the two orientations was the cycle time, the time between refills. With the feed on top the unit called for additional water every 21.5 min, operating about 40 percent longer between refills than the previous orientation. This is likely due to gravity effects, which aid in transporting the water from the supply sponge to the wicks. In a space environment, no gravity forces exist to aid or hinder the water feed and the cycle time would likely be between 15.2 and 21.5 min.

The three other sets of runs were made at higher coolant flow rates, two at the design heat load and one at about 130 percent of the design. A summary of the data obtained in these runs, along with that obtained in the 70 lb per hr runs is given in Table 2-4. Comparison of the runs made at or near the design heat load indicates that the cycle times are relatively independent of the coolant inlet temperature but proportional to the heat load. Also shown are the average maximum and minimum temperatures reached by the outlet temperature during the periods when the unit was refilling itself. It has already been pointed out that the average outlet temperature is a function of the heat load only and independent of the inlet temperature. The difference between the maximum temperature and the average outlet temperature increases with decreasing heat load and with increasing inlet temperatures. This is due partially to the lower average temperature at lower heat loads so that there is a greater temperature change between the average outlet and the outlet temperature when the water is turned on (51°F in the tests). At the same heat load the maximum outlet temperature increases with increasing inlet temperature because as the wick begins to dry out, heat dissipation capacity becomes a function of the amount of water in the wick. Therefore, as the amount of available water decreases, the heat transfer rate decreases and at lower coolant flow rates (higher inlet temperature), the change in the outlet temperature is greater.

TABLE 2-4

BOILER MODULE PERFORMANCE TEST RESULTS

Run Nos.	Q	$T_{c_{in}}$	$T_{out_{ss}}$	$T_{out_{min}}$	$T_{out_{max}}$	Cycle Time	Refill Time
	Btu/hr	°F	°F	°F	°F	Minutes	Minutes
103-106	3250	90	44	42.5	59	15.2	1.82
204-208	2380	76	42	38	57	26.7	1.72
201-203	1540	60	38	35	54	34	1.90
209-211	3260	90	44	43	57	21.5	1.74
101-102	4430	68	47	47	52	15.7	--
113-116	3500	61	46	45	54	15.3	1.33
107-112	3490	76	45	43	55	14.2	1.50

It is also seen that the runs at lower heat loads exhibited larger difference between the steady state and minimum outlet temperature, in other words they had a greater tendency to "undershoot" the steady state outlet temperature. This tendency exists because at the low heat loads, for a given poppet opening, the ΔP and therefore the saturation temperature and pressure are lower. Since for all cases, when water is fed the outlet temperature must be $51^{0}F$ or greater, the poppet openings are about the same (since it is controlled by the temperature). The resulting lower saturation temperature causes increased cooling; pulling the outlet temperature lower until the corresponding smaller poppet opening can compensate and bring the saturation pressure (and therefore the outlet temperature) back up.

For all test conditions it was possible to control the unit. The control band was greater for low flow rates. This is because the heat rate is proportional to the product of the flow rate and the difference in temperature of the coolant from one end of the unit to the other. Therefore the smaller the flow rate, the larger the change in the coolant temperature difference, and this change in the temperature difference is reflected in the control band. Since variation in outlet temperatures above the steady state value were much greater than variations below, better control could be achieved by decreasing the high side variation. This could be done for a unit designed for a specific coolant flow rate by designing the control valve to turn on the water flow at a temperature relatively close to the steady state temperature at full heat load, and by designing the core so that the distance water must travel to feed the wicks is shorter.

OPTIMIZED BOILER MODULE

Based on the wicking investigation and the results of the multi-wick boiler testing, an optimized one-kilowatt wick evaporator was designed. While the optimized module was not constructed, all the concepts incorporated into the design were verified experimentally. Design of this unit incorporated the use of the best overall wick from a boiling coefficient standpoint, optimization of the flow configuration, and minimization of the wicking flow path and steam friction pressure drop while keeping the size and weight of the unit to a minimum. The problem statement to which this unit was designed is given below.

Coolant	62.5% ethylene glycol, 37.5% water
Inlet Temperature	$90^{0}F$
Outlet Temperature	$60^{0}F$
Heat Rejection	one KW

A steady state absolute pressure just upstream of the steam valve of .1040 psia was used in the design. This corresponds to a saturation temperature of $36^{0}F$, sufficiently above the freezing temperature of the expendable fluid. The wick chosen for use in this unit was a .060-in. thick, 15 percent dense, nickel fiber, metal wick. It was selected because it yielded high boiling coefficients and because of its light weight. A similar .030-in. thick wick demonstrated similar boiling coefficients, but could be easily plugged during a braze operation.

A two-pass configuration was employed on the glycol side of the unit and the water feed was designed to be from two faces. The steam plenum was placed at the middle of the unit. This is identical to the final configuration discussed above in the section on Flow Configuration, and was chosen because of the advantages cited there. A sketch of the optimum core design is shown in Figure 2-19 with overall dimensions. As indicated, the unit incorporates 9 wicks and 10 glycol passages. The width of the glycol passages is 1 in. which is also the active wick length. A 1-in. wide steam plenum is shown at the center of the core. The fin surface used on both the glycol and steam sides was 20 fins per inch, .050-in. high, .002-in. thick, with a 1/10-in. offset. Stainless steel was used on the glycol side and nickel on the steam side. The reason for using nickel is to increase the conduction across the steam passage, thereby increasing overall conductance and reducing the required unit size. The glycol flow length is 5 in. per pass.

The active width of the wick adjacent to each glycol pass was limited to 1 in. for several reasons. First, by keeping the capillary flow length short, better control may be realized since liquid can reach the active areas faster when additional feed is required. Second, for operation in 1 g, the thin wicks cannot support a sizable heat flux over a substantial length so it is necessary to limit the length for this reason. Also, the steam pressure drop is smaller for a shorter steam fin length. It is noted from the figure that on each water feed face, there is a distribution plate and a distribution pad. The distribution plate is a plate with small holes ($\sim$1/16 in.) drilled in it at given intervals. It serves to distribute water to all portions of the unit through the distribution pad. The distribution pads are 1/2-in. thick cellulose sponges which serve to store water, to distribute water, and to prevent flooding of the unit. When the wicks begin to dry out and the water feed is turned on, liquid enters the core through the distribution plate. Since it enters at a faster rate than it can be pumped through the wicks or dissipated in evaporation, unless it is stored, it will flow into the steam passages and flood the unit. The sponges damp out this surge of fluid and serve as storage area. Using sponges on two faces speeds up the water distribution to the wicks.

ONE KW MODULE WATER BOILER STACKING STUDY

The ultimate goal in the design of an optimum 1 KW module water boiler is the use of multiples of this module in combination to satisfy the required heat load in a variety of applications. Typical of this type service would be the use of six modules to provide a heat dissipation equal to 6 KW. With this typical problem statement in mind, a series of design layouts was conducted, aimed at evaluating the various methods which could be used to combine six 1 KW modules.

Figure 2-20 (SK51270) shows one arrangement which could be used. This solution was selected because it provides the simplest technique for joining six modules and because it keeps the required piping to a minimum. The boiler modules are joined to each other in a bolted assembly with four bolts through the sideplate of each module. Clearance holes are provided in each

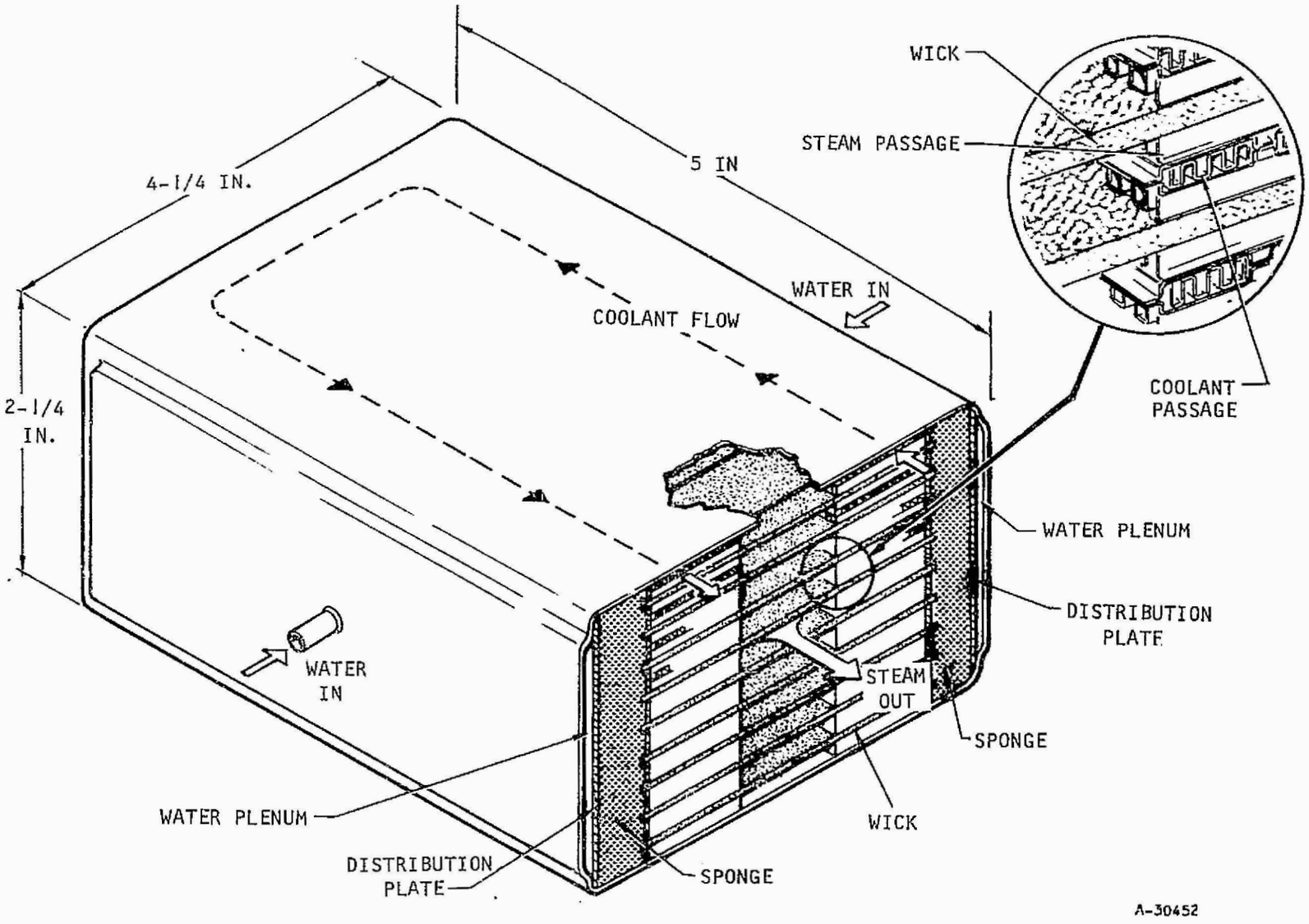

Figure 2-19. Optimized One kw Water Boiler

FOLDOUT FRAME 1

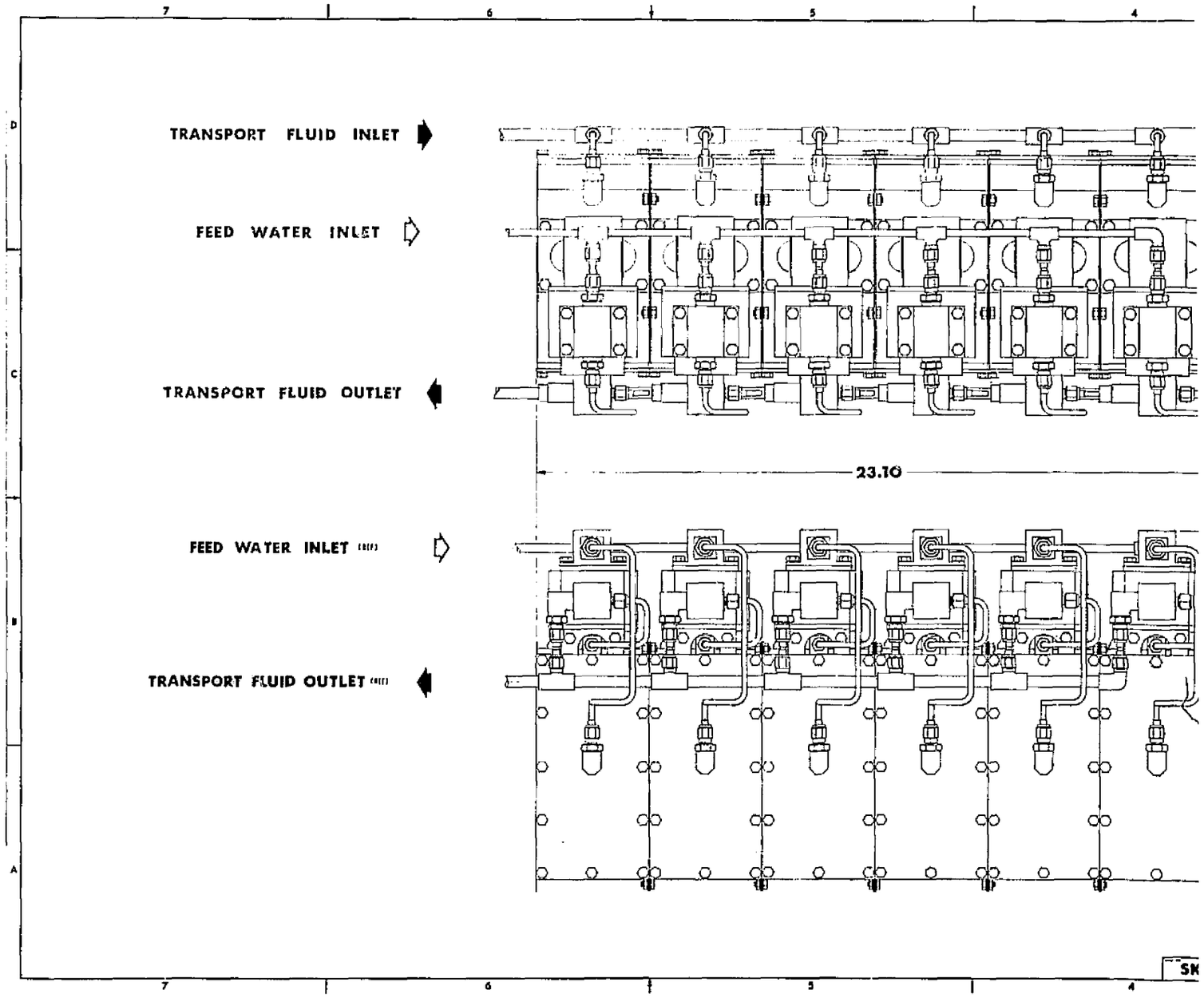

FOLDOUT FRAME 2

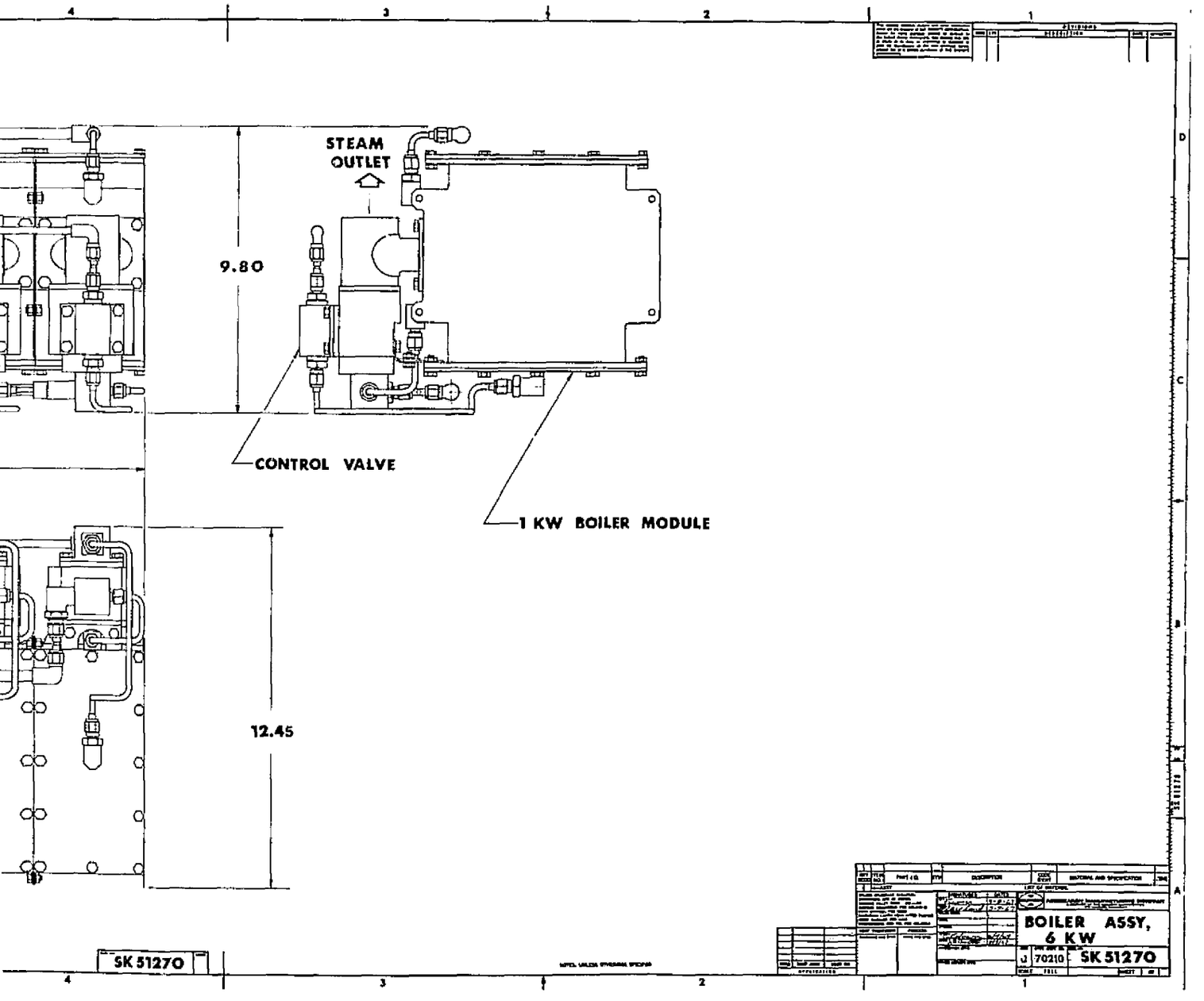

Figure 2-20. Boiler Stacking Study

sideplate such that assembly could be accomplished merely by stacking six units and bolting each to the unit above and below. The heat transport fluid loop can be seen most clearly in the upper left side view of Figure 2-20. The heat transport inlet is uppermost in the drawing and is composed of a single pipe manifolded to each of the six modules. The total flow would be distributed equally to each of the six modules for all modes of operation by an orifice in each manifold sized to equalize the pressure drop in each boiler loop.

The heat transport fluid is ducted from each core through the water on-off valve vernatherm of each unit. After passing through the water on-off valve, the total flow is collected in a single pipe and returned to the heat transport loop. Each boiler module contains its own steam back pressure-feed water flow control valve mounted atop the individual module. This valve, similar to that used on the 1 KW module designed and built during this contract, senses heat transport fluid outlet temperature and controls steam plenum pressure and feed water flow according to the sensed temperature. Feed water is supplied to each of the valves from a single line operating off a pressure source. The use of a separate valve for each module is necessitated by the desire to maintain a versatility for the 1 KW module. Thus if a single back pressure flow control valve were designed for a 6 KW system, the back pressure characteristics of this valve would make it incompatible with a 2 KW or 8 KW system. If a single control valve were used for each different application, the net result would be a change in the nominal control temperature for each new system. The universal application of a single valve would also require a rather complete system of ducting for the steam flow and the heat transport loop outlet flow, which would be different for each application.

The system shown in Figure 2-20 is not, of course, the only possibility for arrangement of six modules. The modules could easily be placed side by side in stacks of two or three and manifolded together to provide a more convenient package size for a particular application. However, the arrangement shown does demonstrate the feasibility of a diversified application of an optimum 1 KW module.

SECTION 3

WATER SUBLIMATOR MODULE

INTRODUCTION

Task II of the heat sink study was an investigation and optimization of a porous plate sublimator module. Analyses were performed to investigate possible sublimation mechanisms, the liquid breakthrough phenomenon, and the effect of steam plenum configuration. An extensive experimental investigation of various porous plates and their operating characteristics was conducted. The effects of the heat flux and water plenum pressure were examined, and performance at startup, restart, steady state, and at no heat load was defined. Several water plenum configurations were tested and the potential advantageous use of hydrophobic coatings was established. A sublimator core incorporating several porous plates was designed, fabricated, and tested. Based on the investigation, an optimized one kilowatt sublimator was designed. The potential of handling large heat loads was investigated in stacking studies.

RECOMMENDATIONS AND CONCLUSIONS

1. An optimum sublimator design should incorporate a steam plenum sized on a maximum pressure drop basis to insure that all areas of the sublimator plates are exposed to pressure levels substantially less than the water triple point pressure. Oversized passages contribute nothing to performance and merely increase unit weight and volume.

2. The use of a supply water plenum height on the order of 0.010 to 0.020 in. eliminates the possibility of a porous plate rupture during sublimator freeze up. The short water plenum does not, however, degrade the unit performance.

3. Varying the heat transport fluid fin area density by increasing the number and thickness of the fins from the hot to the cold end of the unit, will produce the optimum heat transport fluid side sublimator design. The resulting increase in overall conductance allows for operation of the sublimator over its entire length at the maximum allowable heat flux which can be withstood by a given porous plate without breakthrough.

4. Porous plates selected for use in a sublimator should contain pore sizes in the range of 2 to 10 microns. Porous plates with pore sizes smaller than 2 microns are subject to plugging by corrosion and system contaminants. Plates with pore sizes larger than 10 microns demonstrate poor startup characteristics due to the longer period of time required to form an ice block within each pore.

5. In general for porous plates with the same average pore size, the plate with the highest void fraction will demonstrate the best performance, measured in terms of the temperature difference between the heat transport fluid and the sink temperature.

6. Development of the concept of using hydrophobic porous plates will allow elimination of the breakthrough heat flux limitation imposed upon conventional designs, resulting in units more reliable and as much as 50 percent lighter than current sublimators.

7. A series of optimum 1 kw module sublimators may be combined or stacked to provide cooling for a wide variety of heat load applications.

SUBLIMATOR ANALYSIS

Possible Mechanisms

According to the theory presented in Reference 6, the sublimation mechanism is characterized by a layer of ice on the inside face of the porous plate. The main elements of the referenced theory can be summarized as follows:

> [The existance of this ice layer is determined by a combination of the vapor pressure drop characteristics of the porous plate and the heat flux or vapor flow rate. When the vapor pressure drop across the porous plate is less than the triple point pressure the phase change must be from the solid directly to the vapor phase, by sublimation of the ice layer. The thickness of the ice is governed by the rate of heat transfer and the sublimation temperature corresponding to the local vapor pressure at the inlet face of the porous plate. To meet the imposed heat load the ice sublimes at the face of the porous plate and freezes at a corresponding rate at the liquid interface. The generated vapor passes through the porous plate. It can be shown that the normal operating pressure differentials across the porous plate and ice layer are insufficient to extrude the ice into the pores and thus the ice forms a barrier to liquid flow into the pores.
>
> If the input heat flux is increased, the vapor pressure drop across the porous plate increases causing the sublimation temperature to rise accordingly. This results in a reduction in the ice layer thickness in order to satisfy the heat conduction requirements. Eventually the ice layer will disappear completely when the heat flux is sufficient to cause the vapor pressure at the inlet face of the porous plate to be greater than the triple point pressure. It is at this point that the evaporation mechanism begins to occur. However, if the pore size distribution is non-uniform, the heat flux at which this transition occurs will vary with location on the plate due to inequalities in vapor pressure drop, resulting in mixed mode operation.
>
> Typical porous plates contain a random distribution of pores with respect to both size and shape. The point of transition for any single pore is dependent on its equivalent radius and ultimately the vapor pressure drop produced by the pore. In the mixed mode of cooling, phase change occurs at local temperatures above and below the triple point depending on the local pore geometry. An averaging effect exists and if the plate is of reasonable thermal conductivity the effective plate temperature remains constant and very near 32°F over a wide range of heat flux. Design calculations are then simply based on a triple point sink temperature.]

The main elements of the theory are summarized above. Some portions of this theory, however, are not consistent with the experimental data given in Reference 6 or the observations made here at AiResearch. In order to formulate a more consistent theory several "mixed mode" models were proposed and analyzed to check their validity.

The original model assumed both sublimation and boiling taking place at the upstream face of the porous plate with all the vapor passing through the entire plate. Using this model, a pressure drop corresponding to the vapor flow rate fixed by the experimental heat flux may be determined from the reference pressure drop vs flowrate data. This was done for several test modules referred to in Reference 6.

From the experimental heat flux, the vapor mass flux is determined from the equation:

$$W = \frac{Q/A}{\Delta H_b} \qquad (3\text{-}1)$$

where W = vapor mass flus, $lb_{m/hr\ ft^2}$

Q/A = Heat flux, Btu/hr ft^2

ΔH_b = Heat of vaporizationof water, Btu/lb_m

By using experimental nitrogen flow rate vs pressure drop curves for free molecule flow given in the referenced report, and by making a simple water vapor correction (given below) derived from the free molecule pressure drop equation, the pressure drop through the porous plate may be determined.

$$\Delta P_{vapor} = \Delta P_{N_2} \left(\frac{R_{vapor}}{R_{N_2}} \right)^{1/2} = 1.25\ \Delta P_{N_2} \qquad (3\text{-}2)$$

where ΔP_{vapor} = Water vapor pressure drop, lb_{f/in^2}

ΔP_{N_2} = Nitrogen pressure drop, lb_{f/in^2}

R_{vapor} = Water vapor gas constant = 85.8 lb_f ft/lb_m ^oR

R_{N_2} = Nitrogen gas constant = 55.2 lb_f ft/lb_m ^oR

The experimental data and calculated pressure drops are given in Table 3-I. It is seen that the pressure drops obtained in this manner give pressures on the upstream side of the porous plate of from 1.5 to 11 times the triple point pressure. Since ice was observed in the test units, these high pressures obviously could not have been attained, indicating a deficiency in the assumed mechanism.

In order to account for this pressure drop discrepancy, the model was revised, proposing sublimation at the upstream face and boiling near the downstream face. This is essentially the theory given in Reference 6 for "mixed mode" operation. According to this reference, sublimation takes place upstream because the pressure differential is not sufficient to extrude the ice layer into the pores, and the vapor generated passes through the entire plate. Boiling takes place inside the plate, at or near the downstream face giving a small pressure drop. In effect, this model suggests sublimation over some areas of the plate with pressure drop and boiling over the remaining areas with negligible pressure drop, the difference arising from the different sides of the plate at which phase change occurs.

TABLE 3-I

CALCULATED PRESSURE DROP FOR VAPOR FLOW THROUGH POROUS PLATES IN SUBLIMATOR

Porous Plate	Q/A Btu/hr st^2	$P_{ambient}$ psi	T_{pp} ^{o}F	W lb/hr ft^2	ΔP_{vapor} psi
C	470	0.001	33.7	0.385	0.36
	710		34.0	0.582	0.51
	970		34.2	0.795	0.69
	1230		32.0	1.01	0.87
	1475		31.8	1.21	1.03
D	420	~0.002	30.5	0.344	0.151
	475		28.9	0.389	0.140
	580		31.5	0.475	0.156
	610		33.7	0.500	0.162
	690		31.2	0.565	0.168

Q/A = experimental heat flux

$P_{ambient}$ = pressure in vapor passage

T_{pp} = porous plate temperature

W = calculated vapor mass flux

ΔP_{vapor} = calculated vapor pressure drop based upon assumption that vaporization takes place at water side porous plate face

The validity of this model may be tested by experimentally determining the average heat flux over the plate, from this determining the relative magnitudes of the boiling and subliming heat fluxes, and observing whether the values obtained are reasonable. This was done for several test plates from the reference as shown below. The total average heat rate is equal to the sum of the boiling heat rate and the subliming heat rate.

$$q_s A_s + q_B A_B = q_{avg} A_T \tag{3-3}$$

where q_s = subliming heat flux

q_B = boiling heat flux

q_{avg} = average heat flux, experimentally determined value

A_s = area over which sublimation takes place

A_B = area over which boiling takes place

A_T = total plate area = $A_s + A_B$

By defining a "boiling area ratio" $\left(R_B = \frac{A_B}{A_T}\right)$ which is the ratio of the plate area over which boiling takes place to the total plate area and dividing both sides of (3-3) by A_T, one obtains

$$q_s (1 - R_B) + q_B R_B = q_{avg} \tag{3-4}$$

which becomes

$$\frac{q_B}{q_s} = \frac{1}{R_B}\left[R_B - 1 + \frac{q_{avg}}{q_s}\right] \tag{3-5}$$

For a given plate with a known pressure drop as a function of vapor flux, one may determine the maximum possible flow rate per unit area, w_s, which gives a pressure drop low enough to keep the upstream pressure at or below the triple point pressure, thereby assuring the possibility of ice (and sublimation) at the upstream face. This flow rate is then the maximum possible vapor flux over the subliming area, and from this, the maximum sublimation heat flux may be found.

$$q_s = \Delta H_b w_s \tag{3-6}$$

ΔH_b = heat of vaporizaton

w_s = vapor flow rate per unit area

Once q_s is known, Equation (3-5)may be solved for $\frac{q_B}{q_s}$ using values of R_B between 0 and 1. The ratio of boiling heat flux to subliming heat flux was calculated for the referenced published experimental data and typical results are given below for plate D with an experimental average heat flux of 420 Btu/hr ft^2.

q_s $\frac{Btu}{hr\ ft^2}$	Assumed R_B	q_B/q_s
120	1.0 (maximum possible)	3.44
120	0.9	3.72
120	0.8	4.05
120	0.7	4.49

This analysis indicates that if the proposed mechanism is that which occurs, the heat flux over those areas at which boiling takes place is more than three times greater than the heat flux existing over the subliming areas. In order to support such great variation in heat flux, there must be either a correspondingly great variation in the local heat transfer resistance between the heated surface and porous plate or a large variation in the local source temperature. Since neigher of these seems likely in the test modules used, and neither of these seems likely in the test modules used, and neither was reported along with the experimental data, it can only be assumed that the model of sublimation and boiling occurring upstream and downstream of the porous plate, respectively, is inaccurate.

The only model which is compatible with the data is that of sublimation taking place not at the upstream face but within the pores cyclically, with the ice vapor interface receding and again forming when water fills the pores and freezes. Sublimation visualization tests which will be explained below seem to lend credibility to this model.

Breakthrough Analysis

Measurements of liquid breakthrough of porous plates in the literature have shown that the breakthrough pressure can vary from a very small fraction of the gas breakthrough pressure to a number in excess of the gas breakthrough pressure. To better understand this situation an analysis of the phenomena of liquid and vapor breakthrough for capillary tubes with rounded exits of various sharpnesses and for contact angles from 0 to 180 deg was undertaken. The reason for investigating various exit sharpnesses is that in a porous plate of conventional construction, a sharp cornered capillary will not be the typical pore geometry. A sketch of the axially symmetrical model used in the analysis is shown below.

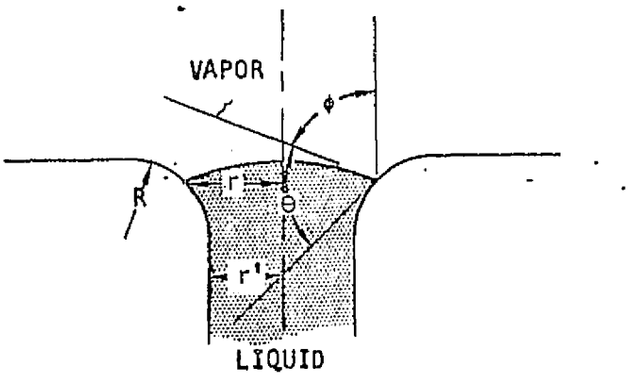

A-21705

Admittedly, the pore exits in a porous plate will probably not have symmetrical shapes; nevertheless, the following analysis is useful in that it provides a better understanding of the breakthrough phenomenon and gives an idea as to the desirable plate and fluid-surface characteristics. For clarity, the following analysis is given for liquid breakthrough; however, it can be shown that the results for liquid breakthrough with a contact angle of θ are the same as those for vapor breakthrough for an angle of $180^0 - \theta$.

A force balance on the vapor-liquid interface gives for $r' \leq r \leq r' + R$:

$$P_L - P_V = \frac{2\sigma}{r} \cos \phi \qquad (3\text{-}7)$$

where P_V = the pressure on the vapor side

P_L = the pressure on the liquid side

σ = the surface tension

From simple geometric relations, one obtains $\cos \phi$ as a function of contact angle θ, r, r', and R; therefore the expression for the interface pressure differential becomes:

$$P_L - P_V = \frac{2\sigma}{r}\left\{-\left[1 - \left(\frac{r'}{R}\right)\left(\frac{r}{r'} - 1\right)\right] \cos\theta + \left[2\left(\frac{r'}{R}\right)\left(\frac{r}{r'} - 1\right)\right.\right. \qquad (3\text{-}8)$$

$$\left.\left. - \left(\frac{r'}{R}\right)^2 \left(\frac{r}{r'} - 1\right)^2\right]^{1/2} \sin\theta\right\}$$

If both sides of (3-8) are divided by $\frac{2\sigma}{r'}$, one obtains the normalized pressure differential $\frac{P_L - P_V}{\frac{2\sigma}{r'}}$. For vapor breakthrough the equation for the interface pressure differentail is the same as (3-8) except there is no minus sign on the

coefficient of the cos θ term. Therefore since cos (180 - θ) is equal to - cos θ, the vapor breakthrough pressure for 180 - θ is equal to the liquid breakthrough pressure for a contact angle of θ.

For a given contact angle θ and "exit sharpness" $\frac{r'}{R}$, the ratio of the pore radius to the radius of curvature of the exit, one can evaluate the normalized pressure differential $\frac{P_L - P_V}{\frac{2\sigma}{r'}}$ for different values of r between r' and $r' + R$ from Equation (3-8), and upon doing so, observes that the normalized pressure differential increases and then decreases with increasing r. An example of this is shown in Table 3-2 for an "exit sharpness" of 1.0 and a contact angle of 100 deg.

TABLE 3-2

NORMALIZED PRESSURE DIFFERENTIAL ACROSS LIQUID-VAPOR INTERFACE FOR EXIT SHARPNESS OF 1.0 AND CONTACT ANGLE OF 100 DEG

r/r'	cos ϕ	$\frac{P_L - P_V}{\frac{2\sigma}{r'}}$	
1.00	0.174	0.174	
1.05	0.474	0.451	
1.10	0.860	0.532	
1.20	0.700	0.584	
1.30	0.825	0.634	
1.40	0.892	0.637	- Breakthrough occurs at this value of r/r'
1.50	0.940	0.626	
1.60	0.972	0.607	
1.70	0.991	0.583	

One notes that for this case the maximum value of $\frac{P_L - P_V}{\frac{2\sigma}{r'}}$ occurs at $r = 1.4\ r'$.

The maximum normalized pressure differential will occur at different values of r/r' for different combinations of θ and $\frac{r'}{R}$. The maximum value of $\Delta P/\frac{2\sigma}{r'}$ is the normalized breakthrough pressure, for if this ΔP is exceeded, the liquid will detach from the capillary opening and breakthrough will occur. to obtain the breakthrough pressure P_B for a given θ and $\frac{r'}{R}$, one first solves for the $\frac{r}{r_T}$ at which breakthrough occurs. This is done by differentiating Equation (3-8) with respect to $\frac{r}{r_T}$.

$$\frac{d\left(\frac{P_L - P_V}{2\sigma/r'}\right)}{d\ \frac{r}{r_T}} = -\left(\frac{r'}{r}\right)^2 \left(1 + \frac{r'}{R}\right) \cos\theta + \left(\frac{r'}{r}\right) \tag{3-9}$$

$$\left[2\frac{r'}{R}\left(\frac{r}{r_T} - 1\right) - \left(\frac{r'}{R}\right)^2 \left(\frac{r}{r_T} - 1\right)^2\right]^{1/2}$$

$$\left[\frac{\frac{r'}{R}\left(1 - \frac{r}{R} - \frac{r'}{R}\right)}{2\frac{r'}{R}\left(\frac{r}{R_T} - 1\right) - \left(\frac{r'}{R}\right)^2\left(\frac{r}{r_T} - 1\right)^2} - \frac{r'}{r}\right] \sin\theta$$

Equation (3-9) is then set equal to zero and solved for $\frac{r}{r_T}$. This value is then substituted into (3-8) and the normalized breakthrough pressure $\frac{P_B}{2\sigma/r'}$ is found.

The results of this analysis are shown in Figure 3-1 for "exit sharpnesses" of 0, 0.01, 0.05, 0.1, 0.5, 1.0, 3, and ∞. Figure 3-2 shows pore size as a function of $2\sigma/r'$ and can be used in conjunction with Figure 3-1 to obtain pore diameter from measured bubble point data. As previously stated, results for vapor breakthrough correspond to liquid breakthrough for the supplementary contact angle. One notes that for an infinitely sharp corner, the liquid breakthrough pressure is independent of θ between 90 and 180 deg and proportional to sin θ between 0 and 90 deg. For a sharpness ratio of 0, the curve takes the form of a cosine curve. Liquid breakthrough pressure is seen to decrease with decreasing contact angle and exit sharpness ratio. Another interesting feature of this plot is that for values of θ to the right of the diagonal broken line, the normalized breakthrough pressure may be represented exactly by $\frac{P_B}{\frac{2\sigma}{r_T}} = \frac{\sin\theta}{1 + \frac{R}{r_T}}$. The reason for this simplified expression has to do with the

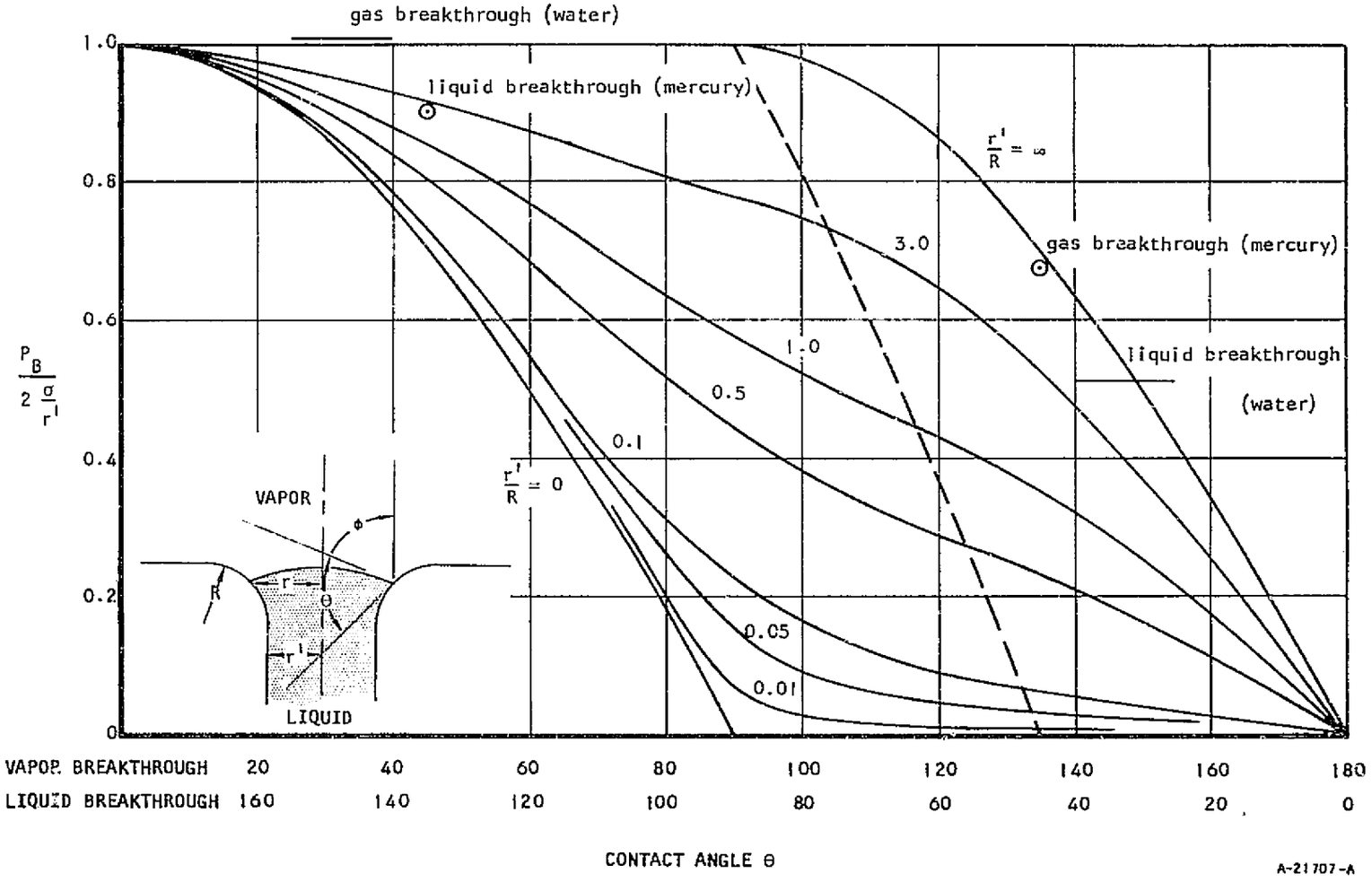

Figure 3-1. Normalized Breakthrough Pressure as a Function of Contact Angle and Exit Sharpness

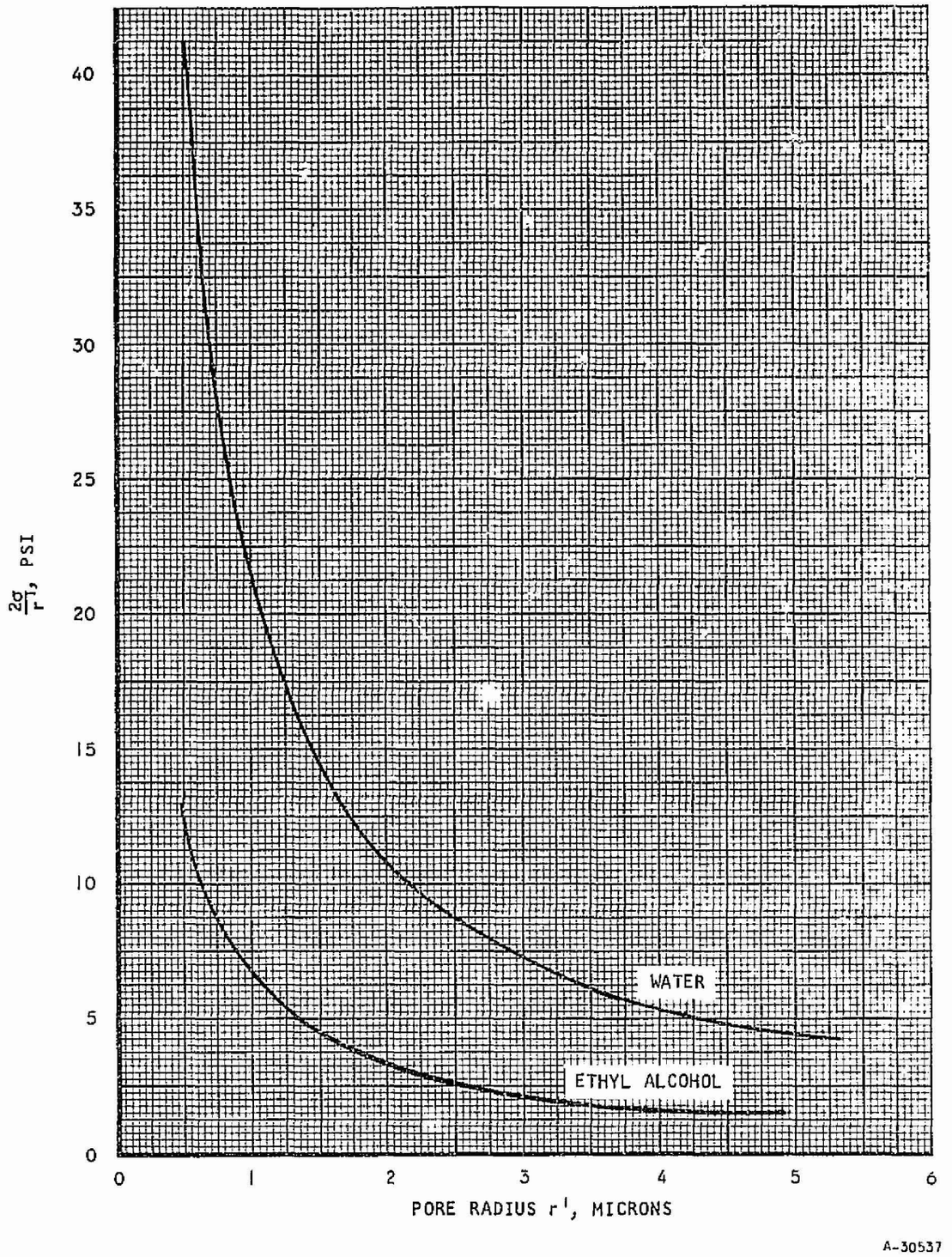

Figure 3-2. $2\sigma/r^1$ as a Function of Pore Radius

point in the capillary exit at which the breakthrough pressure is reached, and this will be explained below.

Figure 3-3 shows the position of the interface prior to liquid breakthrough for a pore with a sharpness ratio of 0.5 for various contact angles. One notes that as the contact angle is decreased, the point of contact moves further out of the pore until it reaches the outer extrimity where $\frac{r}{r'} = 1 + \frac{R}{r'}$. Upon further reduction of the contact angle, the vapor liquid interface contacts the pore wall at the same location. The maximum contact angle for breakthrough at $\frac{r}{r'} = 1 + \frac{R}{r'}$ is given by:

$$\theta_{max} = \arctan \frac{1}{1 + \frac{r'}{R}} \tag{3-10}$$

This means that for all angles less then θ_{max}, breakthrough will occur at $\frac{r}{r'} = 1 + \frac{R}{r'}$ and the defining equation obtained from a force balance is:

$$P_B = \frac{2\sigma}{r_{max}} \sin \theta \tag{3-11}$$

where $r_{max} = r' + R$

Normalization yields:

$$\frac{P_B}{2\frac{\sigma}{r'}} = \frac{\sin \theta}{\frac{r' + R}{r'}} = \frac{\sin \theta}{1 + \frac{R}{r'}} \tag{3-12}$$

This is the equation given above defining $\frac{P_B}{2\frac{\sigma}{r'}}$ for θ to the right of the broken line in Figure 3-1, and it is now seen that this occurs because for all $\theta < \theta_{max}$ in the case of liquid breakthrough ($\theta > \theta_{max}$ for vapor breakthrough) the breakoff point occurs at the pore exit extremity.

Analysis indicates that the breakthrough pressure will always be reached when the interface is at the pore exit. It is obviously impossible to support a liquid head at a rounded pore entrance for a contact angle of less than 90 deg because the surface tension always tends to pull the liquid through the pore; however, for an obtuse contact angle, the liquid vapor interface can exit at the pore entrance for pressures sufficiently less than the breakthrough pressure. Since it seems desirable in sublimators to have the evaporating interface near the pore exit to decrease the vapor flow length and thus the vapor pressure drop, we are interested in the pressure required

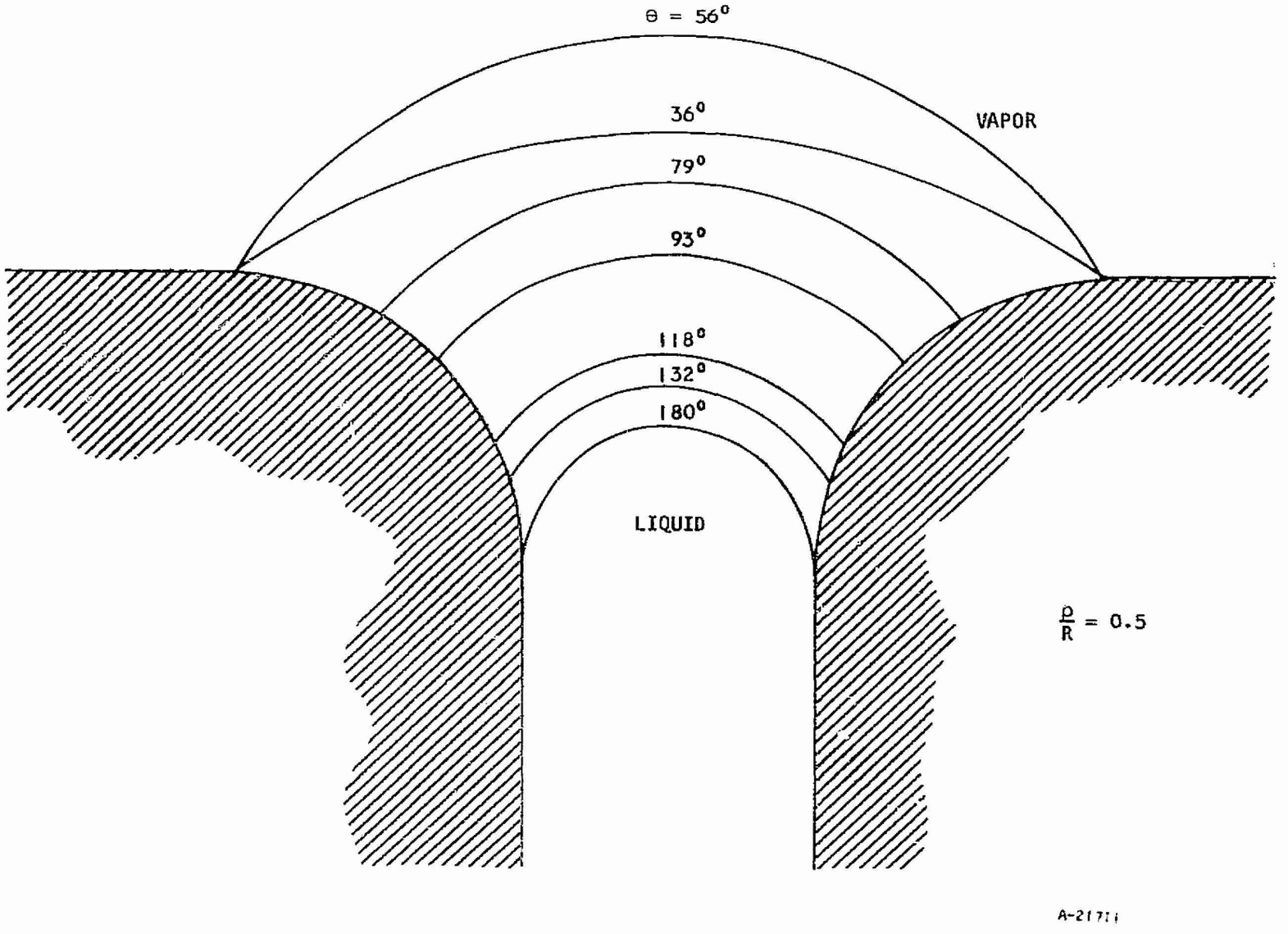

Figure 3-3. Position of Vapor Liquid Interface at Breakthrough for Various Contact Angles

to force the liquid into the pore, the break-in pressure P_{BI}.

A sketch of the pore entrance and liquid-vapor interface is shown below.

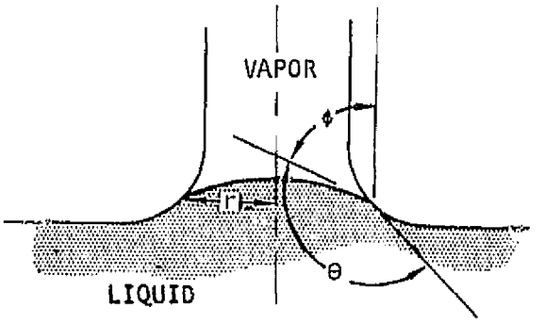

A-21706

Again, a force balance gives

$$P_L - P_V = \frac{2\sigma}{r} \cos \phi \qquad (3\text{-}13)$$

Since the breakin pressure is desired, the maximum value of $P_L - P_V$ must be found, and one observes that as the interface moves into the pore, r and ϕ become smaller and cos ϕ becomes larger. It follows then that $P_L - P_V$ is a maximum when r is a minimum and cos ϕ a maximum. This occurs when $r = r'$, and at that point, $\phi = 180^0 - \phi$ so the normalized breakin pressure becomes:

$$\frac{P_{BI}}{2\sigma/r'} = -\cos \theta \qquad (3\text{-}14)$$

This is of course true only for $\theta \geq 90^0$ since for $\theta < 90^0$ the surface tension forces pull the liquid into the pore. The normalized break-in pressure curve is identical to the $r'/R = 0$ curve in Figure 3-1, and it is seen that this breakin pressure is always less than the breakthrough pressure, indicating that at breakthrough the interface always exists at the pore exit.

It is seen from Figure 3-1 that is is indeed possible for a system to have a liquid breakthrough pressure in excess of the vapor breakthrough pressure, however this is possible only if the contact angle is greater than 90^0. It is seen also that, in general, a system which possesses a relatively high liquid breakthrough pressure will have a relatively low vapor breakthrough pressure. The one exception to this is the system with a contact angle around 90^0 for which both breakthrough pressures are nearly the same. In the sublimator application, a high liquid breakthrough pressure is desirable in order to prevent loss of water while the vapor breakthrough pressure is of little consequence. For this reason, a high contact angle seems desirable in this application.

Tests were performed in order to verify the analytical predictions.

The test apparatus for liquid and vapor breakthrough is shown in Figure 3-4. Stainless steel capillary tubes of known inside diameter were used and were thoroughly cleaned prior to testing. The liquid breakthrough test involved gradually increasing the liquid head and observing the pressure differential at which breakthrough occurred. In the vapor breakthrough test, the gas pressure was slowly increased until the first dynamic bubble appeared from the test fluid.

The tests were performed with water and mercury for sharp cornered capillary tubes in order to verify the $r'/R = \infty$ curve in Figure 3-1. With these fluids, results were obtained for a wetting ($\theta < 90^0$) and a nonwetting ($\theta > 90^0$) liquid.

The results of these initial tests are shown on Figure 3-1. It is seen that fairly good agreement with the analytical predictions was obtained. The normalized gas breakthrough pressures are within a few percent of the predicted values while the liquid breakthrough pressure of mercury is about ten percent less than the analytical prediction. A possible explanation of this might be the value used for the interfacial surface tension of mercury and air. Perry states that the surface tension of mercury is "variable and decreases with time," which could explain the discrepancy. The contact angle of water with stainless steel is shown as a range rather than a point because of the difficulty in determining its exact value. Observation under moderate magnification of the liquid drops on the test apparatus during testing, as well as the protruding liquid-vapor interface, indicated a contact angle in the neighborhood of 30^0. Photographs of water drops on a stainless steel plate were made in order to obtain a more accurate value of the contact angle; however, this was unsucessful due, probably, to contamination of the plate between cleaning and photographing, and contact angles ranging from 30^0 to 90^0 were obtained. The literature gives contact angles of water on "cleaned" stainless steel surfaces of from 0^0 to 42^0, depending on the cleaning procedure and whether the contact angle is the advancing or receding angle.

Effect of Steam Passage Dimensions on Sublimator Design

In the design of a conventional sublimator, the steam passage dimensions are critical. With a high vapor mass flow and a long narrow steam passage, the pressure at the bottom of the passage could approach the triple point pressure even though the pressure at the plenum outlet is quite low, due to the pressure drop of the vapor leaving the plenum. The increased pressure at the bottom of the plenum could lead to liquid breakthrough, especially at startup, since the time required to freeze increases greatly as the ambient pressure approaches the triple point. It is desirable therefore to design the steam passage such that a relatively low pressure is maintained.

The pressure in the steam plenum may be predicted as a function of the operating heat flux (mass flux), vapor flow length, passage height and width, and plenum outlet pressure by solving the basic pressure drop equation:

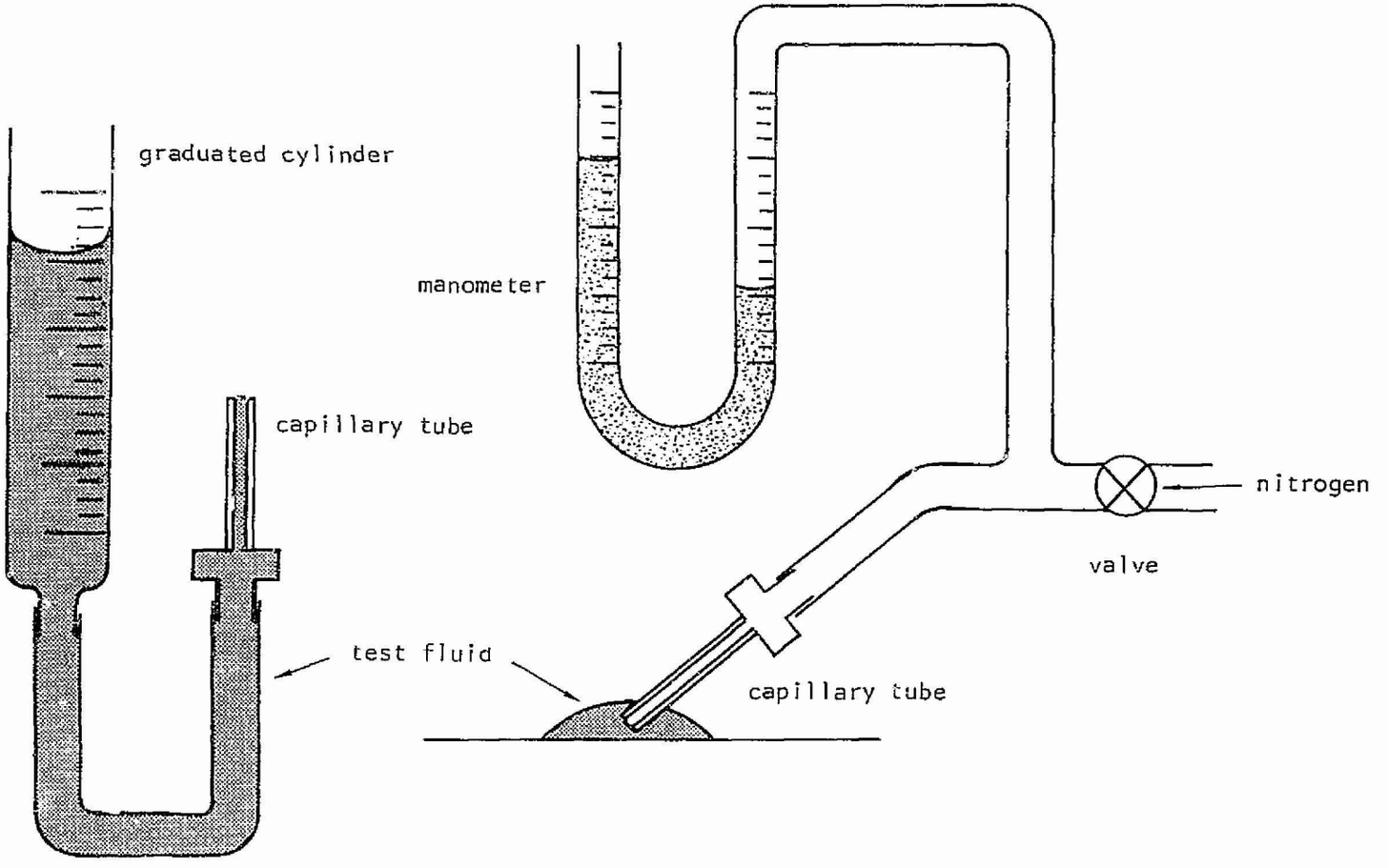

Figure 3-4. Breakthrough Test Apparatus

$$dP = \frac{-G^2}{2g_c\rho} \frac{4f}{D_h} dx \qquad (3\text{-}15)$$

where dP = change in pressure

G = vapor mass flux in direction of flow

ρ = vapor density

f = friction factor

g_c = gravitational constant $= 32.2 \frac{lb_m\ ft}{lb_f sec^2}$

D_h = hydraulic diameter of steam passage

dx = incremental flow length

For the probable limits of heat flux and flow length of 10,000 Btu/hr ft^2 and 1 ft, the flow is in the laminar regime and the friction factor may be approximated to within 2 percent with the equation:

$$f = \frac{14.2 + 9.8\ (1 - \frac{h}{w})^3}{Re} \qquad (3\text{-}16)$$

where RE = Reynolds Number

$\frac{h}{w}$ = passage aspect ratio

Assuming uniform heat flux, the mass flux in the flow direction is directly proportional to x and the defining pressure drop equation becomes:

$$PdP = -\frac{B\ \mu\ RT\ (Q/A)\ x\ dx}{2g_c\ Hs\ h^3} \qquad (3\text{-}17)$$

where μ = viscosity

R = gas constant

T = vapor temperature

Q/A = heat flux

Hs = heat of sublimation

h = vapor passage height

$$B = \left[14.2 + 9.8\ (1 - \frac{h}{w})^3\right]\left[1 + \frac{h}{w}\right]^2$$

Integrating equation (3-17) between x = 0 and L (total flow length) and applying the boundary condition that $P = P_{outlet}$ at x = L, the equation defining the pressure at any position in the plenum is obtained.

$$P^2 = \frac{B\ \mu\ RT\ (Q/A)(L^2 - x^2)}{2g_c\ Hs\ h^3} + P^2_{outlet} \qquad (3\text{-}18)$$

The maximum pressure in the plenum which occurs at the bottom of the passage is obtained by setting x = 0. As indicated previously, the pressure is a function of the heat flux, flow length, passage height, passage width, and the outlet pressure.

To illustrate the effect of passage height on the maximum steam plenum pressure in a typical sublimator, the above equation was solved at x = 0 for a heat flux of 6000 Btu/hr ft^2, a plenum outlet pressure of 0.5 mm Hg (.00965 psia), and $h/w \approx 0$ (no fin in the steam passage). Figure 3-5 shows the maximum plenum pressure as a function of plenum height for various vapor flow lengths.

If the maximum allowable steam plenum pressure is known, the passage design height may be determined from this type of plot. Obviously, in order to prevent breakthrough, it is necessary to maintain the pressure below the triple point in a conventional sublimator, however, how far below the triple point is not known at this time. It has been shown that the time required to freeze small liquid drops exposed to low pressures increases markedly for pressures greater than approximately 50 percent of the triple point pressure,[7] which implies that the pressure in the steam passage should be maintained at least below this value.

Even though it is not possible at this time to pick the optimum pressure level and therefore the minimum allowable height, it is possible in some cases to determine a maximum passage height. For example, for a flow length of 3 inches, no advantage is realized by designing a passage height of .5 inch instead of .3 inch because the pressure reduction obtained is for all practical purposes negligible, as indicated by Figure 3-5.

Sublimator Visualization Test

Early in the sublimator study program a visualization test module was designed. It was thought that through visual observations some insight might be gained into such problems as where the ice forms, whether in or out of the pores, if there is blockage of flow by fins, and what causes breakthrough and under what circumstances does it occur. With this goal in mind, a unit consisting of a heated plate, finned water passage, porous plate, steam passage, and transparent sides and top was fabricated and testing was initiated.

Some difficulty was encountered in observation of the bottom porous plate surface due to the fins and the relatively small height of the water passage (0.175 in.). To alleviate this problem, a similar unit was assembled with no fins and a water passage 0.5-in. high. Figure 3-6 shows the new module in operation. With this unit, observation of the entire plate surface was possible and testing was continued. Photographs were taken for documentation purposes and to allow repeated observation of certain phenomena.

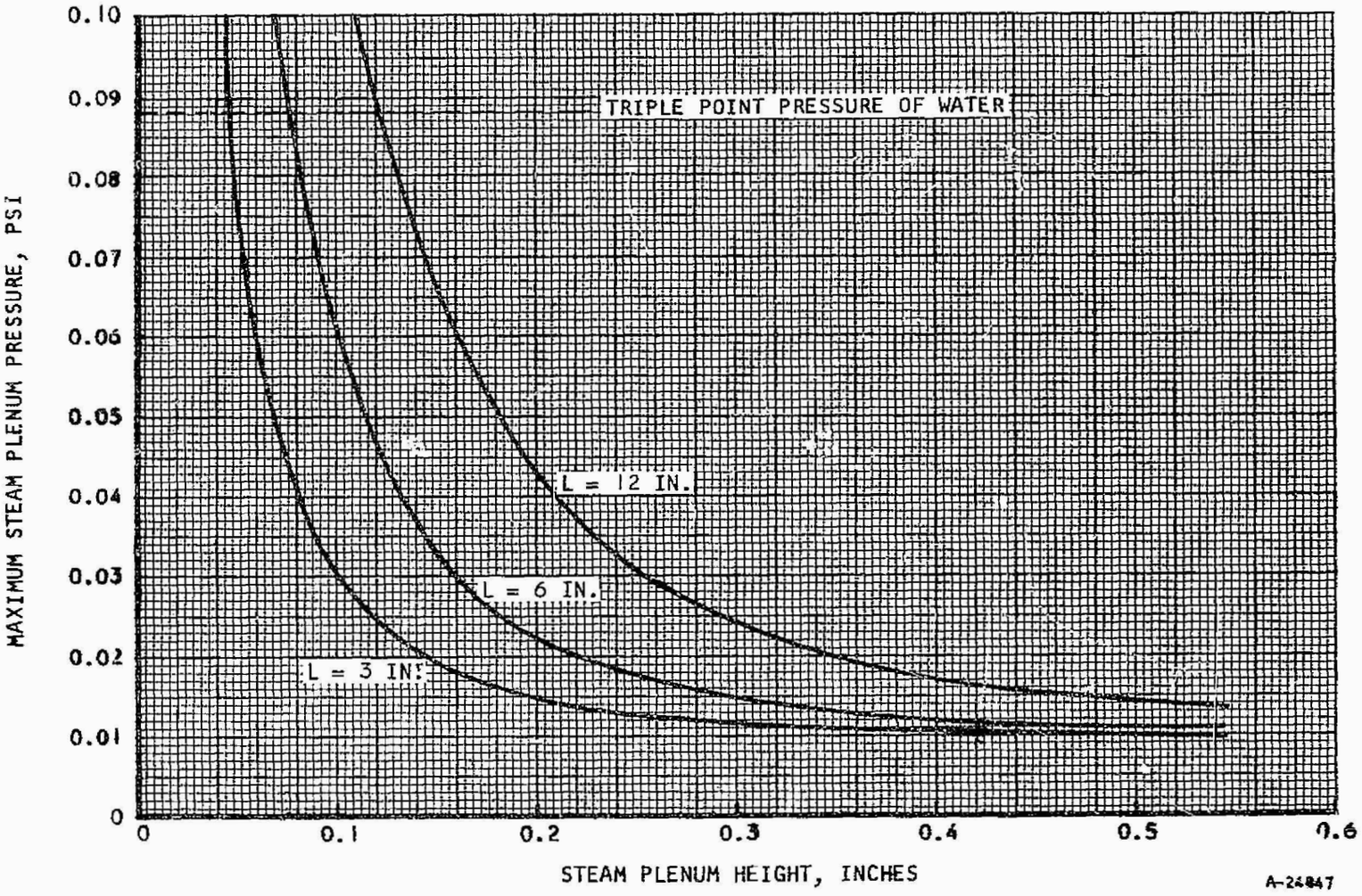

Figure 3-5. Maximum Plenum Pressure In Typical Sublimator

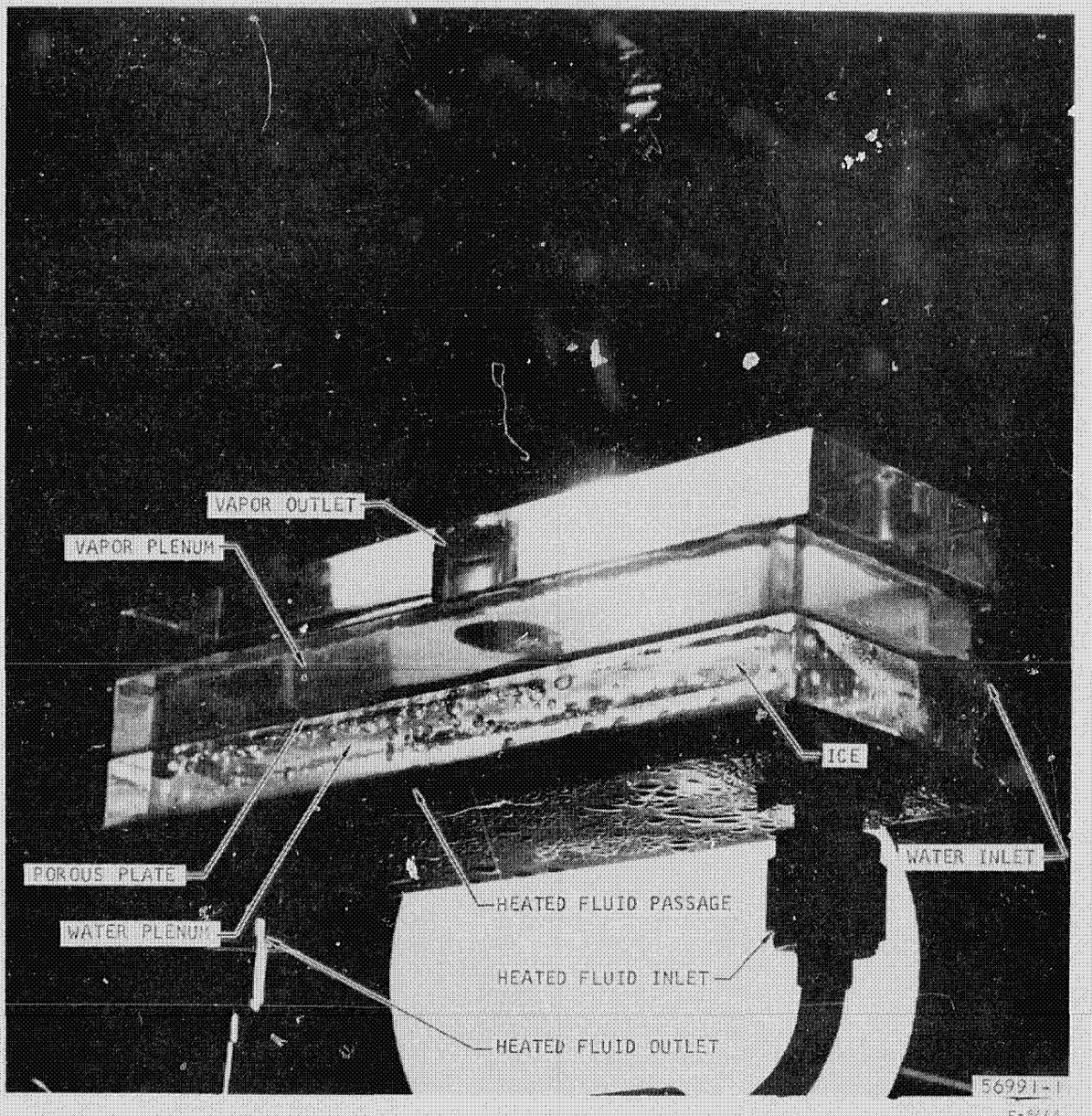

Figure 3-6. Sublimator Visualization Test Module

A schematic and photograph of the test setup are shown in Figures 3-7 and 3-8. As indicated, the water was filtered and metered before entering the water plenum. A measurable heat load was provided by passing a heated fluid through a finned passage and recording inlet and outlet temperatures. Pressures were measured at the point of water supply, in the water plenum, and in the vapor plenum. A bypass of the filter was provided in order that the flow might be reversed without destroying the filter.

Several interesting and noteworthy phenomena were observed. When the unit was run with no heat load, a layer of ice formed over the entire bottom of the plate except along the edges of the unit. (The lack of ice next to the lucite sides was due to heat leaking through from the surroundings.)

Observation of the ice layer on the water passage side revealed a light colored surface, frosty in appearance, at the ice-porous plate interface. Intermittently, portions of these light areas became darkened and when this occurred, small "fingers" of ice appeared at corresponding areas on top of the porous plate. This change in color always proceeded from the edge of the ice layer or from an already darkened area. It is thought that the light areas are small spaces between the ice and the porous plate, formed when the ice sublimes and passes through the plate as vapor. When this space becomes sufficiently large, water rushes in, causing the darkened appearance, and some of the water passes completely through the plate, forming the "ice fingers" at the surface. This ice "breakthrough" occurred over only those portions of the plate which were covered with ice on the water side.

When the plate area covered by ice was reduced by increasing the heat load to the system, this intermittent breakthrough phenomenon continued over that area of the plate covered with ice but ceased to occur over areas covered with liquid water and no visible ice. Increased heat load resulted in the elimination of all visible ice and along with it, elimination of the formation of the "ice fingers" on the low-pressure side. At this point the pressure on the downstream side of the porous plate was increased while maintaining constant all other system variables; profuse water breakthrough occurred when the pressure reached the triple point pressure.

This significant fact indicates that there is ice in the pores which melts when the pressure goes above the triple point, allowing water to break through. The indication of ice existing in the pores when there is no ice visible on the bottom of the plate is an important one, for it implies a cycling mechanism in which the ice-vapor interface recedes and reforms due to either the ice melting or the interface receding all the way out of the pore and water rushing in.

The mechanism which is thought to be that which occurs in a porous plate in a sublimator is shown in Figure 3-9. In Sketch (a), liquid enters the pore. Originally it was thought that the liquid was restrained at the pore exit by surface tension forces, however, the breakthrough analysis indicated that this is possible only for minute water pressures or for hydrophobic surfaces. Therefore the liquid is not restrained until ice is formed.

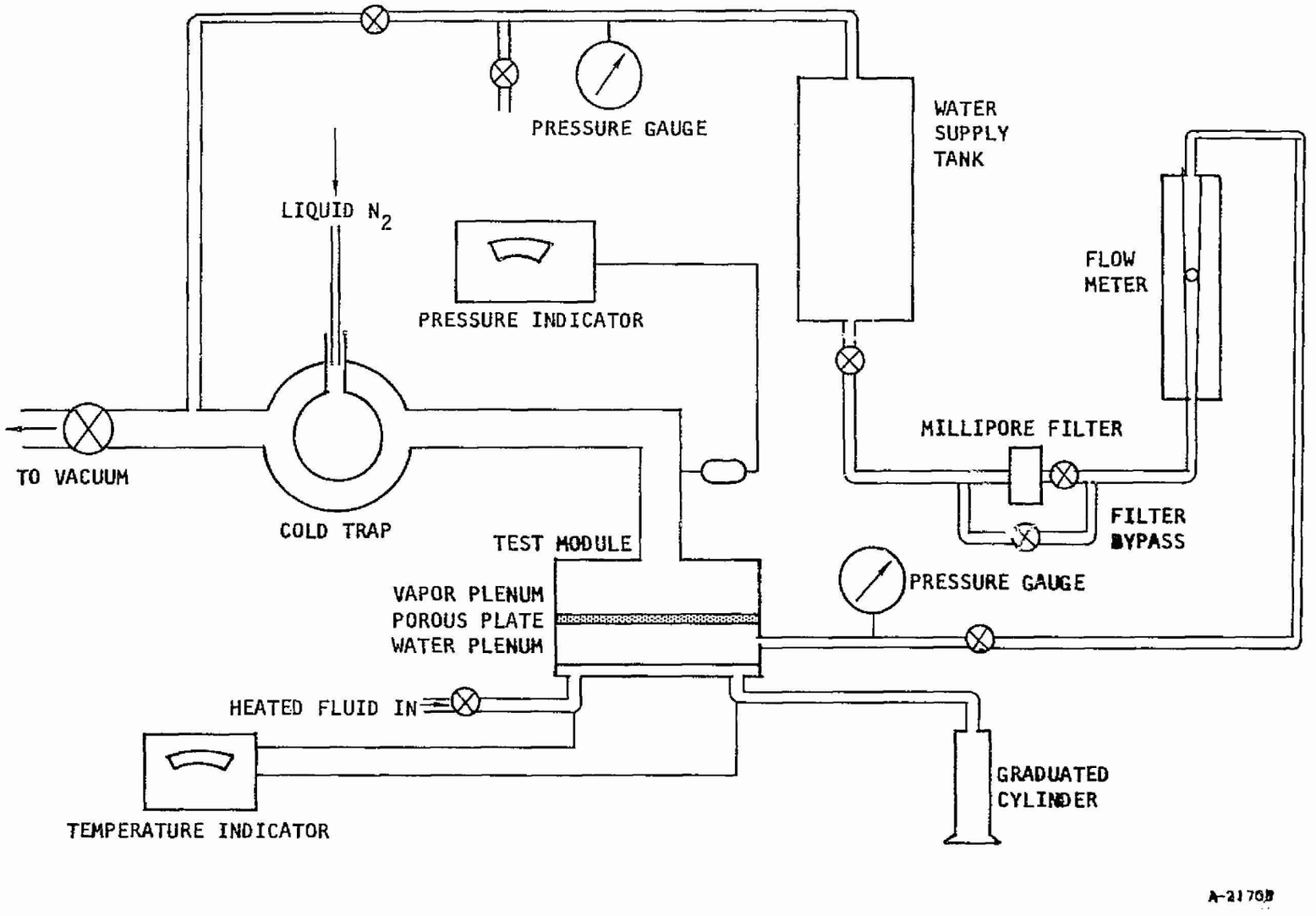

Figure 3-7. Schematic of Sublimation Test System

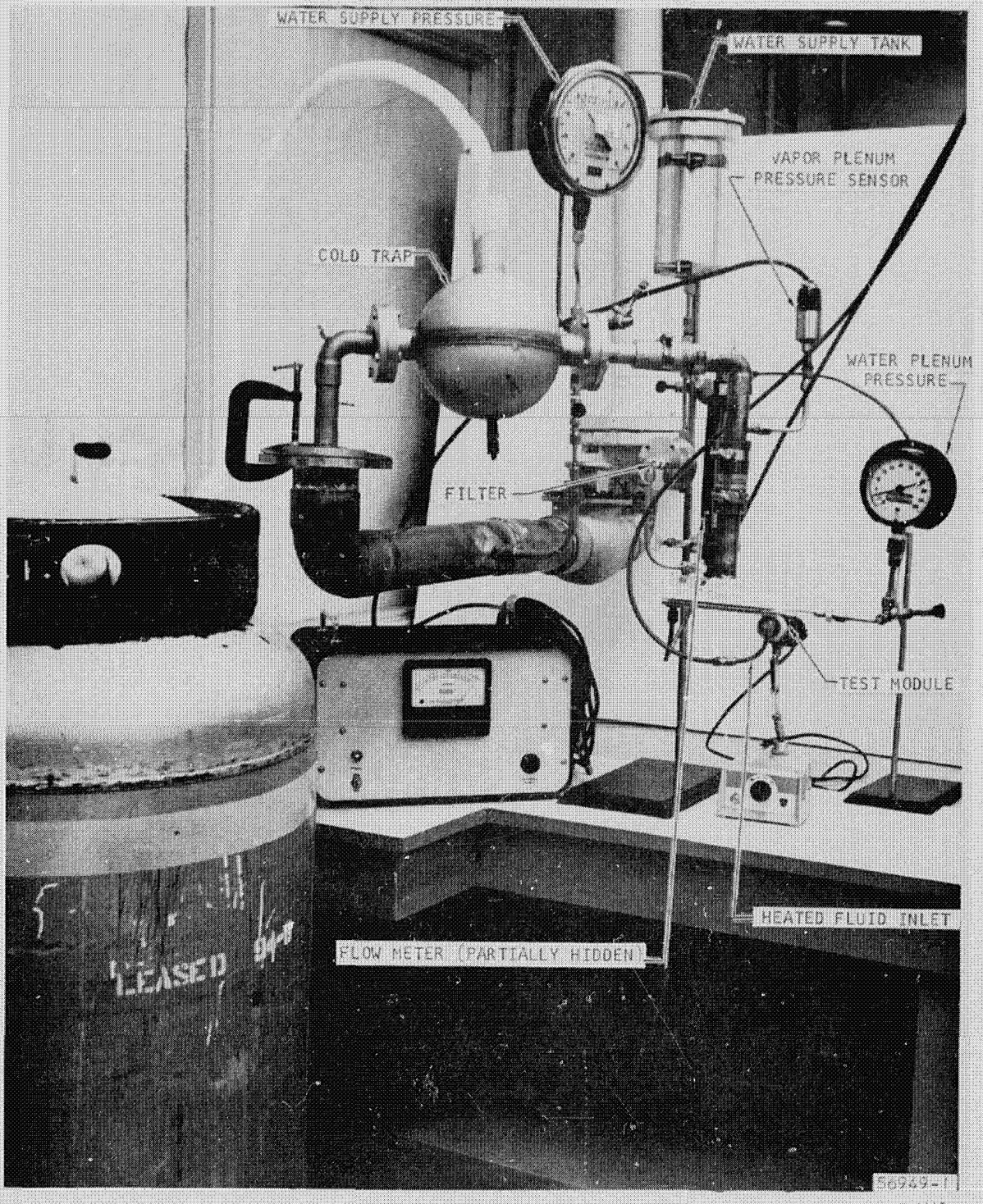

Figure 3-8. Sublimation Test System

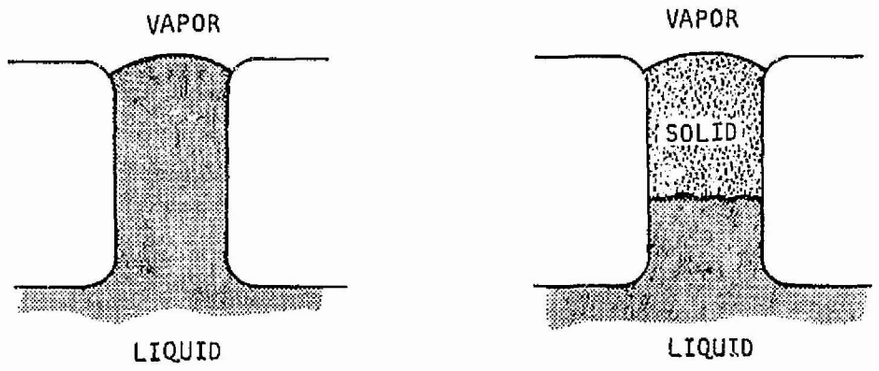

NOTE: Vertical scale has been greatly reduced. Actual length to diameter ratio is of the order 100.

A-21712

Figure 3-9. Possible Sublimation Mechanism When Solid Phase is not Visible on Liquid Side of Plate

Sketch (b) shows solid forming rapidly in the pore as the liquid is exposed to the very low pressure. In Sketches (c) and (d) the solid phase has sublimed, causing the solid-vapor interface to recede further into the plate and also raising the absolute pressure at the interface. At this point it is thought that one of two things happens. Either the solid-vapor interface recedes until all the solid phase has sublimed or the interface pressure increases above the triple point and the solid melts, either of which would allow liquid to reenter the pore (Sketch (e)) causing the cycle to repeat.

POROUS PLATE INVESTIGATION

General

It is well known that the operational characteristics of a sublimator are a strong function of the porous plate which is used in the unit. Optimization of a sublimator therefore includes sllection of an optimum porous plate and an investigation of porous plates is required in order to make such a choice. The investigation performed during this program included simple bench tests to describe the plate characteristics themselves and single module sublimator tests to determine the plates sublimation characteristics.

The majority of plates tested were of sintered metal powder construction as supplied by Clevite, Lockheed, APM and Union Carbide. A limited number of sintered woven wire mesh, porous Teflon and Kel-F, and electro-formed mesh samples were tested. (A list of the plates tested and the type of construction is given in Appendix C.) A few plates coated with Teflon were also tested.

Bench Tests

In order to define the porous plates to be used in sublimator testing and to obtain plate characteristics with which the porous plate sublimation performance could be correlated, a series of bench tests were performed on sample plates. Bubble point in alcohol, water retention pressure, nitrogen permeability to vacuum, and nitrogen permeability to ambient were performed. The results of these tests are tabulated in Appendix C. The majority of plates tested were of sintered particle construction and were obtained from Lockheed (L designation), Clevite (C designation), and Union Carbide (UC designation). As indicated, all of these plates are nickel, ranging in thickness from 0.015 to 0.056 in. Porosities ranged from the smallest of 32 percent for one of the Union Carbide samples to 56.7 percent for a Clevite sample. All the specimens are of sintered particle construction, and Samples C1, C2, and C6 contain a 20 by 20 mesh, 0.007 in. dia wire nickel reinforcement screen. At different times during the program, bubble point data were obtained for the same plate or for plates of the same designation in the same batch. All these data are presented in tables C-1 and C-2, and the pore diameter based upon the average alcohol bubble point is given. The Lockheed plates appear to have the smallest maximum pore diameters, about 2.5 microns, with approximately 80 percent of the pores larger than 1.5 microns. It will be shown below that these plates are the least permeable of all the "L", "C", and "UC" plates tested. The Clevite plates have the largest pores of those tested in this series, from 6 to 8 microns. The Union Carbide plates have more of a spread in maximum equivalent pore diameter, from 2.82 to 6.90 microns, with the 80 percent pore diameters equal to from 57 to 76 percent of the maximum diameters. The other plates tested exhibited a wider range in maximum pore size, from 3 microns to 128 microns.

Permeability data were also obtained for the porous plates, one series with nitrogen discharge to ambient, the other with nitrogen discharge to vacuum (0.093 mm Hg abs to 1.42 mm Hg abs). The results of these tests are shown in

Appendix C. It is seen that just as in pore size, the "L" and "C" series tend to be bunched while the "UC" series is spread over a range. The APM plates were the least permeable and the BM5 plate the most permeable of all plates tested.

Table C-2 shows the bubble point is water and water retetion pressure data obtained. In general the water bubble point pressure is significantly higher than that obtained with alcohol. This is due to the higher surface tension of water. The water retention pressure is in general quite small, and, as was pointed out in the breakthrough analysis this is due to the low contact angle and rounded pore exits.

The opposite trends are evident for the hydrophobic plates (large contact angle). For the Teflon and Kel-F plates the water retention pressure is greater than the bubble point (gas breakthrough) pressure due to the large contact angle as predicted by Figure 3-1. The water retention pressure was increased substantially for the nickel plates with a teflon coating.

Single Module Tests

In order to determine the performance of the sample porous plates and to establish their characteristics in the various modes of operation of a sublimator, a series of tests were performed on single modules. Tests were performed to define the maximum heat flux attainable, steady-state characteristics, operation at startup, restart characteristics, and the effect of freezing or operation at zero heat load. The single porous plate test module consisted of a heat source, a water passage and a porous plate. The heat source was an electrical heater so that precise control of the input heat flux could be maintained. The unit was instrumented with 6 thermocouples in the heater plate and one at the water inlet, and continuous temperature readout was provided. The porous plate module installed in the test rig is shown in Figure 3-10. For some of the thinner porous plate specimens, it was necessary to attach additional cross bar supports to prevent the plates from bowing as shown in the photograph. Not shown, but important to prevent heat losses, were the layers of aluminized mylar placed on the bottom of the module next to the heater plate. A photograph of the test setup is shown in Figure 3-11. The electrically heated test modules were enclosed in a vacuum chamber in order to maintain the vapor pressure below the triple point. Heat flux was controlled by a variac, and voltage and current were indicated on appropriate meters. Water from the supply tank was filtered through a $1/2\mu$ absolute filter and metered before entering the sublimator module.

1. Steady State Performance and Maximum Heat Flux

Initial tests were performed to determine the heat rejection capability of various plates and the maximum heat flux attainable before breakthrough. In some cases the water plenum was a .100 in. gap with a nickel conduction fin in it and in others a .012 in. high water gap. Plots of the heater temperature as a function of heat flux are shown in Appendix C. Plates from Union Carbide, Lockheed, Clevite, Aircraft Porous Media, and Buckbee Mears

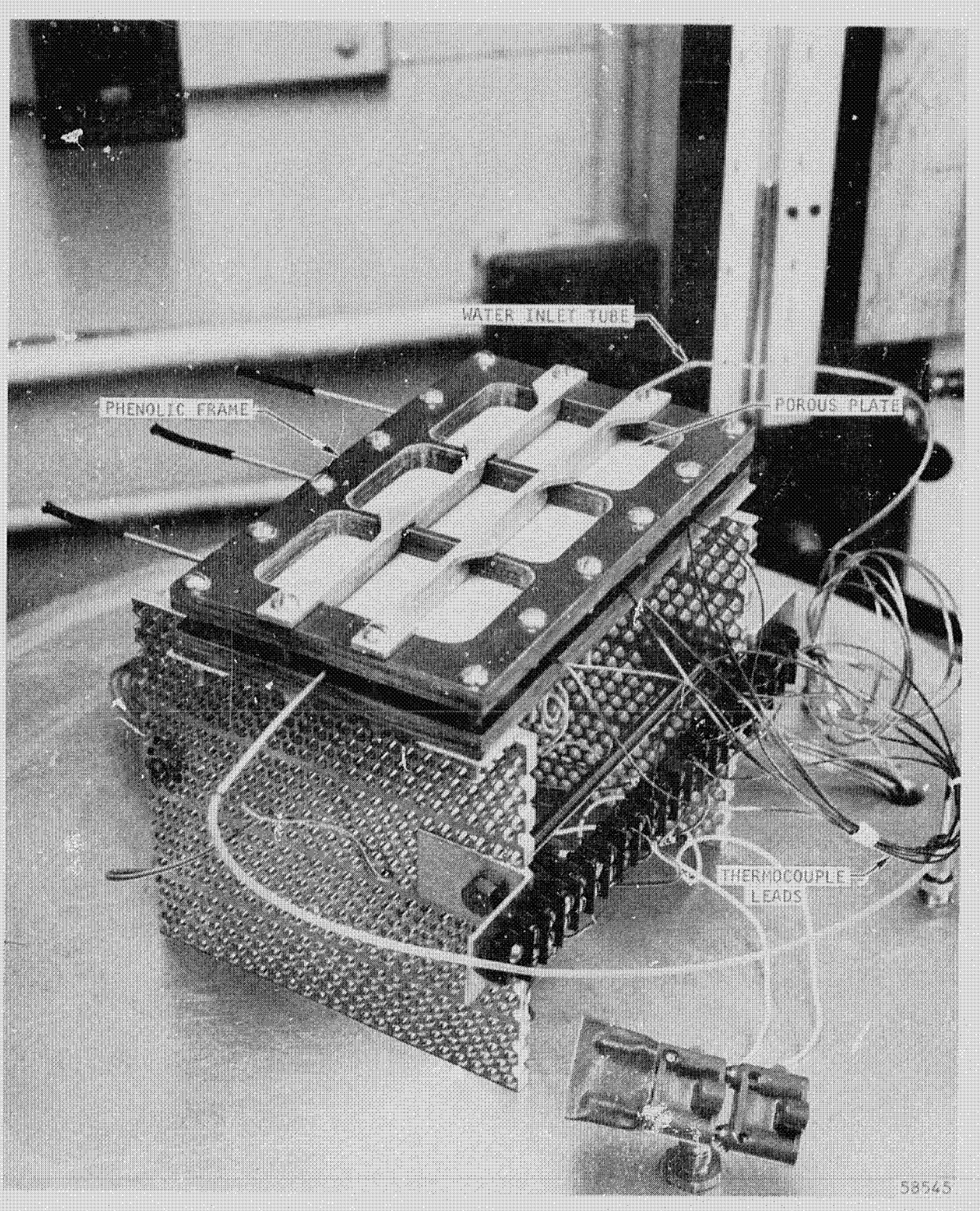

Figure 3-10. Sublimator Test Moduel

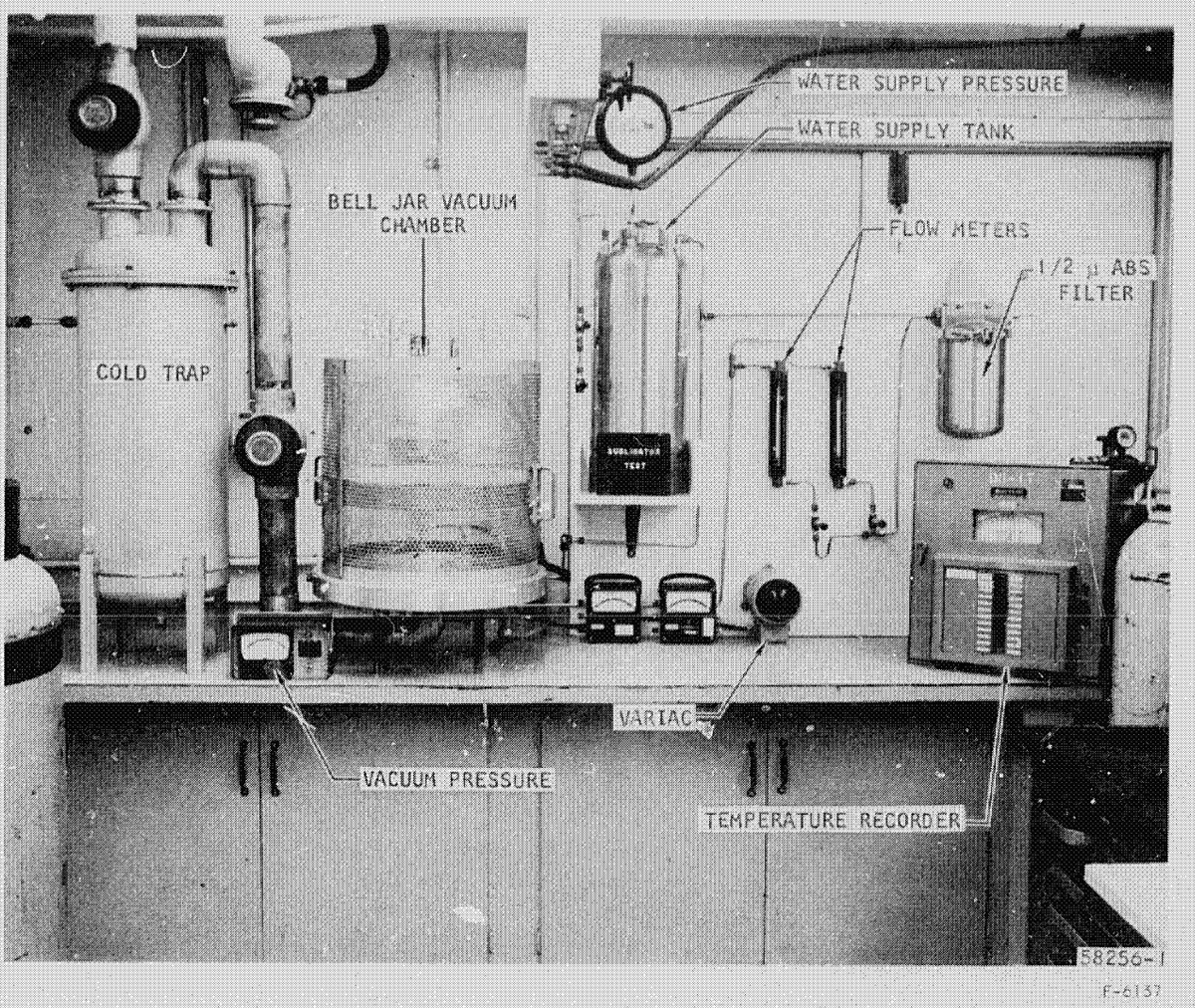

Figure 3-11. Sublimator Performance Test Setup

were tested with the finned water gap configuration. With all these plates it was possible to establish equilibrium operating conditions with heat fluxes of 3500 Btu/hr ft^2 or more. There are two criteria by which the porous plates might be compared on a steady state basis. These are the heater temperature at a given heat flux and the heat flux at which liquid breakthrough begins or becomes uncontrolled. As shown in Table 3-3, of the 25 plates tested at a feed pressure of 3 psi, 9 experienced no uncontrolled breakthrough up to a heat flux of 10,000, 12 failed at 10,000, 3 at 7300 and 1 at 5500. Minor breakthrough occurred at 2000 Btu/hr ft^2 for 1 plate, at 5500 for 3 plates, at 7300 for 7 plates, at 10,000 for 8 plates and did not occur at all for 6 plates. From this data it is evident that a major portion of the plates tested would be suitable for a sublimator application, at least from the standpoint of maximum heat flux attainable before uncontrolled breakthrough.

At the outset it was hoped that the performance of the porous plates could be correlated on the basis of some easily measurable property of the plates such as bubble point or permeability. This was not possible for the breakthrough phenomenon.

The other method of comparing the plates is to compare the heater temperatures required to establish a given heat flux. It is advantageous to have this temperature as low as possible for this means a smaller porous plate area is required to dissipate a given heat rate. It is noted from the plots in Appendix C that, for instance, all the plates but the one Buckbee Mears sample, gave heater temperatures from 46 to 58°F at a heat flux of 5500 Btu/hr ft^2. The plates which give the lower temperature are, of course, better selections for sublimator plates. There does appear to be some correlation between the plates which give the lowest heater temperature and those which have the highest breakthrough heat flux. The average heater temperature at a heat flux of 5500 for the plates which did not experience uncontrolled breakthrough was 47.8°F, 51.6°F for those that broke through at 10,000, and 53.7°F for those that failed at 7,300. Selection of a plate which has a high breakthrough heat flux is therefore compatible with selection of plate with good heat transfer characteristics.

Also given in Appendix C are the results of porous plate tests conducted with a 0.12 in. water gap with no fins in the water plenum. This configuration was tested because of the potential of using this concept to eliminate problems associated with freezing of the unit during zero heat load operation. Tests were performed at feed water pressures of 3, 6, and 9 psia to determine the effect of this variable on performance. From the data it can be seen that in general the heater temperature decreases with higher feed pressures. Also, as indicated by Table 3-4, the uncontrolled breakthrough heat flux decreases with increasing pressure. It should also be noted that the breakthrough heat fluxes at 3 psia for the .012 gap are compatible with those at 3 psia for the .100 gap with fins, indicating that the plenum configuration may have little if any effect on the breakthrough.

TABLE 3-3

SUMMARY OF HEAT FLUX BREAKTHROUGH PERFORMANCE OF PLATES
TESTED WITH 0.10 IN. HIGH FINNED WATER PASSAGE AND 3 PSIA FEED PRESSURE

Plate	Heat Flux for Uncontrolled Breakthrough	Heat Flux for Minor Breakthrough
UC-1A	10,000 Btu/hr ft^2	5,500 Btu/hr ft^2
1B	7,300	5,500
1C	7,300	5,500
2A	>10,000	10,000
2B	>10,000	10,000
2C	>10,000	>10,000
3A	7,300	7,300
3B	10,000	7,300
3C	10,000	10,000
4A	10,000	10,000
4B	>10,000	>10,000
4C	>10,000	>10,000
L1A	10,000	7,300
2A	>10,000	10,000
3A	10,000	7,300
4A	10,000	7,300
5A	10,000	7,300
C2	>10,000	>10,000
3	10,000	10,000
4	>10,000	>10,000
5	10,000	10,000
6	>10,000	>10,000
APM34	10,000	10,000
35	10,000	7,300
BM5	5,500	2,000

TABLE 3-4

UNCONTROLLED BREAKTHROUGH HEAT FLUX FOR .012 GAP

Plate	3 psia	6 psia	9 psia
UC-2B-5	12,300	10,000	7,300
UC-4B-5	12,300	10,000	7,300
UC-4C-6	None	7,300 10,000	7,300 7,300
UC-2C-4	10,000	10,000	10,000
UC-2A-3	10,000	7,300	--
Clevite VI	10,000	--	--

2. Start-up Testing

A conventional sublimator depends upon the existence of ice in the pores of the porous plate in order to prevent water breakthrough for feed pressures above the water retention pressure. Testing has indicated that while a plate may operate in a steady state condition with a feedwater pressure on the order of 9 psia, it may be impossible to achieve start-up with this pressure without breakthrough occurring. For this reason, start-up characteristics were investigated in order to define system start-up limits. A series of start-up tests were performed on single module porous plates of varying pore size and permeability. The plates tested ranged from 0.020 to 0.028 in. thickness and had a subliming surface area of about 18 square in. The test module and test setup used were those shown in Figures 3-10 and 3-11. Heater temperature and water plenum pressure were sensed and recorded. The test module was mounted in a vacuum chamber and the pressure reduced to about 200 microns of mercury absolute. The heater was turned on and the heat flux set at 2,000 Btu/hr ft^2, and when the heater temperature reached 80^0F the water inlet valve was opened. Observations were made as to the severity of breakthrough. Water inlet flow rates of 100, 40 and 20 cc per minute were used. A summary of the start-up data is given in Tables 3-5, 3-6 and 3-7. Permeability and bubble point data are shown along with the type of breakthrough at various feedwater pressures and fill rates. "Minor" and "serious" breakthrough refer to the relative amounts of ice formed on the top of the plate. The time for healing refers to the time at which the plate ceased to form ice on the downstream face. The ice that had formed there sublimed away in time. The plates are arranged in order of increasing permeability which corresponds in general to decreasing bubble point which means increasing pore size.

Table 3-5 gives results for 5 plates tested at pressures of from 3 to 9 psia and at an inlet flow rate of 100 cc/min. The plates tested were chosen because they gave a range in permeability and because they all performed well

TABLE 3-5

SINGLE MODULE START-UP DATA

Plate	ΔP at 2 lb/hr ft² N_2 Flow, psi	Bubble Point in Alcohol		Type of Breakthrough at Given Feedwater Pressure			
		Initial psi	80 Percent, psi	3 psia	4.5 psia	6 psia	9 psia
UC-2C-8	0.57	4.60	7.68	None	Minor, healed in 1.5 min.	Serious, healed in 3 min.	Uncontrolled
UC-4C-1	0.53	3.52	5.99	None	Minor, healed in 1 min.	Serious, healed in 1 min.	Serious, healed in 4 min.
UC-4B-1	0.34	3.10	4.36	Very minor, healed immediately	Very minor, healed immediately	Serious, healed in 2 min. Serious, healed in 5 min.	Uncontrolled
UC-2B-1	0.25	3.56	4.81	Minor, healed in 1 min.	Uncontrolled	Uncontrolled	Uncontrolled
UC-2A-1	0.15	1.81	3.07	Uncontrolled	--	Uncontrolled	Uncontrolled

TABLE 3-6

START-UP DATA AT VARIOUS FEED PRESSURES AND FLOW RATES
FOR A 0.012 INCH HIGH WATER PLENUM

Plate	100 cc/min			40 cc/ min			20 cc/min		
	3 psi	6 psi	9 psi	3 psi	6 psi	9 psi	3 psi	6 psi	9 psi
UC-2C-4	0	S2*	U	0	VM2	VM2	0	0	0
UC-4C-6	0	M2.5	S2	0	0	0	0	0	0
UC-4B-5	0	M.5	U	0	VMO	S.5	0	0	0
UC-2B-5	VM.5	M.8	U	0	VMO	S3	0	0	0
UC-2A-3	0	MO	U	0	M2	S2	0	VM2	0

TABLE 3-7

START-UP DATA AT VARIOUS FEED PRESSURES AND FLOW RATES
FOR A 0.100 INCH HIGH FINNED WATER PLENUM

Plate	100 cc/min				40 cc/min			20 cc/min		
	3 psi	4.5 psi	6 psi	9 psi	3 psi	6 psi	9 psi	3 psi	6 psi	9 psi
UC-2C-9	0	0	0	M.8	VM.2	VM.3	VM.3	0	0	VMO
UC-4C-4	0	0	MO	MI	0	0	VM 0	0	0	0
UC-4B-3					VM 0	VM.3	VM.5	0	0	0
UC-2B-4	M.I	M.75	U	U	VM.2	VM.3	VM.5	0	0	VMO
UC-2A-4	0	MI	U	U	VM.2	VM.3	VM.3	0	0	VMO

Note.
VM-very minor breakthrough
M -minor breakthrough
U - uncontrolled breakthrough
S - serious breakthrough

*The numbers appearing in the tables refer to the time required for healing in minutes. For example, S2 means serious breakthrough which healed in 2 minutes.

in the steady state and maximum heat flux tests. Two trends are evident. The first is an increased tendency to break through with increasing feedwater pressure, an expected characteristic. The second indicates an increased breakthrough tendency for larger pore sizes (lower bubble point).

Table 3-6 shows the start-up characteristics of plates tested with .012 in. thick water plenum with no fins at 3 inlet flow rates and 3 feedwater pressures. Again there was increased uncontrolled breakthrough at higher feedpressures, however the increasing breakthrough tendencies for the plates with larger pores were not so evident as in the previous tests. The effect of decreasing the feedwater flow rate is quite evident. As the flow rate was decreased the breakthrough became less severe and at an inlet water feed rate of 20 cc/min, successful start-up with no breakthrough was achieved with essentially all plates.

Table 3-7 shows results for the same tests performed with the finned water passage. Here again are evident the effects of increasing pressure and increasing pore size. Again start-up is improved by decreasing the plenum fill rate and at 20 cc/min successful start-up with only very minor self-healing breakthrough was achieved for all plates. Comparison of Tables 3-6 and 3-7 indicates that the plenum configuration has little effect on the start-up characteristics.

3. Restart Testing

One method of controlling a sublimator to prevent freezing damage at zero heat load is to monitor the heat load and turn off the water supply when the heat load becomes small. When the heat load is reapplied, the water supply will be turned on and the unit must restart from a completely or partially dry condition in the water plenum. Tests were performed to determine the restart characteristics of various porous plates. The single module test rig was used, and the water plenum configuration was the .100 in. gap with a fin. Equilibrium conditions were established at a heat flux which gave a heater temperature of 60°F. The water feed was turned off, and the heat flux monitored to maintain a heater temperature of approximately 60°F. When the steam plenum pressure dropped off sharply, it was evident the plate was almost dry. The time required for this condition to exist was very nearly equal to the predicted time to sublime the volume of water in the plenum. Two restart conditions were explored. The feedwater valve was opened again at a flow rate of 100 cc/min when the plenum was almost dry and at half the time required to dry the plenum or when it was half dry. The severity of breakthrough was recorded and the results are shown in Table 3-8. Essentially no difference was noted for the two cases. The results were quite similar to the dry plate start-up tests with the same inlet flow rate and plenum configurations with similar dependence on pore size and feedpressure. The data indicate that there is essentially no difference between start-up with a dry plenum and restarting with a partially wet plenum.

TABLE 3-8

RESTART CHARACTERISTICS AT VARIOUS FEED PRESSURES, TWO PLENUM WETNESS CONDITIONS, AND WATER FEED RATE OF 100 CC/MIN FOR A .100 INCH HIGH WATER PLENUM

Plate	Plenum Almost Dry				Plenum Approximately Half Dry			
	3 psi	4.5 psi	6 psi	9 psi	3 psi	4.5 psi	6 psi	9 psi
UC-2C-9		0	0	M.5	0	0	0	0
UC-4C-4		0	0	M 0	0	0	0	MO
UC-4B-3	-	-	-	-	-	-	-	-
UC-2B-4	0	M.2	U	U	0	VMO	U	U
UC-2A-4	0	M.5	U	U	0	M.8	U	U

4. Freeze-Thaw Cycle Testing

A design requirement for thermal conditioning systems is that they be able to operate intermittently. If the heat load to a sublimator is turned off and the unit is maintained in this quiescent state for an extended time, the water in the water plenum freezes, and the accompany expansion may destroy the unit. Methods of designing around this problem may be: (1) maintaining a low heat load on the unit at all times, (2) limiting the duration of the no heat load condition, or (3) turning off the feedwater when the heat load is removed or reduced and allowing the residual heat load to sublime sufficient water to prevent expansion. The first two of these alternatives in effect violate the quiescent operation requirement for they do not allow an indefinite zero heat load condition. The third method appears to be a reasonable alternative; however it does require additional valves and sensing equipment, complicating the system and reducing reliability.

Another alternative was investigated with single modules. The approach is to limit to a small value the linear expansion in the water plenum by reducing the height of the water passage to about 0.010 in. and allowing the water to freeze completely. The 10 percent volume expansion due to freezing expands the passage 0.001 in. in this case, wherease with a 0.100 in. passage the expansion would be 0.010 in. Testing has indicated that the porous plate is flexible enough to allow repeated freeze-thaw cycles with a low water passage, but with a high passage the plate will rupture. Four plates were tested with different passage configurations summarized in Table 3-9. The test procedure in all cases involved initially establishing normal operation of a single module sublimator and then terminating heat load. When the temperature of the heated surface dropped below 32°F it was assured that the water passage was completely frozen. Heat was then reapplied to melt the ice, and to assure this, the pressure in the steam plenum was raised above

TABLE 3-9

FREEZE-THAW CYCLE TESTING

PLATE	WATER PLENUM CONFIGURATION	NUMBER OF FREEZE-THAW CYCLES	DAMAGE
UC-2C-6	A	5	MINOR PLATE BUCKLING AND SURFACE CRACK
UC-2A	A	1	RUPTURED
UC-2B-5	B	10	SLIGHT DEFORMATION
		25	BUCKLING
		100	SEVERE BUCKLING
UC-2B-4	C	100	NONE

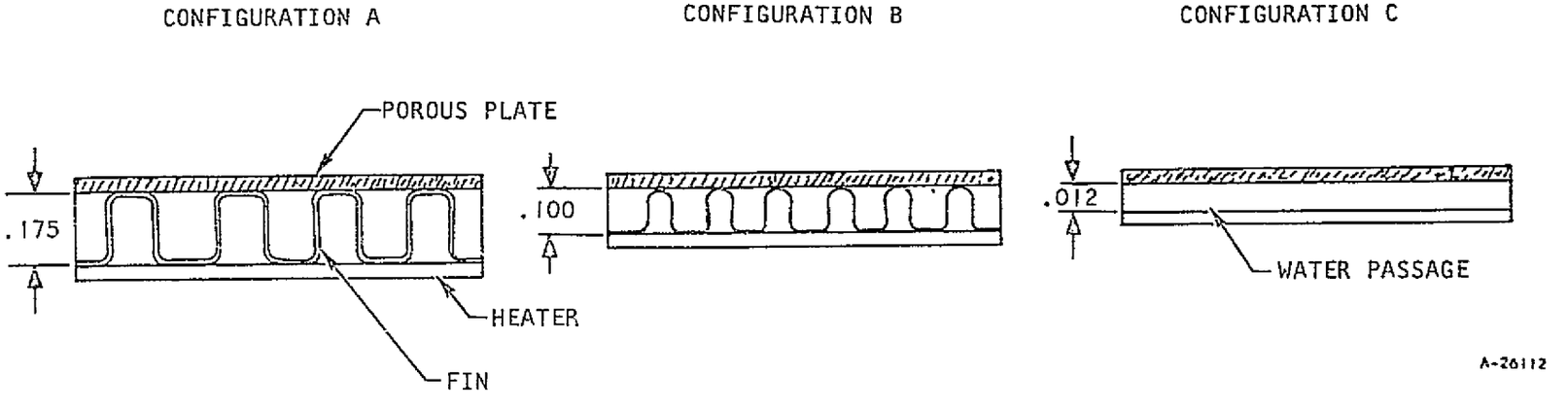

the triple point initiating water breakthrough and precluding the existence of ice. The heat load was again removed and the cycle repeated.

Two plates were tested in Configuration A, the .175 high water gap with fin. Plate UC-2C-6 showed minor buckling and developed a surface crack after 5 cycles, and plate UC-2A cracked severely after one cycle. The damaged plates tested in this configuration are shown in Figure 3-12. Configuration B was similar to A; however the passage height was reduced to 0.100 inch. The plate tested showed severe buckling after 100 cycles (it had deformed .070 inch); however no degradation in bubble point was detected. The third configuration incorporated a .012 in. water passage and the plate run in this configuration exhibited no visible damager after 100 freeze-thaw cycles. This plate was also checked for microscopic damage by performing a bubble point test every 10 cycles, and no decrease in bubble point was detected.

The tests have shown this method to be successful in eliminating plate damage due to freezing. Therefore, this design was used in the multi-porous plate sublimator module construction.

5. Hydrophobic Coatings

It is noted from Figure 3-1 that the liquid breakthrough pressure increases with increasing contact angle. (Two types of liquid breakthrough are discussed in this report. One is that which occurs when the surface tension forces are not sufficient to balance the pressure forces applied to a liquid on one side of a porous plate. The other is that which occurs in a sublimator when sufficient ice is not available in the pores to form a barrier to the liquid. The former type may also occur in a conventional sublimator operating above the triple point (really a force-fed evaporator) if the feed pressure is very near the sink pressure. The liquid breakthrough pressure discussed in the development of Figure 3-1 is, of course, the former type since it deals with surface tension and contact angle. The second type is that discussed in the sections describing start-up, restart, and maximum heat flux characteristics.) Even though conventional porous plates have quite small pores, their liquid retention pressures are low because of the relatively low contact angles and dull pore exits. If, however, plates with large contact angles are developed, larger breakthrough pressures will result, and the dependence upon ice in the pores to prevent failure is eliminated.

There are two approaches to developing this concept for improving sublimator design and operation. One is to use a plate made from a hydrophobic material (one with which water has a large contact angle), and the other is to apply a hydrophobic coating to a conventional porous plate. The latter approach is probably more feasible because of pressure drop considerations. If the entire plate is hydrophobic, the water will be restrained at the upstream face of the plate and phase change will occur there. The resulting vapor pressure drop through the porous plate will raise the pressure above the triple point, thereby increasing the sink temperature and decreasing the heat rejection capability. A hydrophobic coating applied to the downstream face of the plate will restrain the water near the downstream face, provided

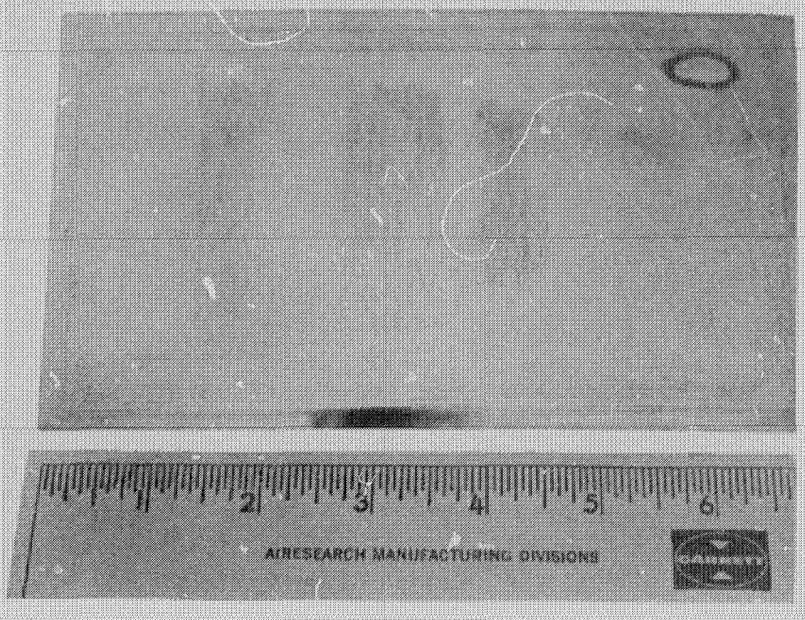

PLATE UC-1C-6

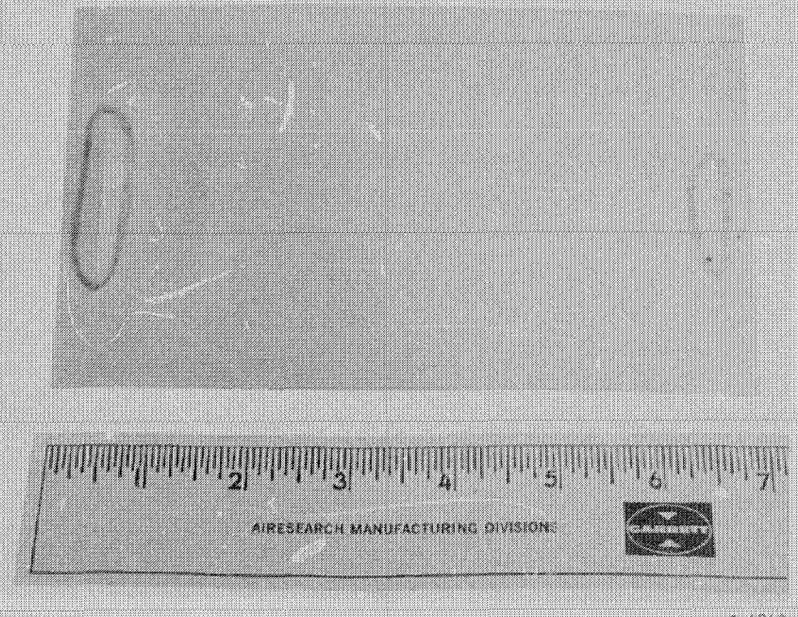

F-6942

PLATE UC-2A

Figure 3-12. Freeze-Thaw Damage to Plates Tested in Configuration A

the coating penetrates to a small depth. Phase change now occurs at the downstream face, and the pressure drop is significantly less since the vapor flow length has been reduced.

Tests were performed to determine experimentally the magnitudes of the effects of hydrophobic coatings on the water retention pressure and permeability of porous plates. A porous plate which performed well in the single module sublimator tests was selected, cut into four sections, and tested for bubble point in water, permeability with vacuum discharge, and water retention pressure.

The plates were then sprayed with a Teflon coating and heated to fuse the coating to the base porous plate. Different spray times and heating temperatures as shown below were employed to determine the effect of these variables.

Plate	Time of Spray Seconds	Heat Treatment °F	Length of Treatment Minutes
1	2	750	10
2	4	750	10
3	2	550	10
4	4	550	10

The coated plates were retested for water retention pressure and permeability, and as predicted, the water retention pressure increased markedly; pressures of 7.8, 10.0, 6.9 and 11.2 psi were obtained for plates 1, 2, 3, and 4 respectively. Plate characteristics before and after coating are shown below.

Plate	Thickness Inches	Bubble Point in H_2O	Water Retention Pressure Before Coating	Water Retention Pressure After Coating
		psi	psi	psi
1	.020	>12.3	.57	7.8
2	.020	>12.3	.54	10.0
3	.020	>12.3	.59	6.9
4	.020	>12.3	.57	11.2

Figure 3-13 shows the permeability of the plates before and after treatment. As indicated, the permeability pf plates 2, 3, and 4 was reduced while that of plate 1 remained essentially unchanged. It appears that the longer spray

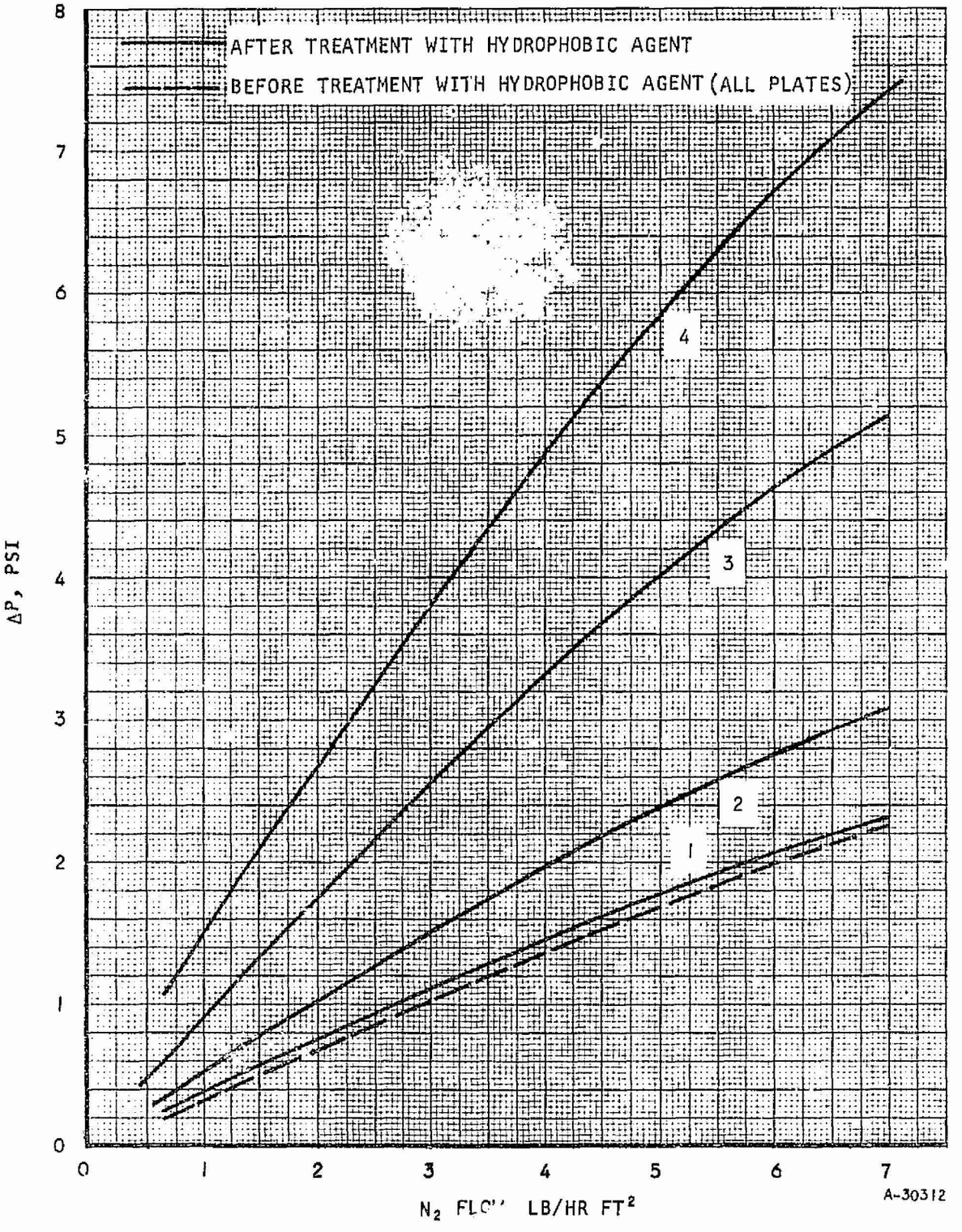

Figure 3-13. Nitrogen Permeability with Discharge to Vacuum Before and After Application of a Hydrophobic Coating

times gave higher water retention pressures while the higher curing temperature gave less permeability reduction. These data indicate therefore that with a suitable coating, the water retention pressure may be increased to the desired level without reducing the permeability of the plate significantly.

MULTI-POROUS PLATE SUBLIMATOR MODULE

General

A multi-porous plate sublimator module was designed, constructed and tested in order that data might be obtained on the performance of a complete unit. The design involved porous plate selection, feedwater plenum design, heat transport fluid passage design, and steam plenum design, as related to operating heat load, maximum heat flux attainable without breakthrough, prevention of freezing damage at zero heat load operation, and maintenance of a pressure sufficiently below the triple point.

Sublimator Design

The selection of a porous plate for a sublimator must be made to a large extent on an emperical basis. This is due to the fact that the sublimation mechanism which occurs inside the individual pores has not been completely defined quantitatively for the irregular passages and undefined geometries of the plates used in current sublimators.

It is well known that as the heat flux across a porous plate is increased, a point is reached at which liquid breakthrough occurs, causing failure of the unit. This breakthrough is due to the elimination of ice within the individual pores, ice which had been restraining the liquid in the feedwater plenum. Data defining this heat flux limit for various porous plates obtained from several vendors was given above in the single module test results. Obviously a plate which has a high breakthrough heat flux should be chosen for use in a sublimator. Plates from the UC-2C series were chosen for use in this sublimator, and it is seen from Table 3-3 that this series experienced no breakthrough to a heat flux of greater than 10,000 Btu/hr ft^2.

Other considerations which must be taken into account in selection of a porous plate are its performance at start-up and restart, and its steady state operation characteristics. As was indicated in the discussion of the single module porous plate tests, the UC-2C series performed among the best of all the plates tested. Breakthrough at start-up was, in general, less likely with this plate, and, for a given heater temperature it was able to dissipate about as great a heat flux as any plate tested.

It should be noted that at a feedwater pressure of 3 psia, it was possible to operate at steady state all of the plates tested. Of these all but one did not experience even minor breakthrough until a heat flux of 5,500 Btu/hr ft^2 was reached, which indicates that if very careful limitations on the start-up and restart conditions could be maintained, almost any of these plates would prove satisfactory for use in a sublimator. This is true even though the maximum pore diameters of the 24 plates vary by a factor of 4 and the permeabilities by a factor of 20.

The design of the feedwater plenum is based upon maintaining a high heat transfer conductance in the plenum to increase the heat flux for a given heated surface temperature and preventing freezing damage associated with

zero heat load operation. High conductance is achieved by placing fins in the water plenum, reducing the height of the plenum to reduce the conduction path, or both. While it is advantageous to increase the heat flux by reducing the heat transfer resistance because this reduces the size of the unit, care must be exercised not to increase the heat flux above the breakthrough heat flux discussed above. The water plenum must be designed so that a high heat flux is maintained but not so high as to initiate breakthrough.

The approach developed in the single module freeze-up tests to reduce zero heat load problems, namely the use of a very short water plenum, was used in the multi-porous plate unit. A water plenum height of .015 in. was used since a height on this order proved satisfactory in the single module tests. A fin was not used in the water plenum. The reason for this was that it was necessary to limit the heat transfer conductance in order to keep the maximum heat flux below the breakthrough limit.

As was stated previously, proper design of the steam plenum is essential in order that too great a pressure is not maintained above the porous plate. This is so that the chances of breakthrough will not be enhanced. The method outlined in the section on sublimator analysis for predicting the pressure drop in the steam plenum as a function of the system parameters was used to design the steam plenum in the multi-porous plate unit. A one-half in. plenum was used in those passages with a porous plate on both sides and a 1/4 in. plenum where there was only one. Steam flow was along the 4 in. dimension of the unit instead of the 7 in. dimension to decrease the flow length and therefore the pressure drop.

Sublimator Fabrication

Assembly of the multi-porous plate sublimator is accomplished with a modular brazing technique similar to that employed to the water boiler. The finned water glycol passages are joined with a nickel base braze alloy in an initial operation with the water supply passages, porous plates and steam passages added in a second braze step. Some difficulty was encountered in the brazing of the porous plates selected for use in this unit. The porous plates showed a tendency to roll and deform at their edges during the brazing operation. It is felt that the porous plates were experiencing a continuation of the sintering process employed during their fabrication, and that this sintering process caused the plates to deform locally. The net result of this plate deformation was local braze voids around the perimeter of the porous material and some minor cracking of the plates in the areas immediately adjacent to the header bars. However, a torch braze repair of the sublimator core after the final braze operation was successful in sealing those leaks which developed. The glycol inlet-outlet pans were added with a torch brazing operation and the water plenum mounting flange machined prior to the final cleaning of the sublimator. Figure 3-14 shows the water inlet and steam outlet faces of the multi-porous plate sublimator.

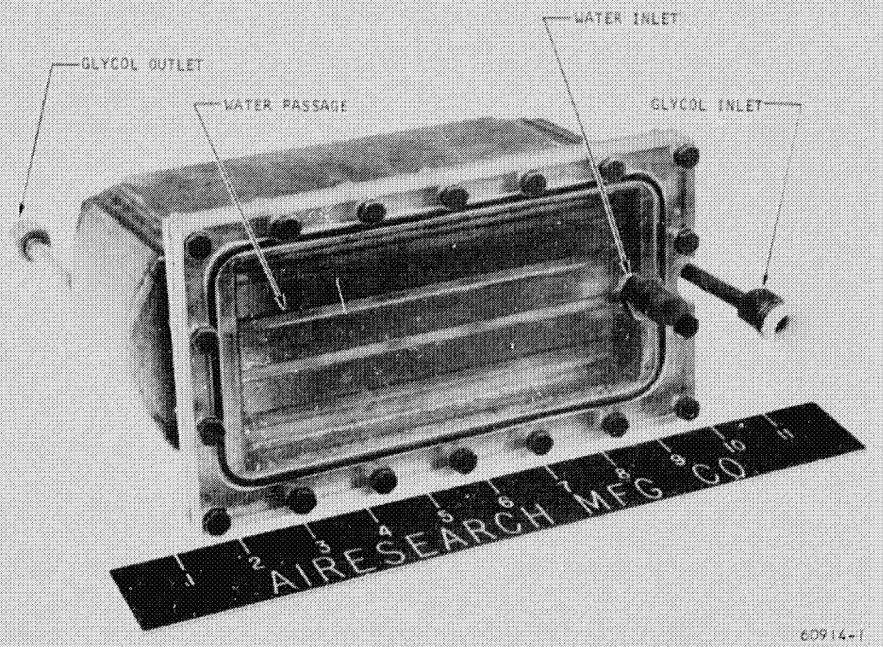

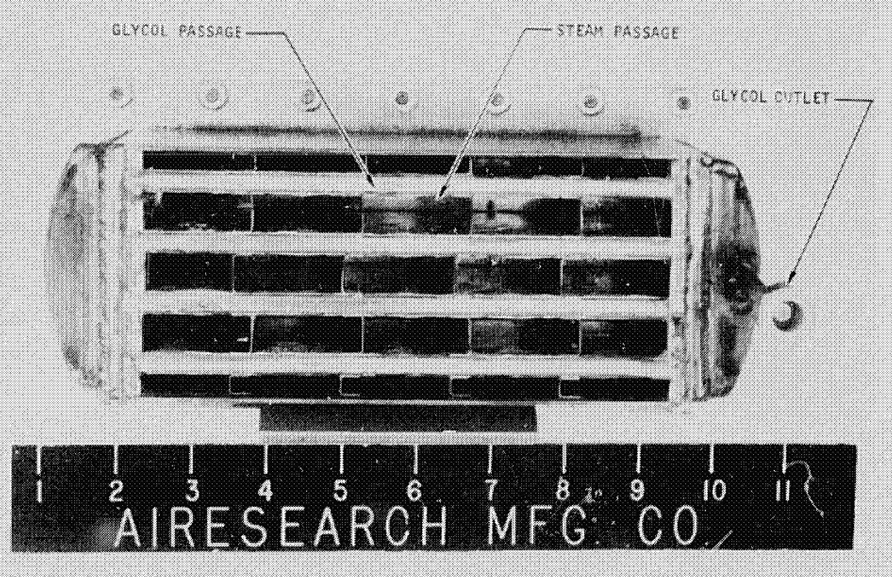

F-8084

Figure 3-14. Multi-Porous Plate Sublimator Module

Sublimator Testing

The multi-module sublimator was tested to verify performance predictions and to investigate problems occurring in a complete sublimator. A 62.5 percent ethylene-glycol and 37.5 percent water solution was used as the heat transport fluid. The unit was mounted in a bell jar attached to a vacuum system. The inlet temperature, outlet temperature, and flow rate of the glycol solution; the supply pressure, flow rate, and temperature of the expendable water; and the absolute pressure downstream of the porous plate were recorded. Visual observations of relevant phenomena were made and recorded.

Initially a set of freeze-up tests were performed on the inlet by filling the water plenum with water at no heat load and allowing the unit to freeze. A heat load was applied to melt the ice and the cycle was repeated. Ten freeze-thaw cycles were performed on the test unit and no visual damage or leaks observed.

Performance tests were conducted with glycol flow rates from 90 to 240 lb/hr and inlet temperature from 50^{0}F to 74^{0}F. Water supply pressures of 3 and 6 psia were used. The test results are shown in tabular form in Table 3-10. Figure 3-15 is a comparison of the test results with the predicted performance in the form of effectiveness versus glycol flow rate. The effectiveness is defined as:

$$E = \frac{T_{g_{in}} - T_{g_{out}}}{T_{g_{in}} - 32} \qquad (3\text{-}19)$$

where $T_{g_{in}}$ = glycol inlet temperature

$T_{g_{out}}$ = glycol outlet temperature

Good agreement between predicted and experimental performance was obtained.

Attempts were made to run with higher glycol inlet temperatures, however this was unsuccessful due to uncontrolled liquid breakthrough. At glycol inlet temperatures much above 75^{0}F it was impossible to sustain steady operation because of liquid pouring through the porous plate in the areas adjacent to the glycol inlet. This problem was thought to be a result of the short water plenum configuration. The conduction path through the water plenum header bar to the porous plate is short enough so that at high glycol inlet temperatures, the porous plate is heated above 32^{0}F and ice cannot form there. Since no ice exists to restrain the liquid, water passes through the plate and causes failure. An analysis of this phenomenum is presented in Appendix D. Two approaches may be utilized to eliminate this problem. One is to attach the porous plate to a "frame" which is in turn brazed to the header bar in order to lengthen the conduction path and increase the temperature drop and thus reduce the temperature of the plate to below 32^{0}F.

TABLE 3-10

MULTI-MODULE SUBLIMATOR TEST RESULTS

Run No.	Glycol Inlet Temperature, °F	Glycol Outlet Temperature, °F	Glycol Flow Rate, lb/hr	Sink Pressure, Microns HgA	Water Supply Pressure, In. HgA	Water Flow Rate, cc/min	Water Supply Temperature, °F	Q Btu/hr
101	58.0	45.0	238	900	12.25	43.5	78.0	2230
102	62.0	42.5	152.5	700	12.25	16.2	72.0	2140
103	60.0	42.0	150.5	700	12.25	14.5	72.0	1950
104	57.0	40.8	150.0	600	12.25	11.5	72.0	1750
105	58.0	4.10	150.5	620	12.25	13.8	72.0	1840
106	60.0	43.8	182.5	700	12.25	14.3	72.0	2130
107	60.0	43.8	183.0	700	12.25	15.5	72.0	2140
108	59.0	37.2	95.0	550	12.25	10.5	72.0	1490
109	59.0	37.2	95.0	550	12.25	10.4	72.0	1490
110	74.2	38.0	91.2	800	12.25	26.2	72.0	2380
201	50.1	39.5	150.	500	6.12	10.0	76.0	1150
202	50.0	39.2	150.	500	6.12	10.0	76.0	1170
203	50.0	41.0	190.	500	6.12	8.0	76.0	1230
204	50.0	41.0	190.	500	6.12	8.0	76.0	1230
205	50.0	40.0	190.	500	12.25	8.0	76.0	1370
206	50.0	40.0	190.	500	12.25	8.0	76.0	1370

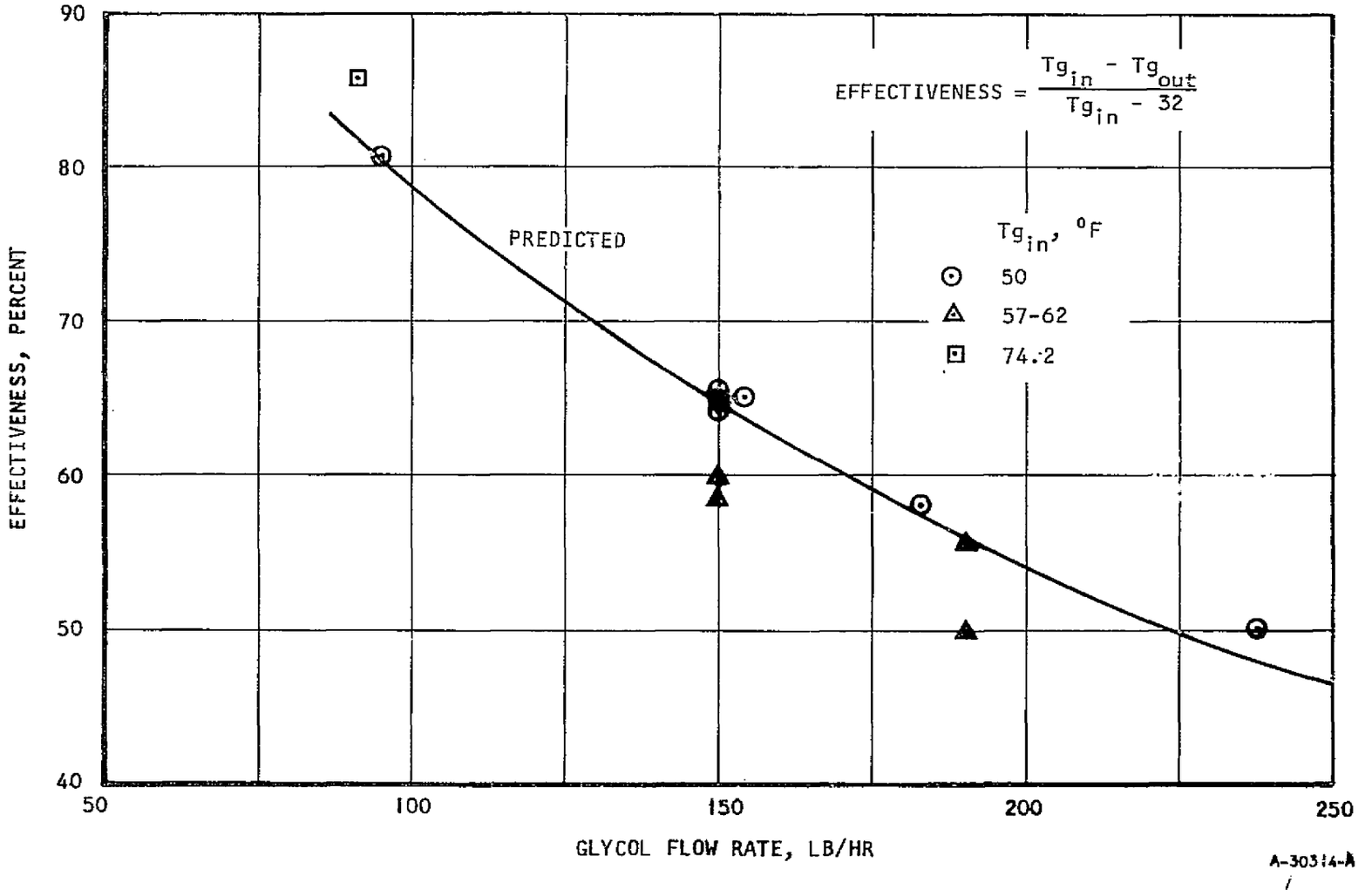

Figure 3-15. Multi-Porous Plate Sublimator Test Results

The other is to use a hydrophobic-coated plate so that ice is not required to restrain the liquid and surface tension forces are sufficient.

As indicated, feedpressures of 3 and 6 psia were used, and no significant difference in steady-state performance was found for the two cases.

OPTIMIZED SUBLIMATOR MODULE

On the basis of the porous plate investigation, the multi-module unit tests, and related analysis, an optimized sublimator was designed. The optimized sublimator module was not constructed; however, all the concepts incorporated into the design (except for the recessed porous plate construction explained below) were verified experimentally. The unit was designed to the problem statement given below.

Heat transport fluid	62.5 percent ethylene glycol, 37.5 percent water
Inlet temperature	90°F
Outlet temperature	60°F
Heat rejection	1 kw
Available sink pressure	0.5 mm Hg

The porous plate selected for the optimum design was the UC-2C series as this plate gave the best overall performance during start-up and steady-state operation. A sketch of the optimum core is shown in Figure 3-16. The heat transport fluid makes one pass through the unit in three passages and the water enters at one face and the steam leaves at the opposite face. The water plenum is 0.015-in. high so that freezing at zero heat load will not damage the plates. No fins are used in the water passage. The heat transport fluid passage is a finned passage, 0.100-in. high. The finned surface is varied in the flow direction. The reason for this is that it is desired to keep as nearly a uniform heat flux as possible in order to minimize the size of the unit. Single-module tests indicated that porous plates for sublimators are heat flux limited; that is, there is a heat flux above which breakthrough will occur. The core must be designed so that heat fluxes greater than the maximum limit are not exceeded. Since the temperature difference between the heat transport fluid and the effective sink temperature decreases along the glycol flow length; if the same heat transfer surfaces are used throughout the unit, the heat flux will decrease also. However, if the heat transfer conductance is increased along the unit by varying the finned surface, a fairly uniform heat flux may be achieved and the resulting unit will be smaller. In the optimum design, different finned surfaces were used in a 2-in. section at the inlet, a 2-in. section at the middle of the core, and at a 3-in. section adjacent to the outlet of the glycol passage. They are all 0.100-in. high offset fins, 0.002-in. thick. The first section used eight fins per inch, the second 15, and the third 29 fins per inch. Using these three fins, the average heat flux is approximately 89 percent of the maximum allowable. By using more different fin sections, it is possible to increase this percentage; however, the gain becomes smaller with each additional section. For comparison, a unit was designed with the same maximum heat flux but with the same finned surface throughout. For this particular problem statement, the resulting unit was 25 percent larger than the 3-section configuration.

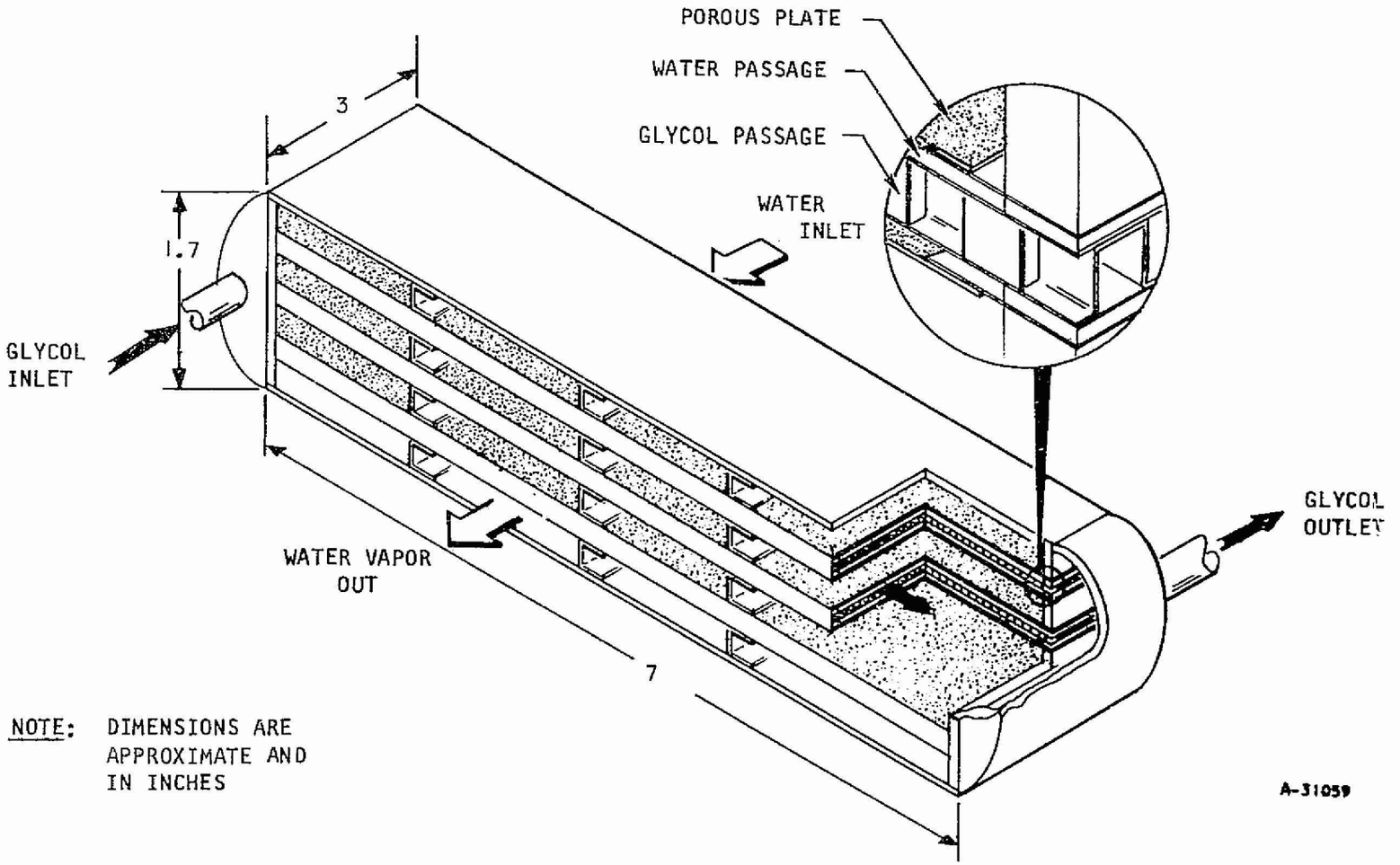

Figure 3-16. Optimized One Kw Sublimator

The steam passages were designed using the analysis presented above in the analytical section. The passages between two porous plates are 0.30-in. high and those at the side of the unit 0.20-in. high. This limits the maximum plenum pressure to 0.015 psia, about one-sixth the triple point pressure, which is low enough to prevent breakthrough due to too high a sink pressure.

An expanded detail of a glycol passage-water passage sandwich is shown in Figure 3-16. Of interest in this detail is the attachment of the porous plate. As indicated, the porous plate is not brazed directly to and between the header bars but is welded to a frame which is, in turn, brazed between header bars. The reason for this is to increase the metal conduction length from the glycol passage to the porous plate through the header bar. As was mentioned in the discussion of the sublimator module tests, with a short water plenum, this conduction length is small, and as was experienced in these tests, with the porous plates brazed to the header bars, at high glycol inlet temperature ($> \sim 75^0$F) the porous plate is heated above 32^0F and breakthrough occurs. In order, therefore, to realize the advantages of the short water plenum without initiating breakthrough, it is necessary to locate the porous plate at a short distance from the header bar, thus, the frame design.

Spacers are located in the water plenum and steam plenum for structural purposes.

It is obvious that with a heat flux limitation on porous plates, the size of a unit designed for a given heat load is pretty well fixed. It is not possible to increase the conductance by using fins in the water passage or more compact surfaces in the glycol passage because this increases the heat flux above the allowable limit. Therefore, in order to decrease unit size, a way must be found to increase this heat flux limit or to do away with it altogether. Indications are that the development of the concept of hydrophobic plates will allow elimination of the breakthrough heat flux limit. Development of a suitable hydrophobic coating will eliminate the need for ice in the porous plates and will allow the use of compact high conductance geometries to achieve higher heat fluxes and reduce unit sizes by 50 percent or more.

ONE KW MODULE SUBLIMATOR STACKING STUDY

As with the water boiler design, the ultimate goal in the design of an optimum 1 kw module sublimator would be the use of several single modules stacked together to provide cooling for a variety of heat load applications. A typical service condition would be the use of six modules to provide a total heat dissipation equal to six kw. Using this as a problem statement, a series of design layouts were conducted aimed at evaluating the various techniques for stacking six 1 kw modules. Figure 3-17 (SK51280) shows an arrangement which could be used to combine the six units. This solution provides the simplest technique for joining the six units and for providing inlet and outlet heat transport fluid flow to each of the modules. The sublimator modules are joined to each other in a bolted assembly with a bolt pattern included in the side plate of each unit. The units are assembled one atop the other and joined at the four corners.

FOLDOUT FRAME 1

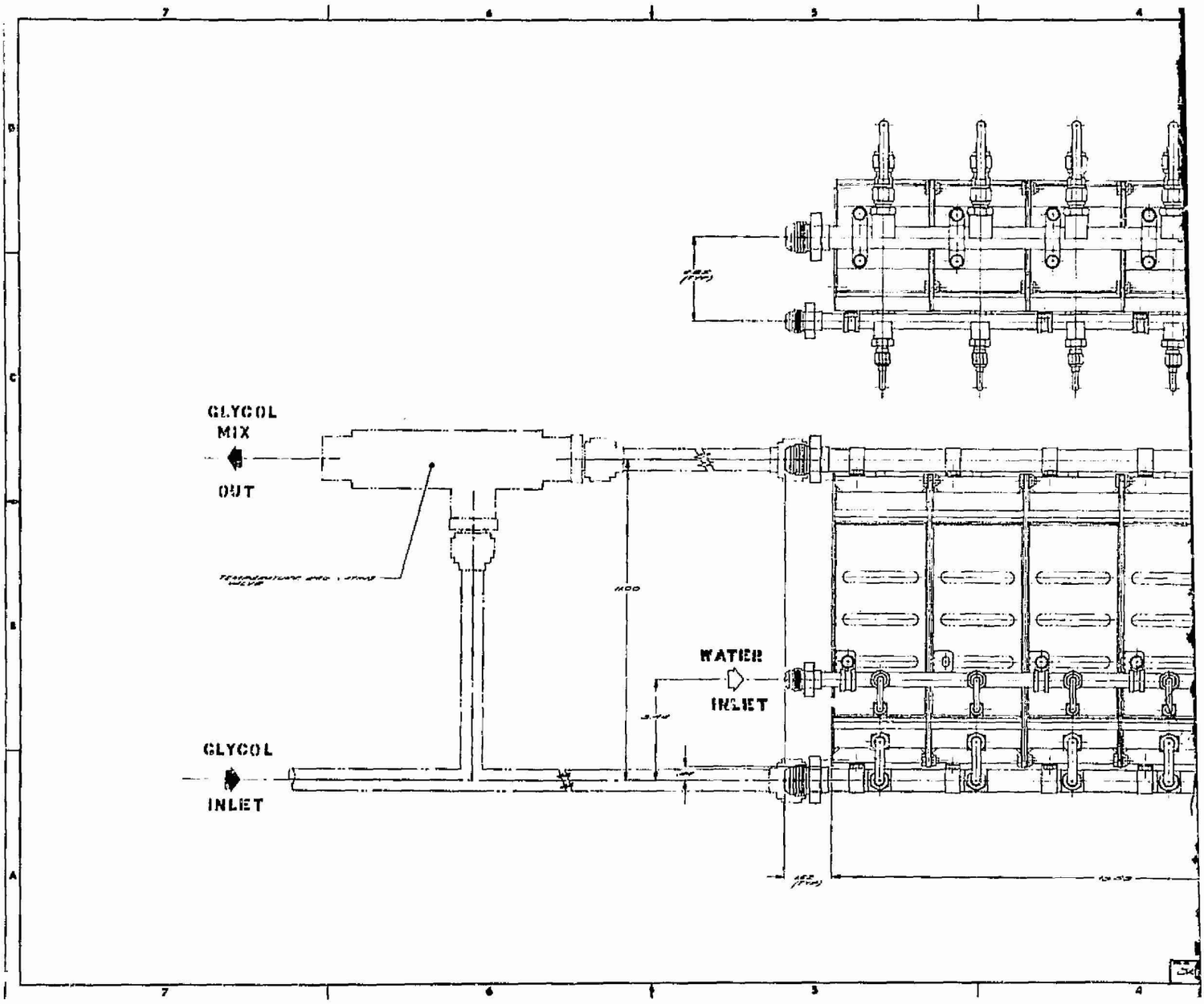

FOLDOUT Frame 2

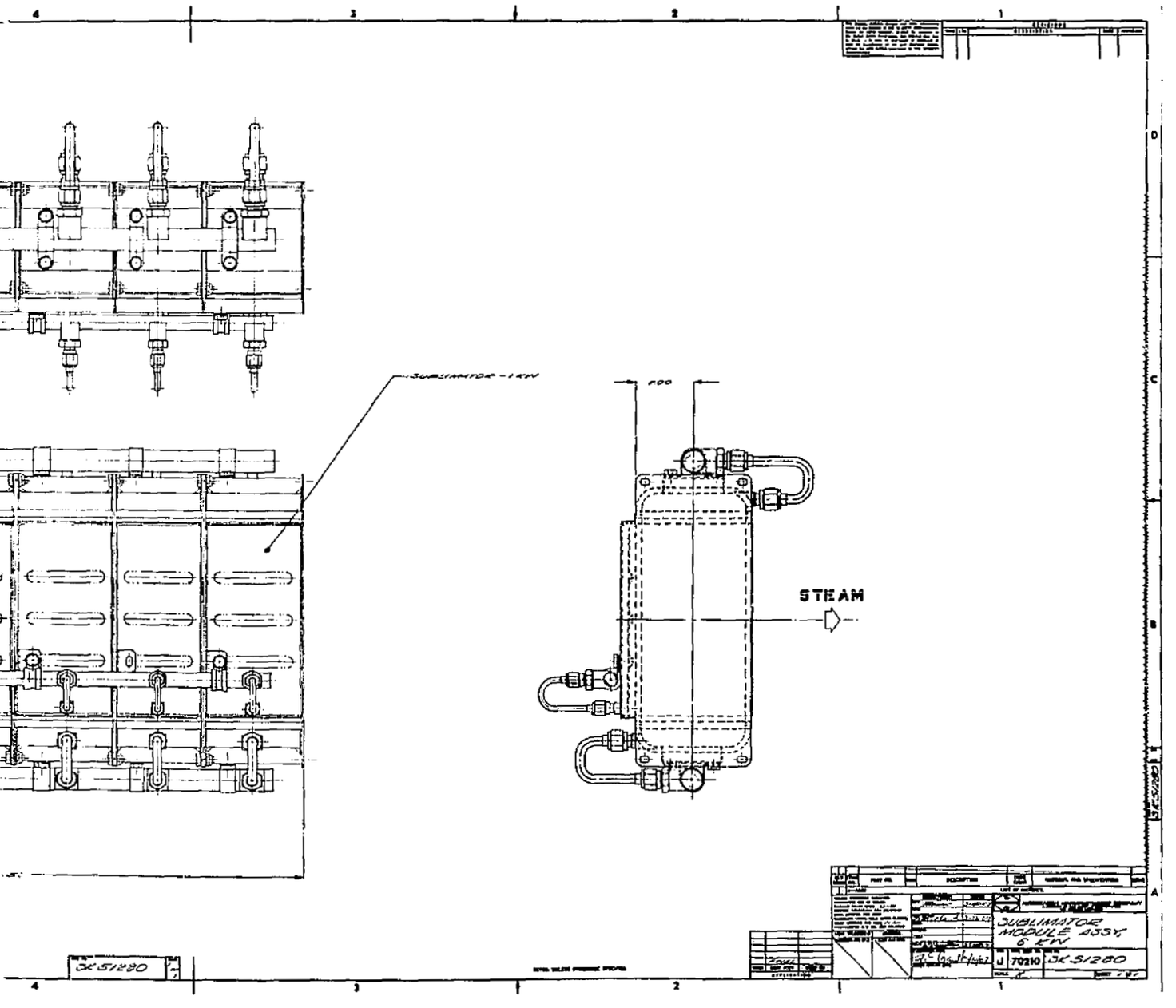

Figure 3-17. Sublimator Stacking Study

The heat transport fluid loop can most clearly be seen in the lower right hand view of Figure 3-17. The water glycol flows to the unit in a single pipe and is distributed to each of the cores through small tubes. The total glycol flow would be distributed among the six modules for all heat levels by an orifice located in the inlet tube to each core and sized to equalize pressure drop through each sublimator loop. The glycol inlet line is supported by ring clips around the line and bolted directly to the sublimator. The glycol flow would make a single pass through each sublimator and be collected in an outlet manifold which is also attached to the modules with ring clips. Downstream of the unit the glycol outlet flow travels through a bypass valve. The bypass valve senses the mixed temperature of the inlet and outlet heat transport fluid by means of a Vernatherm element. Upon increase in glycol mix temperature the valve moves toward the closed position and increases the amount of heat transport fluid traveling through the sublimator. At a decrease in mixed temperature, the valve moves toward the open or full bypass position, in order to maintain a constant mix temperature. Due to the nature of this valve, a single valve could be designed which would handle the control function for a variety of heat loads from one to six kw. Feedwater supply is from a pressurized source and is brought to the sublimator by means of a single line individually manifolded to each unit. As with the 1 kw water boiler module, the sublimator modules could also be arranged in a manner different from that depicted. However, Figure 3-17 does represent the simplest stacking arrangement possible in terms of joining the basic modules and in providing the minimum amount of ducting.

SECTION 4

THERMAL CONDITIONING PANELS

INTRODUCTION

In a space vehicle, cooling of electronic packages located remotely to an active thermal conditioning system without resorting to lengthy and elaborate plumbing systems is possible only by providing the units with their own ultimate heat sinks. Since obviously it is not practical to design a unique thermal conditioning unit for each heat producing electronic package or experiment in the vehicle, it becomes advantageous to develop an entirely self-contained thermal conditioning panel, capable of being located anywhere in the vehicle, upon which the various heat producing components may be mounted. The requirements of such a unit are as follows:

a. Thermal conditioning panel will be self-contained and not dependent on the external power or pumping requirements to distribute evaporant within the panel.

b. The thermal conditioning panel will include its own water supply and control system.

c. The panel will be capable of dissipating heat from components mounted on its surface and/or normal operation with an independent prime mover for conditioning of electronic packages with internal cooling shrouds.

d. The panel will deliver maximum thermodynamic performance and allow evaporant water to vent inboard to the spacecraft without the discharge of liquid water or ice.

e. Heat loads for the thermal panel will be typical of those for the Saturn IU thermal panels (420 watts) with locations of high heat flux varying with each particular application.

f. The structural integrity of the thermal panel will be sufficient to withstand the environment of the Saturn IU.

Since nondependence upon external power is a primary requirement, another method of distributing coolant over the large thermal panel area (30 in. x 30 in.) must be used. In the zero-gravity environment of a space vehicle, capillary forces become the dominant fluid transport forces and may be utilized to advantage for liquid distribution. Wicking materials are therefore an important and necessary component of a self-contained thermal panel independent of external power.

Just as zero-gravity is utilized by taking advantage of the dominance of the capillary forces, the essentially zero-pressure characteristic of the space environment may be advantageously used in dissipating heat. The ultimate heat sink in this type unit is provided by the latent heat of an expendable

fluid, in this case water, and the low pressure of the space environment allows phase change at a temperature necessarily lower than the desired control temperature level.

CONCLUSIONS AND RECOMMENDATIONS

The experimental and analytical investigation yielded the following conclusions and recommendations in the area of thermal conditioning panels.

1. The heat pipe-sublimator and single wick boiler are feasible panel concepts for thermal conditioning of electronic equipment in a zero g environment. Development tests conducted on panel sections representing each of these concepts have demonstrated that both panels will successfully dissipate heat loads typical of those encountered on the Saturn IU. The test sections achieved thermal control within a band of $\pm 10^{0}$F.

2. The two panels studied can be equipped with mechanical controls and an integral water storage capacity making them independent of external loops or power requirements. The control system would be driven by a melting-wax vernatherm element and water would be supplied from a rechargeable storage tank within the panel.

3. Analytical techniques available for predicting the performance of the heat-pipe sublimator and the simple wick boiler have proved quite accurate yielding predicted values within 10 percent of test results.

4. The heat pipe-sublimator and simple wick boiler panel test sections fabricated under this program can be further evaluated with startup tests (frozen and unfrozen wicks) and tests under transient heat load conditions.

5. Based on the panel study results the optimum design should be selected and a full size, flight type, thermal conditioning panel should be fabricated and tested to verify its performance and structural capabilities.

HEAT PIPE - SUBLIMATOR

Principle and Mode of Operation

A conceptual design of the Heat Pipe-Simulator thermal panel is shown in Figure 4-1. In this design, high thermal conductivity fins are brazed to the equipment mounting face of the panel on one side and to a wick material on the other. The remote coolant loop is a multi-pass finned passage attached to the other side of the wick. This thermal panel design incorporates as the ultimate heat sink, a single module sublimator, which may be located anywhere on the panel because of the ability of the heat pipe to transport heat to the coldest location. The heat which is generated by the electronic equipment mounted on the panel surface is conducted through the high conductivity fins to the wick surface where evaporation of the heat pipe working fluid occurs. The vapor thus generated locally condenses on the colder portions of the panel which may be any unheated section or the area adjacent to the sublimator heat sink. The latent heat of the vapor which condenses adjacent to the sublimator heat sink is conducted across the wick to the sublimator where it is dissipated in sublimation of water from an expendable supply. When the heat input is from the remote coolant loop fluid, heat is transferred from the fluid by convection to the finned surfaces in the coolant loop passage and by conduction through the fins, plate and wick-fluid matrix. Evaporation occurs at the wick surface and the rest of the heat dissipation mechanism is identical to that which occurs with the heat input from the equipment mounting surface. There is no net loss of working fluid from the heat pipe; evaporation and condensation occur at different locations simultaneously and fluid is resupplied to the evaporating areas by capillary forces in the wick material. Very uniform temperatures are maintained along the mounting surface, an inherent characteristic of a properly designed heat pipe. In Figure 4-1, the sublimator heat sink is located in an extended area which also serves as the expendable water supply storage. Although for purposes of clarity the water storage area is shown as an extended section, it may be desirable from a packaging standpoint to locate the water storage section and sublimator heat sink on the rear face of the panel.

Test Module Design

In order to evaluate the heat pipe concept for use in thermal conditioning panels the test section shown in Figure 4-2 was fabricated and tested. This unit is 30-in. long in order to examine the effect of the longest possible thermal panel dimension on heat pipe operation. The heat pipe uses 0.250-in. thick nickel fiber metal in the evaporating section to provide maximum water pumping capacity and 0.250-in. high copper fins in the steam passage to obtain maximum heat conductance with low pressure drop. The condensing wick, located adjacent to the ultimate heat sink, is 0.060-in. thick nickel fiber metal. Electrical heaters were fixed to the face of the panel for heat input and thermocouples were attached for temperature measurement. The heat removed from the condensing water vapor is dissipated by a single passage

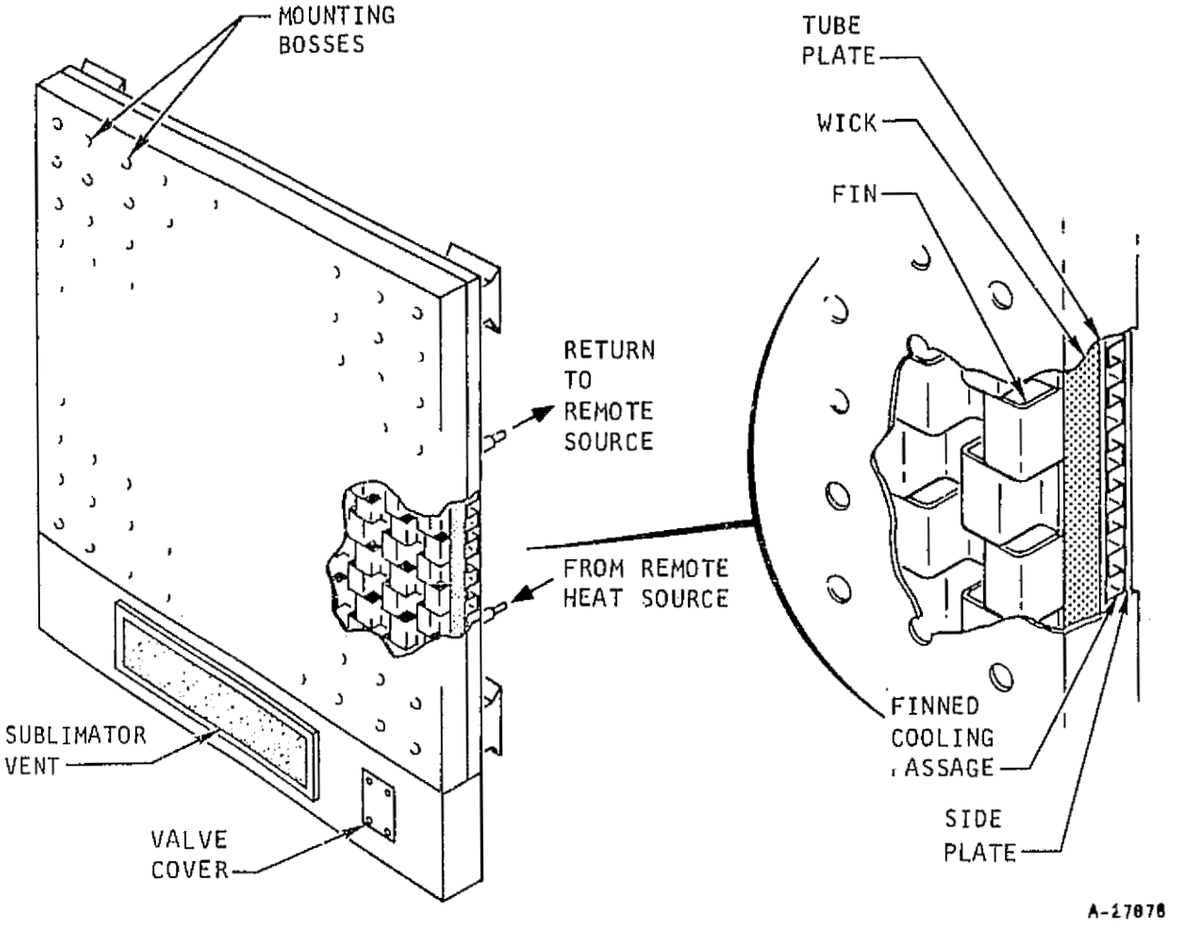

Figure 4-1. Heat Pipe - Sublimator Thermal Conditioning Panel

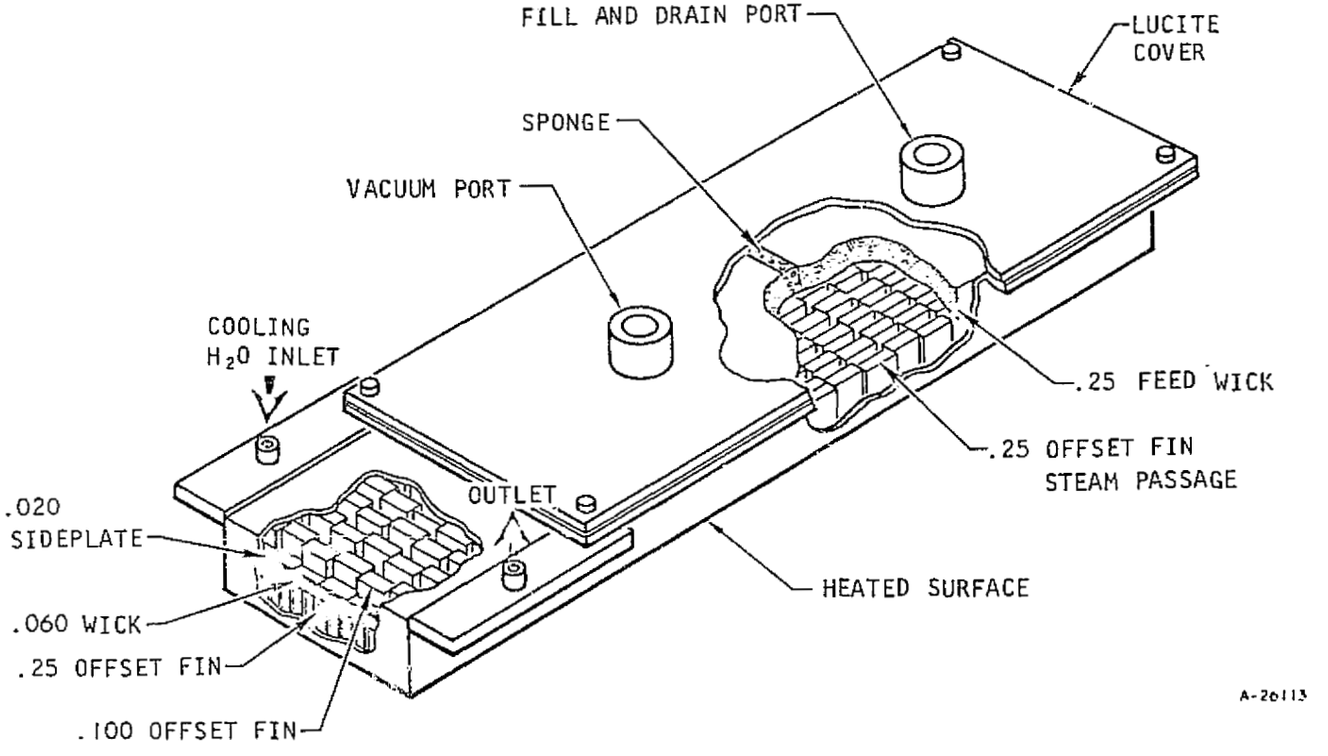

Figure 4-2. Heat Pipe Thermal Panel Test Section

liquid heat exchanger in the test module. This form of ultimate heat sink allows even control of condenser surface temperature and determination of accurate heat balances during testing of the heat pipe. The test module did not utilize a sublimator as the ultimate heat sink since extensive single module sublimator tests had been performed and since the primary objective was to establish the feasibility of using the heat pipe concept in a thermal panel. Therefore design of the test module was essentially a heat pipe design problem.

The design of a heat pipe is primarily a matter of minimizing the temperature drops along the path of heat transfer and assuring sufficient fluid transport from the condensing area to the evaporating area.

Selection of appropriate wick materials for the various areas of the heat pipe is an important item. Since the evaporating area must be supplied with sufficient liquid at all times, the wicks must provide good capillary pumping and will probably have relatively large pores, since in a zero gravity environment the pumping rate increases with pore size. Over the condensing area, since condensation occurs at the saturated wick surface, all the heat must be conducted across the liquid-wick matrix to the ultimate heat sink. Since the ratio of condensing area to evaporating area is small, the condensing heat flux is significantly larger than the evaporating heat flux, and it is necessary therefore, to minimize the condensing wick thickness to reduce the ΔT at this location. While a thin wick will not pump as much liquid, in the condensing area the pumping distance is short and it may be possible to supply sufficient liquid to the thicker evaporating wick with a relatively thin condensing wick. The wick thickness over the condensing surface is determined then by optimizing both the pumping requirements and the heat conduction ΔT.

The vapor passage must be sized to prevent excessive friction pressure drop associated with the flow of vapor from the evaporating surface to the condensing surface. The vapor flux driving potential is approximately equal to the difference in vapor pressures corresponding to the fluid temperatures at the evaporating and condensing interfaces. Since the condensing temperature is fixed for a given design and heat flux, the surface temperature at the evaporating area will be a function of the pressure drop. If the driving potential is not sufficient to transport the vapor flux corresponding to the operating heat flux, the pressure at the evaporating surface will increase, causing an increase in temperature there due to the increase in saturation temperature. If the friction pressure drop is small, the required pressure differential and therefore the ΔT from one end to the other is minimized.

The above considerations were taken into account in the heat pipe thermal panel test module design. It should be noted that a conservative approach was taken in the design, primarily from the standpoint of incorporating thicker wicks than the analytical calculations indicated were necessary. The reason for this was that it was desired to assure operation of the unit even if the wicks became slightly contaminated and suffered degradation in pumping ability so that sufficient heat transfer data could be obtained to determine the operating characteristics.

For test purposes the heat input to the thermal panel section was supplied with electrical strip heaters bonded to the panel surface. Thermocouples are located in rows along the length of the panel in order to measure temperature distributions over its entire surface. The heat pipe section is also equipped with pressure taps and lucite cover plate which provides visual observation of the wicks during filling and panel operation. Heat fluid temperature is measured by mixing sections and the performance tests were carried out in a large vacuum chamber to insure a minimum of heat leak and no gas leakage into the heat pipe. The assembled test module with the attached instrumentation is shown in Figures 4-3 and 4-4.

Testing and Test Results

The heat pipe thermal panel module was tested with input heat rates up to 620 Btu/hr and input heat fluxes up to 1000 Btu/hr ft^2. This heat flux is the maximum flux which the actual panel will experience and the heat rate is about half the design heat rate. (The module is 30 in. x 5 in. so that half the full-sized panel heat rate was being dissipated over about 1/6 the full sized panel area.) Heat was applied along the entire length of the panel or at one end or the other for the various tests. The panel temperatures were predicted analytically by summing the ΔTs throughout the system for the test heat rates. The temperature drops in the system were:

1. ΔT associated with heat conduction through the fins and with evaporation at the fin-wick interface

2. ΔT associated with the difference in saturation temperature from one end to the other due to the pressure drop resulting from vapor flow from the evaporating areas to the condensor

3. ΔT associated with condensing

4. ΔT associated with conduction of heat through the wick-water matrix to the ultimate heat sink

5. ΔT associated with transferring heat from the heat pipe wall to the heat transfer fluid flowing through the ultimate heat sink heat exchanger

Summing the system ΔTs and adding the total to the mean sink fluid temperature one obtains the predicted panel maximum surface temperature. A comparison of the predicted and experimental panel temperatures is shown below.

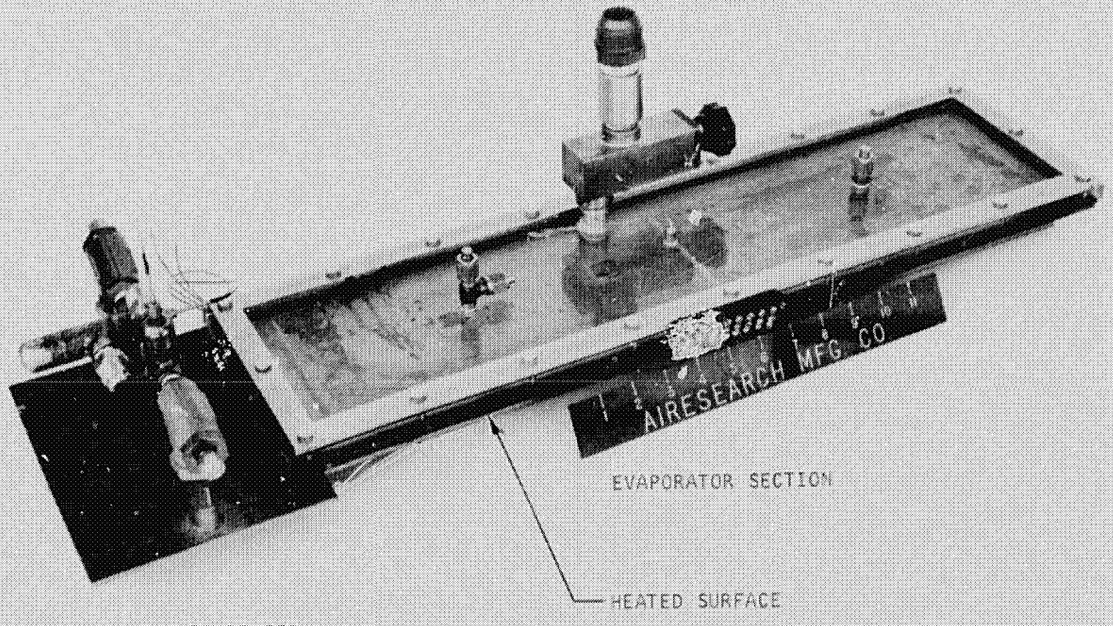

59891-2

F-7619

Figure 4-3. Heat Pipe Thermal Panel Test Module

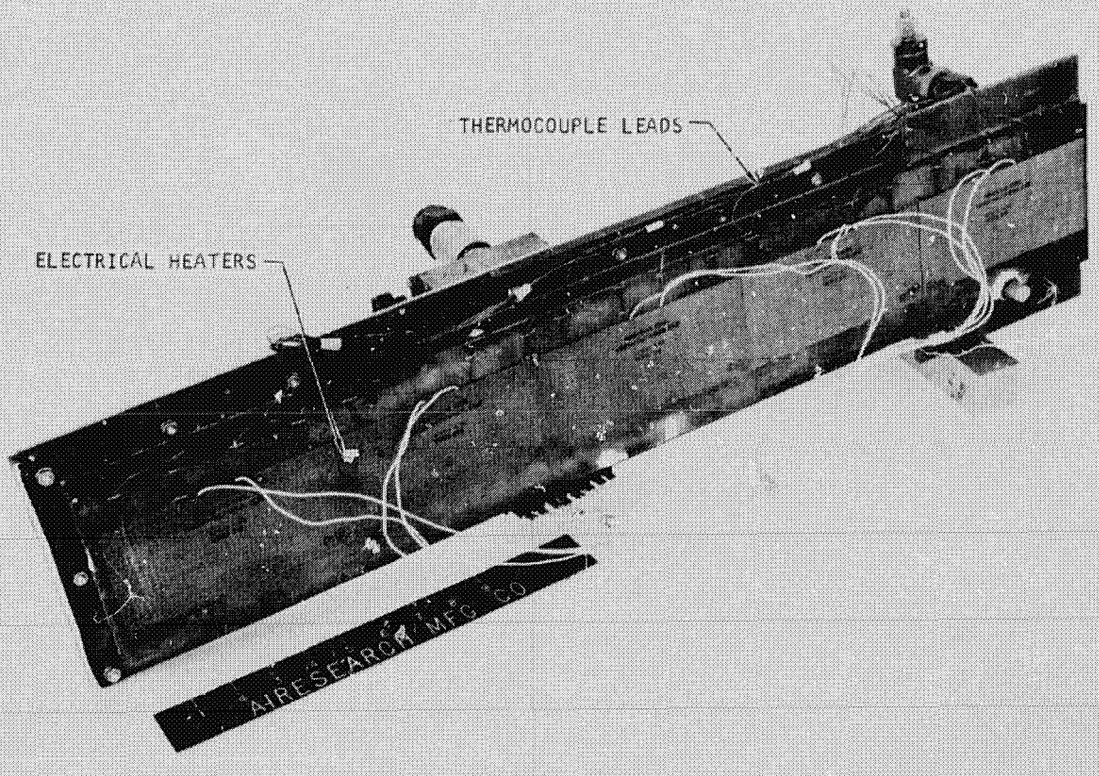

59891-1

F-8103

Figure 4-4. Instrumented Heat Pipe Thermal Panel Test Module

Run No.	Q Btu/hr	$T_{max\ analytical}$ °F	$T_{max\ experimental}$
301	212	59.1	58.5
302	212	59.1	57.8
303	440	67.3	67.0
304	440	67.3	67.2
305	617	73.5	72.6
306	617	73.5	73.3
307	126	59.5	62.3
308	248	61.2	62.3

As indicated, good agreement is obtained with the predicted maximum temperatures. For the cases of maximum heat rate, the wall temperature between the condenser wick and the ultimate heat sink heat exchanger was about 53°F giving a ΔT through the heat pipe alone of about 20 degrees. Of this it was calculated that a conduction ΔT of 11.4 degrees occurred across the condenser wick. This is the major temperature drop in the system and may be reduced significantly with a larger condenser section The total ΔT occurring in a full size thermal panel would be on the order of 10 to 12 degrees at the maximum heat load.

Initial tests conducted with this unit gave ΔTs of about 45 degrees at the maximum heat rate instead of the 20 degrees reported above. This was thought to be due to the presence of noncondensables in the system. The literature stresses the detrimental effect noncondensables have on heat pipe performance since they collect at the cold end and retard condensation. To alleviate this problem, a tap was installed in the unit at the condenser end and gas was allowed to escape while heat was applied. After a short period the tap was closed and the tests reported above were conducted. The performance improved markedly, indicating the noncondensables had been driven off and verifying the importance of removing all gases other than water vapor.

It may be concluded from these tests that (1) it is practical to use a heat pipe for thermal control of a panel which may receive heat loads of various magnitudes at random positions; (2) it is possible to predict the performance of such a unit; and (3) it is essential to remove all the noncondensable gases from such a system.

SIMPLE WICK BOILER

Principle and Mode of Operation

The other thermal conditioning panel concept investigated during this program was the Simple Wick Boiler. This design shown in Figure 4-5 incorporates two fiber metal wicks between the remote coolant fluid passage and the equipment mounting surface. These two wicks, an evaporating wick covering the equipment mounting face and a thicker water supply wick, are separated by a small steam plenum. A heat input from either the mounted equipment

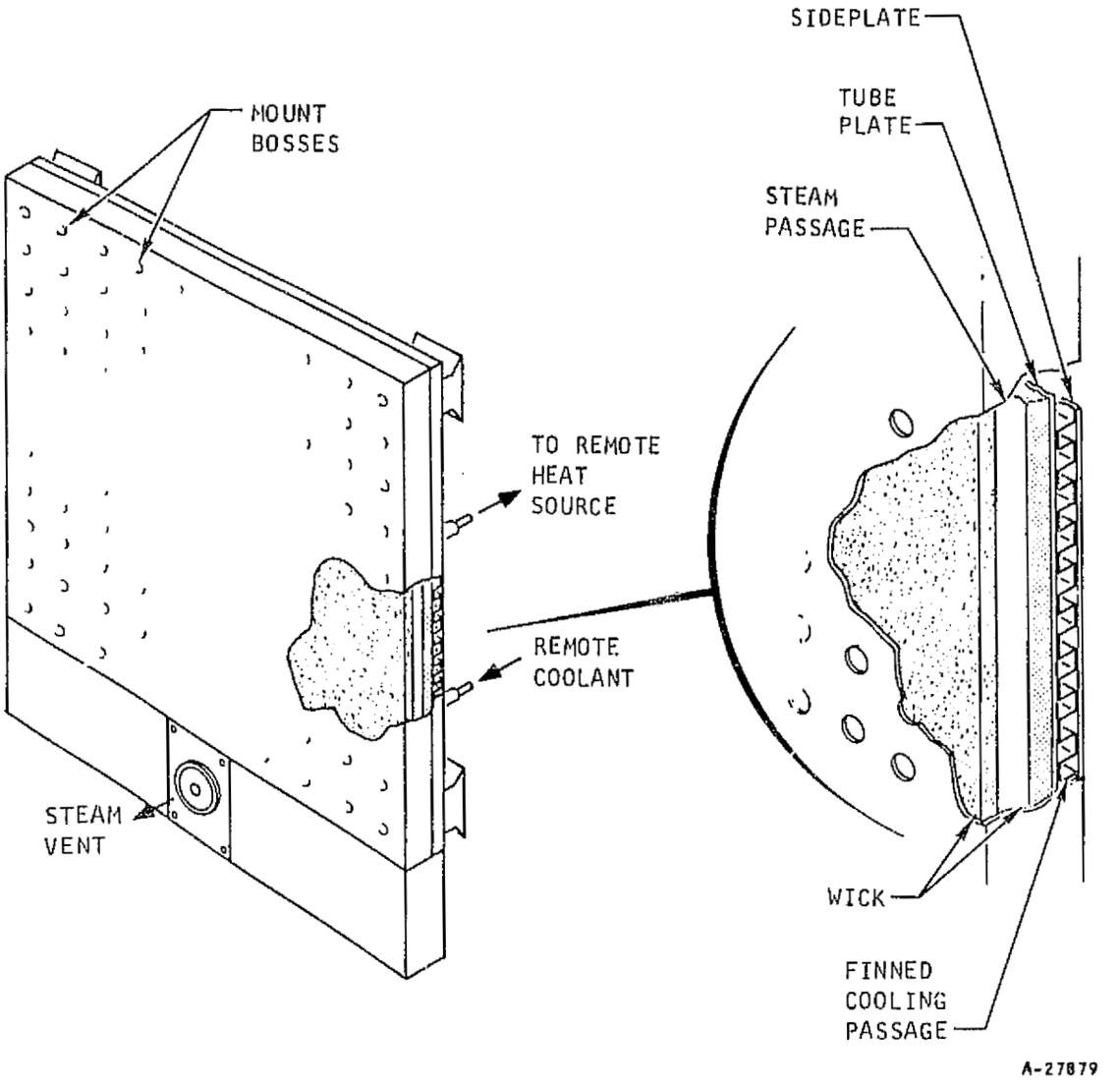

Figure 4-5. Simple Wick Boiler Thermal Conditioning Panel

or from the remote coolant source is dissipated in evaporating water at the surface of the adjacent wick. As the water in the thinner wick is dissipated, additional cooling water is drawn from the supply wick through cellulose sponge material located around the inside perimeter of the thermal panel and between the wicks. In turn, water is wicked from the water storage area to the water supply wick to refill it. The vapor generated passes along the steam plenum and is vented to the interior of the spacecraft. With this design, as in the heat pipe-sublimator, the heat input may occur anywhere on the panel since the wicks will supply fluid to all areas. Temperature control of a Simple Wick Boiler thermal panel is achieved by controlling the pressure of the steam plenum to the desired saturation pressure level. Either a thermistor actuator system or a vernatherm type valve could be used for control of pressure level.

Test Module Design

The 12-in. square simple wick boiler test section is shown in Figure 4-6. (A photograph of this unit with heaters and thermocouples attached is shown in Figure 4-7.) This section represents approximately one quarter of a full-size thermal panel and employs a 0.060-in. thick, 20 percent dense, nickel felt metal wick on the evaporating surface. The supply wick is 0.125-in. thick nickel felt metal and feeds the evaporative wick through cellulose sponge packed on three sides of the test section. The fourth side of the test section is a lucite cover plate which allows visual evaluation or fill procedures and examination of the wicks during operation of the unit. Electrical heaters are mounted on the surface adjacent to the thinner wick, and the unit is instrumented with fourteen thermocouples and two pressure probes. Temperature control of the panel test section is accomplished by manual adjustment of a back pressure valve utilizing panel temperature and/or steam plenum pressure to determine the correct valve setting.

Testing and Test Results

Startup and steady state tests were performed, and the unit was operated in two orientations, with the heated surface up and with it down. The unit mounted in the test setup is shown in Figure 4-8. In the steady state tests the wicks were saturated with water and the unit was allowed to come to temperature equilibrium at 60^{0}F. The heaters were turned on and the pressure maintained at a specified level. Surface temperatures were recorded as a function of time. As predicted the surface temperature remained 1 to 3 degrees hotter than the saturation temperature depending on the heat flux. After a period of time, the temperature at certain locations started to rise, slowly at first and then at a rate greater than 1^{0}F per minute, indicating that these areas were beginning to dry out and that the wicks had pumped themselves as dry as possible. In the inverted position, the unit operated longer before the rapid increase in temperature occurred. This was due to the fact that in this position, gravity forces aided in transporting water from the supply wick to the evaporating wick.

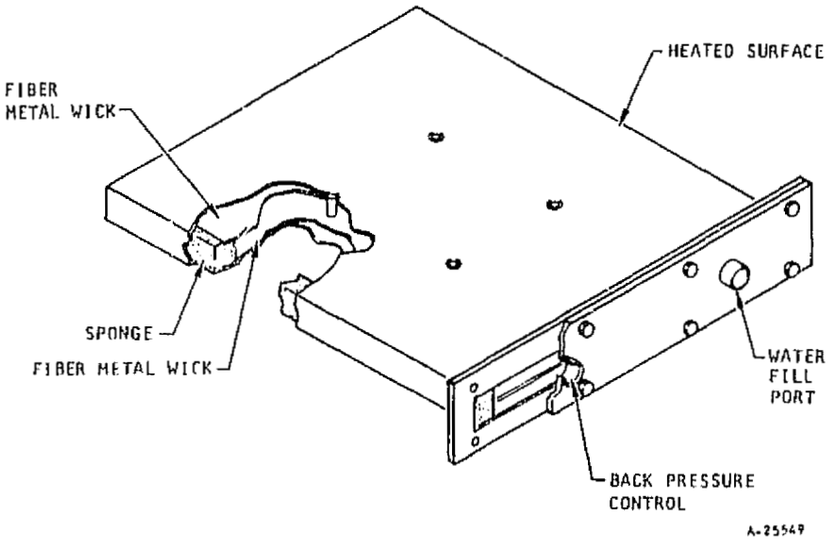

Figure 4-6. Simple Wick Boiler Thermal Panel Test Section

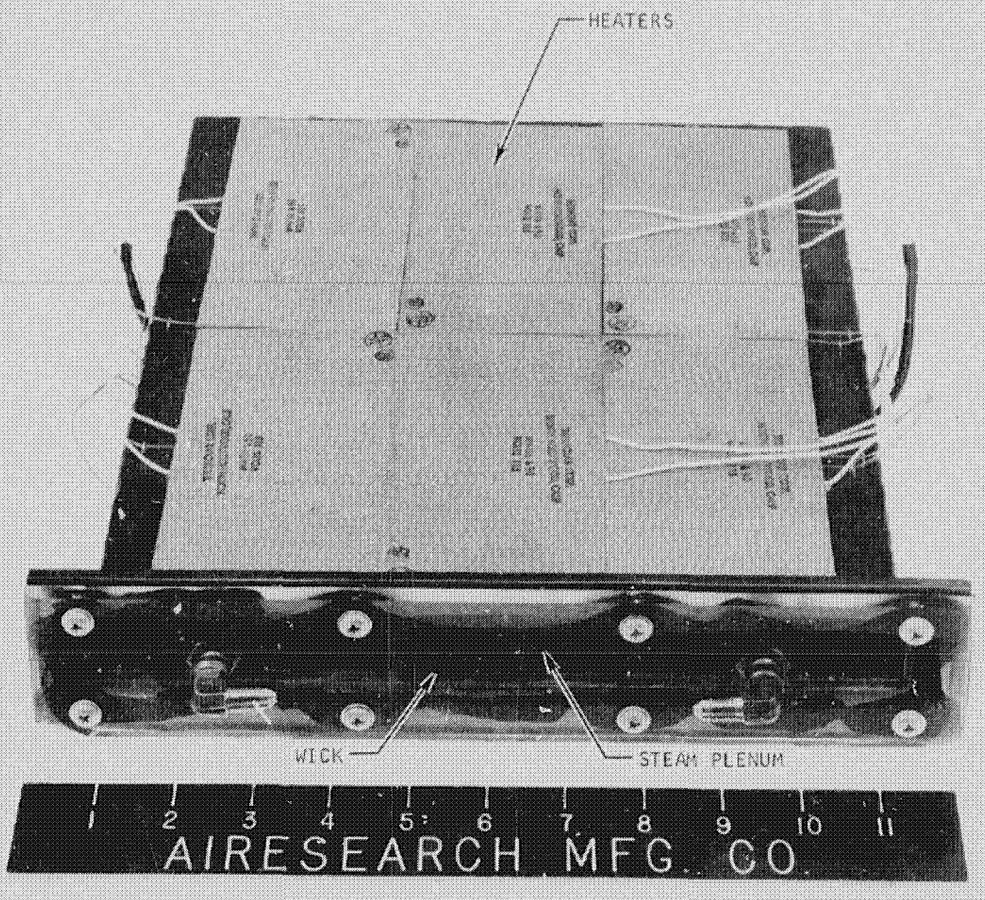

60032-1

F-7621

Figure 4-7. Simple Wick Boiler Thermal Panel Test Module

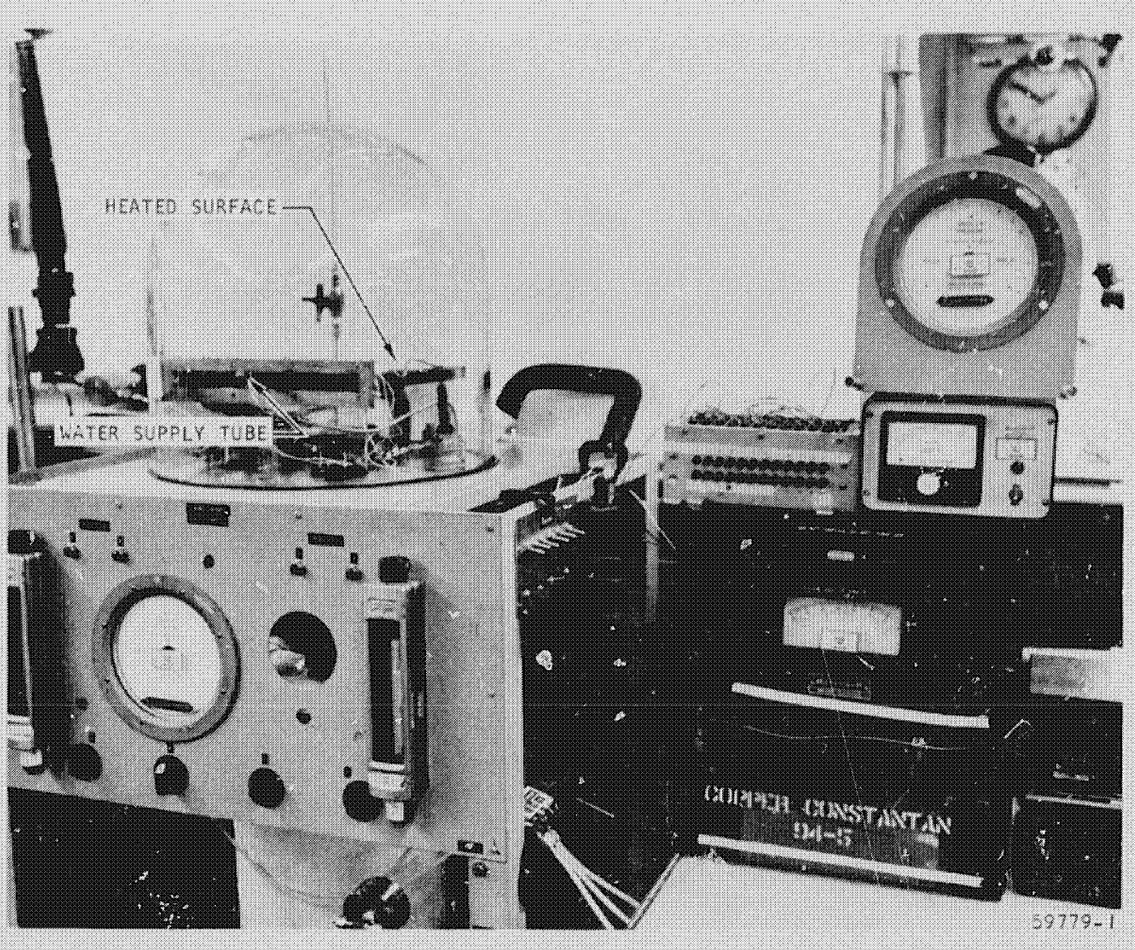

Figure 4-8. Simple Wick Boiler Test Apparatus

A typical set of data is shown in Figure 4-9 for a test in which a heat flux of 1000 Btu/hr ft^2 was applied over the 108 square inches of heater area. The solid circles are temperatures recorded at various locations on the heat input surface; the open circles are those recorded on the unheated surface. The saturation temperature was maintained at 71°F by controlling the pressure level. The data indicate that all locations except one remained a few degrees above the saturation temperature. The one thermocouple which heated to 90° before the test was terminated was located in the exact middle of the heated surface. The increase in temperature was due to an insufficient supply of water to this area. As the heat input was dissipated in evaporating water and venting it from the unit, more water was pumped by capillary forces from the bottom supply wick. Eventually, since a wick cannot pump itself dry, the wick could not supply water to the heated surface at a sufficient rate and the temperature therefore began to increase rapidly. One would expect the center portion of the heated surface to heat up first because this location is most remote from the supply and water must be pumped furthest to reach this point, and this is indeed the case. At this heat load the rapid increase of greater than 1°F per minute occurred at about 40 minutes and for the same heat flux with the unit inverted it occurred at 52 minutes, the increase in time due to the aiding affect of gravity. For heat fluxes of 750 and 350 the "drying out" occurred at 80 and 185 minutes respectively.

In the startup test, the wicks were filled with water, the pressure in the unit was reduced and the unit sealed, and a heat flux of 1000 Btu/hr ft^2 applied over 1/3 of the face of the unit. Temperatures were recorded as a function of time and a plot of the temperatures recorded immediately adjacent to the active heaters and at the areas furthest from the active heaters is shown in Figure 4-10. The maximum difference between surface temperatures was 8 degrees, the hottest locations being those adjacent to the operating heaters and the coldest those thermocouples located at the extreme end. The fact that the temperature at the unheated end follows the heated end temperature quite closely indicates that as the unit starts up, it operates as a heat pipe with vaporization and condensation occurring at different sections tending to keep a uniform surface temperature. This means that at startup of this type of unit, control may be achieved by sensing the temperature at any location since for reasonable temperature levels, the temperature differences at various locations are relatively small.

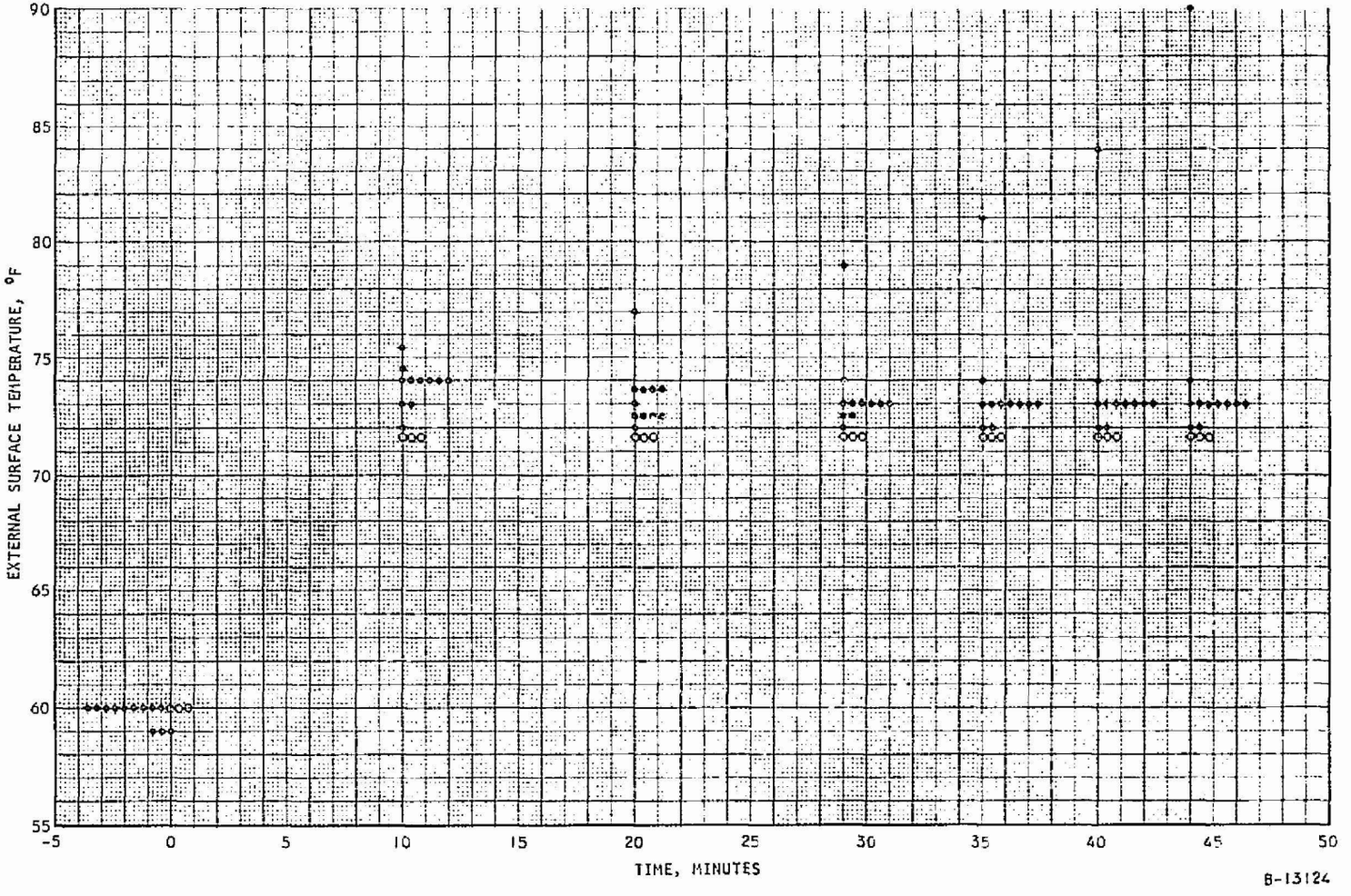

Figure 4-9. Simple Wick Boiler Module Test Results

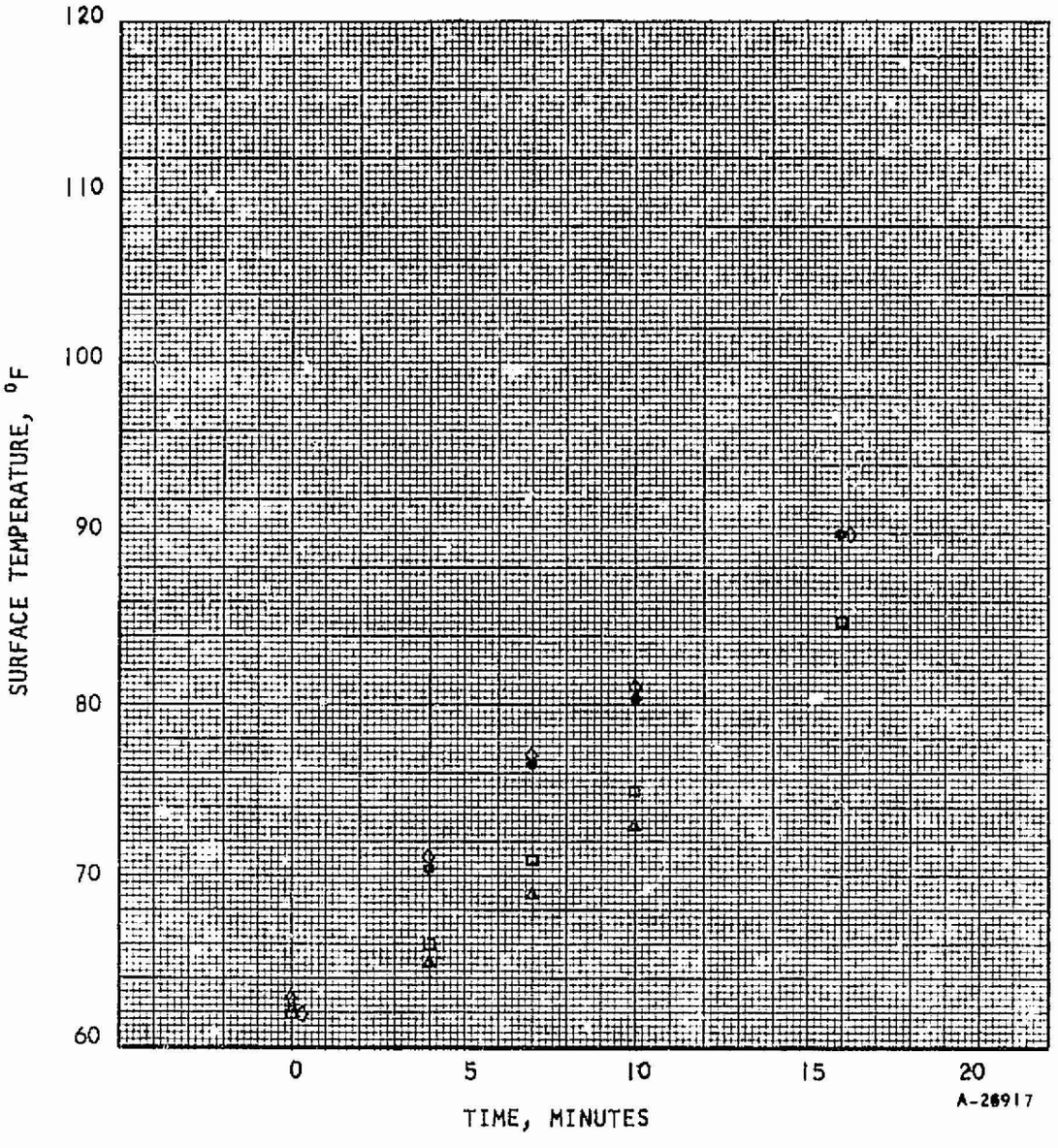

Figure 4-10. Simple Wick Boiler Module Start-up Characteristic

REFERENCES

1. K. Ginwala, "Engineering Study of Vapor Cycle Cooling Equipment for Zero-Gravity Environment", WADD TR 60-776, January, 1961.

2. L. Langstron, Sherman, A., Hilton, B., "Third Quarterly Report, Vapor Chamber Fin Studies," NASA CR-54989, April 1966.

3. R. Siegel, "Transient Capillary Rise in Reduced and Zero Gravity Fields," Journal of Applied Mechanics, Trans. ASME, June 1961, pp. 165-170.

4. G. Pickett, "Rate of Rise of Water in Capillary Tubes," Journal of Applied Physics, Vol. 15, 1944, p. 623.

5. L. Tong, "Boiling Heat Transfer and Two-Phase Flow," John Wiley and Sons, Inc., New York, N. Y., 1965.

6. "Porous Plate Water Boiler Design Study" - Final Report, HSER 3509, Hamilton Standard Division of United Aircraft Corporation, Windsor Locks, Connecticut, May 20, 1965.

7. John B. Gayle, Egger, Carl T., Bransford, James W., "Freezing of Liquids on Sudden Exposure to Vacuum," Journal of Spacecraft, Vol. 1, No. 3, May-June 1964.

APPENDIX A

ANALYSIS OF CAPILLARY FLOW IN WICKS

The following discussion reviews the fundamentals of capillarity, after which equations are derived which can be used to predict the characteristics of capillary induced flow in a wick.

FUNDAMENTALS OF CAPILLARITY

The pressure difference across a curved liquid surface has been shown to be

$$\Delta P = \sigma \left[\frac{1}{R_1} + \frac{1}{R_2} \right]$$

where ΔP = pressure differences, σ = surface tension, R_1 and R_2 = principal radii of curvature of the surface. If the surface is spherical, R_1 and R_2 = R and

$$\Delta P = \frac{2\sigma}{R} \tag{1}$$

Considering the case of a capillary tube of diameter D where the liquid contacts the solid at an angle θ, D and R are related by

$$R = \frac{D}{2 \cos \theta}$$

Therefore, Equation (1) becomes

$$\Delta P = \frac{4\sigma \cos \theta}{D} \tag{2}$$

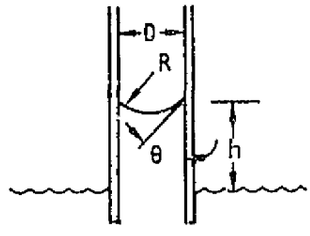

Wettability of a surface is usually defined in terms of the contact angle, θ. A zero contact angle would indicate complete wettability, and an increase in θ indicates a lower degree of wetting. For water and glass or metallic surfaces the contact angle is between zero and 90°.

If one end of a capillary tube is immersed in a pan of liquid, the liquid will rise or fall until the force due to the curved surface is balanced by the liquid head, giving

$$\frac{4\sigma \cos \theta}{D} = \frac{g}{g_0} h (\rho_1 - \rho_2)$$

where h = height difference between fluid in tube and the pan, g = acceleration of gravity, g_0 = gravitational constant, ρ_1 and ρ_2 = densities of the fluid and the surrounding atmosphere, respectively. Under most conditions, ρ_2 is much smaller than ρ_1 and can be neglected so

$$h = \frac{g_0}{g} \cdot \frac{4\sigma \cos \theta}{\rho D} \tag{3}$$

Obviously, as gravity is reduced, h increases.

If flow in a capillary tube is of interest, the pressure drop due to flow must be considered. Small diameter tubes and low flow rates are involved so laminar flow is assumed. Using the friction factor correlation for flow in round tubes yields the following equation for the frictional pressure drop with flow in a capillary tube

$$\Delta P = 32 \frac{L \mu G}{\rho g_0 D^2} \tag{4}$$

where L = flow length
G = average mass velocity
μ = fluid viscosity

During transient conditions, there is a change of momentum in the capillary tube which could affect the force balance used to analyze capillary dynamics. However, it can be shown that for the passage diameters of interest in wick boilers, the momentum term in the force balance equation is completely negligible relative to the other terms in the equation. The absence of the momentum term greatly simplifies the following analysis.

WICK DYNAMICS

The application of the above equations to wicks involve a number of assumptions because the diameter of the flow passage varies in a given wick material and the fibers in the wick material are oriented in various directions. However, comparison of the results of the following analysis with experimental data on wick dynamics verifies the assumptions that are used.

Wick Pumping Rate

The purpose of this analysis is to derive an equation for the maximum flow rate that can be provided by capillary forces in a wick. It is assumed that the liquid is being vaporized at the surface of the wick by a constant heat flux as shown in the sketch. The derivation for other heat flux boundary conditions follows the same procedure.

At the top of the wick the flow is zero, as all the liquid entering the bottom of the wick has been vaporized. The assumed constant heat flux boundary conditions yields a linear variation with distance of liquid flow rate.

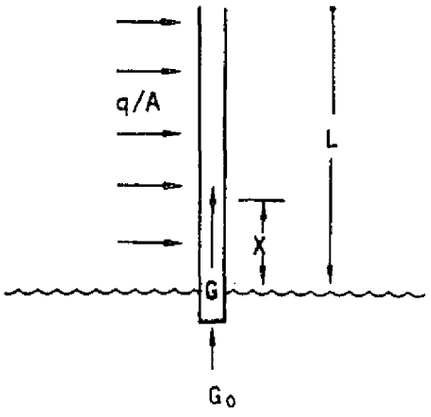

$$G = G_o \left(1 - \frac{X}{L}\right) \qquad (5)$$

The friction pressure gradient at any position is obtained by combining Equations (4) and (5).

$$\frac{dp}{dx} = \frac{32\mu\, C\, G_o\, (1 - X/L)}{\rho g_o D^2} \qquad (6)$$

where C = the ratio of the actual flow length through the randomly oriented fibers to the wick length. The mass velocity, G_o, for a wick is obtained by dividing the total liquid flow rate by the product of wick cross section area A_w and porosity, ϵ. The free flow area $A_c = A_w \cdot \epsilon$.

The total frictional pressure drop is obtained by integrating Equation (6) from X = 0 to X = L with the following result

$$\Delta p = 16\, \frac{\mu\, G_o\, C\, L}{\rho g_o D^2} \qquad (7)$$

The available pressure drop is equal to the difference between the capillary driving force, given by Equation (2), and the head of liquid in the wick.

$$\Delta p = \frac{4\sigma \cos\theta}{D} - \rho \frac{gL}{g_o} \qquad (8)$$

At steady state the pressure drops given by Equations (7) and (8) must be identical; solving these two equations for the mass velocity pumped by the wick yields

$$G_o = \frac{W_o}{A_c} = \frac{\rho g_o D^2}{16\mu L C} \left[\frac{4\sigma \cos\theta}{D} - \rho \frac{g}{g_o} L\right] \qquad (9)$$

The importance of gravity to wick performance is measured by the value of the last term in brackets relative to the value of the first term. Results obtained from Equation (9) for the maximum wick pumping rate for water are presented in Figure A-1 as a function of wick length and pore diameter. The increase in pumping capacity which results from the removal of gravity is shown by the comparison between the dashed and solid lines.

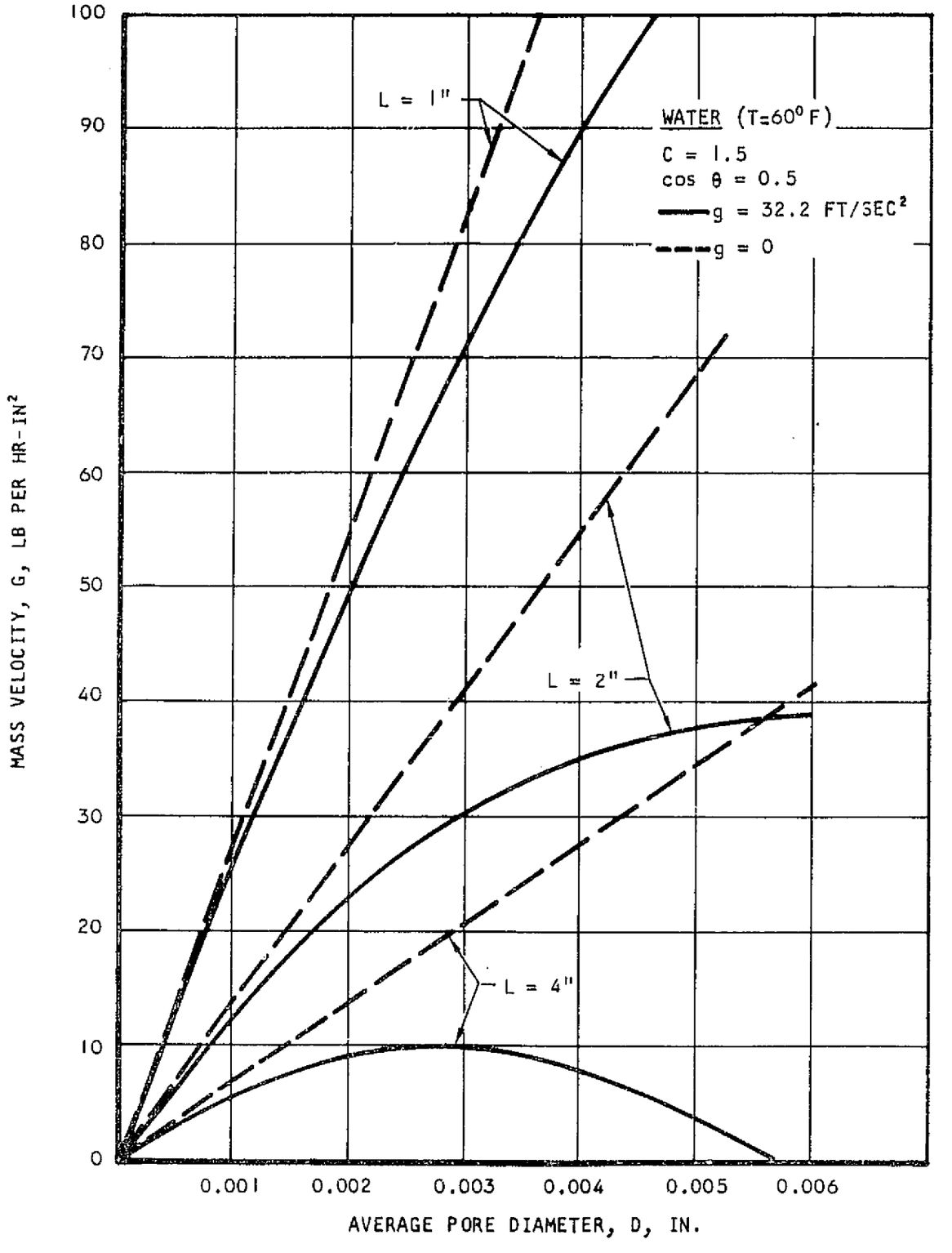

Figure A-1. Wick Pumping Rate

A similar analysis which describes the operation of a wick while evaporation is taking place from its surface is used to develop an equation for the height to which a wick can deliver water at various heat fluxes. Again:

$$G = G_0 \left(1 - X/L\right) \tag{10}$$

The mass entering the wick at the bottom per unit time is equal to the rate of evaporation. For evaporation occurring on both sides of the wick:

$$G_0 \, Ac = \frac{2(Q/A) \, w \, L}{\lambda} \tag{11}$$

The friction pressure gradient is:

$$\frac{dP}{dX} = \frac{32 \, \mu \, C \, G_0 \left(1 - X/L\right)}{\rho \, g_0 \, D^2} \tag{12}$$

which becomes:

$$\frac{dP}{dX} = \frac{64 \, \mu \, C \, (Q/A) \, (L-X) \, dX}{D^2 \, g_0 \rho \, \lambda \, Ac/w} \tag{13}$$

Integrating (13) between X = 0 and X = L:

$$\Delta P = \frac{32 \, \mu \, C \, (Q/A) \, L^2}{D^2 \, g_0 \, \rho \, \lambda \, Ac/w} \tag{14}$$

and setting this equal to the difference between the capillary driving force and the liquid head one obtains:

$$\frac{32 \, \mu \, C \, (Q/A) \, L^2}{D^2 \, g_0 \, \rho \, \lambda \, Ac/w} = \frac{4 \, \sigma \, \cos \, \theta}{D} - \rho \, \frac{g}{g_0} \, L \tag{15}$$

or:

$$L^2 + \frac{D^2 \, g \, \rho^2 \, \lambda \, (Ac/w)}{32 \, C \, \mu \, (Q/A)} \, L - \frac{g_0 \, D \, \sigma \, \cos \, \theta \, \rho \, \lambda \, (Ac/w)}{8 \, \mu \, C \, (Q/A)} = 0 \tag{16}$$

This equation may then be solved for L as a function of Q/A for a given wick in any gravity field. It is noted that in zero g the second term in equation (16) becomes zero.

Transient Wicking Height

The following analysis develops an equation for the time it takes liquid to reach various heights in a wick after the end of a dry wick has been brought into contact with the liquid. It is assumed that there is no heat or mass transfer from the sides of the wick; the flow rate of liquid is the same at each level at any one time.

Assuming that momentum changes are negligible reduces the force balance equation to three terms: gravity, friction, and surface tension. The pressure drop due to friction, given by Equation (4) is equal to the pressure drop provided by the excess of capillarity over gravity as given by Equation (8).

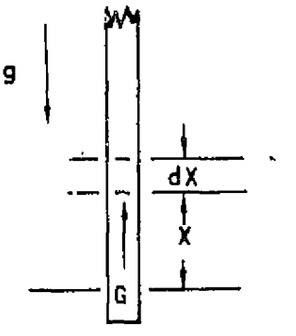

$$\frac{4\sigma \cos \theta}{D} - \frac{\rho g X}{g_o} = \frac{32\ C\ X\ \mu\ G}{\rho g_o D^2} \tag{17}$$

The change of height with time is equal to the liquid velocity at any time. Combining this with the definition of mass velocity yields

$$G = \rho V = \rho \frac{dX}{dt} \tag{18}$$

Substituting Equation (31) into Equation (30) and solving for dt gives

$$dt = \frac{32\ \mu\ C}{g_o\ D^2} \quad \frac{X\ dX}{\left(\frac{4\ \sigma \cos \theta}{D} - \frac{\rho\ g\ X}{g_o}\right)} \tag{19}$$

Integrating Equation (32) yields the final equation for the time it takes liquid to reach each height in the wick.

$$t_{g \neq o} = \frac{32\ \mu\ C}{\rho\ g\ D^2} \left[\frac{4\ \sigma \cos \theta\ g_o}{\rho\ g\ D} \log \left(\frac{1}{1 - \frac{\rho\ g\ D}{4\ \sigma \cos \theta\ g_o}\ X} \right) - X \right] \tag{20}$$

Note that Equation (33) breaks down when gravity exactly equals zero. It is however applicable to verify transient wick tests performed on earth. Under zero gravity conditions the corresponding equation obtained by setting g = 0 in Equation (32) and then integrating is

$$t_{g=o} = \frac{4\ \mu\ C\ X^2}{g_o\ D\ \sigma \cos \theta} \tag{21}$$

APPENDIX B

SINGLE MODULE WICK BOILING TEST DATA AND ONE KW BOILER TEST DATA

In order to determine the heat transfer performance of various wick materials and to obtain data upon which water boiler and thermal panel design could be based, evaporation tests were performed on various wicks. The results of these tests are shown in the form of effective boiling coefficient as a function of heat flux at three saturation pressures. The effective coefficient is determined by dividing the heat flux (based upon projected wick area) by the difference in the heater and saturation temperatures. Wick identification numbers are tabulated in Section 2 of the text.

Figures B-16 through B-22 show traces of the inlet and outlet heat transport fluid temperatures obtained in the one kw boiler test. The significance of the results are explained in Section 2, Water Boiler Module.

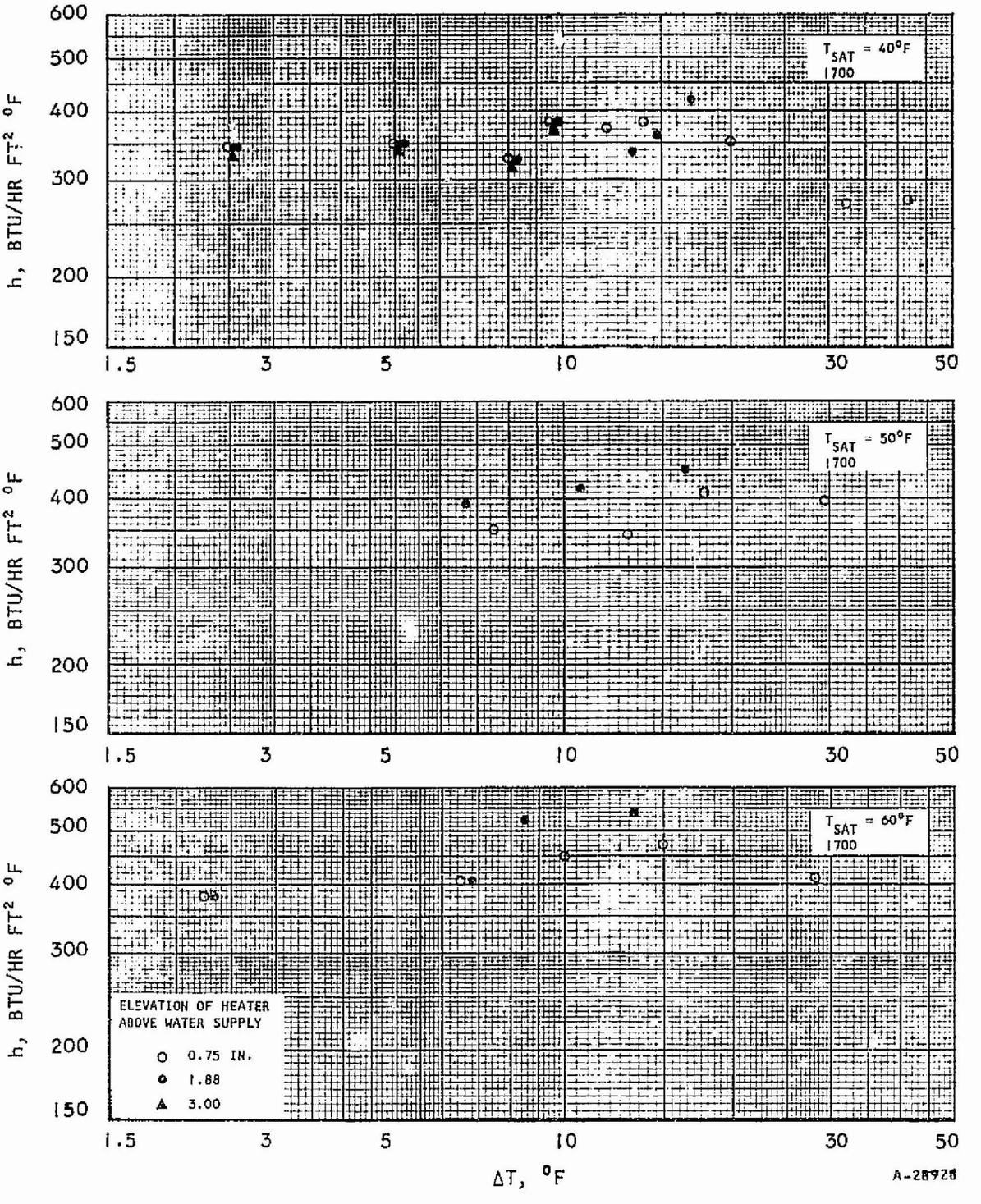

Figure B-1. Boiling Performance of Wick No. 1700

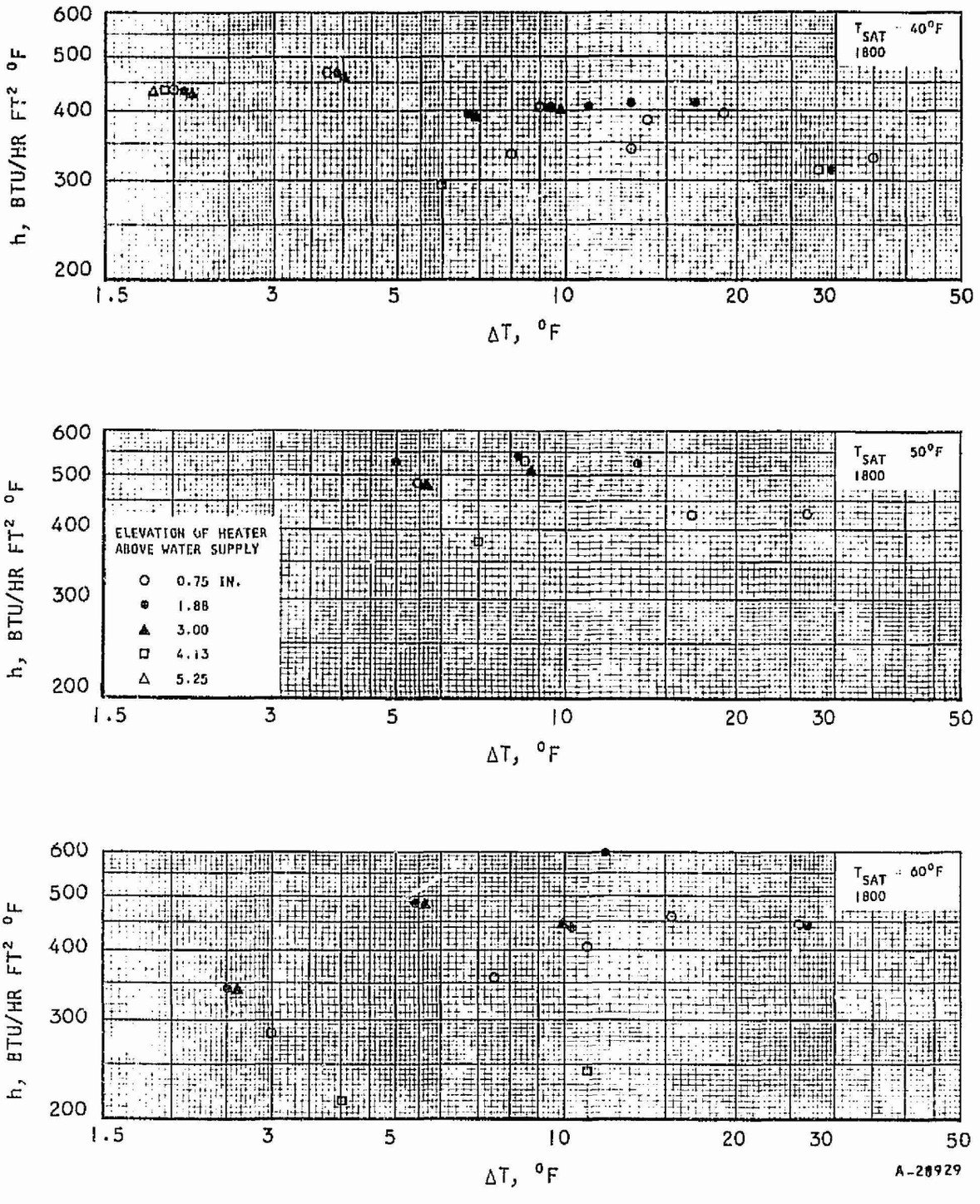

Figure B-2. Boiling Performance of Wick No. 1800

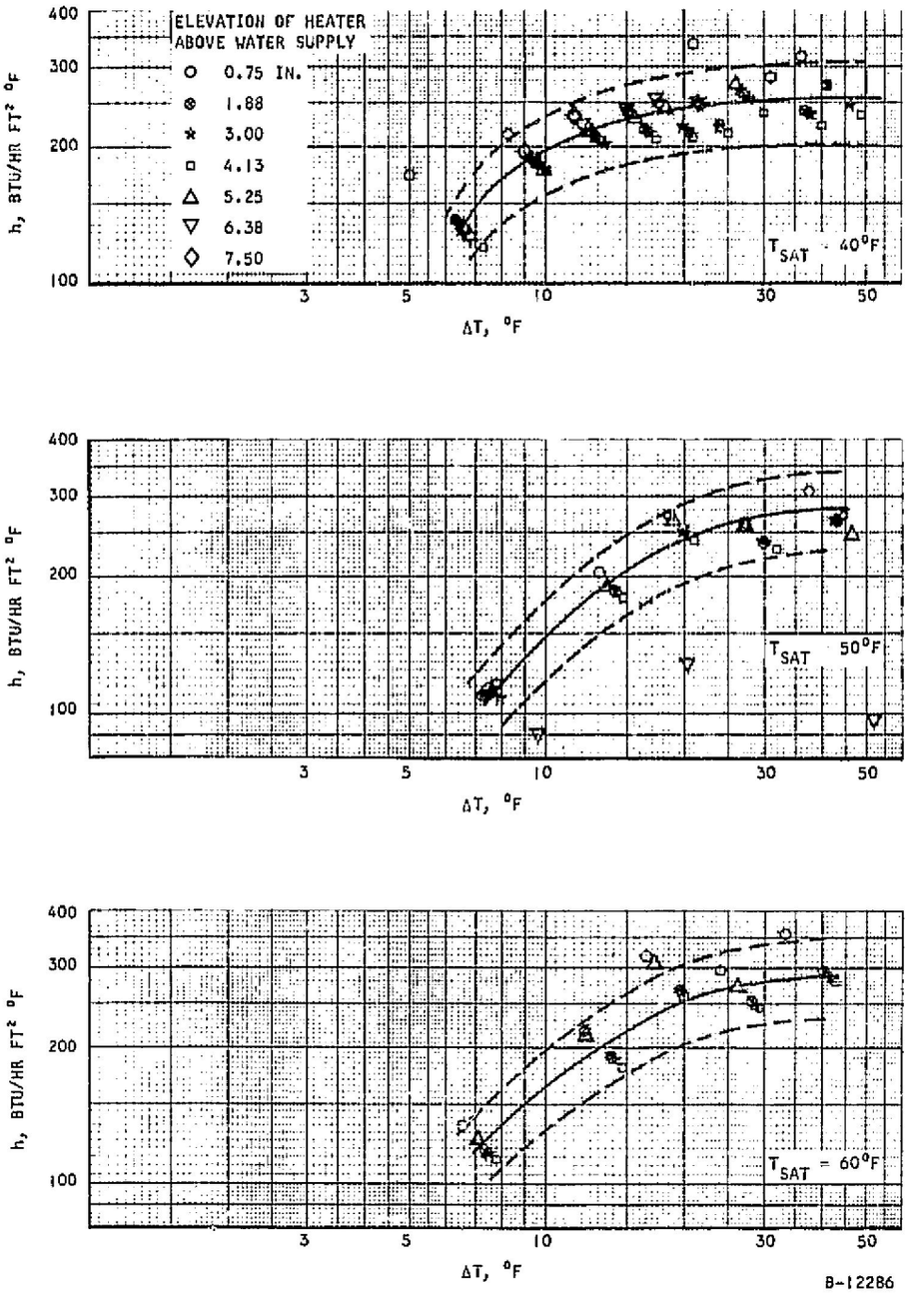

Figure B-3. Boiling Performance of Wick No. 1100

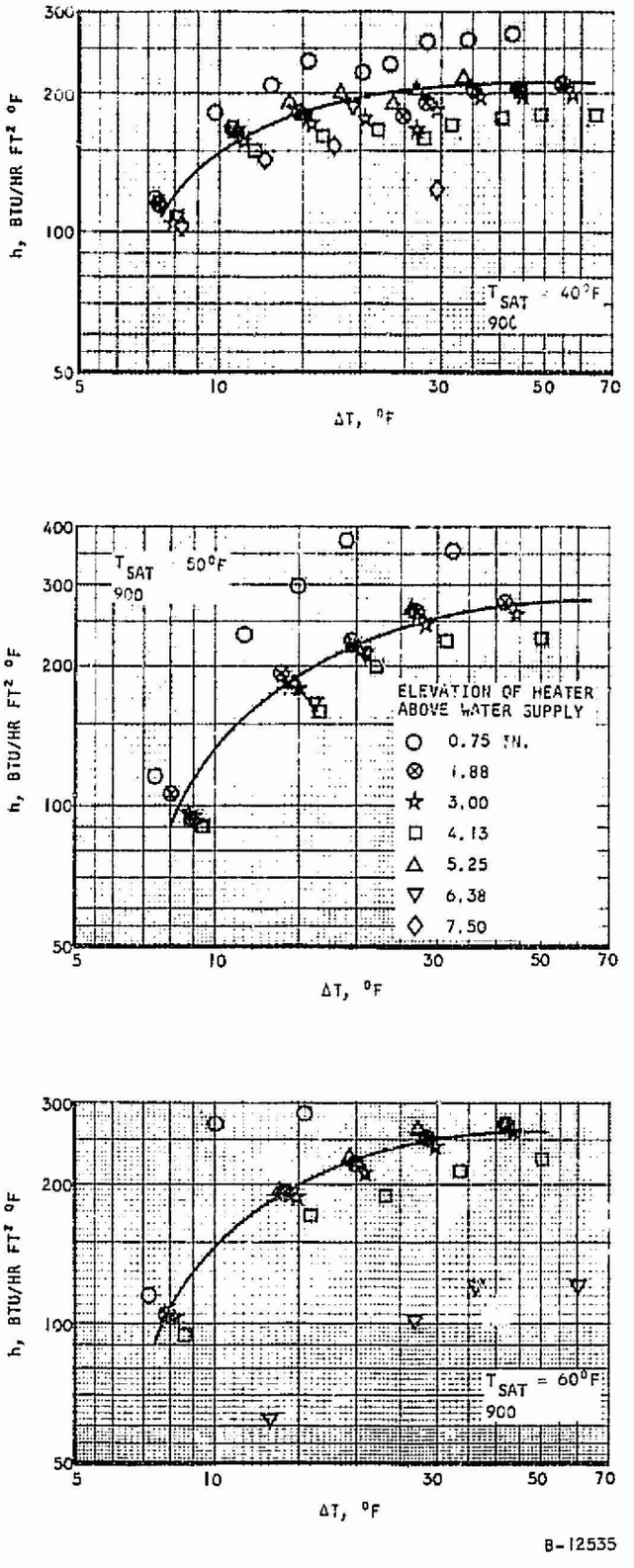

Figure B-4. Boiling Performance of Wick No. 900

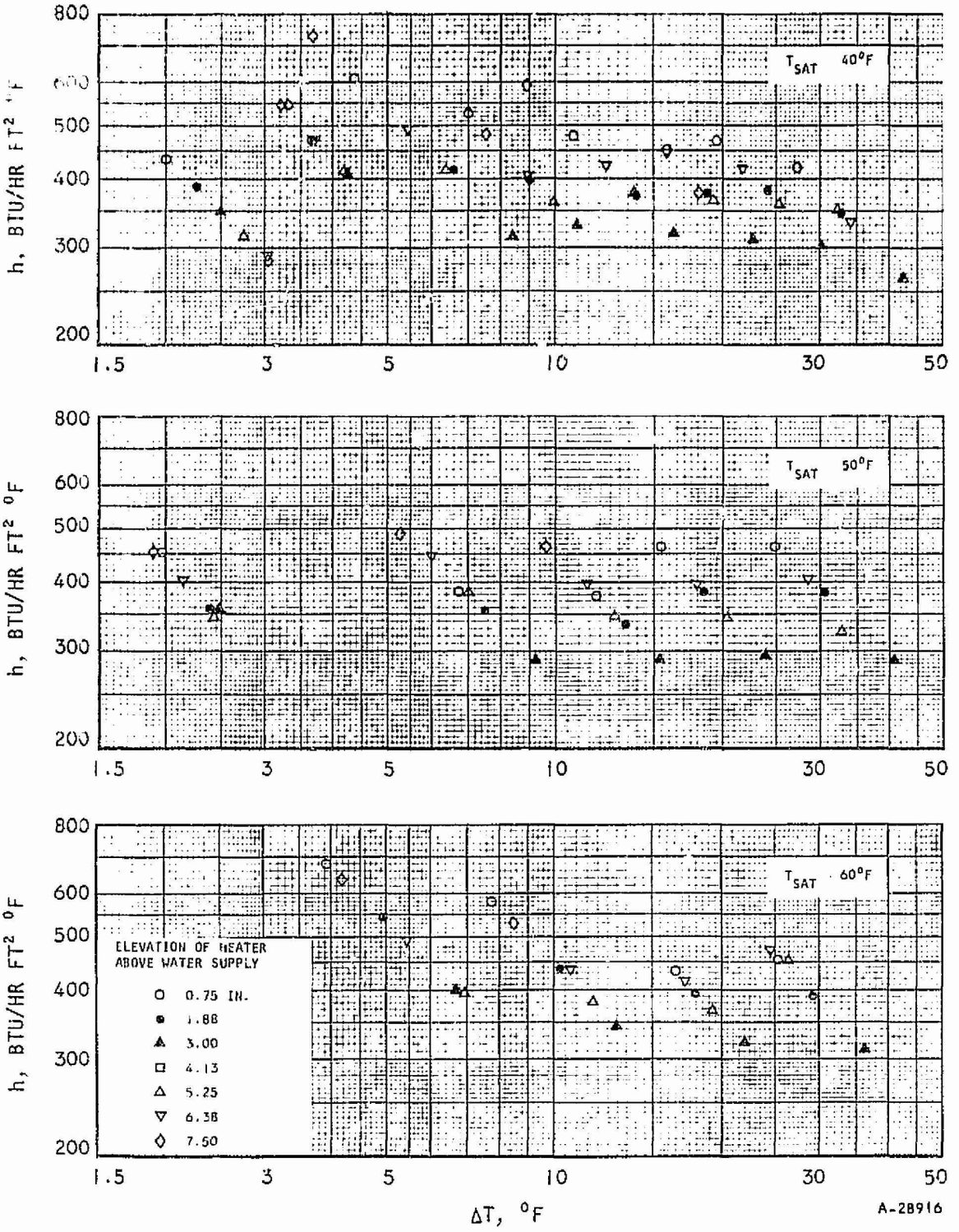

Figure B-5. Boiling Performance of Wick No. 1900

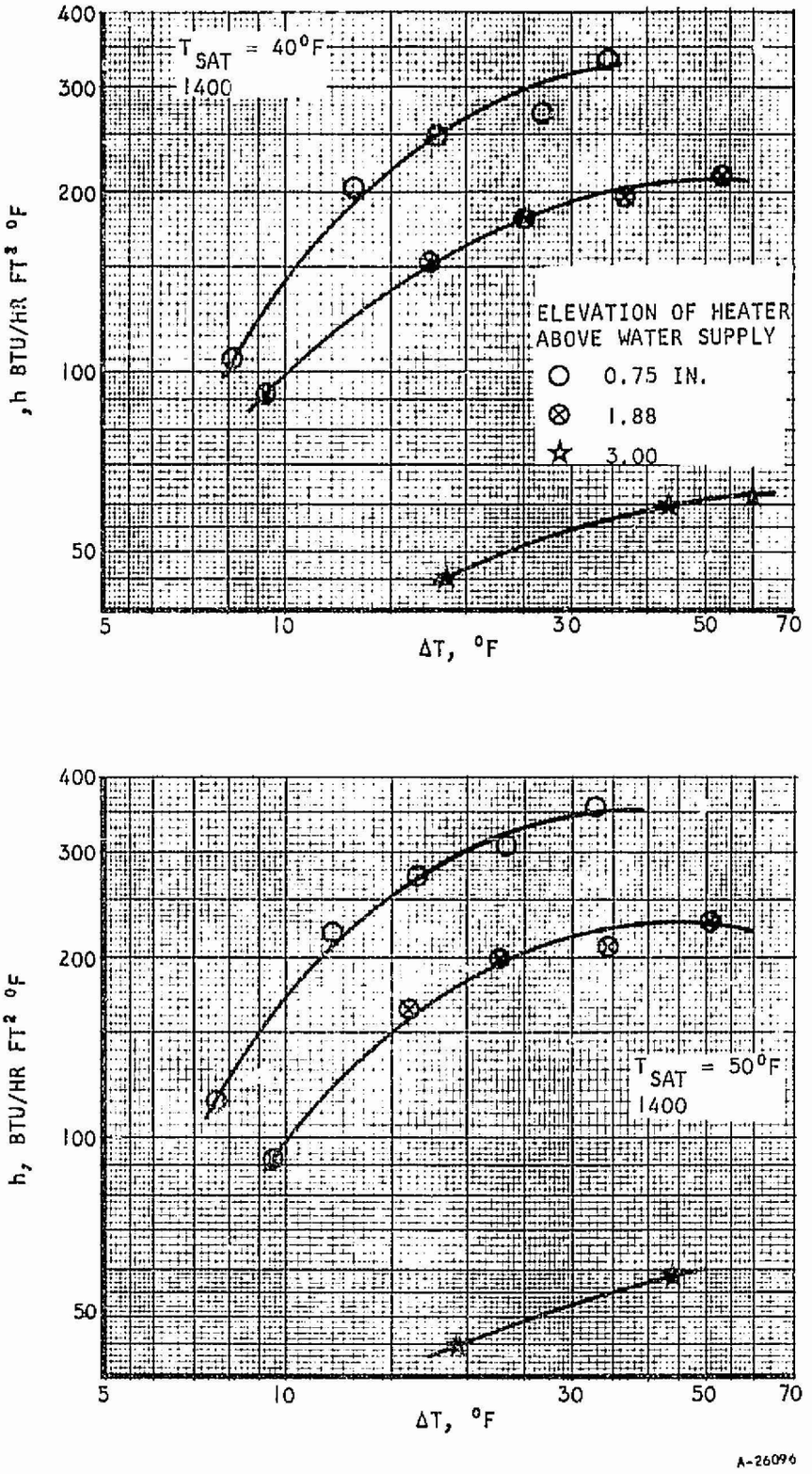

Figure B-6. Boiling Performance of Wick No. 1400

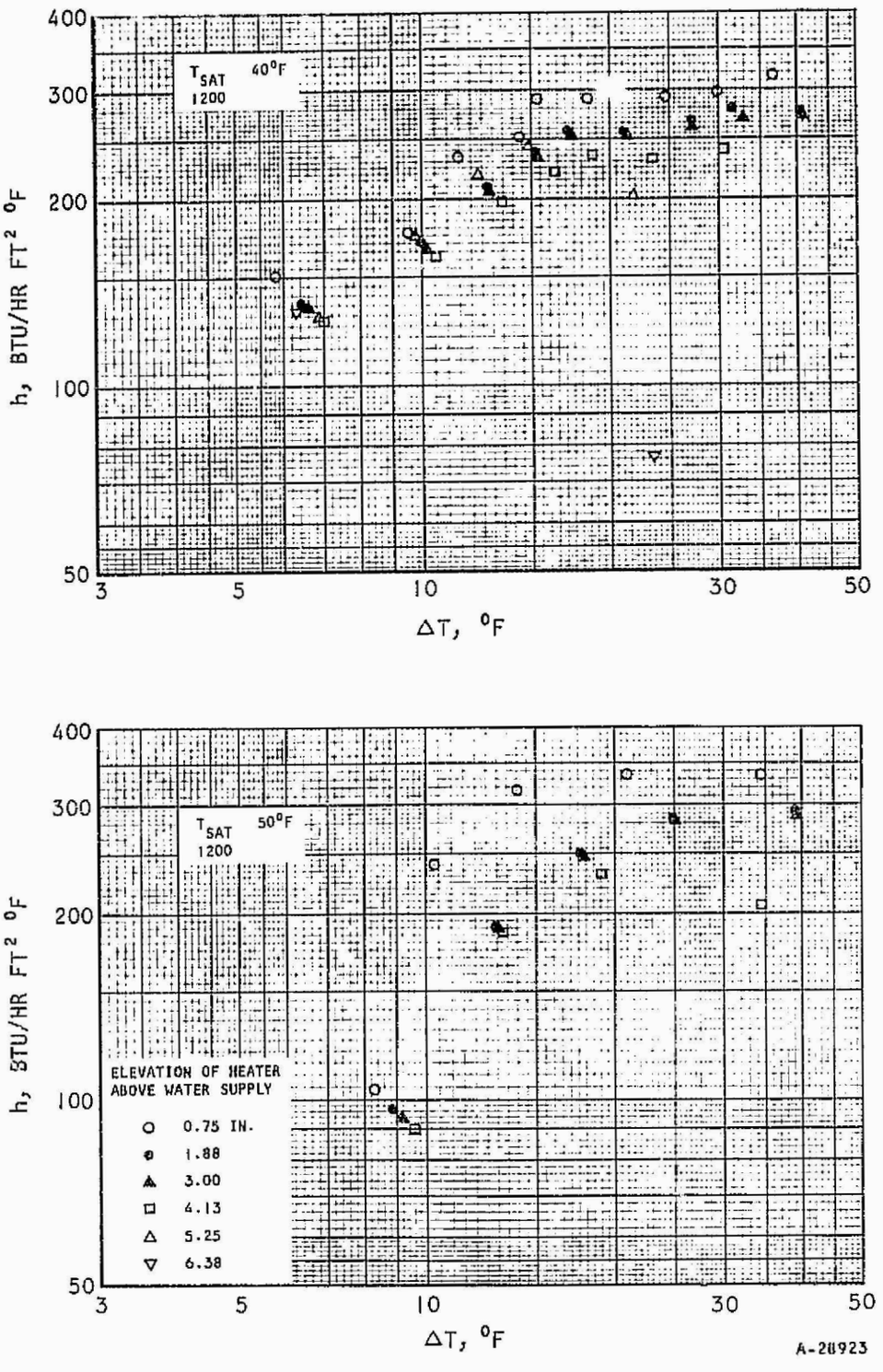

Figure B-7. Boiling Performance of Wick No. 1200

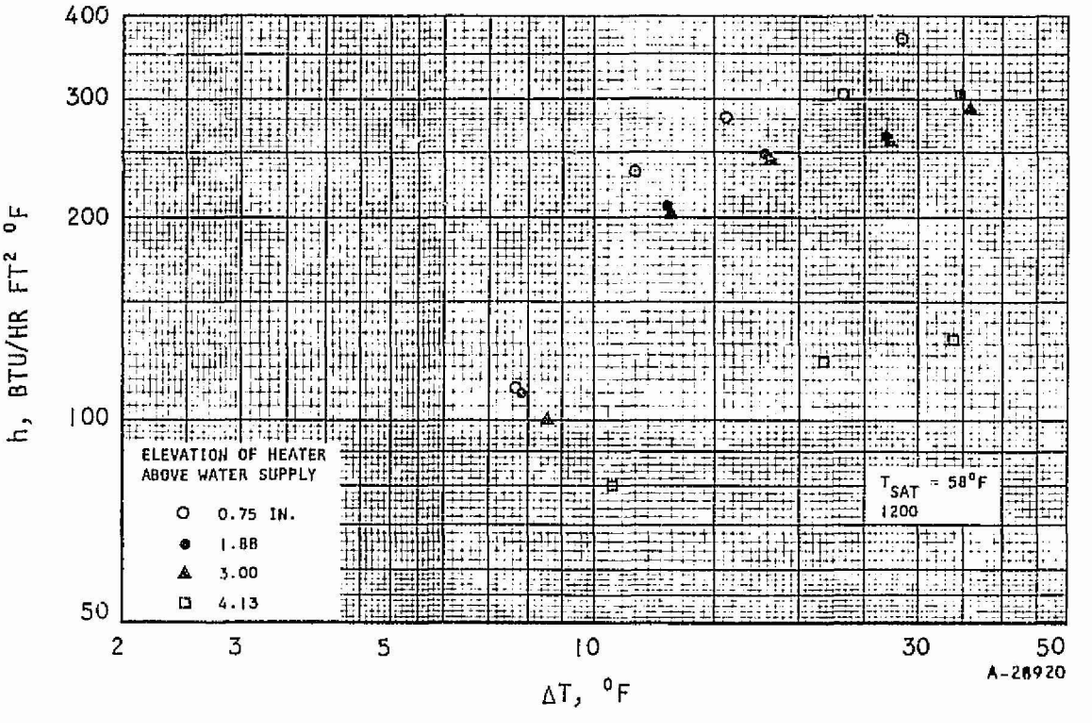

Figure B-8. Boiling Performance of Wick No. 1200

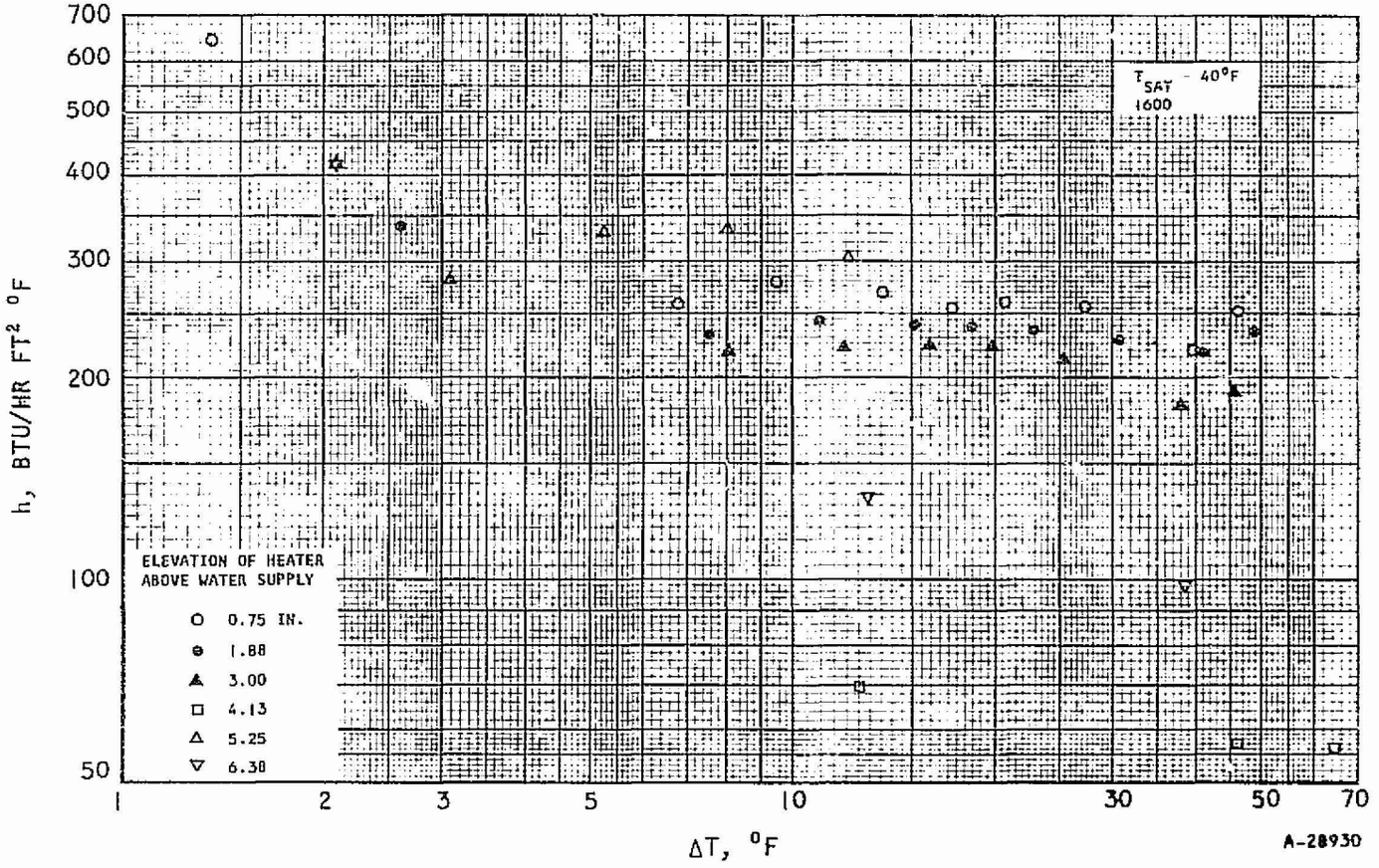

Figure B-9. Boiling Performance of Wick No. 1600

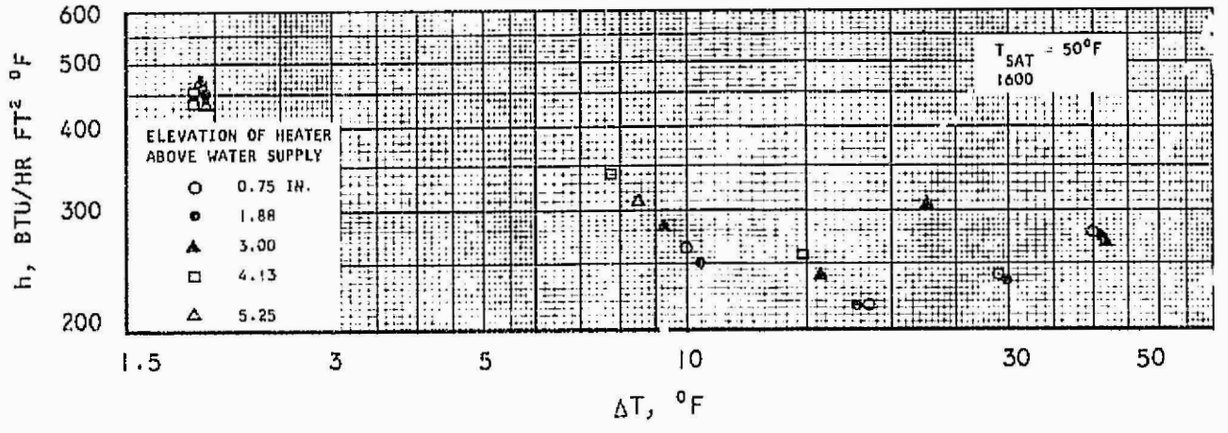

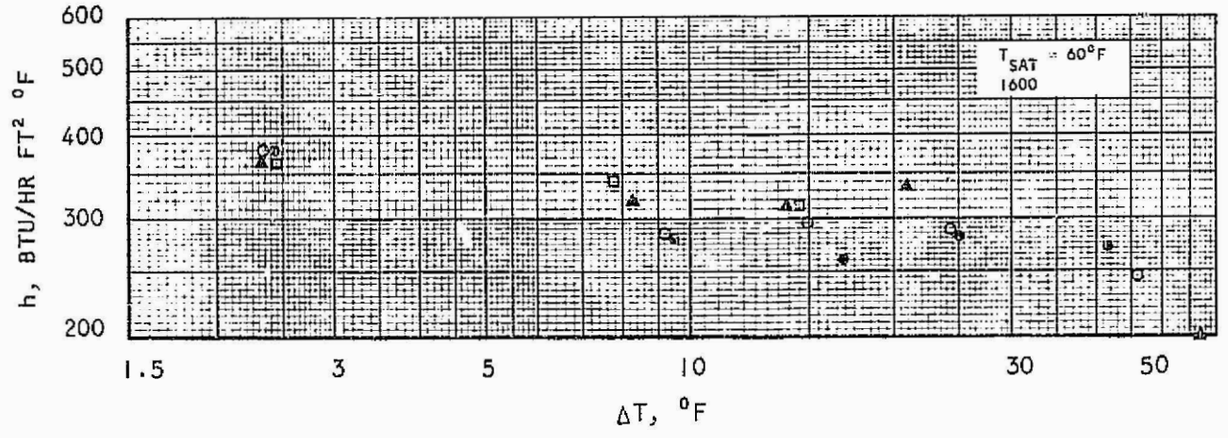

Figure B-10. Boiling Performance of Wick No. 1600

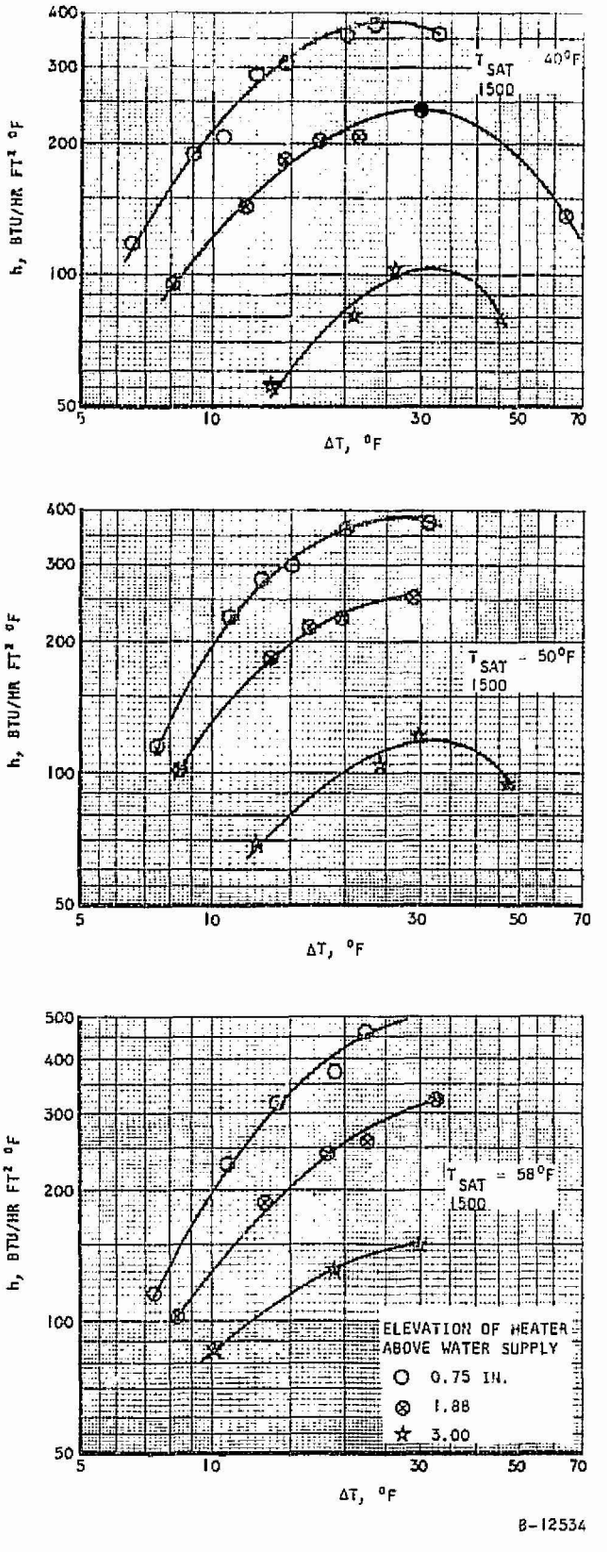

Figure B-11. Boiling Performance of Wick No. 1500

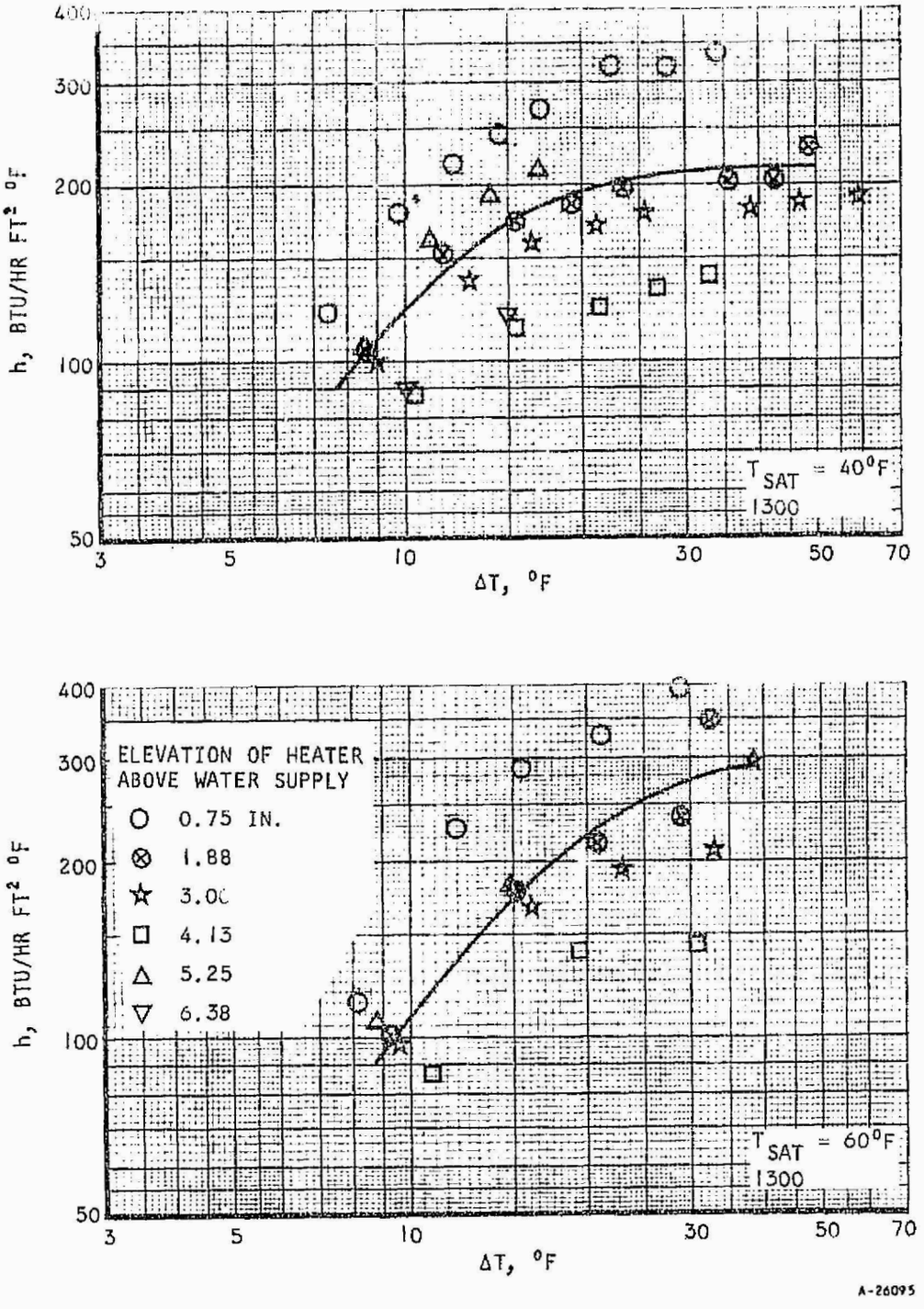

Figure B-12. Boiling Performance of Wick No. 1300

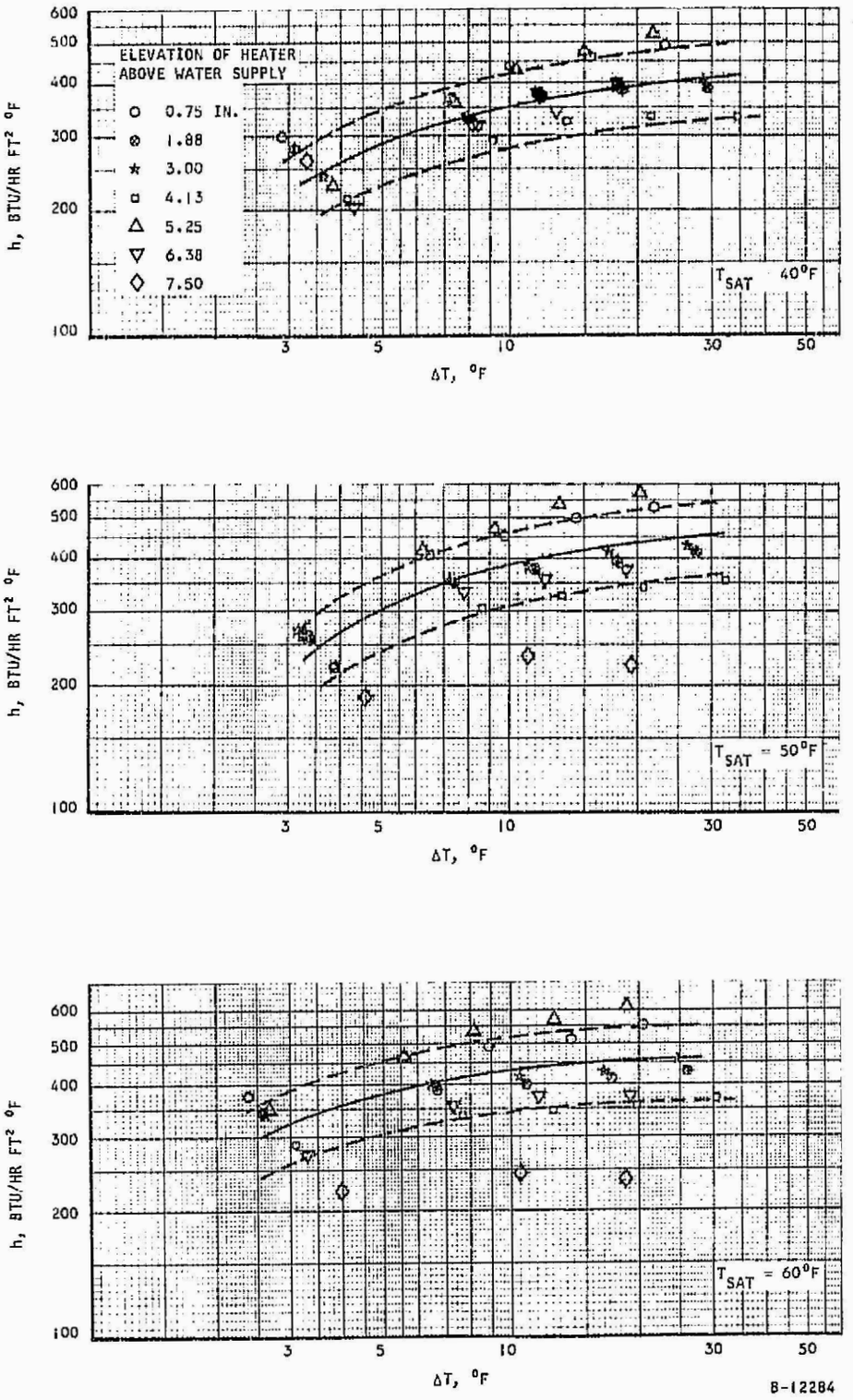

Figure B-13. Boiling Performance of Wick No. 700

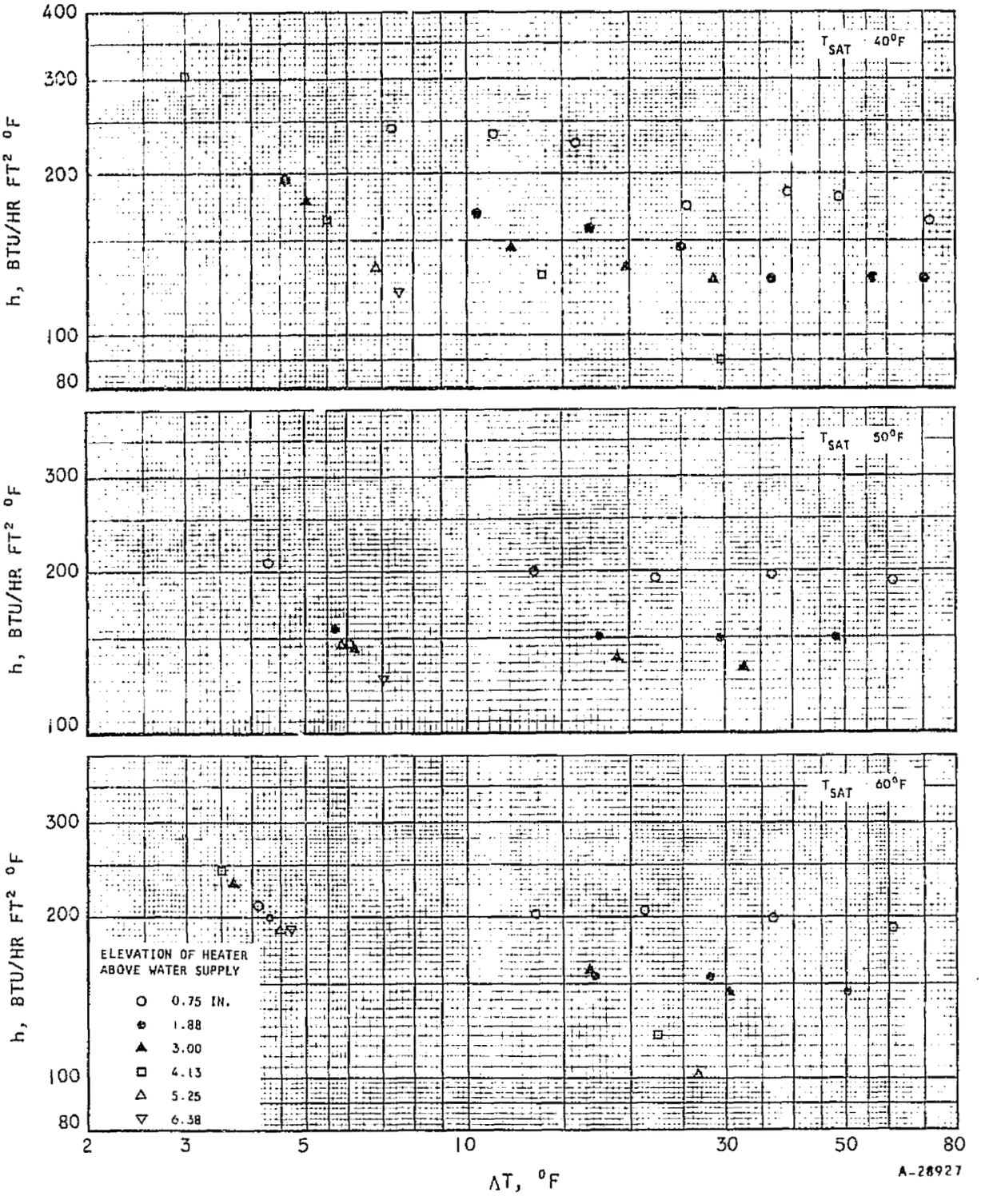

Figure B-14. Boiling Performance of Refrasil Wick

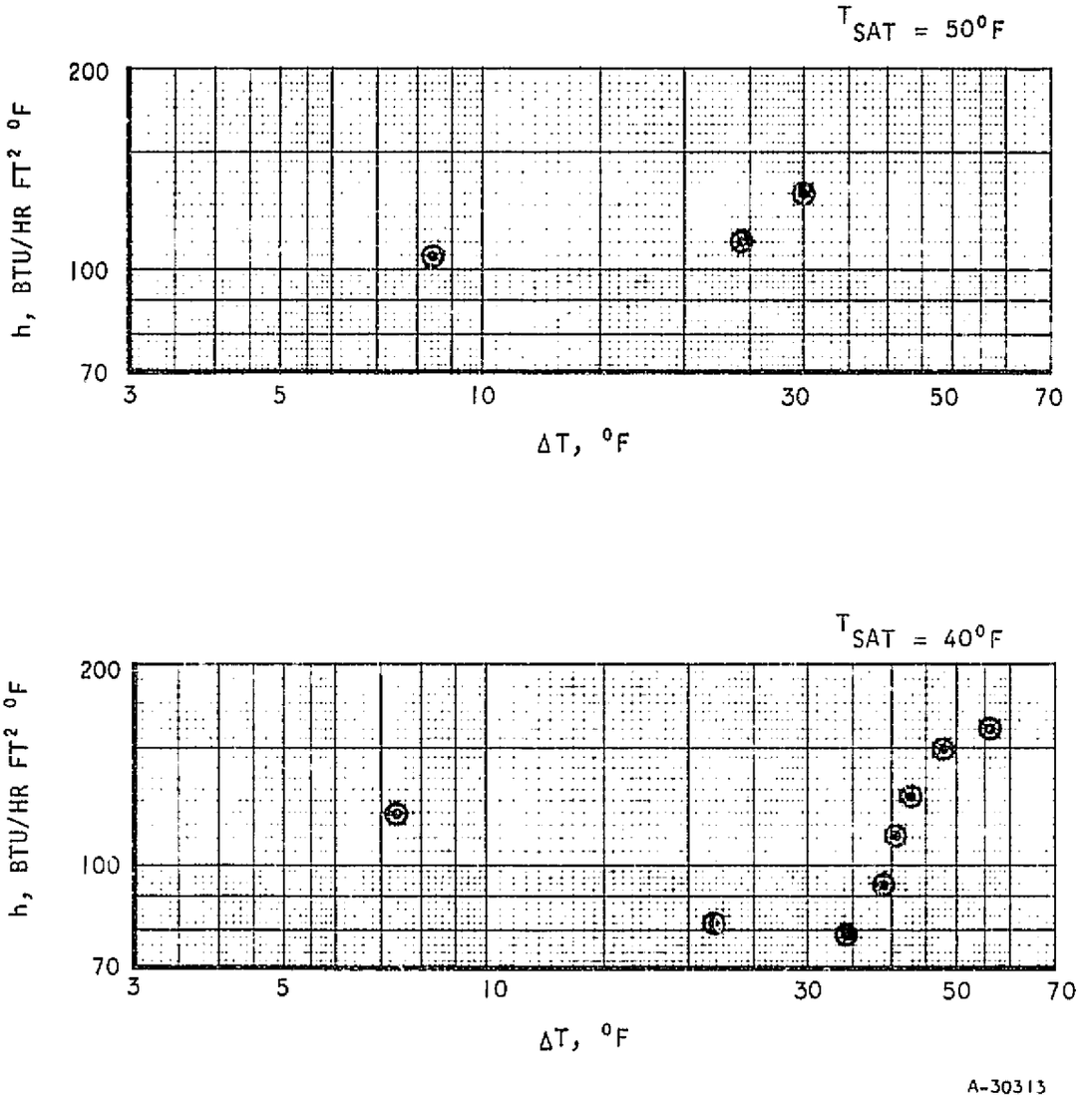

Figure B-15. Boiling Performance of Copper Wick

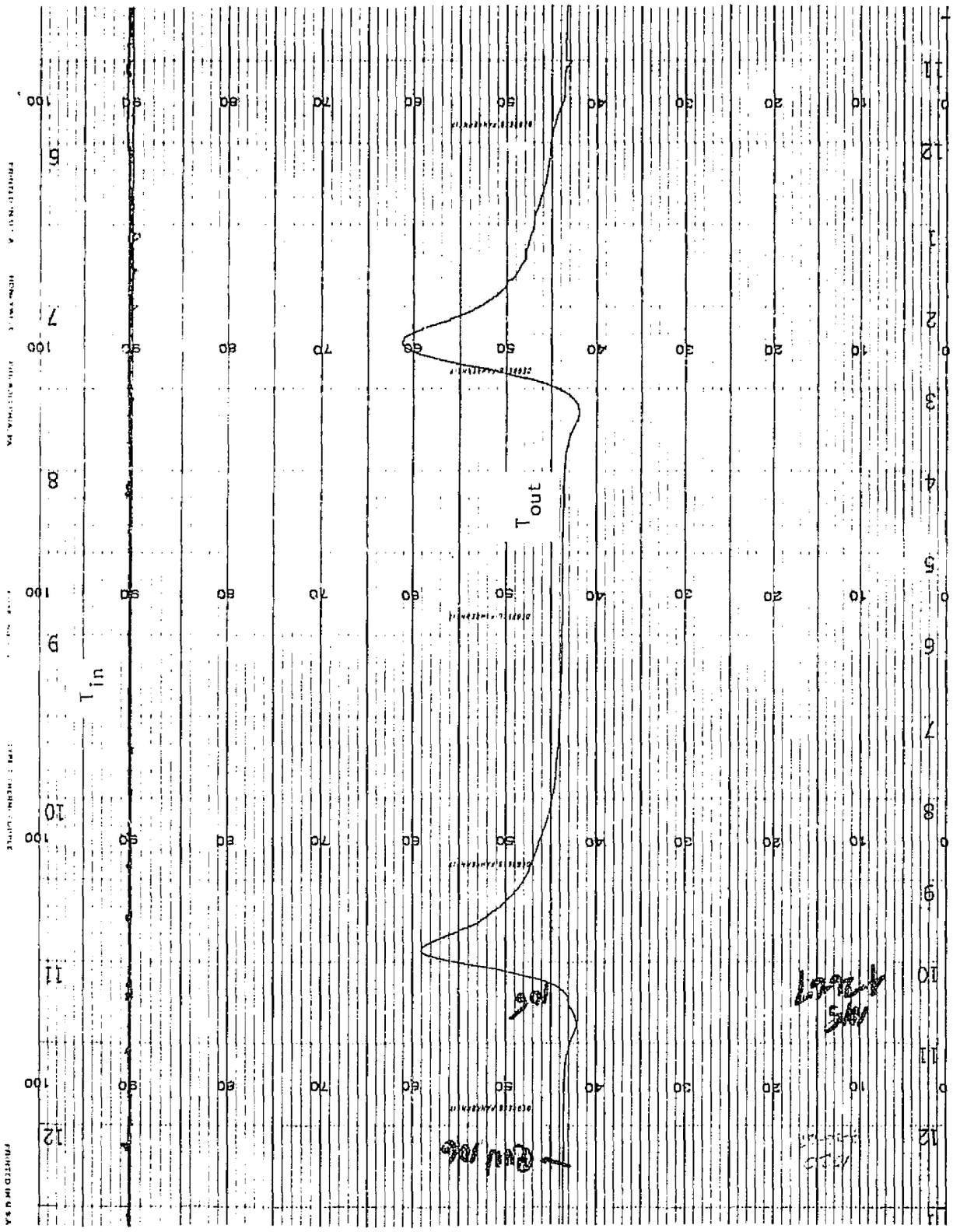

Figure B-16. One KW Boiler Heat Transport Fluid Temperature Trace for Runs 103-106

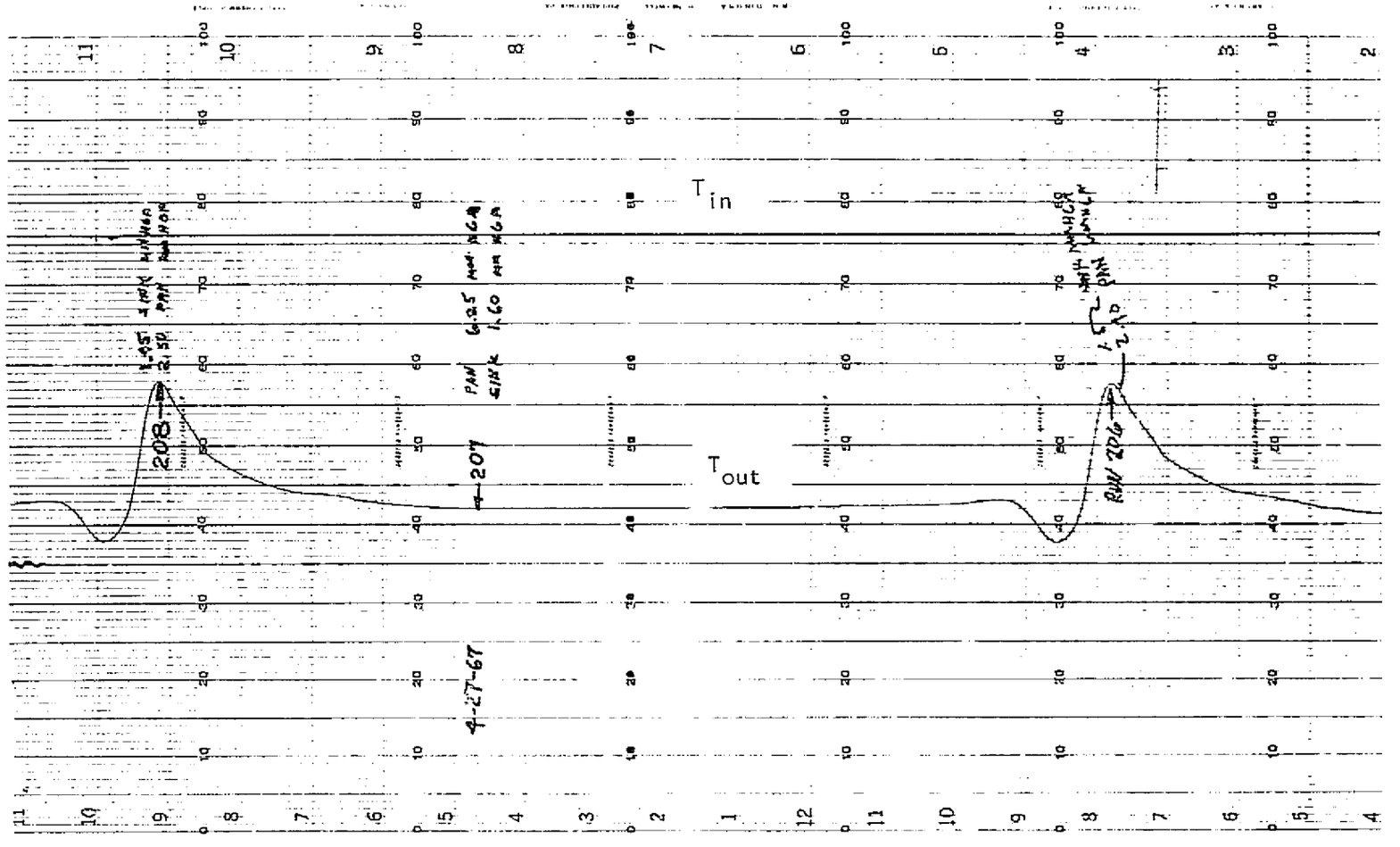

Figure B-17. One KW Boiler Heat Transport Fluid Temperature Trace for Runs 204-202

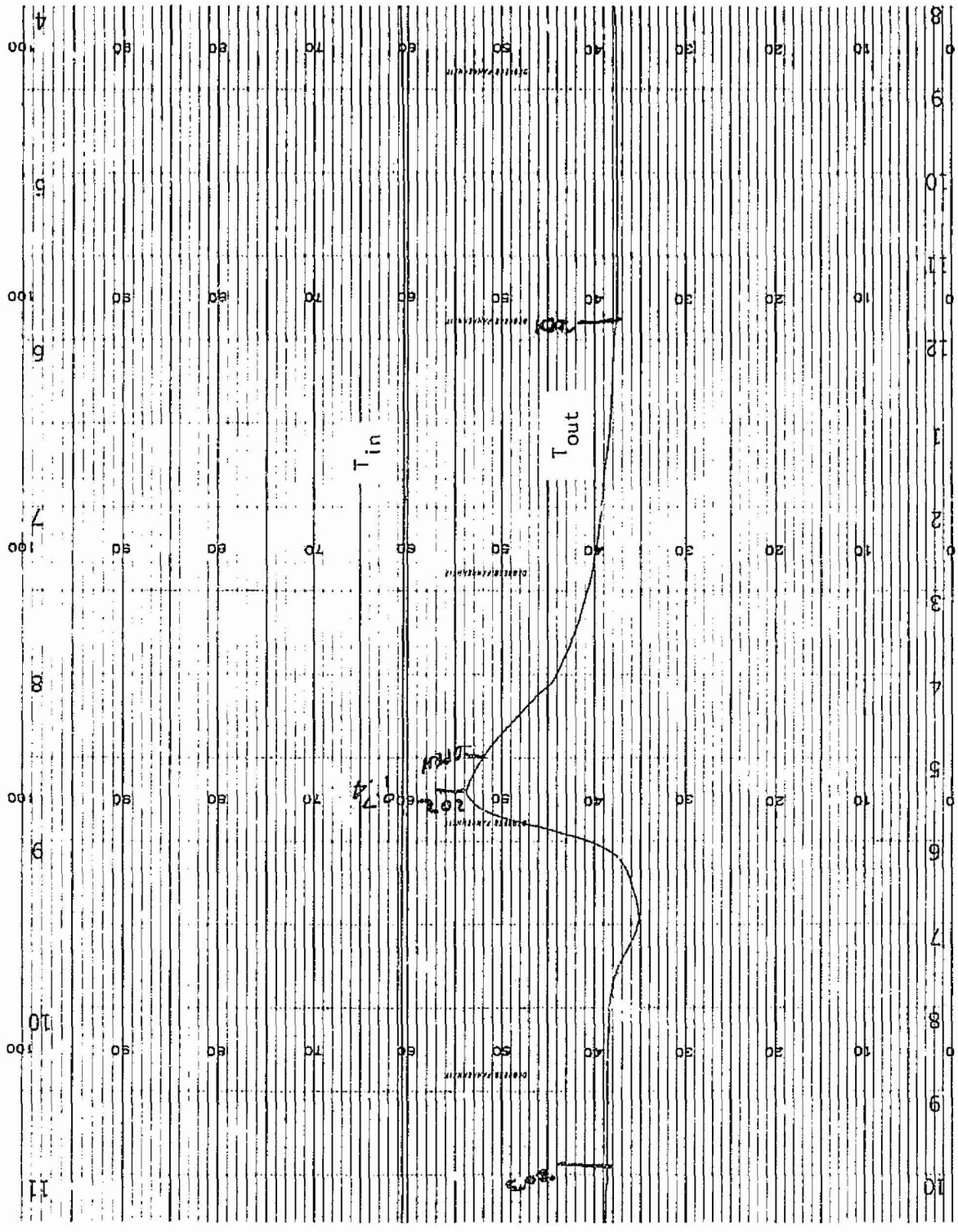

Figure B-18. One KW Boiler Heat Transport Fluid Temperature Trace for Runs 201-205

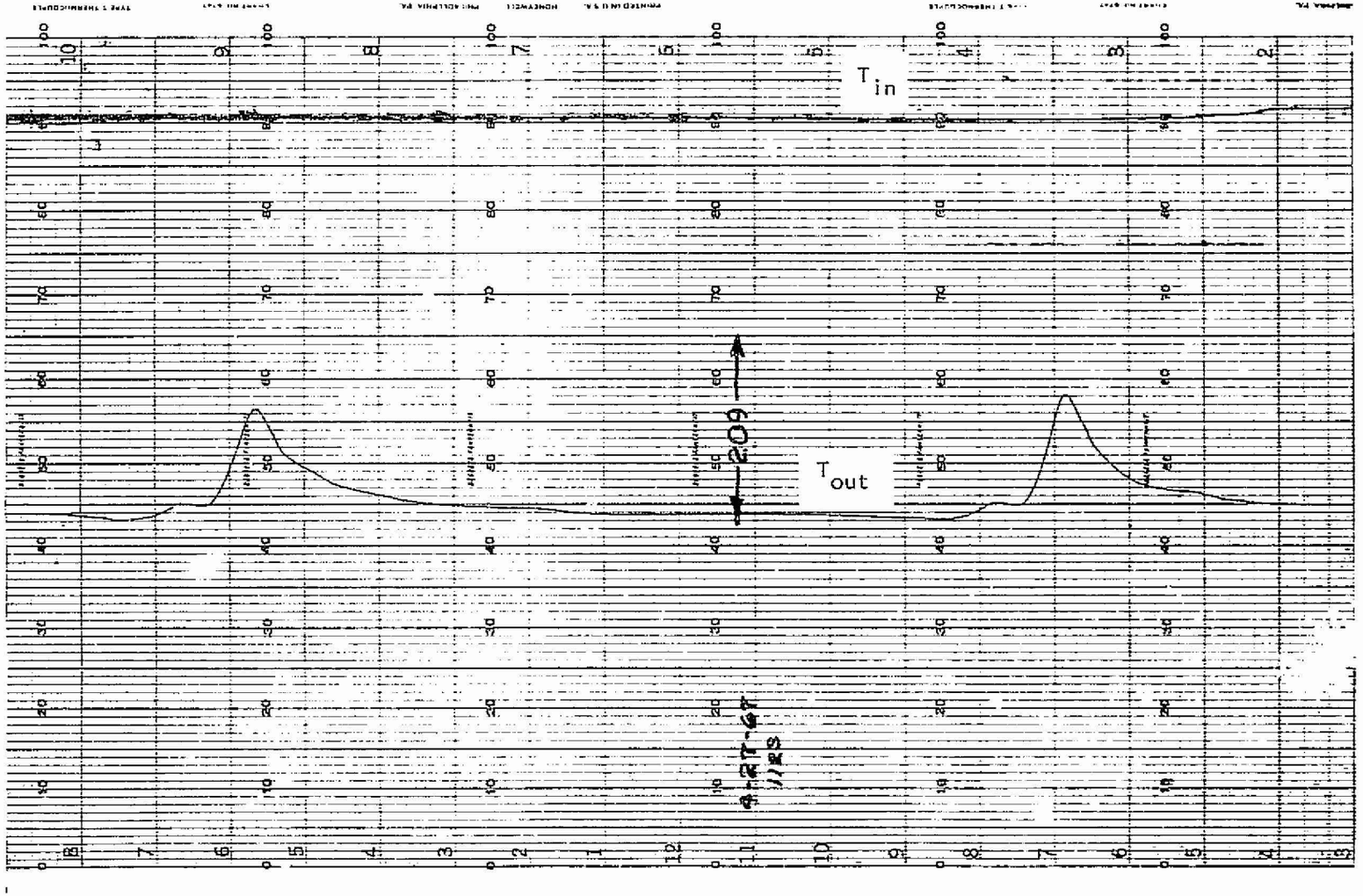

Figure B-19. One KW Boiler Heat Transport Fluid Temperature Trace for Runs 209-211

Figure B-20. One KW Boiler Heat Transport Fluid Temperature Trace for Runs 101-102

Figure B-21. One KW Boiler Heat Transport Fluid Temperature Trace for Runs 113-116

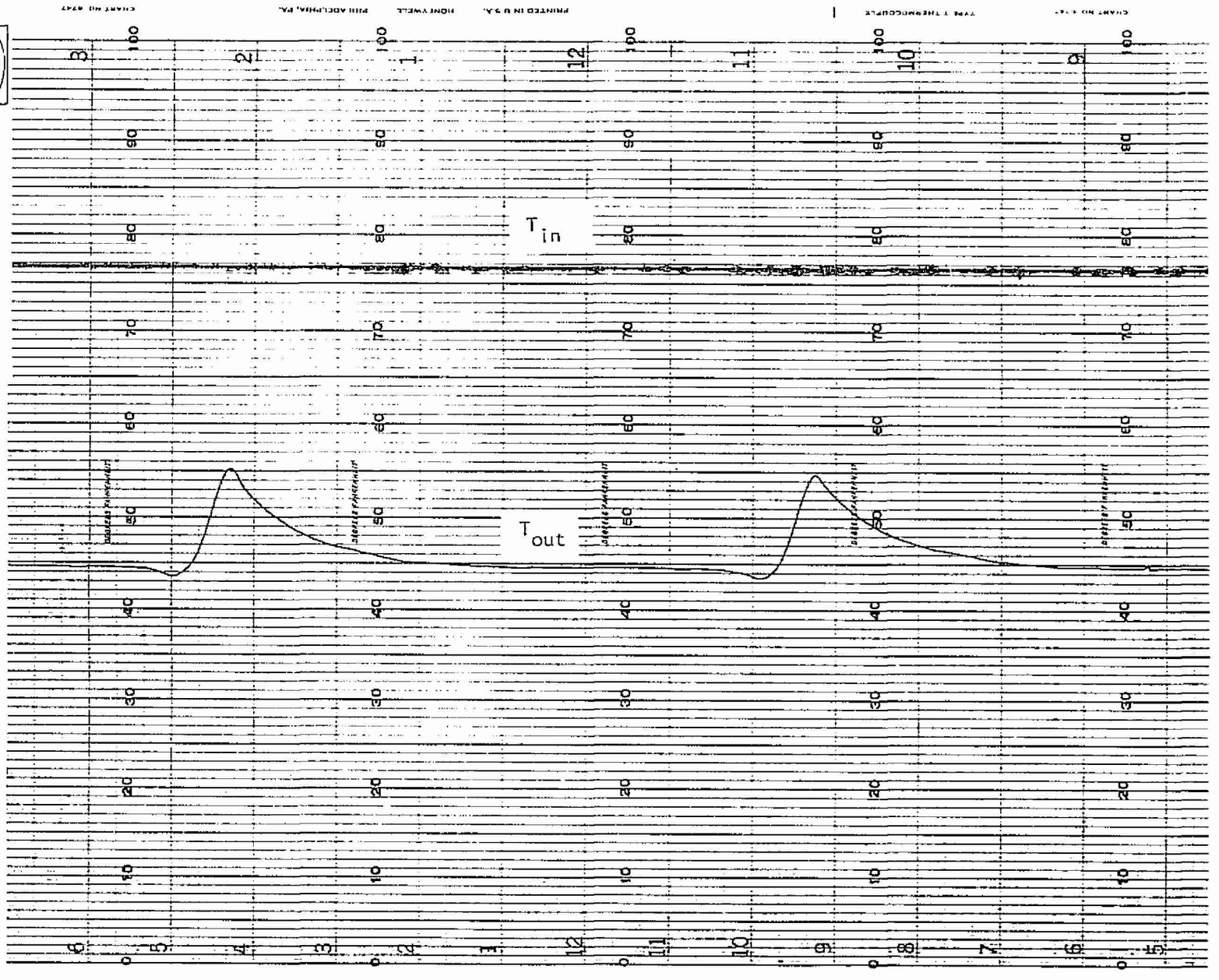

Figure B-22. One KW Boiler Heat Transport Fluid Temperature Trace for Runs 107-112

APPENDIX C

POROUS PLATE BENCH TEST AND SINGLE MODULE SUBLIMATION TEST RESULTS

POROUS PLATE BENCH TESTS

A series of bench tests were performed on porous plates. The results of these tests are given in Tables C-I and C-2 and in Figures C-I through C-8. A brief outline of the tests and test procedures is given below.

Water Breakthrough Pressure

Distilled one-half micron filtered water is supplied at steadily increasing pressure to the back face of a porous plate clamped in a holder. The pressure is recorded for water to initially form on the top face.

Bubble Point in Water

Distilled one-half micron filtered water is poured onto the top face of a porous plate clamped in a holder, sufficient to form a layer approximately one-half inch thick. Air is applied to the bottom face at a slowly increasing pressure. The pressure is recorded when the first dynamic bubble is seen and when 80 percent of the surface is seen to be bubbling.

Bubble Point in Alcohol

The same procedure as above is used except that 95 percent ethyl alcohol is substituted for water.

Nitrogen Permeability - Vacuum Discharge

Filtered nitrogen gas is supplied to the back face of a porous plate in a holder which is situated in an evacuated bell jar. The pressure drop across the plate is recorded at various flow rates, the downstream pressure being maintained at less than 500 microns pressure.

Nitrogen Permeability - Ambient Discharge

The same procedure as above is used except that the plate and holder are situated in laboratory ambient conditions.

The following handling procedure is used to insure cleanliness of the plates. Any contamination of the plates can produce serious errors in the results.

a. All testing is carried out in a clean area.

b. All plates are thoroughly cleaned prior to testing by heating in a vacuum furnace at 900^{0}F.

c. All plates are kept in nylon bags when not in use.

d. The surface of the plates are handled only when wearing clean rubber gloves.

SINGLE MODULE PERFORMANCE TESTING

To evaluate the performance of various porous plates, single module sublimation tests were performed. The results of a portion of these tests are shown in Figures C-9 through C-17 in the form of heated surface temperature versus heat flux. The significance of the results are discussed in Section 3, Water Sublimator Module.

TABLE C-I

POROUS PLATE CHARACTERISTICS

Plate	Material	Thickness in.	Porosity percent	Initial Bubble Point in Alcohol psi	Average Initial Bubble Point for Plates in Same Batch psi	80 Percent Bubble Point in Alcohol psi	Maximum Equivalent Pore Diameter Based on Average Bubble Point microns
L1A	Nickel	0.030		5.75		8.20	2.40
L2A		0.030		5.30		8.65	2.60
L3A		0.030		5.35		8.40	2.58
L4A		0.030		5.25		8.30	2.63
L5A		0.030		4.80		8.64	2.88
C1		0.053	56.7	--		--	
C2		0.046	49.5	1.81		2.24	7.62
C3		0.053	48.5	1.52		1.81	9.07
C4		0.056	50.0	1.88		2.16	7.33
C5		0.056	46.7	1.66		1.81	8.30
C6		0.052	54.1	1.59	1.50	1.73	
				1.40		1.74	9.20
UC-1A		0.020	48	2.92		4.26	4.72
UC-1B		0.018	42	--		--	--
UC-1C		0.015	32	4.59		6.50	
				4.61		7.08	
-1				4.47	4.44	4.91	
-2				4.87		6.00	3.11
-3				3.93		5.85	
-4				4.18		6.64	
UC-2A		0.024	47	1.91		2.67	
				2.26		3.48	
				1.62		2.75	
-1				1.03	1.81	3.14	7.62
-2				2.60		3.39	
-3				1.57		2.90	
				1.67		3.14	
UC-2B		0.022	41	3.83		5.05	
				3.49		5.75	
-1				3.74	3.56	4.19	3.88
-2				3.15		3.94	
-5				3.59		5.11	

TABLE C-I (Continued)

Plate	Material	Thickness in.	Porosity percent	Initial Bubble Point in Alcohol psi	Average Initial Bubble Point for Plates in Same Batch psi	80 Percent Bubble Point in Alcohol psi	Maximum Equivalent Pore Diameter Based on Average Bubble Point microns
UC-2C	Nickel	0.028	32	4.62		8.15	
-2				5.65		7.87	
				5.80		7.71	
-3				5.60		8.11	
-4				5.15		7.61	
				4.13		6.34	
-5				3.37	4.60	6.81	3.00
-6				3.61		8.79	
				3.29		6.93	
-8				5.60		7.56	
				4.09		--	
-9				4.87		7.82	
-10				3.90		8.32	
UC-3A		0.023	48	4.26	4.25	5.60	
				4.23		5.75	3.25
UC-3B		0.020	44	2.64	2.58	3.68	
				2.51		4.37	5.35
UC-3C		0.018	34	2.10	2.35	3.61	
				2.60		3.54	5.86
UC-4A		0.024	48	1.88	1.90	2.56	
				1.91		--	7.26
UC-4B		0.022	32	2.71		4.70	
-1				3.59	3.10	4.23	
-2				2.90		3.68	4.45
-5				3.20		4.81	

TABLE C-I (Continued)

Plate	Material	Thickness in.	Porosity percent	Initial Bubble Point in Alcohol psi	Average Initial Bubble Point for Plates in Same Batch psi	80 Percent Bubble Point in Alcohol psi	Maximum Equivalent Pore Diameter Based on Average Bubble Point microns
UC-4C		0.020	29	3.72		6.14	
-1				3.39		5.55	
-2				3.84		6.10	
				3.74		5.11	
-3				3.78		6.74	
-5				4.08	3.52	6.98	3.92
-6				2.90		6.10	
-7				3.69		5.11	
-8				3.20		6.40	
-9				2.90		5.70	
APM 28		0.034		2.46		3.93	5.60
30		0.032		2.46		3.68	5.60
34		0.029		3.93		6.87	3.51
35		0.028		4.66		7.85	2.96
BM 1	Nickel	0.002		2.72		5.06	5.07
3		0.002		1.08		2.72	12.8
5		0.002		0.62		1.81	22.2
Rigimesh 1	Nickel	0.012		2.38		2.78*	5.80
Teflon A	Teflon	0.136		.613		.67*	22.5
Teflon C	Teflon	0.075		1.34		1.36*	10.3
KEL-F B		0.119		.119		.145*	116.
KEL-F D		0.071		.108		.134*	128.

*Tenth bubble point

TABLE C-2

POROUS PLATE CHARACTERISTICS

Plate	Initial Bubble Point in Water psi	Water Retention Pressure psi	
L1A	>10	---	
L2A	>10	---	
L3A	>10	---	
L4A	>10	---	
L5A	>10	---	
C1	3.8	---	
C2	5.3	---	
C3	4.9	---	
C4	5.2	---	
C5	5.2	---	
C6	4.5	0.072	
UC-2A-3	---	0.065	
UC-2C-4	10.8	---	
-5	8.4	---	
UC-4C-I	>12.3	0.57	
-II	>12.3	0.54	
-III	>12.3	0.59	
-IV	>12.3	0.57	
UC-4C-I	---	7.8	
-II	---	10.0	After coating
-III	---	6.9	with Teflon film
-IV	---	11.2	
UC-4C-A	12.0	0.34	
-B	12.1	0.25	
-C	12.1	0.20	
-D	10.6	0.20	
UC-4C-C	8.4	7.9	After coating
-D	8.1	7.5	with Teflon film
BM1	---	0.30	
BM3	---	0.03	
BM5	---	0.03	
Rigimesh 1	0.74	1.6	
Teflon A	0.065	1.95	
Teflon C	0.123	4.1	
KEL-F B	0.134	0.24	
KEL-F-D	0.072	0.20	

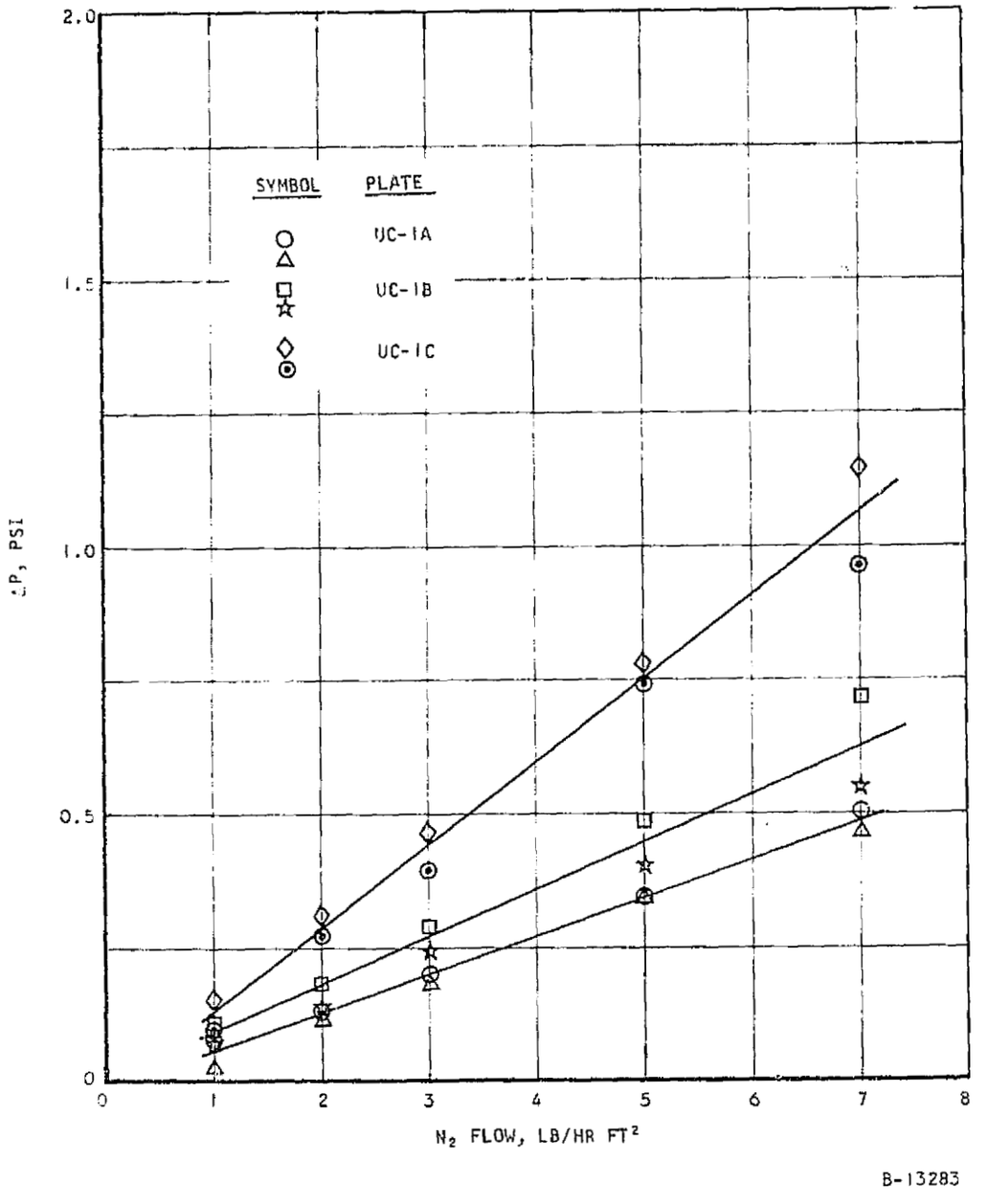

Figure C-1. Nitrogen Permeability with Discharge to Vacuum

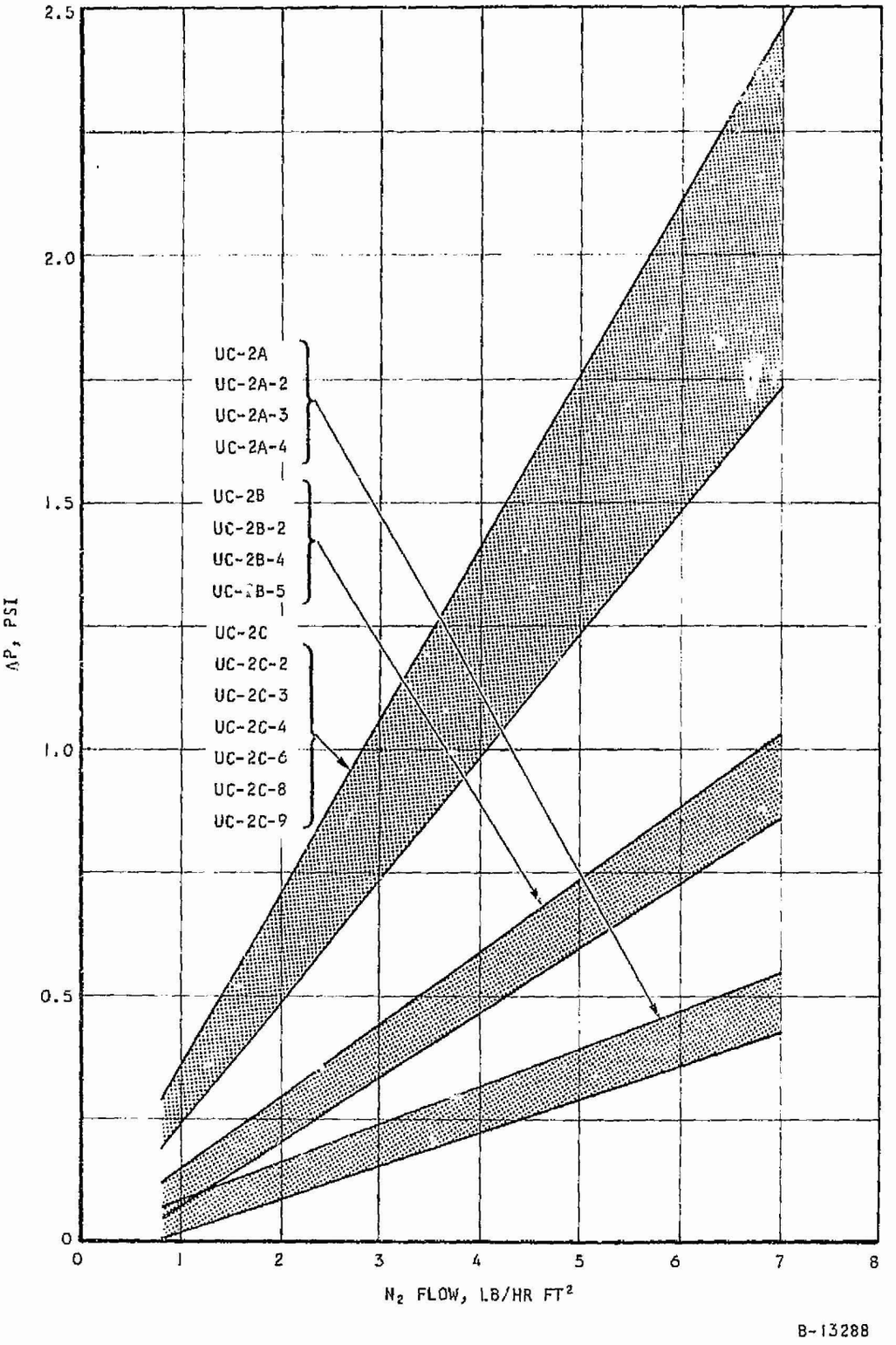

Figure C-2. Nitrogen Permeability with Discharge to Vacuum

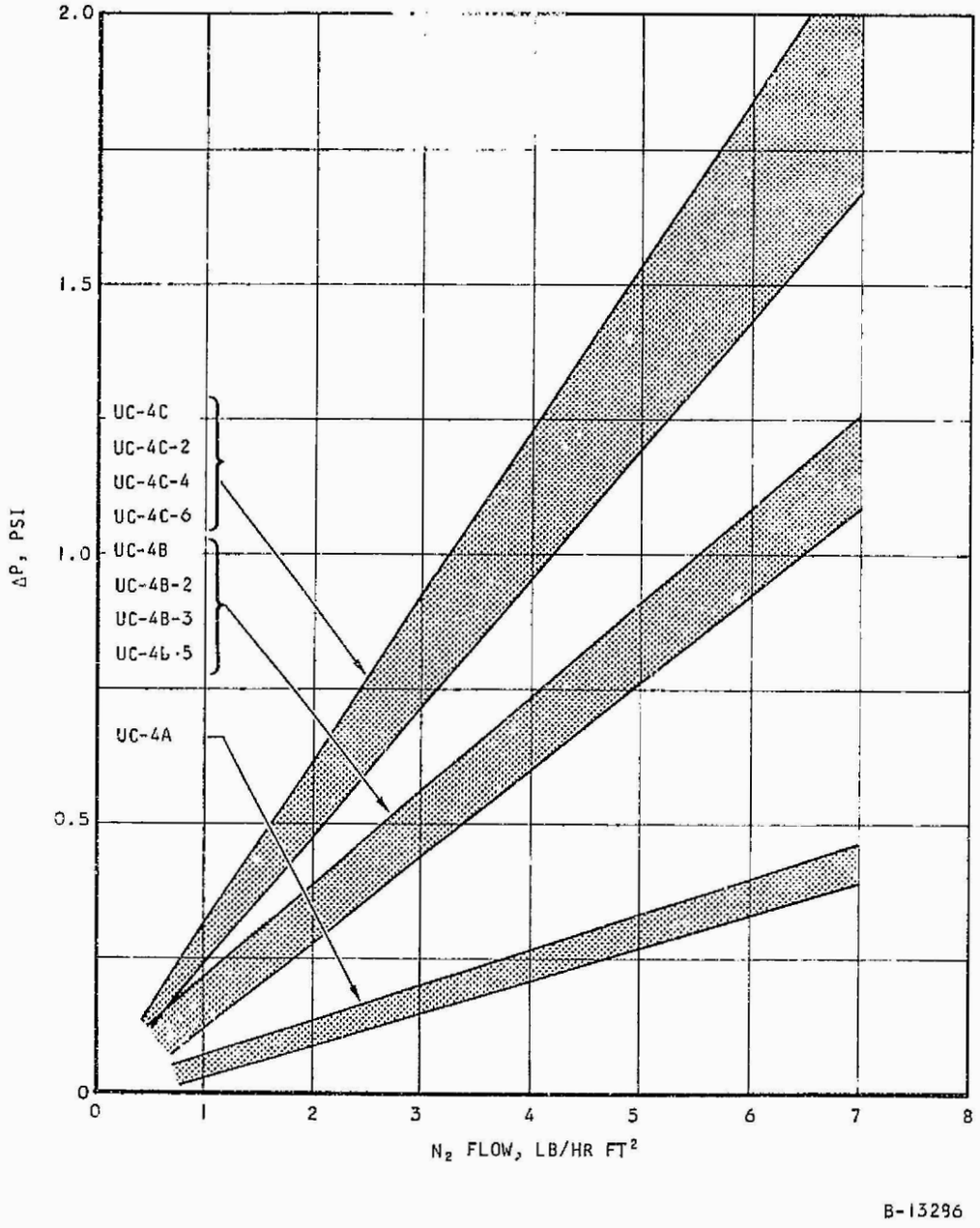

Figure C-3. Nitrogen Permeability with Discharge to Vacuum

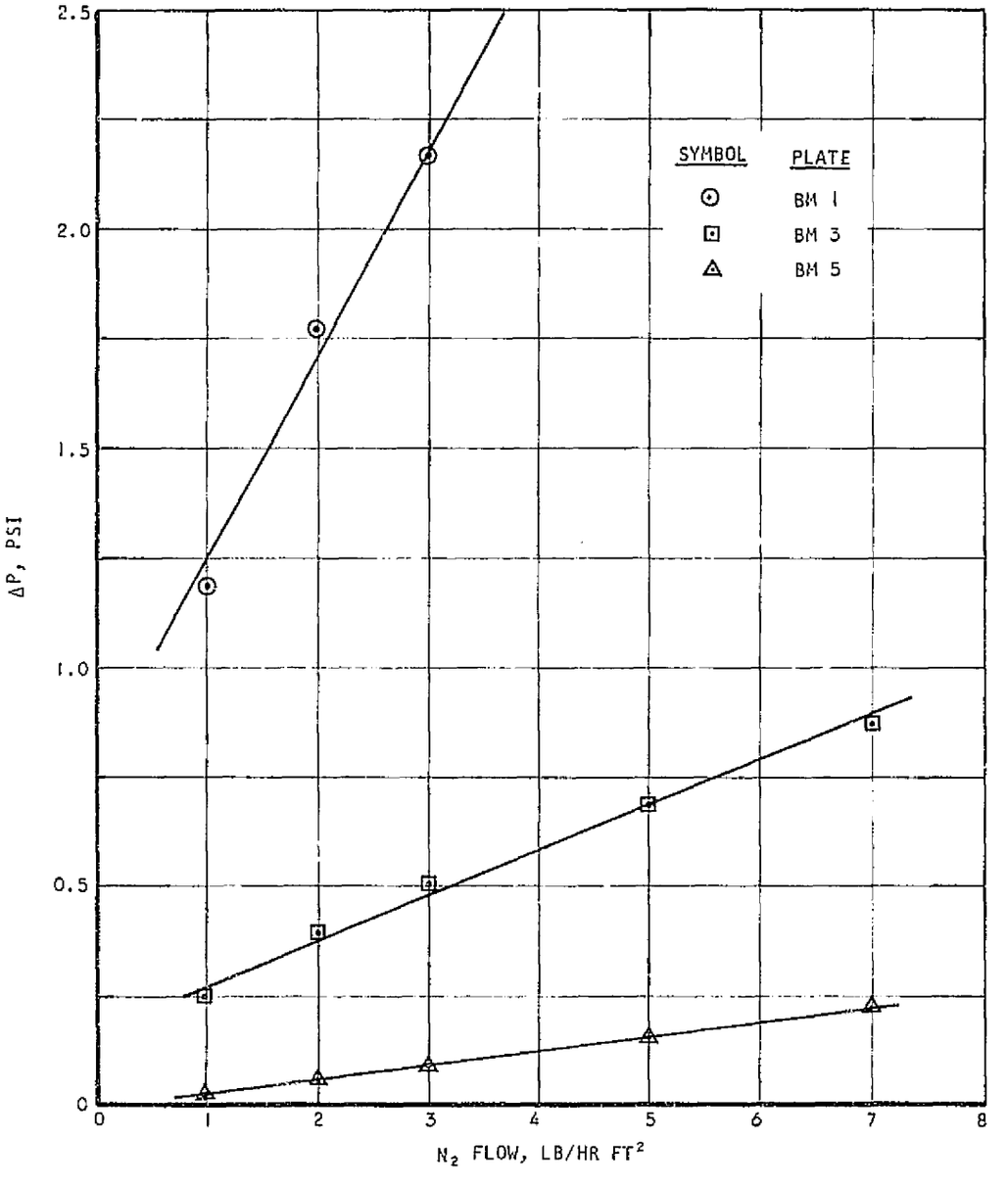

Figure C-4. Nitrogen Permeability with Discharge to Vacuum

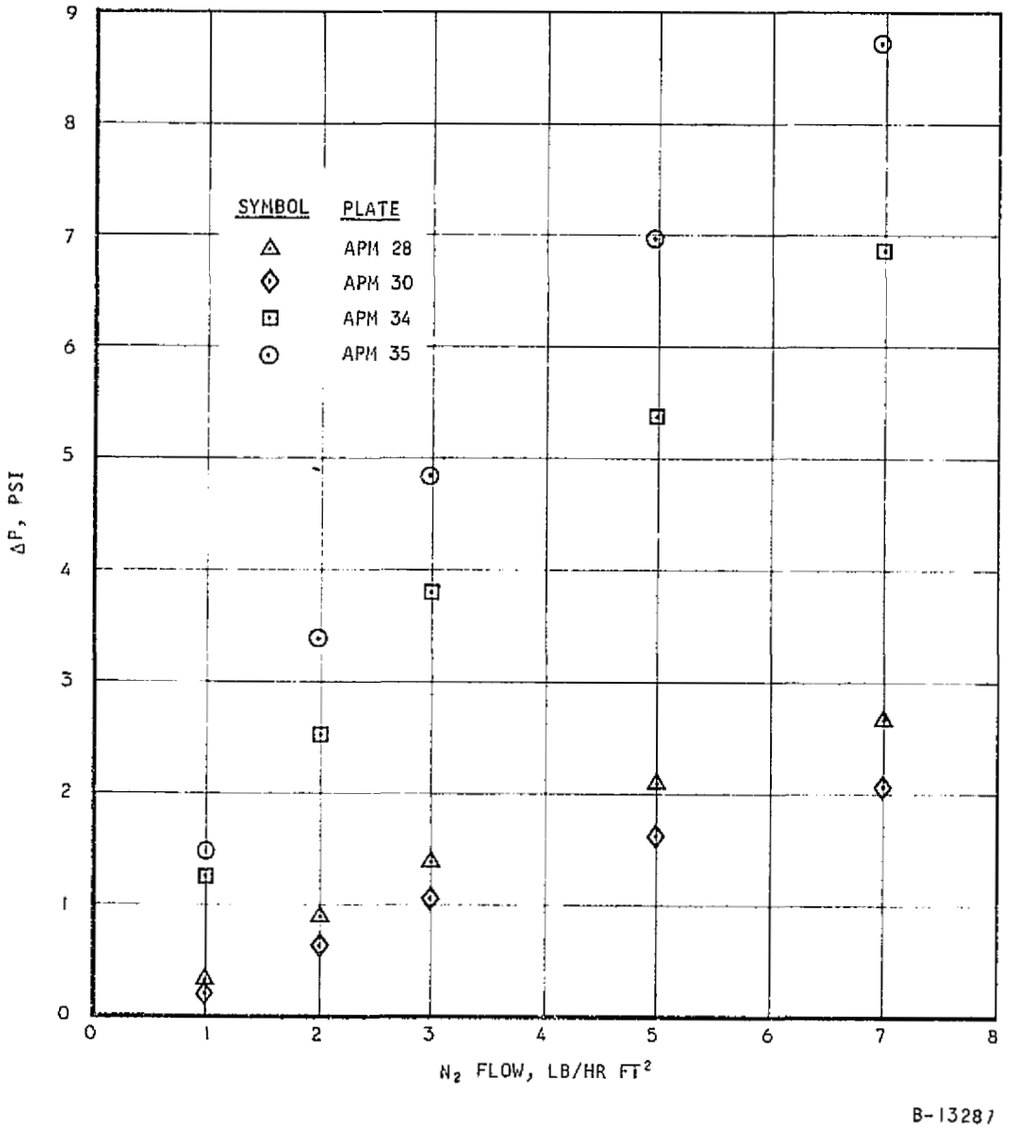

Figure C-5. Nitrogen Permeability with Discharge to Vacuum

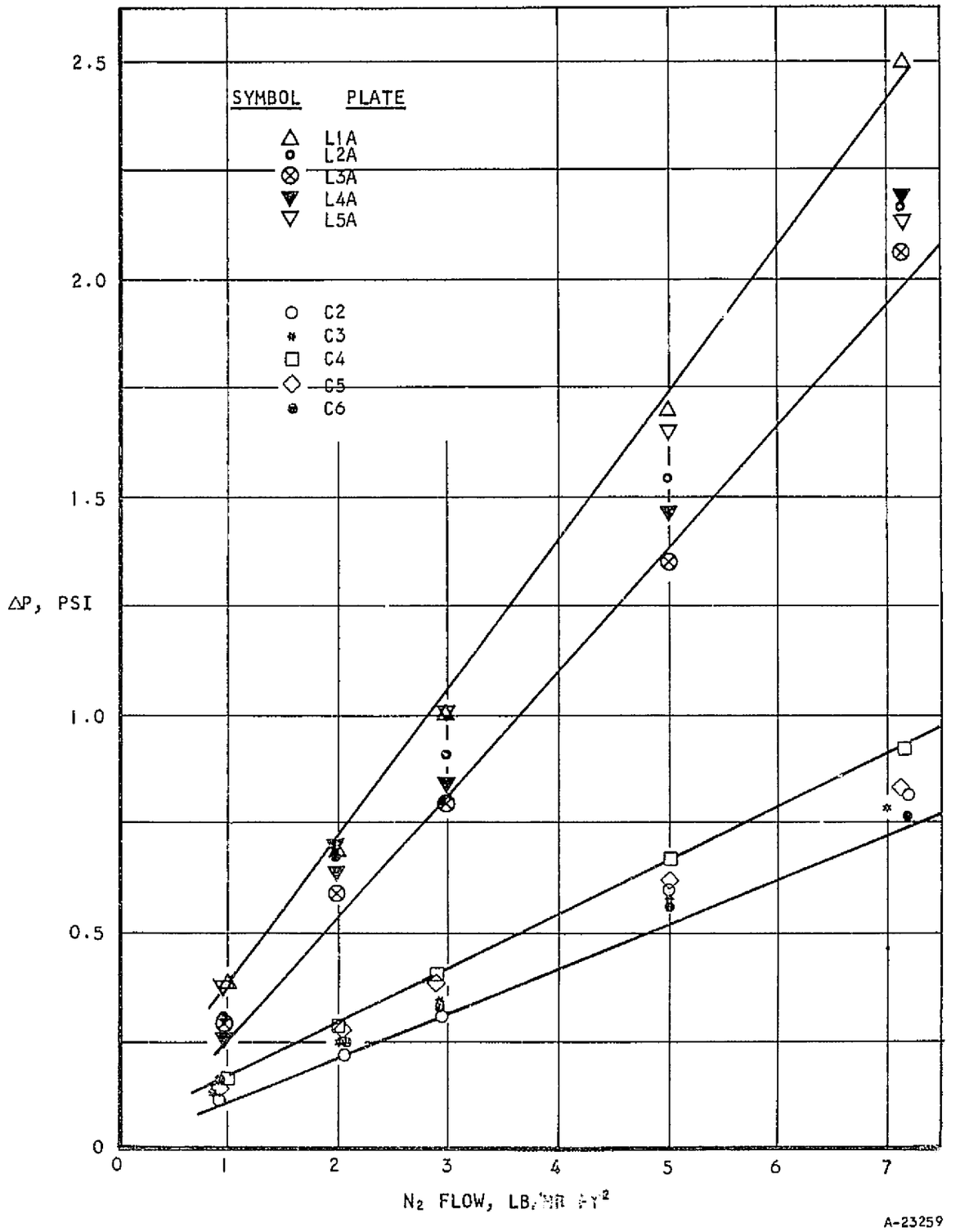

Figure C-6. Nitrogen Permeability with Discharge to Vacuum

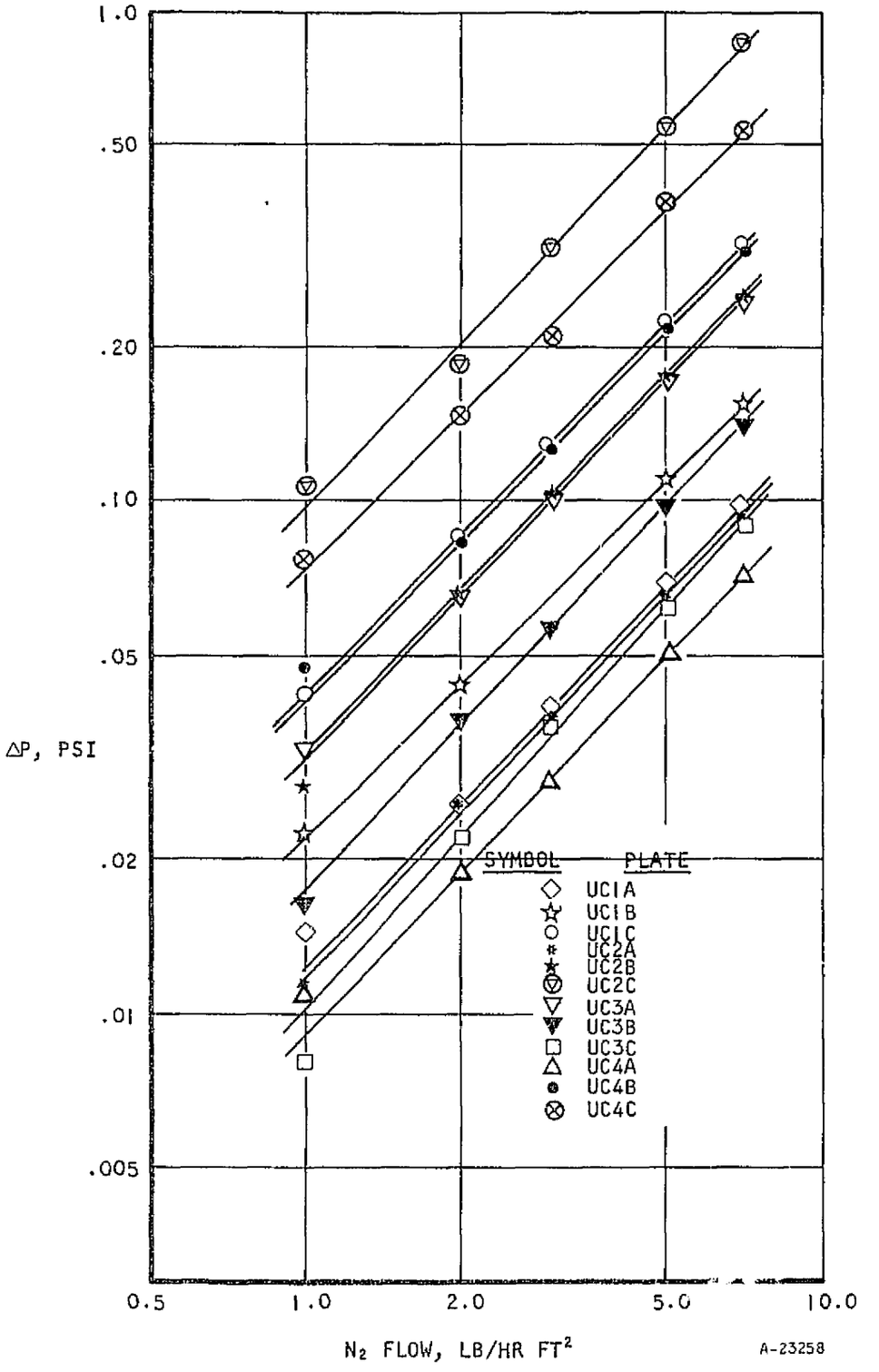

Figure C-7. Nitrogen Permeability with Discharge to Ambient

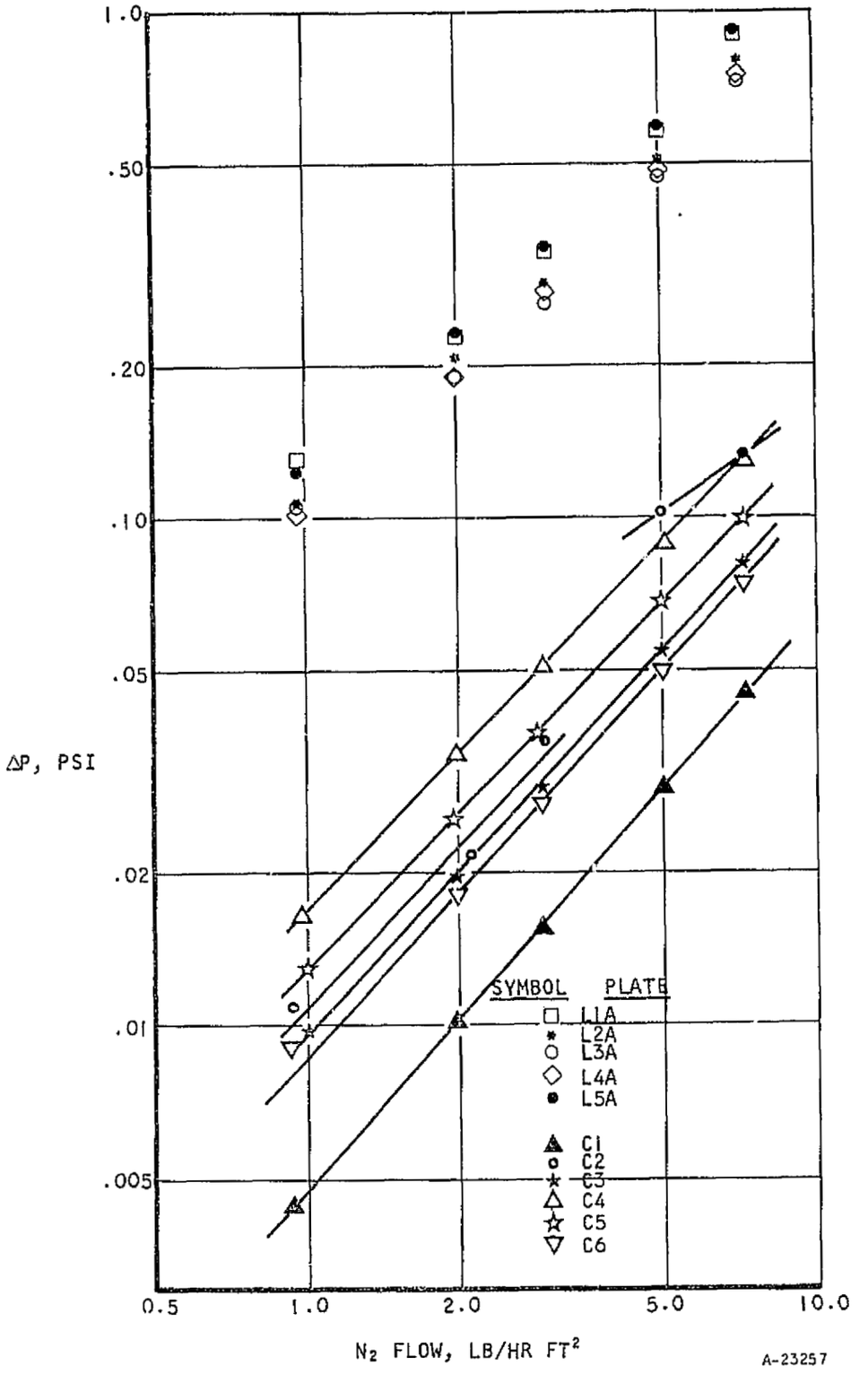

Figure C-8. Nitrogen Permeability with Discharge to Ambient

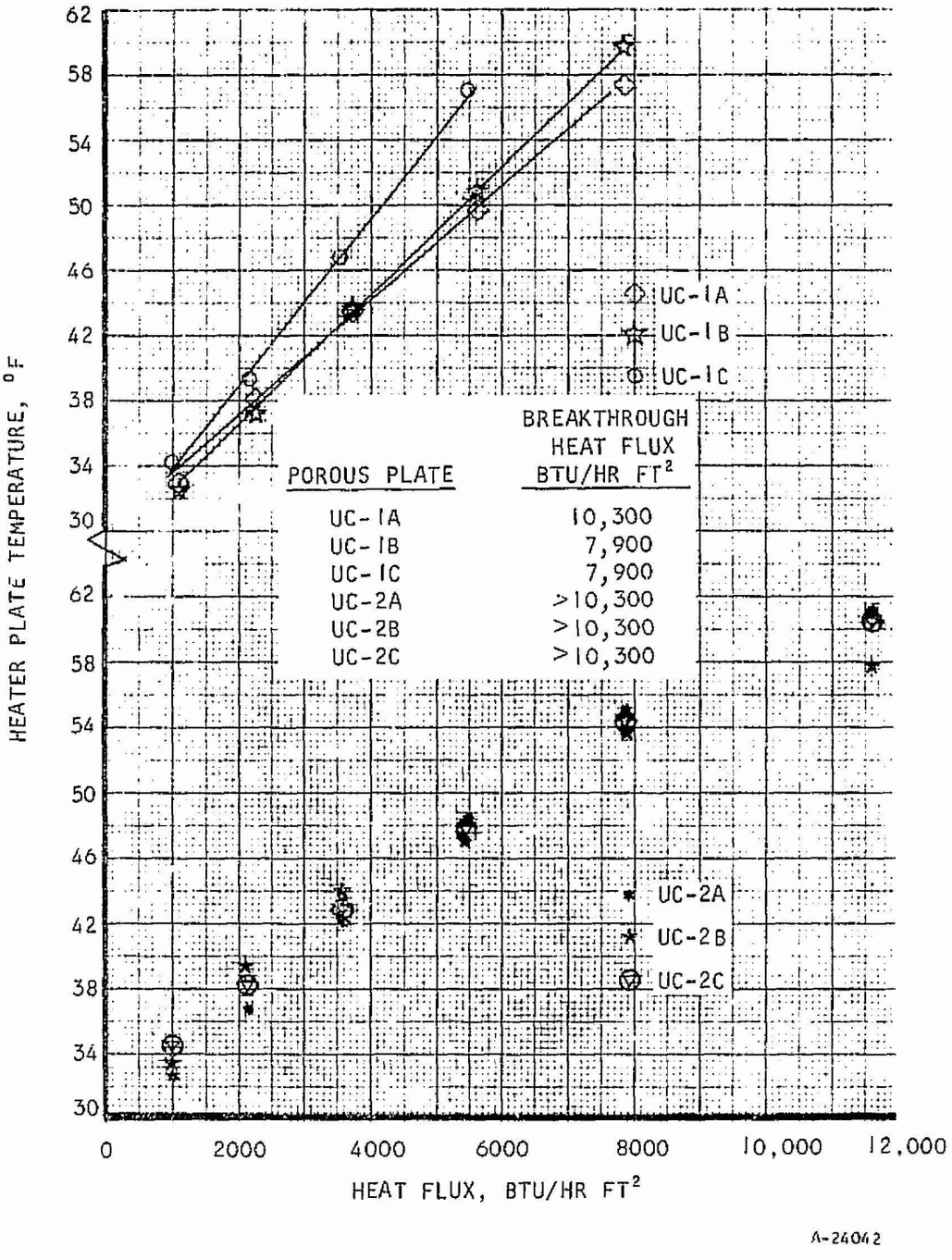

Figure C-9. Single Module Sublimator Performance

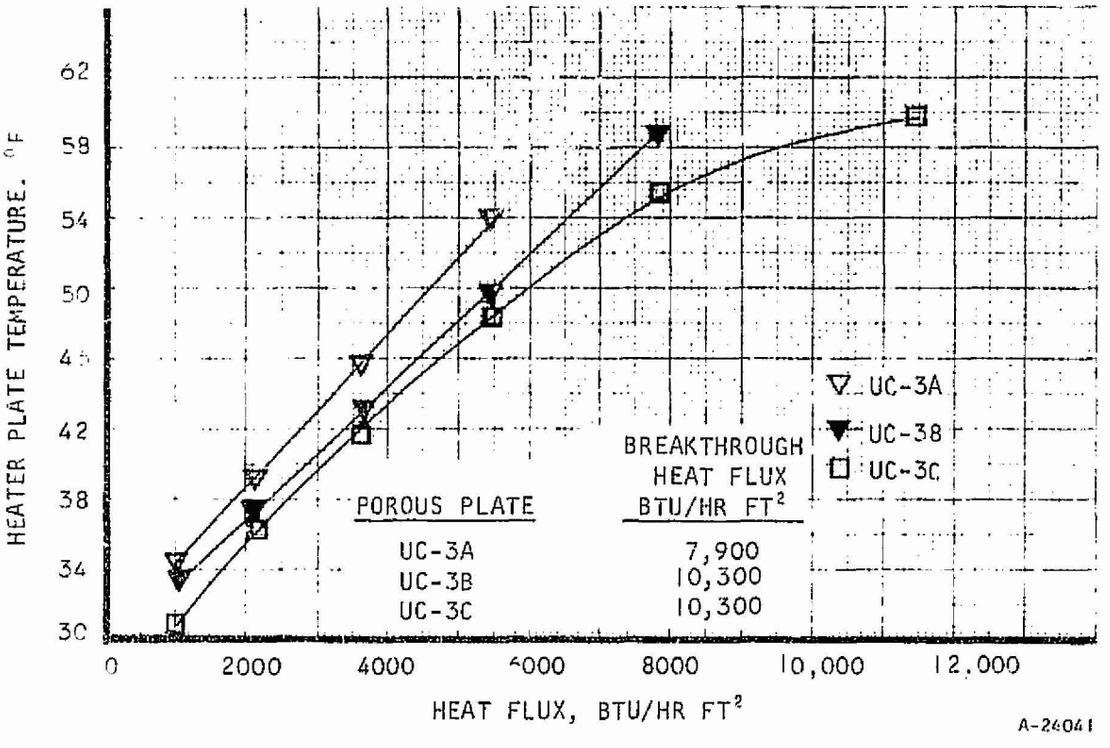

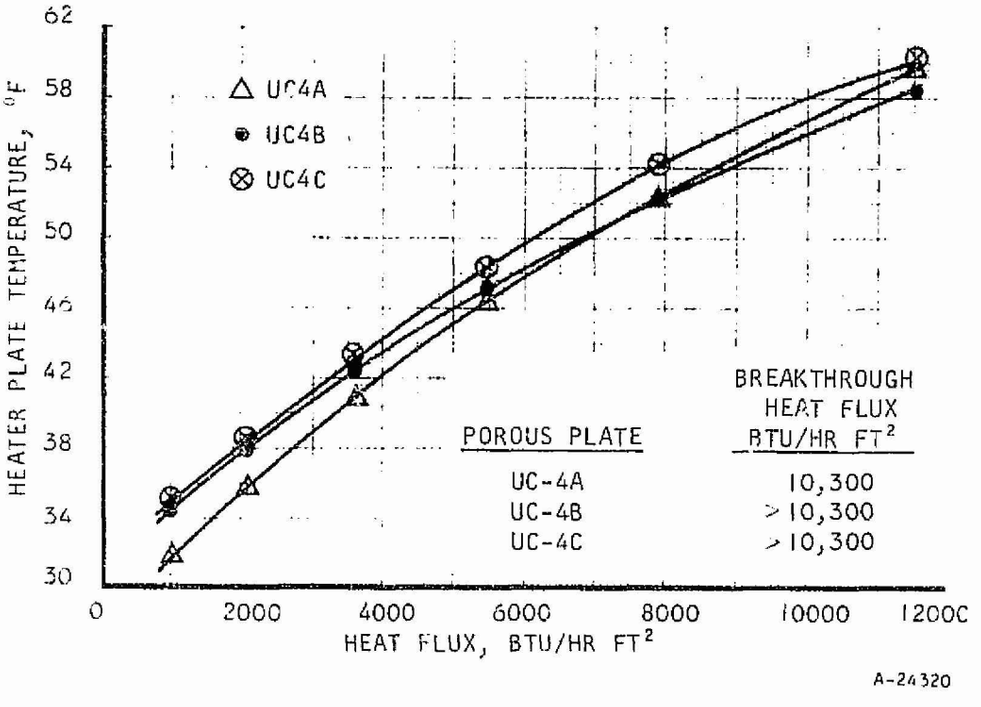

Figure C-10. Single Module Sublimator Performance

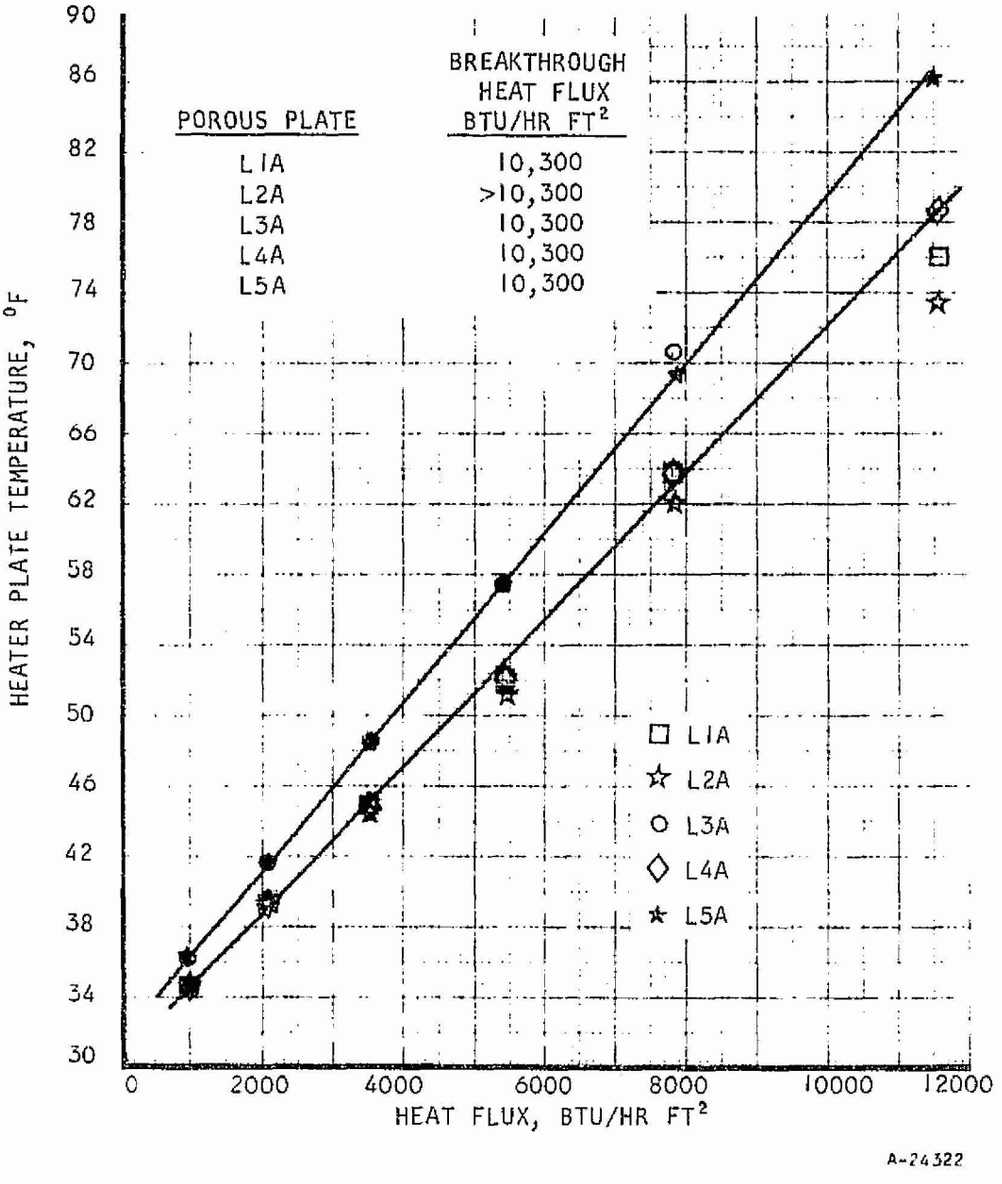

Figure C-11. Single Module Sublimator Performance

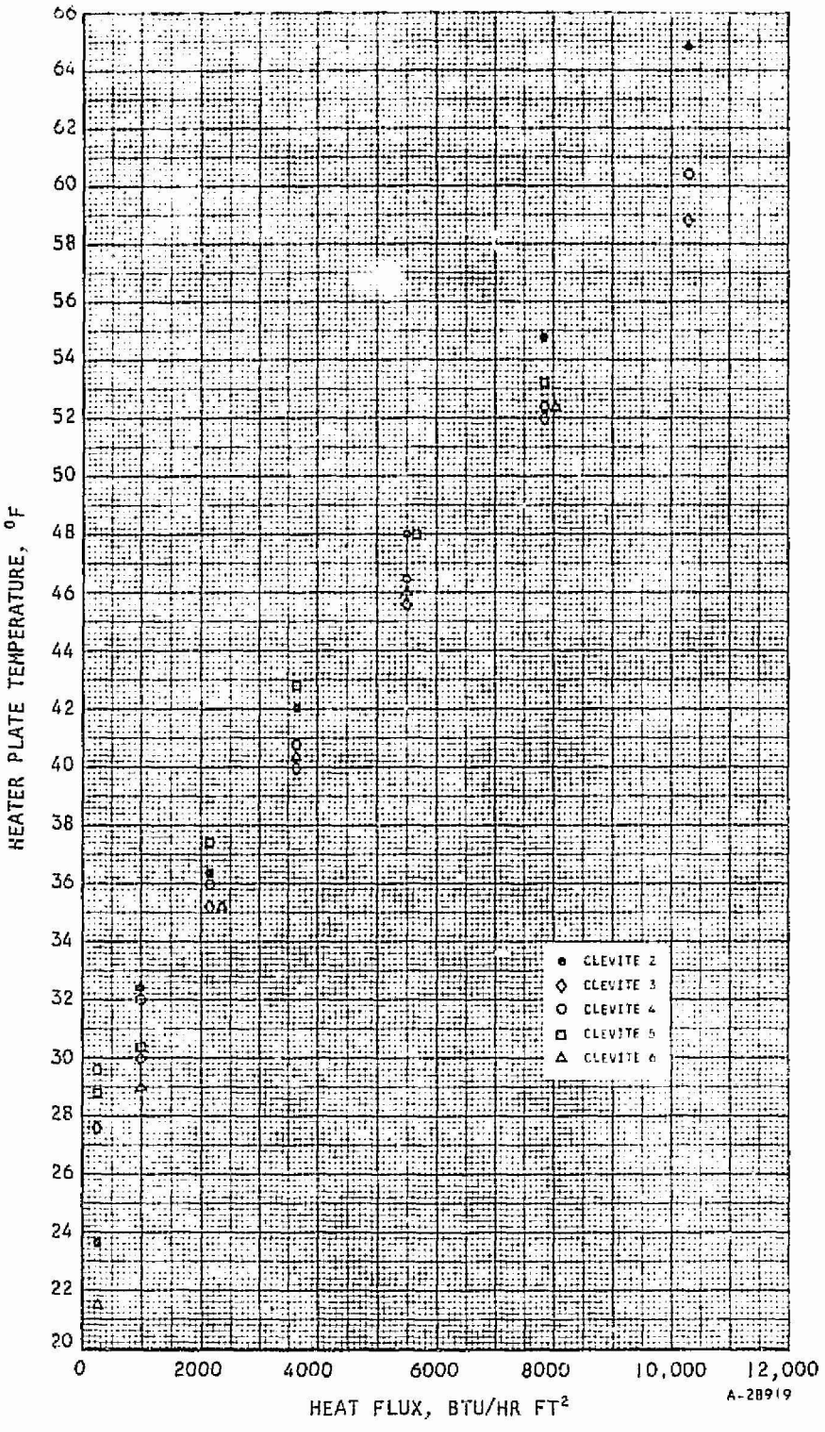

Figure C-12. Single Module Sublimator Performance

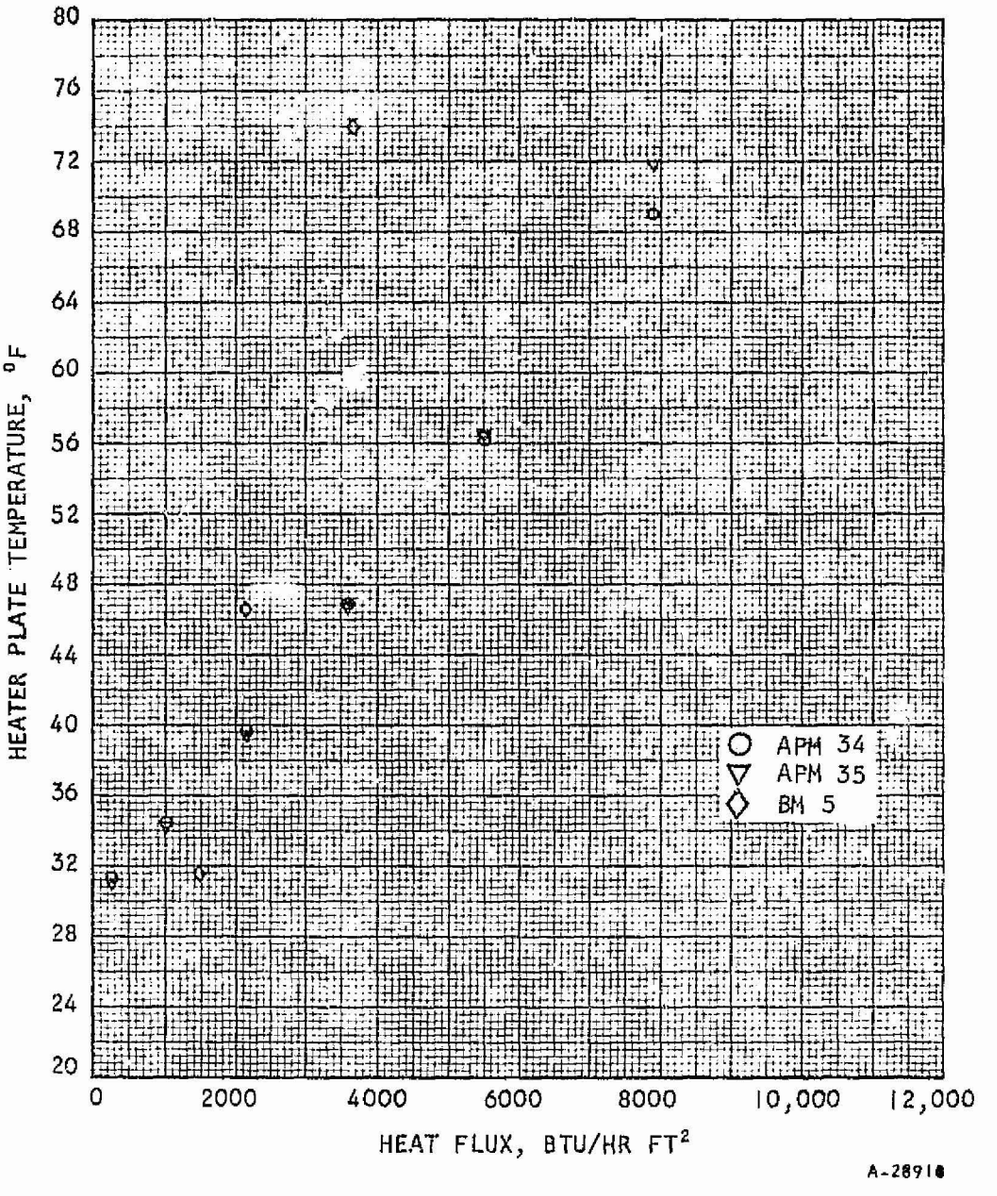

Figure C-13. Single Module Sublimator Performance

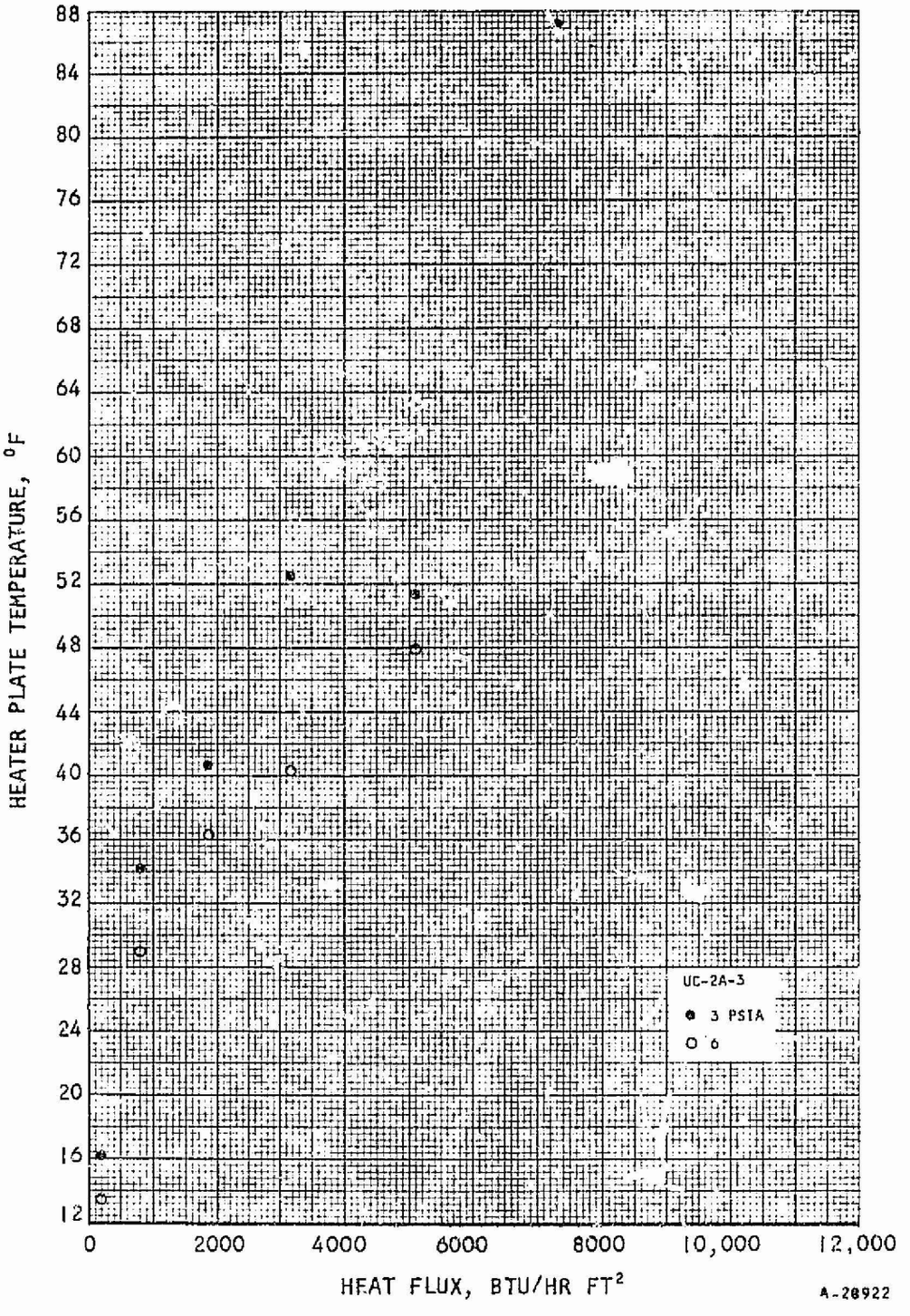

Figure C-14. Single Module Sublimator Performance with 0.012 in. Water Plenum

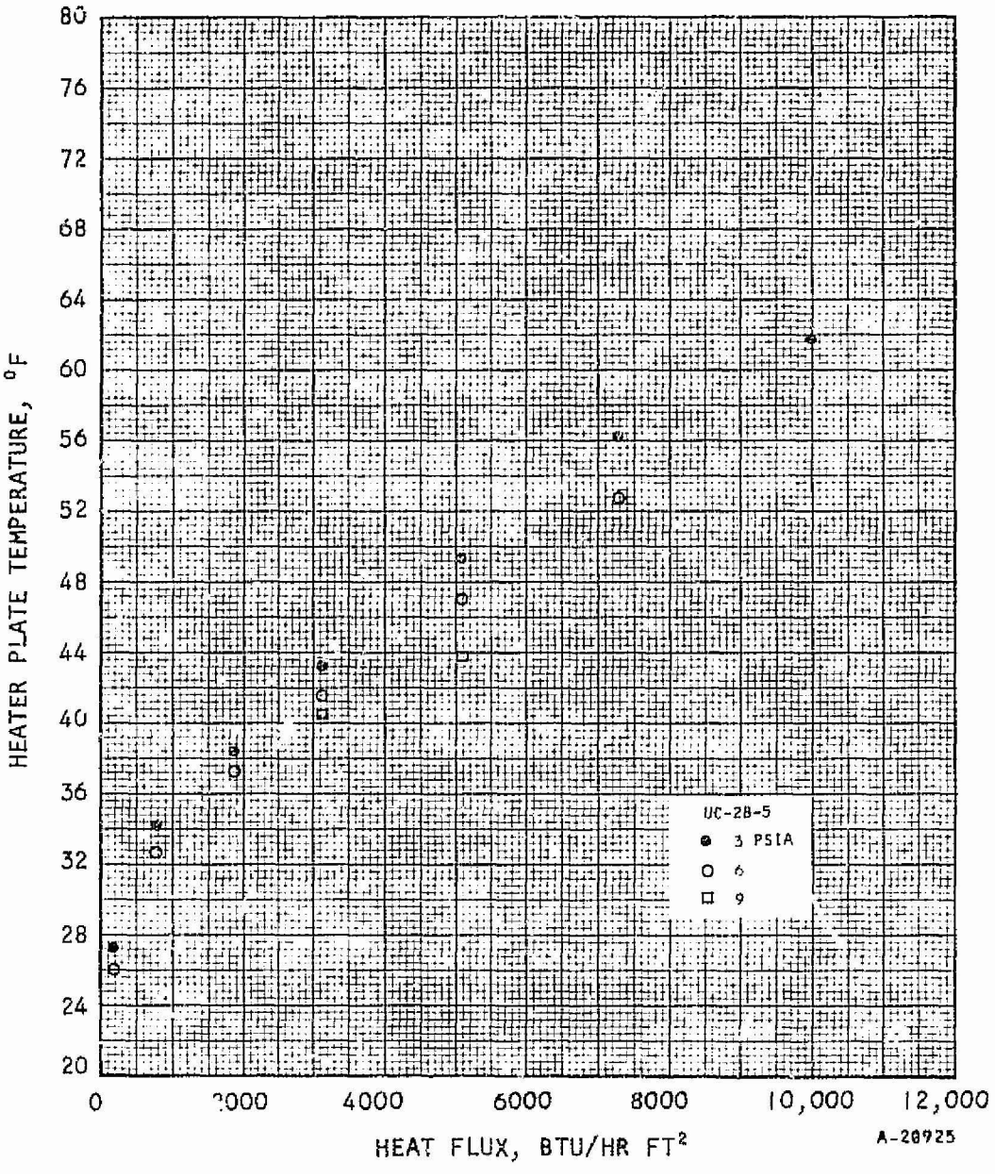

Figure C-15. Single Module Sublimator Performance with 0.012 in. Water Plenum

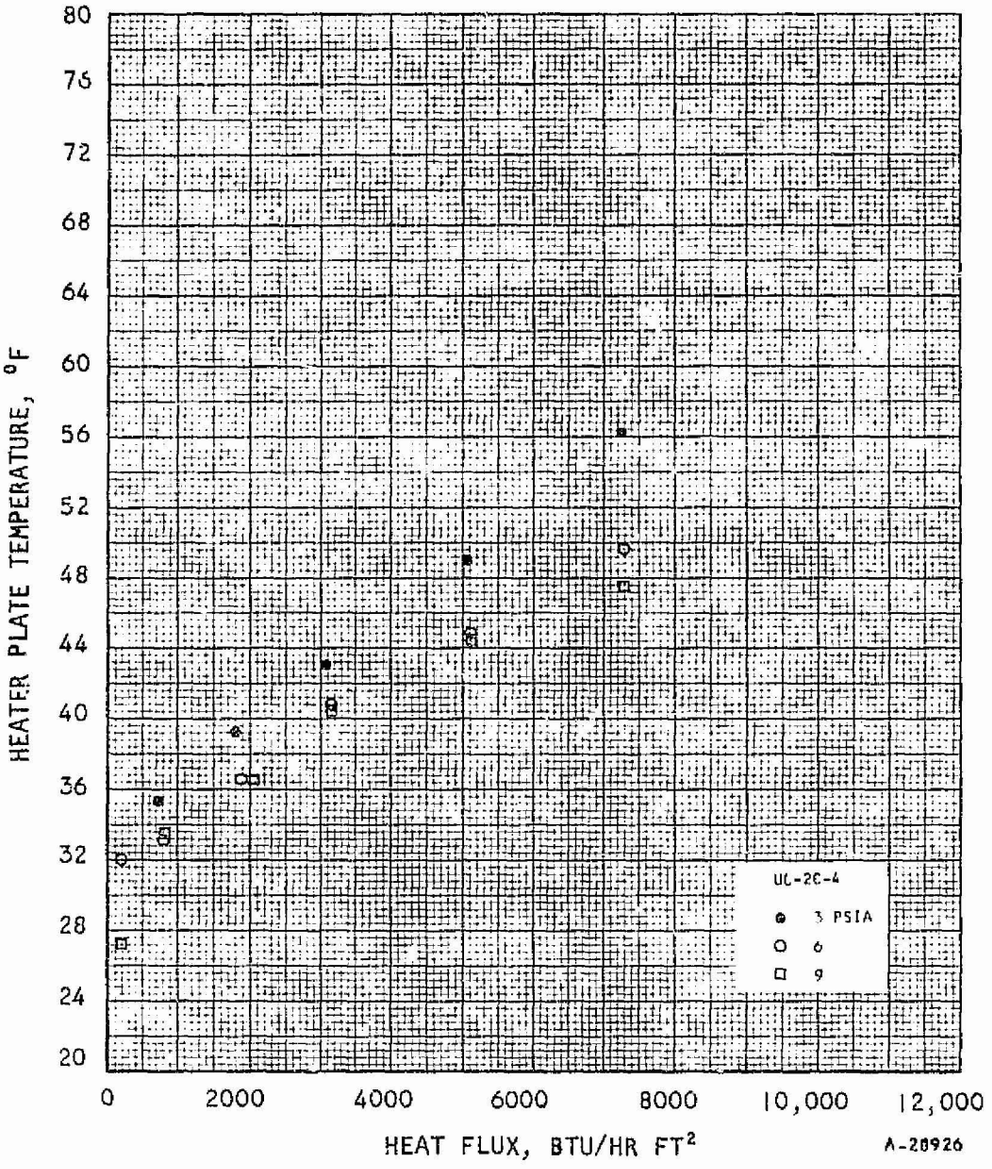

Figure C-16. Single Module Sublimator Performance with 0.012 in. Water Plenum

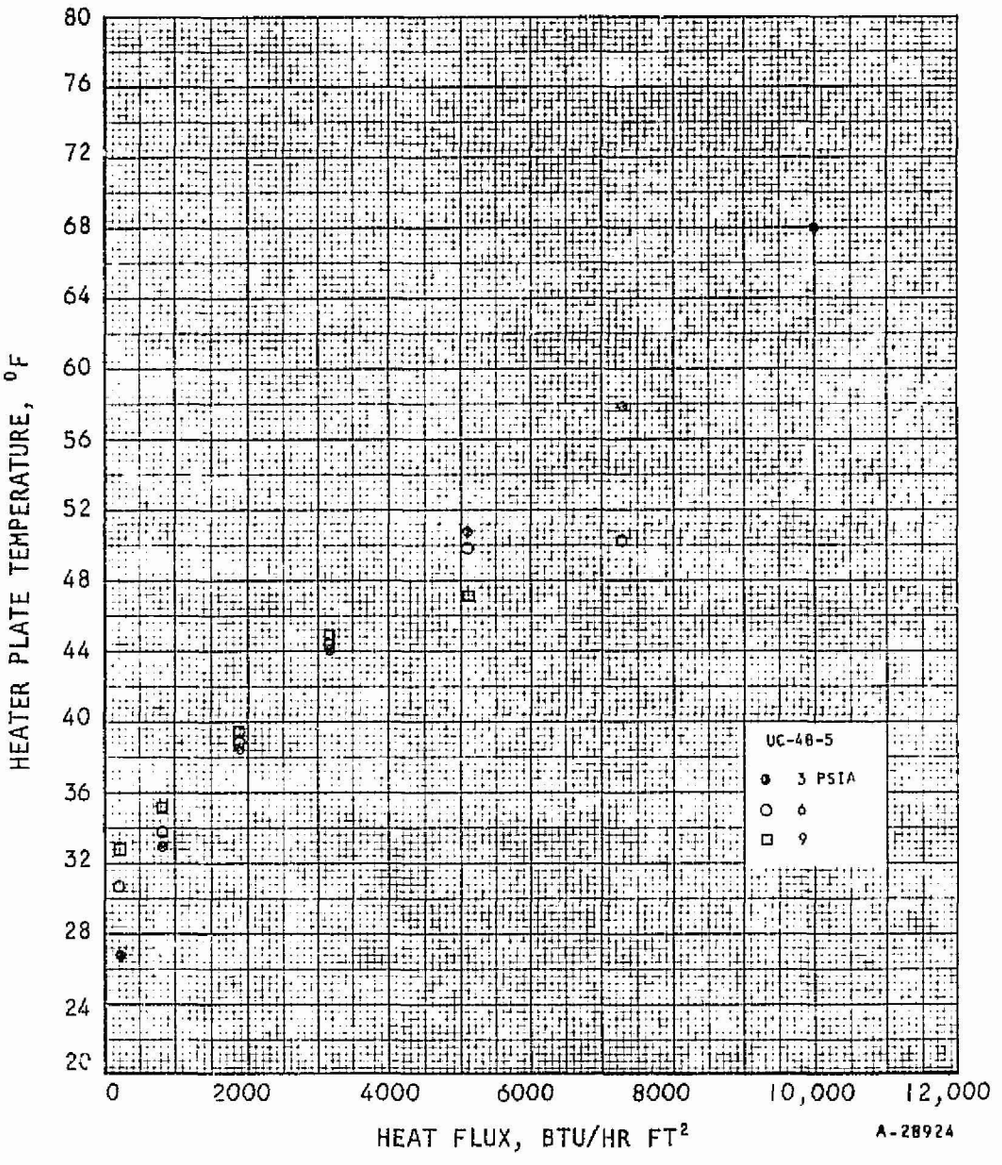

Figure C-17. Single Module Sublimator Performance with 0.012 in. Water Plenum

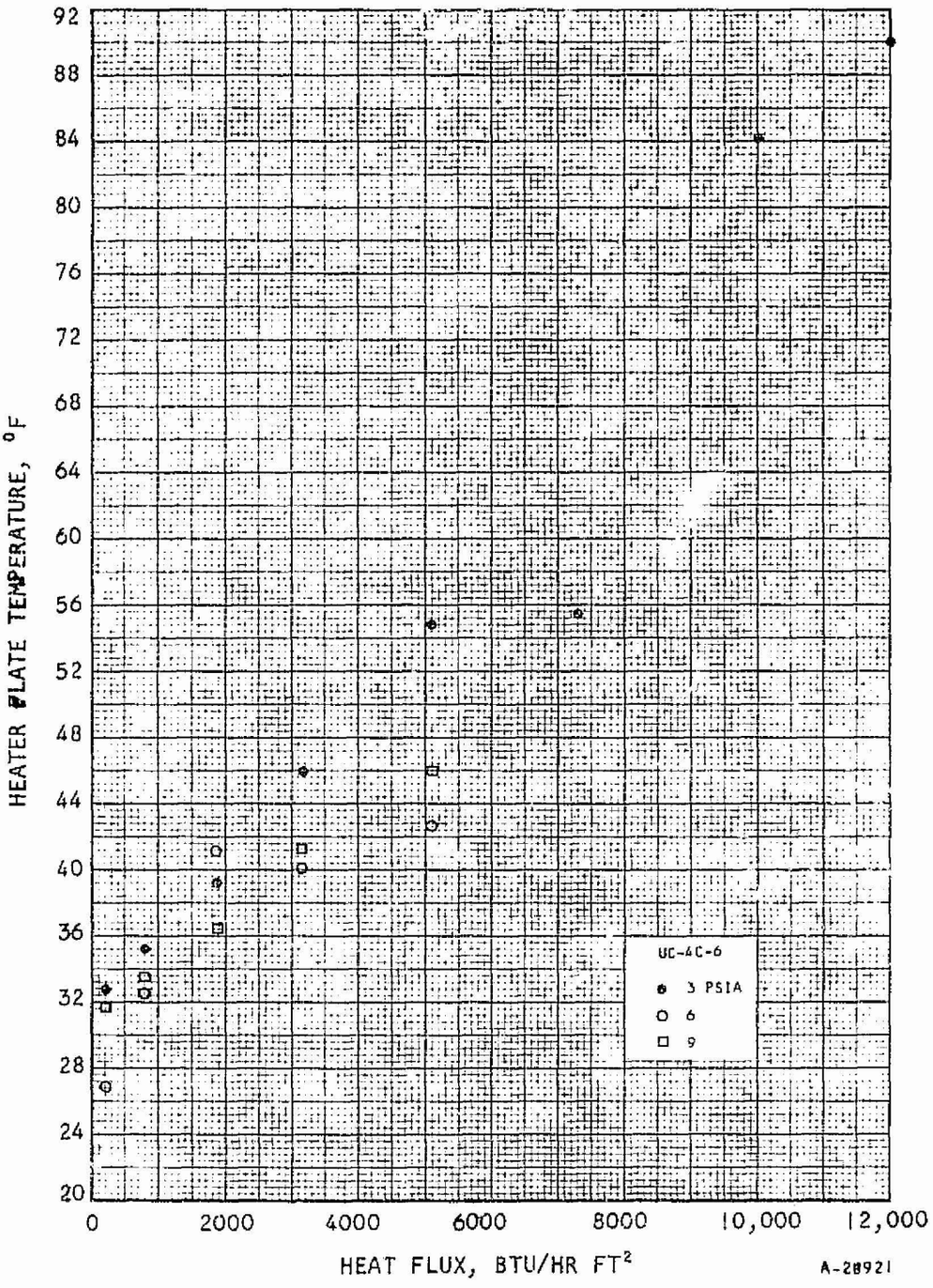

Figure C-18. Single Module Sublimator Performance with 0.012 in. Water Plenum

APPENDIX D

GLYCOL INLET HEAT FLUX BREAKTHROUGH

While the short water plenum eliminates the plate damage problems associated with freeze-thaw cycling, some difficulty is encountered with breakthrough at higher glycol inlet temperatures. This is due to the relatively short heat conduction path through the water plenum header bar which results in the porous plate being heated to above 32°F in this region and liquid passing through the plate. The following analysis develops the equation which defines this phenomenon. The geometry is defined below.

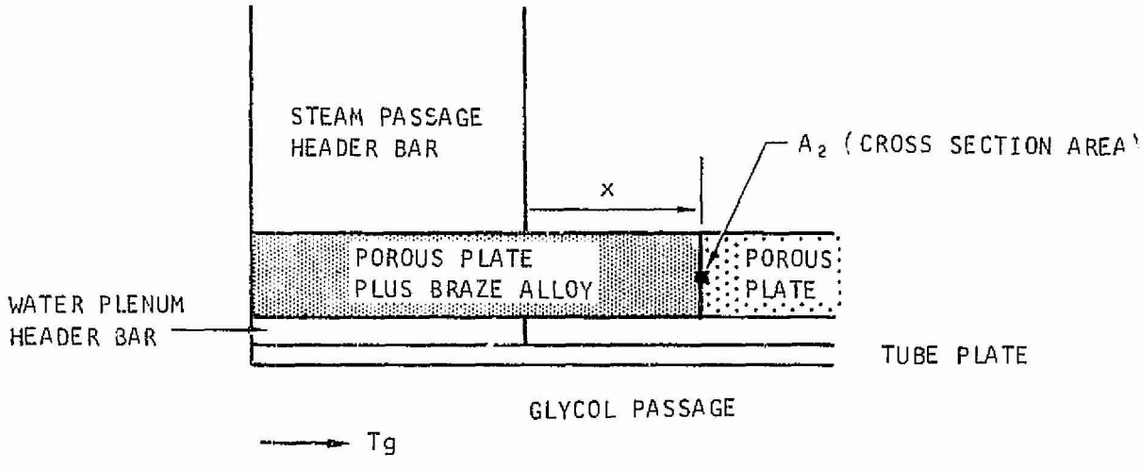

Glycol enters at a temperature T_g and heat is transferred by convection to the tube plate. The heat is conducted along the water plenum header bar and porous plate which in this region is filled (or partially filled) with braze alloy. Heat is conducted along the alloy filled porous plate (A_2) where it is eventually dissipated in the sublimation process. The conduction equation defines heat transfer through the alloy filled porous plate from $x = 0$ to x.

$$\frac{Q}{A_2} = \frac{k}{x} (T_B - 32) \qquad (1)$$

where $\frac{Q}{A_2}$ = heat flux through A_2

k = effective thermal conductivity of porous plate - braze alloy matrix

x = distance over which braze alloy fills porous plate

T_B = temperature at porous plate - header bar junction

It is assumed that at x the maximum plate temperature is 32°F since if it is hotter, no ice will form and breakthrough will occur.

The convection equation defines heat transfer from the glycol to the porous plate. The porous plate - header bar combination is treated as a fin whose base temperature is T_B.

$$\frac{Q}{A_1} = \eta_o h_{eff} (T_g - T_B) \tag{2}$$

where $\frac{Q}{A_1}$ = heat flux through A_1

η_o = fin effectiveness of porous plate and header bar

h_{eff} = effective heat transfer coefficient over A_1

T_g = glycol inlet temperature

Equation (2) may be rearranged to obtain

$$T_B = T_g - \frac{(Q/A_1)(A_2/A_1)}{\eta_o h_{eff}} \tag{3}$$

Solving equation (1) for x and inserting (3) in the resulting equation, one obtains:

$$x = \frac{k}{Q/A_2}\left[T_g - \frac{(Q/A_2)(A_2/A_1)}{\eta_o h_{eff}} - 32\right] \tag{4}$$

Equation (4) defines the minimum distance x which must be filled with braze alloy in order that the plate temperature does not exceed the 32°F required for ice formation. As indicated, x is a function of Q/A_2, the maximum heat flux along the porous plate which the plate can support without causing breakthrough. Since this heat flux is not know, it is not possible to solve (4) exactly for a given geometry. However, to get a rough idea of how x varies with T_g, equation (4) was solved for assumed values of the various parameters and the results are shown in Table I. The thermal conductivity of the sintered nickel porous plate taken to be 20 B/hr ft °F. Values of A_2/A_1 and $\eta_o h_{eff}$ were obtained from the experimental unit designed during this study program and were 0.112 and 149 B/hr ft^2 °F, respectively. Q/A_2 was assumed tc be 20,000 Btu/hr ft^2. Using these values, the following distances were obtained as a function of T_g:

T_g, °F	x, in.
90	0.515
75	0.336
60	0.156
45	0.024

As indicated, relatively small changes in x may result in a significant increase in the glycol inlet temperature.

Additional analysis and/or testing is required to define absolute values of k and Q/A_2 so that accurace predictions of the relationships between T_g and x may be made.